THE THERMAL DECOMPOSITION OF PERFLUOROCYCLOPROPANE

A Thesis submitted for the
Degree of Doctor of Philosophy
of the University of London

by

David James McKeagan

Department of Chemistry,
Imperial College of Science
and Technology,
London S.W.7.

August 1967

ABSTRACT

The thermal decomposition of perfluorocyclopropane has been studied in a static reactor. Pressure changes during the reaction were followed with a pressure transducer and products analyzed by gas-solid chromatography. Reagents were purified by preparative scale gas-solid chromatography.

The reactions can be explained by the following mechanism:

$$\overbrace{CF_2 \cdot CF_2 \cdot CF_2} \xrightarrow{k_1} CF_2 = CF_2 + CF_2$$

$$2CF_2 \xrightarrow{k_2} CF_2 = CF_2 \; ; \; \frac{d[C_2F_4]}{dt} = k_2 [CF_2]^2$$

$$CF_2 + CF_2 = CF_2 \xrightarrow{k_3} \overbrace{CF_2 \cdot CF_2 \cdot CF_2}$$

The differential rate equation describing the kinetics of the above reactions has been integrated by numerical methods using a computer. The following expressions describe the high pressure variation of the rate constants with temperature:

$$k_1^{\infty} = 8.41 \times 10^{14} \exp.(-42.55/RT) \text{ sec}^{-1} \qquad (230 - 320^{\circ}C)$$

$$(k_3/k_2^{\frac{1}{2}})^{\infty} = 1510 \exp.(-7030/RT) \text{ (l./mole sec)}^{\frac{1}{2}} \qquad (230 - 289^{\circ}C)$$

Values of the equilibrium constant for perfluorocyclopropane decomposition and heat of formation of perfluorocyclopropane have been determined.

The reaction described by k_1 is a homogeneous unimolecular reaction. k_1 begins to falloff at about 20 cm of Hg pressure. The variation of k_1 with pressure has been studied at 230 and 253°C down to 0.0015 cm of Hg.

The theory of unimolecular reactions has been sketched in some detail and results of the present study applied to Kassel, Slater and Transition-State approaches. A number of previously unreported fundamentals for perfluorocyclopropane have been observed in the far infra-red. This has facilitated a more complete vibrational analysis of the molecule and aided in the application of the above theories.

ACKNOWLEDGEMENTS

The author wishes to thank his supervisor, Dr B. Atkinson, whose unfailing patience and continual encouragement was an inspiration during this work, and Professor R.M. Barrer for providing laboratory facilities in the Department of Chemistry. He is grateful to Professor G. Wilkinson for the use of infra-red spectroscopy equipment in the Inorganic Chemistry Section.

Grateful acknowledgement is due to the Department of Education in the Province of Quebec and the National Research Council of Canada for Scholarships which enabled the author to devote full time to research activities.

A considerable debt is owed Mrs U. Fowler and Mrs J. Lee for their accurate transcription of the original manuscript.

CONTENTS

LIST OF FIGURES

LIST OF TABLES

LIST OF SYMBOLS

It has been found impossible to find a completely discrete set of symbols for all the different quantities used. It was felt advisable not to try to do so as it would be necessary to express many equations using terminology so different from that of the original authors as to make comparison to the original papers very inconvenient. However where confusion might result from similar symbols used in the theoretical discussions it seems appropriate to specify their meaning in tabular form. Unless otherwise noted the following symbols have the meaning indicated.

M : any molecule

m : mass of a molecule

μ : reduced mass

t : time

T : temperature

T' : kinetic energy

τ : lifetime of an active molecule

k : rate constant

$\underline{k}$: Boltzmann's constant

$\underline{\underline{k}}$: Transmission coefficient

K : equilibrium constant

q : distance coordinate

Q : normal coordinate

$\bar{Q}$: partition function

s : number of Kassel Oscillators

s' : Rice-Ramsperger square terms

S : entropy

P : pressure

$\bar{P}$: probability

E : energy per mole

ϵ : energy per molecule

N : number of molecules

n : number of Slater oscillators

$\bar{v}$: average velocity

V : potential energy

h : Planck's constant

h' : distribution function of active molecule lifetimes.

In the Results section, frequent reference is made to a number of symbols whose meaning should be stated clearly:

k_1 : rate constant for initial step in perfluorocyclopropane decomposition.

k_1^{∞} : theoretical infinite pressure value of k_1

Pr : partial pressure of perfluorocyclopropane

Po : initial value of Pr

Y : Pr/Po

a : $3k_3/2(2k_2RT)^{\frac{1}{2}}$

k_3, k_2 : rate constants for subsequent steps in perfluorocyclopropane decomposition

α : $a\left(\frac{P_o}{k_1}\right)^{\frac{1}{2}}$

Two frequently used chemical symbol abbreviations which should be noted are:

$c\text{-}C_3F_6$	perfluorocyclopropane
$c\text{-}C_4F_8$	octafluorocyclobutane

FOREWORD

The present work was undertaken to compare various kinetic effects in the thermal breakdown of perfluorocyclopropane to those in the structurally similar cyclopropane. The latter compound has been the subject of much experimental and theoretical study in the field of first order homogeneous unimolecular reactions. This would also extend work which has been done on fully halogenated cyclobutane compounds to the cyclopropanes. Fluorinated cyclobutanes and hydrocarbon cyclopropane and cyclobutane rings have high pre-exponential factors in the Arrhenius expressions for the variation of reaction rate constant with temperature; the fully fluorinated C_3 ring has not been studied in this respect. In addition, perfluorocyclopropane has been postulated as an intermediate in the reactions of octafluorocyclobutane; perfluorocyclopropane was never isolated from the products of these reactions nor the mode of decomposition of the pure material considered under the same conditions.

A study of the principal currently held theories of unimolecular reactions forms the main part of the background to the thesis. This, along with an outline of the chemistry of both perfluorocyclopropane and difluoromethylene, whose presence it was necessary to postulate

to explain the decomposition of perfluorocyclopropane, make up the Introduction to the thesis. An Experimental section describes the equipment and conditions used in the preparation, handling, purification, reaction and analysis of perfluorocyclopropane and analysis of its reaction products. The results of the kinetic studies are presented in the Results section. In the Discussion section the results are compared to the known behaviour of other compounds under similar conditions and to the theories which attempt to predict this behaviour.

Page

1. INTRODUCTION

1. INTRODUCTION

1.1 The Theory of Unimolecular Reactions

A unimolecular reaction is one which takes place without collision. It might be described as a spontaneous disruption or transformation of the reacting molecule.

It is now firmly established that a molecule undergoing a chemical unimolecular reaction obtains sufficient energy to do so by collision with other molecules. The overall reaction is, however, described by first order kinetics, i.e.

$$-\frac{dc}{dt} = kc,$$

where c and t represent concentration and time respectively, k, a proportionality constant, has units of $(\text{time})^{-1}$. The variation of k with temperature obeys the Arrhenius expression:

$$k = A \exp.(-E/RT),$$

where R is the gas constant per mole, and T is the absolute temperature. In this equation, A is called the "pre-exponential factor" or "A factor" and E the "activation energy".

For reactions which occur in the gas phase, the "homogeneity" of the reaction is significant in the mechanistic interpretation of numerical results. Thus a reaction is described as homogeneous if the effect of the containing surface on the kinetics can be neglected.

A considerable body of theory exists which attempts to predict the rate constants for unimolecular reactions and their variation with reaction conditions. Unimolecular reaction theory in its present state may be considered to have evolved from the initial ideas of Lindemann (1) and Hinshelwood (14). They proposed that molecules gain sufficient energy to react by collision with other molecules and that a definite time lag exists between collision and actual reaction. Molecules with sufficient energy to react are considered "activated". In the reaction medium there are three simultaneous processes occurring: activation, deactivation, and reaction. For a reacting molecule B, its activated form B*, and any third body M, these steps may be represented by the following equations with respective rate constants:

$$B + M \longrightarrow B^* + M, \; k_1$$

$$B^* + M \longrightarrow B + M, \; k_2$$

$$B^* \longrightarrow \text{products}, \; k_3$$

Thus:

$$d[B^*]/dt = k_1[B][M] - k_2[B^*][M] - k_3[B^*].$$

If a steady state concentration of B* is assumed, then:

$$[B^*] = k_1[B][M]/(k_2[M] + k_3),$$

and

$$\frac{d[\text{prods.}]}{dt} = k_3[B^*] = k_3k_1[B][M]/(k_2[M] + k_3).$$

Thus, the observed rate of reaction is dependent upon the relative effects of the three processes. At high

pressures, the value of [M] is large and since $k_2[M] >> k_3$,

$$\frac{d[\text{prods.}]}{dt} = \frac{k_3 k_1}{k_2}[B].$$

The observed behaviour would be first order. At low pressures [M] is small and $k_2[M] << k_3$, so that:

$$\frac{d[\text{prods.}]}{dt} = k_1[B][M].$$

The observed behaviour would be second order.

These effects are in fact observed when unimolecular reactions are studied at low pressure. There is a "fall off" of the apparent first order rate constant; behaviour approaches second order. The quantitative evidence substantiates the Lindemann-Hinshelwood idea that a time lag does exist between activation and reaction.

The theory of unimolecular reactions is of considerably wider interest than the reactions to which the present study can be suitably compared. It is of importance in such fields as atom recombination reactions and reactions associated with mass spectra. Of specific interest are those molecules which undergo thermal unimolecular reactions and which are sufficiently complex for the falloff region to be conveniently observed. It is the theory which is applied to these reactions which will be sketched. Emphasis will be placed on the assumptions upon which the theories are based rather than on precise mathematical

derivation. In cases where the intention is to apply certain of the theories to the experimental data, more detail will be given.

1.1.1. Rice-Ramsperger-Kassel-Marcus (R.R.K.M.) Theory

(a) The Strong Collision assumption

One common notion in most theories of unimolecular reactions is that effectively all collisions of activated molecules are deactivating. This is known as the strong collision assumption. Thus in the Lindemann-Hinshelwood scheme k_2 is the rate constant for collision of activated molecules.

Benson (35,p.212) has shown very clearly how increase in reaction rates with temperature can be explained by the fact that reaction is primarily due to molecules of unusually high energy. Intuitively then it might be expected that a collision in which a high energy molecule became involved would result in a drastic reduction in its energy content; such molecules are rare and the molecules they collided with will have considerably less energy. Chemical activation experiments in which molecules are generated in an activated state, usually in a narrow energy range, in the presence of various "inert" molecules, give information concerning the deactivation process. Except for discrepancies in the case of some simple molecules ($N < 6$) the evidence is strongly in favour of the strong collision assumption (19).

Hoare (32), has considered the effect of "weak" collisions on unimolecular processes. Mahan (34) has argued from sonic experimental evidence that a considerable number of collisions may be required to remove a molecule from a vibrationally excited state. His work points the way to more precise calculations of k_2 but it is not of immediate practical use; the expressions used require large approximations and are not based on molecular interactions which are strictly vibrational-vibrational interactions.

(b) The Hinshelwood Approach

The Lindemann-Hinshelwood mechanism results in an expression for the overall rate constant:

$$k = \frac{k_3 k_1}{k_2 + k_3/P} \qquad (1)$$

where now P, the pressure has replaced [M] the total concentration of all molecules. This may also be written:

$$\frac{1}{k} = \frac{k_2}{k_3 k_1} + \frac{1}{k_1 P} \qquad (1^a)$$

The term $\frac{k_2}{k_3 k_1}$ is the value of k at high pressure, usually written k^{∞}. Thus the theory predicts that a plot of $1/k$ vs. $1/P$ in the fall-off region, will be a straight line. This prediction is not observed in practice.

On the surface, the Lindemann-Hinshelwood scheme seems difficult to justify in terms of experimental results.

At high pressure the scheme assumes negligible rates of reaction relative to collision; the observed values of k_1 are in fact greater than simple collision theory would predict. But simple collision theory assumes that the vibrational energy would be contained in one degree of freedom and Lindemann's suggestion that several degrees of freedom are in fact active results in a prediction of a much higher proportion of active molecules and more realistic rates.

Hinshelwood (5) has derived an expression, based on classical mechanics, for the chance that a molecule possesses energy greater than E distributed at random among 2f square terms considered equivalent to f vibrational degrees of freedom. This gives an approximate expression for the proportion of activated molecules:

$$\frac{k_1}{k_2} = \frac{\exp.(-E/RT)\ (E/RT)^{f-1}}{(f-1)!} \qquad (2)$$

From above:

$$k^{\infty} = \frac{k_3 k_1}{k_2} = A \exp.(-E/RT)$$

$$\text{and } k_3 = \frac{k_2}{k_1} A \exp.(-E/RT)$$

$$= \frac{A\ (f-1)!}{(E/RT)^{f-1}}$$

If the Hinshelwood approach is assumed valid, a value of k_3/k_2 can be determined from a plot of $1/k$ against $1/P$ (see eqn 1[a]), where:

$$\frac{k_2}{k_3} = \frac{\text{intercept}}{\text{slope}}$$

Assuming k_2 to be the collision frequency, then k_3 can be calculated and f determined.

The determination of f, the number of active vibrational degrees of freedom is useful for the sake of comparing different molecules. However the observed non-linearity of the $^1/k$ against $^1/P$ plot remains to be explained; in effect this curvature vitiates the whole method of calculating f. Implicit in the Hinshelwood approach as given above is the assumption that reaction is dependent on molecules having an amount of energy greater than a critical value E, but that the rate of step 3 does not depend on the magnitude of the excess energy present. In fact a more correct expression for the general rate constant of equation (1), would be:

$$k(E)\, dE = \frac{k_3(E)k_1(E)dE}{k_2 + k_3(E)/P} \quad , \qquad (3)$$

in which both k_1 and k_3 are functions of the energy content E of B*. The integration would be performed over all E from the minimum value needed for reaction to ∞. It seems reasonable to assume that k_3 will be very low for molecules which have only a small amount of energy in excess of the critical value and that k_3 will be higher for a higher excess of energy.

At high pressure where the time between collisions is short it must be fairly highly energized molecules which make the most significant contribution to reaction. At low pressures where the time between collisions is longer the lower energy, more slowly reacting molecules, make a more important contribution. It is interesting to consider the effect of low pressure on the energies of molecules which react. The Maxwell-Boltzmann energy distribution of molecules which applies at high pressure is described by a curve such as the solid line in figure 1.1.a, where N is the number of molecules with energy E. Only those with at least ε_o can react. The distribution is affected in a manner shown by the dotted line at low pressure by the reduction in concentration of activated molecules. At high pressure the number of active molecules N* which react would be described by the solid line of figure 1.1.b. At low pressures where the actual number of molecules reacting decreases, the maximum is shifted towards lower energies since the longer time between collisions gives the lower energy molecules a greater contribution, as in the dotted curve of figure 1.1.b. This effect has been demonstrated by the numerical results of Atkinson**. He has assumed the form of equation (2) for k_1/k_2 and for k_3:

** Atkinson, B., unpublished results.

Distribution of Energies in Reacting Molecules.

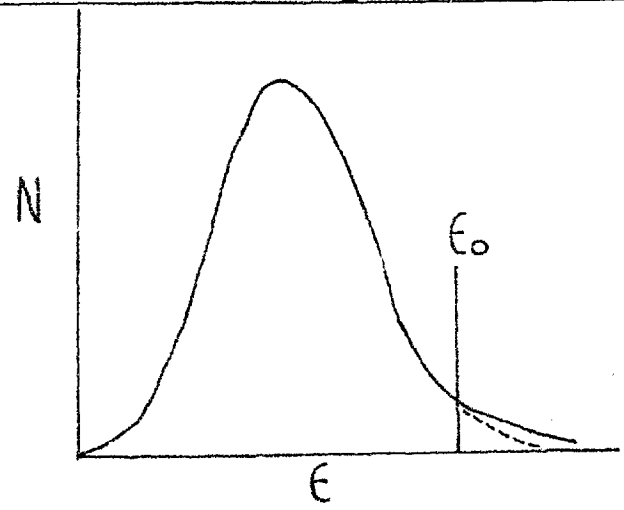

Figure 1-1a

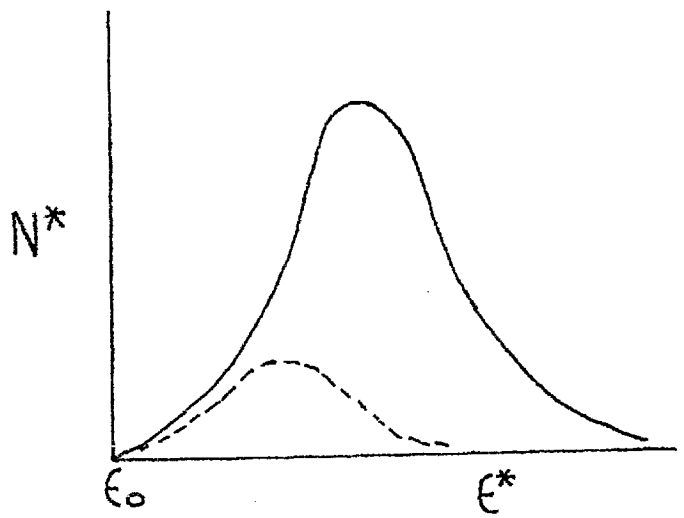

Figure 1-1b

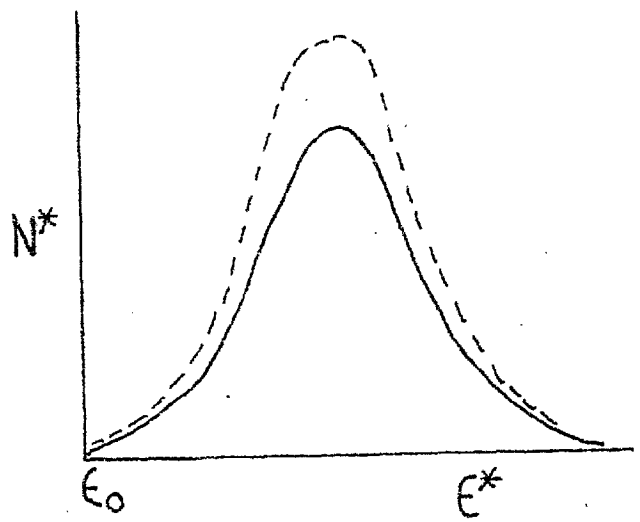

Figure 1-1c

$$k_3 = A \left(\frac{\epsilon - \epsilon^*}{\epsilon}\right)^{f-1} .$$

By taking k_2 as that predicted from collision theory he was able to show for several values of f that the behaviour of figure 1.1.b is indeed observed.

The effect may be imagined in another way. If the effect of reduced deactivation/reaction ratio from longer intervals between collisions is alone considered, then the dotted curve of figure 1.1.c would be the observed effect on the distribution of molecules which react. Low energy molecules have little chance of reaction anyway and their reaction probability is not greatly affected; high energy molecules always have a relatively high probability of reaction and their distribution will not change greatly. If now the reduced concentration of activated molecules (figure 1.1.a) is imposed on this curve then it would be expected to become like that of 1.1.b (dotted line) since as ϵ^* increases, its concentration reduction also increases.

(c) The Simple Harmonic Oscillator Approximation

In elementary models for calculation of unimolecular decomposition rates, the internal vibrations of a molecule have been described in terms of simple harmonic motion. The resulting motion of a number of atoms where vibrations interact is quite complicated even if the individual motions are harmonic. In fact however a number of basically simple

motions arise which result from the interactions of the individual simple harmonic motions. These motions have characteristic frequencies and are referred to as the normal mode vibrations of the molecule. A normal mode is a characteristic motion of the whole molecule, not of a particular internal distance or angle.

For a single particle carrying out simple harmonic motion of frequency ν the displacement x is given by:

$$x = x^{o} \cos (2\pi \nu t + \theta),$$

where x^{o} is the amplitude, t the time and θ a phase constant. The restoring force F may be expressed:

$$F = -4\pi^{2} \nu^{2} m x,$$

where m is the mass of the particle. Since force is the negative derivative of the potential energy with respect to displacement, the potential energy V of the particle may be expressed:

$$V = bx^{2}/2,$$

where $b = 4\pi^{2} \nu^{2} m$, and is called the force constant. The kinetic energy, T', may in turn be expressed:

$$T' = m\dot{x}^{2}/2,$$

where $\dot{x} = dx/dt$.

For a molecule consisting of a number of atoms the positions are described using some type of coordinates. Analogous to the case of a single particle whose movements may be described in terms of a single distance coordinate x, Cartesian coordinates are often used in the case of a many

particle system. The restoring force to equilibrium for each atom could be expressed as a power series in the Cartesian coordinates with force constants relating the motion of each atom to any other. For small displacements however, only the linear terms of this relation need be considered. Thus, the potential energy of the atoms which is zero in the equilibrium position may be expressed (15, p.73):

$$V = \frac{1}{2} \sum_{ij} (b^{ij}_{xx} x_i y_j + b^{ij}_{yy} y_i y_j + b^{ij}_{zz} z_i z_j) +$$

$$\sum_{ij} (b^{ij}_{xy} x_i y_i + b^{ij}_{xz} x_i z_i + b^{ij}_{yz} y_i z_j),$$

where x_i, x_j, y_i, y_j, z_i and z_j are the Cartesian coordinates of the atoms with respect to their individual equilibrium positions, and the b are the appropriate force constants. Because the equilibrium position of each atom is the origin of a different set of Cartesian coordinates, these are also often referred to as displacement coordinates. Similarly, the kinetic energy can be written:

$$T' = \sum_i \frac{1}{2} m_i (\dot{x}_i^2 + \dot{y}_i^2 + \dot{z}_i^2),$$

where m_i is the mass of atom i. Thus the total energy which is $(T' + V)$ would be an expression in the squares of the coordinates and momenta of the component atoms.

In fact any vibrational motion of a system of particles such as a molecule may be represented as a superposition of normal vibrations with suitable amplitudes.

Another frequently used type of description is in terms of normal coordinates which are linearly related to displacement coordinates. As pointed out by Kassel (8) any system whose Hamiltonian (T' + V) contains only terms in the squares of coordinates and momenta may be transformed to a new set of coordinates so that the Hamiltonian has the same form. Thus in terms of normal coordinates the Hamiltonian still only contains terms in the squares of coordinates and momenta.

The theories of Rice and Ramsperger, Kassel and Slater are all based on molecular models made up of harmonic oscillators.

(d) Transition-state Theory

The Transition-state Theory of chemical reactions is usually associated with the names: Glasstone, Laidler and Eyring(13). Its application to unimolecular reactions directly is not of great quantitative importance. However, some of the concepts developed in it are of significance in the evolution of more modern theories such as those of Marcus and Slater.

Attention is focused by this theory on a potential energy surface which describes the possible configurations of the molecule. For the reaction:

$$B \longrightarrow C$$

it is assumed that some coordinate X-Y in B must be extended to a distance ℓ for the molecule to become C.

The potential energy of B rises as X-Y is extended to ℓ and the region of configuration space where this condition is fulfilled is called the "transition state". A minimum energy E_B cal./mole above the lowest energy state of B must be possessed by the molecule to be in this region; when it is in this region it is designated by B^+ and X-Y will have values in the range ℓ to $\ell + \delta$, where δ is small.

An equilibrium condition is assumed which is described by the equation :

$$B \rightleftharpoons B^+ \rightleftharpoons C ,$$

where $[B^+]$ is the equilibrium value. In the above sequence of reactions:

$$K^+ = \frac{[B^+]}{[B]}, \text{ an equilibrium constant.}$$

As the equilibrium is dynamic, half of $[B^+]$ is passing from B to C and half from C to B. Call the portion passing forward $[B^+]_f$. Thus:

$$K^+ = \frac{2[B^+]f}{[B]}$$

The majority of molecules which react will have more internal energy than E_B and at least part of this excess energy will appear as kinetic energy of the internal motion in which X and Y move apart. The average life of B^+ is given by $\delta/\bar{V}$, where $\bar{V}$ is the average velocity of increase in X - Y at ℓ for molecules of different energy. The equilibrium distribution of energies and hence velocities give, from Maxwell's equation:

$$\bar{V} = \left(\frac{2\underline{k}T}{\pi m}\right)^{\frac{1}{2}} ,$$

where m is the effective mass for motion along the co-ordinate X - Y. The average life is then $\delta/\bar{V}$. Thus the rate of reaction can be expressed as:

$$-\frac{d[B]}{dt} = \frac{[B^+]_f}{\text{av. life of } B^+}$$

$$= \frac{K^+ [B]}{2\delta} \left(\frac{2kT}{\pi m}\right)^{\frac{1}{2}}$$

In normal circumstances K^+ could be written in terms of partition functions:

$$K^+ = \frac{\bar{Q}_r^+ \; \bar{Q}_v^+}{\bar{Q}_r \; \bar{Q}_v} \exp.(-E_B/RT).$$

Actually one of the vibrational degrees of freedom of B^+ is a kinetic motion or translation along X - Y inside the distance δ. This translation is expressed by the standard formula:

$$\bar{Q}_t = (2\pi \; m \; \underline{k} \; T)^{\frac{1}{2}} \; \delta/h,$$

so that:

$$-\frac{d[B]}{dt} = \frac{K^{\ddagger} \; (2\pi \; m \; \underline{k} \; T)^{\frac{1}{2}}}{2\delta} \cdot \frac{\delta}{h} \left(\frac{2 \; \underline{k} \; T}{\pi m}\right)^{\frac{1}{2}} [B].$$

whence:

$k^{\infty} = \underline{k} \; T \; K^{\ddagger}/h$, the rate constant, where $K^{\ddagger}$ differs from K^+ in that there is one less term, the vibration become translation in $\bar{Q}_v{}^+$.

$K^{\ddagger}$ may be expressed in thermodynamic terms:

$$\ln K = \frac{-\Delta H^{o}}{RT} + \frac{\Delta S^{o}}{R},$$

Thus:

$$k^{\infty} = \underline{\underline{k}}\,\frac{kT}{h} \exp.\ (\Delta S^{\ddagger}/R)\ \exp.(-\Delta H^{\ddagger}/RT),$$

where:

$\Delta H^{\ddagger}$ is the heat of activation

$\Delta S^{\ddagger}$ is the entropy of activation.

The expression has been multiplied by $\underline{\underline{k}}$, the "transmission coefficient" which is the fraction of crossings of the potential energy barrier which are successful. In effect it allows for the possibility of a peculiar shape in the energy barrier and the possibility that all the molecules which reach the transition state do not proceed to reaction. Giddings and Eyring (20) have considered the transmission coefficient and its relation to unimolecular reactions in detail. They have shown by comparison to Kassel theory that $\underline{\underline{k}}$ depends on molecular constants and that for many reactions its value is unity. They have extended the application of the theory to low pressure by considering the effect of pressure on the transmission coefficient. Slater (4, ch.9) has criticized the general approach of transition state theory as being one which considers only the properties of the reacting species; it is incapable of adequately handling the process of arriving at the activated complex condition.

Simple transition state theory is characterized by the fact that an equilibrium or Maxwell Boltzmann distribution of activated complexes is assumed. For unimolecular reactions where k is less than k^{∞} the reaction rate $k_3[B^*]$ becomes significant and the equilibrium distribution for B^* or B^+ can no longer be assumed. For this reason transition state theory is usually only discussed in terms of high pressure rate constants. The theory also assumes that the product C is not removed and is still present to take part in maintaining the equilibrium concentration of B^+.

(e) The Kassel Approach

Kassel (8) has developed a theory of unimolecular reactions from the Lindemann-Hinshelwood scheme which adopts the more reasonable assumption that the rate of the final step depends upon how much activation energy is given to the molecule in excess of the critical amount. He derives an expression which is the temperature independent probability for decomposition and expresses:

$$k_3(\epsilon) = A\left(\frac{\epsilon-\epsilon_o}{\epsilon}\right)^{s-1}, \qquad \epsilon \geq \epsilon_o \qquad (1)$$

$$\text{and } k_3(\epsilon) = 0, \qquad \epsilon < \epsilon_o$$

where ϵ_o is the minimum energy for reaction, s is an integer related to the number of vibrational or other degrees of freedom, and A is a proportionality constant which turns out to be the high-pressure pre-exponential factor.

The molecular model which Kassel has used is one of a number of simple harmonic oscillators "weakly coupled" so that energy exchange can occur between them in the interval between collisions. In the theory as first developed (7), Kassel has assumed the vibrations to be purely classical. The expression he derives for the fall-off of rate constant is:

$$\frac{k}{k_\infty} = \frac{1}{(s-1)!(\underline{k}T)^s} \int_0^\infty \frac{\exp.(-x/kT)}{\frac{1}{x^{s-1}} + \frac{A/w}{(x+\epsilon_o)^{s-1}}} dx \qquad (2)$$

where

$x = -\epsilon_o + \epsilon$

w = collision rate

p = pressure

s = number of Kassel oscillators

A = high pressure pre-exponential factor

ϵ_o = high pressure activation energy/molecule

$\underline{k}$ = Boltzmann's constant.

In practice this expression is integrated numerically. Schlag and co-workers (11) have evaluated this integral for a range of A/w and s; interpolation of a graphical representation of their figures is possible in a particular case.

Kassel (8) subsequently developed a quantum form of his theory and demonstrated that this reduced to the above expression (2) in the classical limit. The quantum development of the theory will be described.

If there are s oscillators all of frequency ν, then the quantum weight of the state of energy $jh\nu$ is:

$$\overline{P}_j = \frac{(j + s-1)!}{j!\,(s-1)!}$$

Under conditions where the rate of collision is high enough that reaction is negligible relative to deactivation, a Maxwell-Boltzmann distribution of energies is assumed in the molecules. Thus the number of molecules which have j quanta may be expressed:

$$N_j = \frac{N\frac{(j + s-1)!}{j!\,(s-1)!}\exp.(-jh\nu/\underline{k}T)}{\sum_i \frac{(i + s-1)!}{i!\,(s-1)!}\exp.(-ih\nu/\underline{k}T)}, \qquad (3)$$

where N is the total number of molecules, the sum is taken over all possible states, and i is the number of quanta in each state.

The denominator of the expression (3) may be written:

$$\sum_i \frac{(i + s-1)!}{i!\,(s-1)!}\exp.(-ih\nu/\underline{k}T) =$$
$$1 + s\exp.(-h\nu/\underline{k}T) + \frac{s(s+1)}{2!}\exp.(-2h\nu/\underline{k}T) + \ldots$$
$$= [1 - \exp.(-h\nu/\underline{k}T)]^{-s}.$$

Thus,

$$N_j = \frac{N(j + s - 1)!}{j!\,(s-1)!}[1 - \exp.(-h\nu/\underline{k}T)]^s \exp.(-jh\nu/\underline{k}T).$$

Now the high pressure rate constant may be written

$$k^{\infty} = \frac{-1}{N}\frac{dN}{dt} = \frac{\sum_j k_j \bar{P}_j \exp.(-\epsilon_j/\underline{k}T)}{\sum_i \bar{P}_i \exp.(-\epsilon_i/\underline{k}T)},$$

where the ϵ are the energies of the particular states. In order to calculate the individual rates for each state, k_j is assumed proportional to the fraction of molecules with j quanta which, at equilibrium, would have at least m quanta in a selected degree of freedom. The proportionality constant is dependent on the nature of the molecule, but is independent of j. The chance that when s oscillators have j quanta, a selected one of them will have at least m quanta is:

$$\frac{j!\,(j-m+s-1)!}{(j-m)!\,(j+s-1)!}$$

whence $k_j = A \dfrac{j!\,(j-m+s-1)!}{(j-m)!\,(j+s-1)!}$, (4)

where A is the proportionality constant.

When the expressions for $\bar{P}_j$ and k_j are substituted into the expression for k^{∞} and the result expanded by the binomial theorem and simplified, it reduces to:

$$k^{\infty} = A \exp.(-m\, h\, \nu/\underline{k}T) \qquad (5)$$

In order to arrive at an expression for the reaction rate constant at low pressure, the concentration of activated molecules is determined from the balance of

deactivation and reaction. The rate of activation to molecules with j quanta is ZNN_j, where Z is the kinetic theory collision factor. If y_i is the actual concentration of activated molecules, their rate of destruction is ZNy_i if the "hard collision" approach is assumed, i.e. all collisions deactivate. The rate of reaction is $k_j \times y_j$, so that:

$$ZNN_j = ZNy_j + k_j y_j,$$

$$\text{and } y_j = \frac{N_j}{1+k_j/ZN} \qquad (6)$$

The general expression for the reaction rate constant at any pressure is:

$$k = \frac{1}{N} \sum_{j=m}^{\infty} k_j y_j$$

If k_j is assumed as in equation (4), the fall-off of k at low pressure may be expressed:

$$\frac{k}{k^{\infty}} = [1-\exp.(-h\nu/\underline{k}T)]^s \sum_{j=m}^{\infty} \frac{\frac{(j+s-1)!}{j!(s-1)!}\frac{j!(j-m+s-1)!}{(j-m)!(j+s-1)!}\exp.\left(\frac{-jh\nu+mh\nu}{\underline{k}T}\right)}{1+\frac{A}{ZN}\frac{j!(j-m+s-1)!}{(j-m)!(j+s-1)!}} \qquad (7)$$

Arriving at this expression necessitates the assumption from equation (6) that the activation process ZNN_j gives a distribution of energies identical to that at high pressure. In defending this assumption Kassel (8) has considered in detail an example where the average energy of the molecules is considerably less than the amount required for it to be

activated. Suppose the average energy for a molecule with s = 15 is 4 quanta and 27 quanta is the critical energy. Consideration of probabilities and resulting distributions leads to the conclusion that the most important activated molecule contains 31 quanta and that the most important collisions for their production involves 35 quanta in the two molecules which collide. Of these collisions only 3.3% involve activated molecules. The effect on the production, or the resulting distribution, of activated molecules by activated molecules is thus low; it is from molecules of much lower energy and collisions between them that activated molecules are produced. If it can be assumed, as seems reasonable, that at low pressures the energy distribution of non-activated molecules is unaffected, then the energy distribution of active molecules produced from them will be similarly unaffected.

Kassel (8) has pointed out that the assumptions which have been discussed are less valid at high temperature. The ratio of the critical energy to the average energy of the molecule is reduced with increasing temperature and the contribution of activated molecule collisions to the distribution of active molecules becomes more important.

Schlag (21) has considered further the circumstances under which Kassel's approximations become untenable.

Kassel (8) has shown how his quantum expression (7) reduces to the classical form (2) when j is large since for $j >> s$:

$$\frac{(j+s-1)!}{j!(s-1)!} = \frac{j^{s-1}}{(s-1)!} .$$

Schlag (21) has pointed out that the average energy of reacting molecules may lie only slightly above the critical and that this effect would be magnified at low pressures. He has compared calculations by both classical and quantum models for s = 15, and $\epsilon_o/\underline{k}T = 40$. The quantum model falloff prediction is shifted to higher pressure regions when compared to the classical prediction; the effect is magnified as $h\nu/RT$ is increased from 1.0 to 2.0 to 5.0.

Kassel (9) has shown how the quantum derivation can be extended to the case of a model having less than completely degenerate frequencies. The results of the simple quantum case are not altered. Schlag (21) has applied this to the case of cyclopropane with $\epsilon_o/\underline{k}T = 44$; comparing the case of complete degeneracy with s = 21, and $h\nu/RT = 2.0$ to that for three groups of seven frequencies with $h\nu/RT$ = 1.0, 2.0 and 4.0 for respective groups, he finds that the fall-off curve is shifted slightly into a higher pressure region in the three frequency case, although the effect is not greater than a factor of 1.5 to 2 in the specific rate constants.

Schlag (21) has shown that data for cyclopropane can be fitted for s = 21 by the quantum Kassel theory whereas s = 11 is found in the classical case. This fact emphasizes the discrepancy between the two approaches which may occur.

Wilson (33,37) has pointed out that the Kassel expression (1) for the individual rate of reaction for active molecules implies a random distribution of energy among the oscillators every $^{1}/_{A}$ seconds on the average. The randomness of this process makes any distribution of energy among the oscillators independent of the preceding distributions. The coupling between oscillators is described as strong for this reason. If the intramolecular processes are based on a Markov model where any distribution is dependent on the previous ones then the coupling between the oscillators may be termed weak. The effect of such assumptions has been shown (33) qualitatively to broaden the fall-off region; fall-off starts at a higher pressure but reaches second order behaviour in the same pressure region as with strong coupling.

(f) The Rice-Ramsperger Approach.

Rice and Ramsperger (6) arrive at an equation for the value of (k/k^{∞}) which is not fundamentally different from that of Kassel. The derivation is classical. The parameter which indicates the effective complexity of the molecule, s in Kassel's case, is s' in the Rice-Ramsperger case. In fact s'=2s comparing the two since the latter workers treat with the number of square terms, of which there are two per oscillator.

(g) The Marcus Approach

Marcus (16,17,18) has developed a theory of unimolecular reactions which may be simply described as an application of the random lifetime assumption implicit in the Rice-Ramsperger-Kassel approach to transition state theory. By making certain assumptions about the nature of the transition state of the reacting molecule, account is taken of rotations in the reaction process. The expressions derived give approximations to both quantum and anharmonic effects on the vibrations within the molecule.

The scheme describing the unimolecular reaction of a molecule B to form C is somewhat different from the earlier description:

$$B + M \underset{k_2}{\overset{k_1}{\rightleftharpoons}} B^* + M \qquad (1)$$

$$B^* \xrightarrow{k_a} B^+ \qquad (2)$$

$$B^+ \xrightarrow{k_3} C \qquad (3)$$

The various conditions of B are described as B^*, an active molecule with internal energy greater than some critical minimum, and B^+ an activated complex in the spirit of the transition state theory.

The description of the theory which will be given is close to that of Bunker (19). This author has revised the Marcus approach in the light of recent thinking that all the vibrational degrees of freedom are active in the sense that they contribute energy to the bond breaking process. "Critical surface" terminology is used in the description of the theory; this was first used by Slater (4, chs.9 and 10) and then later by Buff and Wilson (39) and others in recent more rigorous approaches to unimolecular rate theory.

The lifetime τ of an active molecule B^* is considered. In the classical phase space which describes an active molecule there is a hypersurface of constant total energy and angular momentum on which the molecule moves. In the absence of collisions the molecule eventually crosses some boundary of the hypersurface and has reacted. The lifetime τ is the time taken to

reach the boundary. The random lifetime assumption is made which means that τ has a random distribution and for a particular molecule, energy and configuration, the lifetime to dissociation is not precisely determinable. In terms of probability this may be appropriately expressed:

$$\bar{P}(\tau) = k_a \exp.(-k_a\tau) \tag{4}$$

where k_a is some constant .

Since collisions are random and if strong collisions are assumed, the probability that a molecule does not become de-energized in time τ where ω is the collision frequency, is:

$$\exp.(-\omega\tau). \tag{5}$$

Now the rate constant for attainment of energy E at phase points with lifetime τ is:

$$\omega\bar{P}(E)\bar{P}(\tau)d\tau dE, \tag{6}$$

where $\bar{P}(E)$ is the probability of energy E. All those molecules which do not suffer a subsequent collision will react. Combining equations (5) and (6) and substituting in equation (4), gives the expression:

$$k(E)dE = \omega\bar{P}(E) \int_o^\infty k_a \exp.(-k_a\tau) \exp.(-\omega\tau)d\tau dE$$

for the rate constant of dissociation at energy E. Integrate over τ and divide through by ω; thus:

$$k(E)dE = \frac{k_a\bar{P}(E)dE}{1 + k_a/\omega} \tag{7}$$

The identity of this k_a to that of equation (2) becomes apparent.

In order to estimate k_a consider the case where there is complete equilibrium; reaction (3) does not take place. The rate constant for the back reaction of equation (2) is assumed to be k_3 and for equilibrium:

$$\frac{d[B^+]}{dt} = \frac{d[B^*]}{dt} = 0.$$

Thus:

$$\frac{[B^+]}{[B^*]} = \frac{k_a}{k_3}$$

When reaction (3) is taking place the value of $[B^*]$ is assumed unaffected and:

$$\frac{[B^+]_r}{[B^*]} = \frac{2k_a}{k_3} .$$

This corresponds to a value of $[B^+]$ one half that at complete equilibrium; the approximation is identical to the approach of transition state theory to the situation where B^+ is not in equilibrium with C.

The ratio of the equilibrium concentrations of B^+ and B^* of the same energy equals the relative number of quantum states per unit of energy of B^+ and B^* in phase space respectively, which is written:

$$\frac{[B^+]_r}{[B^*]} = \frac{G(E^+)}{G(E^*)} = 2\,\frac{k_a}{k_3} .$$

Whence:

$$k_a = \frac{k_3\, G(E^+)}{2\, G(E^*)} . \qquad (8)$$

The quantity G in this expression is the density of quantum states per unit energy level. By definition:

$$E^+ = E^* - E_o,$$

where E_o is the activation energy.

$\bar{P}(E)$ can be related via quantum statistics to G(E); thus:

$$\bar{P}(E)dE = G(E^*)\ \exp.(-E^*/\underline{k}T)\ dE/\bar{Q}, \qquad (9)$$

where $\bar{Q}$ is the partition function of the reactant.

Consider the factor $k_3 G(E^+)$. A part E_t^+ of E^+ will be associated with a translational motion perpendicular to the critical boundary. There is a different k_3 for each E_t^+ and:

$$G(E^+) = \int_o^{E^+} G(E^+ - E_t^+)\ G(E_t^+)\, dE_t^+$$

$$\text{or } k_3\, G(E^+) = \int_o^{E^+} G(E^+ - E_t^+)\ G(E_t^+)\ k_3\, dE_t^+ \qquad (10)$$

k_3, the frequency of decomposition of B^+ may be expressed as in the transition state theory, as the ratio of velocity in the critical coordinate to a small length δ along it.

Thus:

$$k_3 = (2\ \underline{k}T/\pi m)^{\frac{1}{2}} / \delta.$$

In this case the mass m is replaced by μ, the reduced mass of the separating fragments. From the kinetic theory definition:

$$\text{velocity} = (2\ E/m)^{\frac{1}{2}}$$

and in the present case $\underline{kT}/\pi = E$ so that:

$$k_3 = (2E_t^+/\mu)^{\frac{1}{2}} / \delta . \qquad (11)$$

From the quantum mechanical expression for the energy levels of a particle in a 3-dimensional box, the analogous expression in the one dimensional case is:

$$E_t^+ = h^2\ n^2/8\ \mu\ \delta^2,$$

where n is the appropriate quantum number and h Planck's constant. Re-arranging:

$$n = (8\ E_t^+\ \mu\ \delta^2/h^2)^{\frac{1}{2}}.$$

Now:

$$G(E_t^+) = d\ n/d\ E_t^+$$

$$= \frac{\delta}{h}\ (2\ \mu/E_t^+)^{\frac{1}{2}}.$$

Substitution of this expression into equation (10) and the result in turn with equation (11) into equation (8) gives:

$$k_a = \frac{1}{h\ G(E^*)} \int_o^{E^+} G(E^+ - E_t^+)\ dE_t^+.$$

The integral is taken over the quantum state density of the internal motions of B^+, exclusive of the critical translational one. This form is suitable for use where the activated complex can be represented by a unique structural configuration. If however the postulated complex exists in Δ isomeric forms, k_a must be multiplied by Δ to account for the full degeneracy of the quantum states.

Thus:

$$k_a = \frac{\Delta}{hG(E^*)} \int_0^{E^+} G(E^+ - E_t^+)\, dE_t^+ \,. \qquad (12)$$

$G(E^*)$ must now be evaluated. This involves assumptions concerning the energy contribution of rotations to the breaking bond. The case of inactive rotations is first considered since the same expressions are used to evaluate the inactive part of $G(E^*)$ in the case where rotations are active. In common with the transition state theory the assumption is made that molecular vibrations and rotations are individually separable.

Inactive rotations affect only the phase volume available to B^+ and B^*. Their effect can be expressed approximately by multiplying k_a by the following partition function ratio:

$$\frac{\bar{Q}^+_{3-r}}{\bar{Q}^*_{3-r}} \simeq \frac{\bar{Q}^+_{3-r}}{\bar{Q}_{3-r}} = \frac{\prod^{3-r} (I_i^+)^{\frac{1}{2}}}{\prod^{3-r} (I_i)^{\frac{1}{2}}} \,, \qquad (13)$$

where there are r active rotational degrees of freedom, and I_i are the moments of inertia.

For $G(E^*)$ the semiclassical formula used by Marcus (16, p.896) in the case of no active rotations is:

$$G(E^*)_{r.i.} = \frac{(E^* + E^*_{zp})^{f-1}}{(f-1)!} \left(\prod_{i=1}^{f} h\, \nu_i^* \right)^{-1} \,, \qquad (14)$$

where the ν_i^* are the frequencies of the f vibrations of B^* and E^*_{zp} is their zero point energy:

$$\frac{1}{2}\sum_{i=1}^{f} h\nu_i^*$$

An analogous expression pertinent to k_a is:

$$G(E^+-E_t^+)_{r.i.} = \frac{(E^+-E_t^+)^{f-2}}{(f-2)!}\left(\prod_{i=1}^{f-1} h\nu_i^+\right)^{-1} \qquad (15)$$

If this is integrated over E_t^+ and a zero-point correction applied, the result is:

$$\int_o^{E^+} G(E^+-E_t^+)_{r.i.}\, dE_t^+ = \frac{(E^+-E_{zp}^+)^{f-1}}{(f-1)!}\left(\prod_{i=1}^{f-1} h\nu_i^+\right)^{-1}. \qquad (16)$$

If r of the B^* rotational degrees of freedom are active and can contribute energy to the breaking bond, the following form is used for $G(E^*)$:

$$G(E^*)_{r.a} = \int_o^{E^*} G(E^*-E_r^*)\, G(E_r^*)\, dE_r^*. \qquad (17)$$

The factor $G(E^*-E_r^*)$ is vibrational and is given by the expression $G(E^*)_{r.i.}$ for inactive rotations, i.e. equation (14).

$G(E_r^*)$ may be written:

$$G(E_r^*) = \left(\frac{E_r^*}{kT}\right)^{(r/2)-1} \frac{\bar{Q}_{r.a.}^*}{kT\,\Gamma(r/2)}, \qquad (18)$$

where $\bar{Q}_{r.a.}^*$ is the partition function of the active rotations given by:

$$\bar{Q}_{r.a.}^* = (\Pi^{\frac{1}{2}}/\sigma)\, gn \prod_{i=1}^{r} (8\pi^2 I_i\, kT/h^2)^{\frac{1}{2}} \qquad (19)$$

with σ the symmetry number and gn the degeneracy factor.

The correction factor of partition function ratios for inactive rotations is still applied to k_a, for those which are considered as such. In addition for the case of active rotations:

$$\int_o^{E^+} G(E^+-E_t^+)_{r.a.}\, dE_t^+ = \frac{\overline{Q}^+_{r.a.}}{\Gamma(1+r/2)} \int_o^{E^+} \left(\frac{E^+-E_t^+}{kT}\right)^{r/2} G'\, dE_t^+ , \tag{20}$$

where G' is given by the expression (15) for $G(E^+-E_t^+)_{r.i.}$, and Γ is the gamma function.

The product $k_a \overline{P}(E)$ of equation (7) may now be expressed from equations (9), (12) and (13) as:

$$k_a\overline{P}(E) = \frac{\Delta}{h\bar{Q}} \frac{\overline{Q}^+_{3-r}}{\overline{Q}^*_{3-r}} \int_{E_o}^{\infty}\left[\int_o^{E^+} G(E^+-E_t^+)\, dE_t^+\right] \exp(-E^*/kT)\, dE^* \tag{21}$$

At high pressures the term k_a/ω in equation (7) can be neglected and the result is:

$$k^{\infty} = \int_{E_o}^{\infty} k_a\, \overline{P}(E)\, dE. \tag{22}$$

The integral may be evaluated from equation (21) by substituting the appropriate expressions for active or inactive rotations as the case may be.

At any pressure the general expression for the rate constant from equation (7) is:

$$k = \int_{E_o}^{\infty} \frac{k_a\, \overline{P}(E)\, dE}{1+ k_a/\omega} \tag{23}$$

The expression for k_a from equations (12) and (13) is:

$$k_a = \frac{\Delta}{hG(E^*)} \frac{\overline{Q}^+_{3-r}}{\overline{Q}^*_{3-r}} \int_o^{E^+} G(E^+ - E_t^+)\, dE_t^+. \qquad (24)$$

The integral (23) can now be evaluated from equations (24) and (21), again substituting the appropriate expressions depending on the role of the rotations.

Marcus (17) has described the application of these equations to various types of molecule.

1.1.2. Slater Theory

(a) The Critical Configuration Approach

Polanyi and Wigner (10) noted that the value of the A factor in the Arrhenius equation was about 10^{13}-10^{14} sec^{-1} for many reactions. This is a vibration frequency in order of magnitude. They were able to relate the high pressure rate constant and especially the A factor in the expression for this constant, to the normal vibrational modes of the molecule. The internal motion of the molecule was described in terms of the normal modes. Reaction was assumed to occur when the motions characterized by these normal modes caused a critical stretch in some particular bond.

(b) The Slater Approach

The theory of Slater (4) is an application of the approach initiated by Polanyi and Wigner to the Lindemann

idea of the reacting molecule. He proposes a model molecule of simple harmonic oscillators which does not change its internal energy distribution between collisions; this happens only on collision. Reaction can occur when some critical coordinate is stretched beyond a minimum value. The possibility of this occurring will depend upon the amount of energy possessed by the molecule and will take a finite amount of time to come about even when the requisite energy is present.

Slater uses normal coordinates in building up his theory. In terms of the normal coordinates $Q_1, Q_2, \ldots Q_n$, the kinetic and potential energies may be expressed:

$$T' = \sum_1^n a_i \dot{Q}_i^2$$

$$V = \sum_1^n \ell_i Q_i^2$$

where a_i and ℓ_i are arbitrary constants, and a_i/ℓ_i determinate. These equations may be expressed:

$$T' = \sum_1^n \dot{Q}_i^2 / \lambda_i$$

$$V = \sum_1^n Q_i^2 .$$

This then represents a linear harmonic oscillator of frequency ν_i, where:

$$\lambda_i = 4\pi^2 \nu_i^2 .$$

The solution of the motion is:

$$Q_i = A_i \cos 2\pi(\nu_i t + \psi_i)$$

$$(0 \leq \psi_i < 1) ,$$

where A_i is the amplitude and ψ_i the phase constant. There are therefore n normal modes, one for each coordinate Q_i.

If the energy in the i^{th} mode is $\epsilon_i = T_i' + V_i$, then substituting the above expression for Q_i into the relation: $\epsilon_i = \dot{Q}_i^2 / \lambda_i + Q_i^2$, gives:

$$A_i^2 = \epsilon_i .$$

Thus:

$$Q_i = (\epsilon_i)^{\frac{1}{2}} \cos 2\pi(\nu_i t + \psi_i).$$

It will be useful to evaluate the total energy in the modes (ϵ') which is:

$$\epsilon' = \sum_1^n \epsilon_i .$$

The transformation from normal coordinates to the more usual displacement coordinates $q_1, q_2, \ldots q_n$ is:

$$q_r = \sum_1^n \alpha_{ri} Q_i, \quad (r = 1, \ldots n),$$

where the α_{ri} are called amplitude factors, and are characteristic of the particular coordinate under consideration. The solution of the motion in terms of these coordinates is:

$$q_r = \sum_1^n \alpha_{ri} (\epsilon_i)^{\frac{1}{2}} \cos 2\pi(\nu_i t + \psi_i).$$

This can be regarded as the superposition of n oscillators; in any one normal mode the coordinates $q_1, \ldots q_n$ have the same frequency ν_i, and the same ψ_i; the amplitudes are proportional to $|a_{1i}|, \ldots, |a_{ni}|$.

To summarize so far, the configuration of the molecule can at any time be expressed in terms of n independent internal coordinates q or their corresponding normal coordinates Q. The coordinates vary in such a fashion that the atomic motions may be described in terms of simple harmonic motion; the vibrations are characterized by normal mode frequencies $\nu_1, \nu_2, \ldots \nu_n$, which are mutually independent. The amplitudes and phases of the normal coordinates remain unchanged between collisions unless reaction occurs.

Attention is focussed on a particular coordinate q_1. The molecule reacts when q_1 reaches a critical value q_o. A molecule is capable of reacting if q_1 can reach q_o; so that

$$\Sigma \left|a_{1i}\right| (\epsilon_i)^{\frac{1}{2}} \geq q_o, \qquad (1)$$

is a condition which must be satisfied for reaction.

A certain minimum total amount of energy, ϵ'_o, will be required before reaching the critical configuration is possible. If $\epsilon_{10}, \epsilon_{20} \ldots, \epsilon_{n0}$ are the values of ϵ_i for which ϵ' is a minimum such that:

$$\Sigma |a_{1i}| \ (\epsilon_i)^{\frac{1}{2}} = q_o,$$

then:

$$\epsilon_{io} = q_o \, \alpha_{1i}^2 \, / \, \alpha^4 \, ,$$

where:

$$\alpha^2 = \sum_1^n \alpha_{1i}^2 . \quad \text{See (4, p.88).}$$

Whence, the minimum total energy $\Sigma \epsilon_{io}$ for dissociation is:

$$\epsilon_o' = q_o^2 \, / \, \alpha^2 \qquad (2)$$

The general expression for the rate constant of unimolecular reactions may be written from equation (3) of section 1.1.1(b):

$$k(E) \, dE = \frac{P k_3(E) \, k_1(E) \, dE}{k_2 \, P + k_3(E)} \, .$$

If it is assumed that a distribution function can be found which expresses the proportion of molecules in an active state and the energy they possess, this would be of the form:

$$f(E) = \frac{k_1(E)}{k_2(E)} \, .$$

Assuming that all collisions deactivate, we can write for the rate of the collision process:

$$k_2 P = \omega$$

where ω is the collision frequency.

The general rate expression then becomes:

$$k(E) \, dE = \omega \, \frac{k_3(E) \, f(E) \, dE}{\omega + k_3(E)} \, .$$

In Slater theory, $k_3(E)$ is replaced by the function L, the frequency with which the critical coordinate q_1 reaches the value q_o. Thus, on the single molecule basis used by Slater:

$$k(\epsilon)\, d\epsilon = \omega L f(\epsilon) d\epsilon/(\omega+L) \tag{3}$$

which at high pressures becomes:

$$k(\epsilon)\, d\epsilon = L f(\epsilon)\, d\epsilon \tag{4}$$

From statistical mechanics it can be shown that for an assembly of simple harmonic oscillators, the proportion having energy ϵ to $\epsilon + d\epsilon$ is:

$$\exp.(-\epsilon/\underline{k}T)\, d\epsilon/\underline{k}T. \tag{5}$$

If the molecules are each equivalent to a set of n simple oscillators with energies $\epsilon_1, \epsilon_2, \ldots \epsilon_n$, the proportion having simultaneously energies ϵ_1 to $\epsilon_1+d\epsilon_1, \ldots, \epsilon_n$ to $\epsilon_n+d\epsilon_n$ is their respective oscillators is a product of expressions of the form equation (5), and so is:

$$\exp.(-\epsilon'/\underline{k}T)\, d\epsilon_1 \ldots d\epsilon_n/(\underline{k}T)^n.$$

This is the Maxwell--Boltzmann distribution which is a good estimate of $f(\epsilon)$ at high pressures. Thus equation (4) becomes:

$$k^{\infty} = \int k(\epsilon) d\epsilon = \int \ldots \int_o^{\infty} \frac{L \exp.(-\epsilon'/\underline{k}T)\, d\epsilon_1 \ldots d\epsilon_n}{(\underline{k}T)^n} \tag{6}$$

Slater has derived a formula for L, based on the simple harmonic model of the molecule. Upon substituting this into the equation (6) and carrying out the integration,

the expression for the high pressure rate constant becomes:

$$k^{\infty} = \nu \exp.(-q_o^2/a^2 \underline{k}T),$$

or from equation (2):

$$k^{\infty} = \nu \exp.(-\epsilon_o'/\underline{k}T). \qquad (7)$$

ν may be expressed:

$$\nu = \sum_1^n (a_{1i}^2 \nu_i^2 / \sum_i^n a_{1i}^2)^{\frac{1}{2}},$$

and is defined as the root mean square of the normal frequencies $\nu_1, \nu_2 \ldots \nu_i \ldots \nu_n$, weighted with the amplitude factors $a_{11}, a_{12}, \ldots a_{1n}$ of the respective normal modes as they effect q_1, the coordinate of interest. The evaluation of L depends on a number of approximations including that from the model of the vibrating molecule where the amplitudes $a_{ri}(\epsilon_i)^{\frac{1}{2}}$ and the frequencies ν_i describing the motion are all nearly equal.

The general expression for the rate constant k in equation (3) is solved by assuming the same distribution function $f(\epsilon)$ as at high pressure. A more approximate form of L must be used. The final expression obtained by Slater is:

$$k = \nu \exp. (-\epsilon_Q'/\underline{k}T) \; I_{\frac{1}{2}(n-1)} (\theta),$$

and $\frac{k}{k^{\infty}} = I_{\frac{1}{2}(n-1)} (\theta)$.

Values of the integral:

$$I_m(\theta) = \frac{1}{m!} \int_o^{\infty} \frac{x^m \exp. (-x) \, dx}{1+x^m \theta^{-1}},$$

have been tabulated by Slater (4, p.169), for various m and θ. The following relations explain the symbols used:

$$m = \tfrac{1}{2}(n-1)$$

$$\theta = \frac{w}{\nu} Y_n \, b^m$$

$$b = \epsilon_o'/\underline{k}T$$

$$Y_n = \Gamma\left(\frac{n}{2} + \frac{1}{2}\right) (4\pi)^{\frac{1}{2}(n-1)} \, \mu_1 \cdots \mu_n$$

$$\mu_i = \frac{\alpha_i}{\alpha}$$

$$\Sigma \mu_i^{\,2} = 1.$$

At high pressures, ω and θ tend to infinity and $I_m(\theta)$ approaches 1.

In practice the experimental high pressure activation energy per molecule is used for ϵ_o' in order to evaluate fall-off behaviour; a complete vibrational analysis of the molecules is of course required.

(c) Developments and Comparisons of the Approaches.

The similarity of the expressions for falloff of k in the Kassel and Slater theories has been demonstrated by the latter (4). Schlag and co-workers (11), have shown that for a normal value of b = 40, n = (s+1)/2 up to n approximately 4, falloff predictions by both theories are similar. Above this n increases more rapidly for the same falloff behaviour and at n about 18, n = s.

Gill and Laidler (12), have compared the application of both approaches to data for several materials. They have done this by comparing the rate of energization or the limiting low pressure bimolecular rate observed to that predicted by the theories.

In section 1.1.1(b) it was shown that the Lindemann-Hinshelwood mechanism results in the expression:

$$\frac{1}{k} = \frac{k_2}{k_3 k_1} + \frac{1}{k_1 P} \qquad (1)$$

If a straight line relationship is assumed between 1/k and 1/P, then the rate of energization, k_1, may be determined from the slope of such a plot.

Hinshelwood (5) has derived an expression from classical mechanics which gives the chance that a molecule possesses energy greater than E_o distributed at random among s vibrational degrees of freedom as:

$$\frac{k_1}{k_2} = \frac{\exp.(-E_o/RT)(E_o/RT)^{s-1}}{(s-1)!}$$

The k_1 and k_2 are respectively the rate constants for activation and deactivation in his scheme of unimolecular reactions. If the strong collision assumption is made then k_2 is ω, the collision frequency and:

$$k_1 = \frac{\omega \exp.(-E_o/RT)(E_o/RT)^{s-1}}{(s-1)!} \qquad (2)$$

At low pressures unimolecular reactions have been shown to become bimolecular due to the eventual complete dependence of reaction on activation. Slater (4, p.141) has indicated how at low pressure the difference between Hinshelwood and Kassel theory disappears so that the expression (2) also applies to the latter approach in this region, for predicting the rate of activation or the rate bimolecular reaction.

Slater (4) has shown that the limiting second order constant k^o in his case can be given by:

$$k^o = Z\Lambda,$$

where Z is the collision factor. Λ is the equilibrium proportion of interesting molecules evaluated from:

$$\Lambda = \int_{L>0} \exp.(-\epsilon'/\underline{k}T)d\epsilon_1 \ldots d\epsilon_n/(\underline{k}T)^n.$$

By assuming the amplitude factors μ_i to be roughly similar in magnitude, the following approximation to Λ results:

$$\Lambda = (4\pi b)^{(n-1)/2} \chi_n(b) \exp.(-b)\ \mu_1\mu_2 \ldots \mu_n,$$

where:

$$b = \epsilon_o'/\underline{k}T$$

$$\chi_n = 1 - \frac{(\underline{n-1})(\underline{n-2})}{4b} + (n-1) \ldots$$

$$+ \frac{(\underline{n-4})}{2!(4b)^2} - \ldots$$

Gill and Laidler (12) have approximated the result by letting $\chi_n = 1$, so that:

$$k^{o} = Z\left(\frac{4\epsilon_{o}'\pi}{kT}\right)^{(n-1)/2} \prod_{1}^{n} \mu_{i} \qquad (3)$$

The experimental results determined by equation (1) or the observed bimolecular rate are thus compared to the predictions of equations (2) and (3). These authors point out that Slater theory works for molecules where the flow of energy between modes is likely to be low. For simple molecules like N_2O, H_2O_2 and C_2H_6 there is a small number of modes. Hence a greater amount of energy must be concentrated in each mode and anharmonicity effects will be greater. Thus the Kassel approach as expected works better since it is based on the assumption of energy flow between modes. For more complicated molecules like N_2O_5, C_2H_5Cl and cyclopropane, the energy per mode is less; the behaviour is more strictly harmonic, there is little coupling between the oscillators and flow of energy. Slater theory is applicable in this case. The Kassel approach can be used for these more complex molecules only if a value of s less than the actual number of vibrational degrees of freedom is assumed. These authors have further pointed out that at lower pressures in the fall-off region anharmonicity effects may become apparent in the more complicated molecules since now the average life of active molecules is longer and redistribution of energy has a greater chance of occurring. Thus at very low pressures Slater theory may give a poor description.

Slater (22) has pointed out that implicit in the definition of $k(\epsilon)$ is the assumption that the lifetime to dissociation of an active molecule is a random event like collisions. If τ represents the time gap between arrivals at the critical configuration for a molecule of particular energy, then the distribution function h' of τ for a given energy is of the form:

$$h'(\tau) = L \exp.(-L\tau), \text{ for random life times}$$

which gives rise to a value for the specific rate:

$$k(\epsilon) = \frac{\omega L}{\omega + L} f(\epsilon)$$

In what is referred to as Slater's "new approach" (22; 4, ch.9), $\frac{\omega L}{\omega+L}$ is replaced by $\phi(w)$ which is of the form:

$$\phi(w) = \int \omega \exp.(-\omega t') \, d\psi \ \ldots \ ,$$

where t' is the time of internal motion from a particular energy and configuration to dissociation and is a function of the internal coordinates and momenta of the molecule. Such an assumption might give rise to a distribution function h' of the form:

$$h'(\tau) = \tau^{a} \exp.(-b\tau)$$

where a and b are constants. The "random gap" is no longer implied and the lifetimes to dissociation of activated states are more precisely defined.

Thiele (23) has shown how the random gap assumption is implicit in the approaches of Kassel (8) and Giddings and Eyring (20) (transition state) and compared these to the original formulation of Slater (4). Wilson and Thiele (30,31) have used the "new approach" to evolve a quantum theory for the unimolecular rate constant and point out the classical character of assuming precisely defined times for collision and reaction processes. They base their studies on a wave packet analysis. A more precise definition of the character of these wave packets will be required before the theory can be applied to experimentally observed reaction systems.

Slater (4, ch.10) has evolved a quantum version of his original theory i.e. assumption of random gaps. He combines a quantized distribution of normal mode energies with the classical dissociation probability L. This approach results in the same form for k/k^{∞} and hence the same shape of the fall-off curve. In the quantum case however a given value of k/k^{∞} will be observed at a lower pressure compared to the classical.

Bunker (19, ch.3) has reviewed the results of trajectory studies on simple molecules. The models are set up and the effects of the internal vibrations and rotations for molecules of various energies and starting configurations can be examined. One result of these

studies is information concerning the lifetime distribution of active molecules. In these small molecules it is found that non-randomness is associated with large differences between atomic masses or molecular vibration frequencies. For the more complex molecules which are usually the subject of fall-off studies in unimolecular reactions, these effects are likely to be small. This evidence tends to support the random lifetime assumption which is retained in the Marcus approach.

Wilson (33) has shown that the non-random gap assumption leads to the conclusion that a plot of k vs. pressure should go through a maximum and then diminish. Flowers and Frey (36) have shown experimentally that for the unimolecular isomerization of 1,1-dimethylcyclopropane such a phenomenon is not observed; they studied the reaction from the region of 10 mm where falloff begins to 1596 mm and found no significant variation in k^{∞}.

Buff and Wilson (38) have formulated recenty suggested refinements of unimolecular reaction theory in more elegant mathematical terms. They have concluded from their studies that anharmonicity effects and the assumption of inefficient transfer of energy on collision, both lead to broadened pressure transition range of k from its high to low pressure limit.

1.1.3. Multiple Critical Oscillators

Gowenlock (24) has described an unusually high A factor in an unimolecular reaction as one which is $10^{14.5}$ or greater. This represents an entropy of activation greater than +7 e.u. and a transition state that is looser than the initial state; this allows for example, more rotational freedom than is permissible in the ordinary molecule.

High A factors seem to be characteristic of the isomerization and decomposition of C_3 and C_4 ring compounds, as shown in Table (1.1). In the decomposition of cyclopropane it is plausible to suggest that there is greater freedom of torsional movement in one C-C bond in the activated state.

High A factors have also been explained, for example in mercury dialkyl and azoethane decompositions (24), by the mechanism of multiple fragment decomposition where the activation energy is "spread out" into more than one bond. The behaviour of some C_3 and C_4 ring compounds may also be treated as acting in this way, especially where there is a decomposition involved.

Pritchard (25) has developed a classical expression for the high pressure rate constant of molecules which decompose by concentrating a critical amount of energy in more than one oscillator. He has based his treatment

Table 1.1

High Pressure Arrhenius Equation Constants for the Isomerization and Decomposition of Cyclopropanes and Cyclobutanes.

Reaction	Temperature range studied (°C)	A (sec^{-1})	E (k.cal/mole)	Ref.
$CH_2.CH_2.CH_2 \rightarrow CH_3.CH=CH_2$	420 - 435	1.98×10^{15}	65.08	(140)
$CH_3.CH.CH_2.CH_2 \rightarrow$ butenes	440 - 490	2.8×10^{15}	65.0	(141)
$CH_3.CH_2.CH.CH_2.CH_2 \rightarrow$ pentenes	454 - 484	2.5×10^{14}	61.6	(142)
$CH_2.CH_2.CH_2.CH_2 \rightarrow 2C_2H_4$	420 - 468	4.0×10^{15}	62.5	(137)
$CH_3.CH_2.CH.CH_2.CH_2.CH_2 \rightarrow C_2H_4 + CH_3.CH_2.CH=CH_2$	420 - 460	3.6×10^{15}	62.0	(145)
$CH_2.CF_2.CF_2.CF_2 \rightarrow 2C_2F_4$	520 - 590	8.9×10^{15}	74.1	(143)
$Cl.CF.CF_2.CF_2.CF.Cl \rightarrow 2C_2F_3Cl$	425 - 502	2.5×10^{15}	65.3	(26)
$CF_3.CF.CF_2.CF_2.CF.CF_3 \rightarrow 2CF_3.CF=CF_2$	410 - 500	$1.2 - 4.3\times10^{15}$	64.2	(138)

on the approach of Hinshelwood, and uses the expression:

$$k = \lambda \exp.(-\epsilon_o/\underline{k}T) \sum_{r=o}^{s-1} \frac{1}{r!} (\epsilon_o/\underline{k}T)^r, \qquad (1)$$

where r is the total number of vibrations and s the number contributing to the reaction coordinate. λ has the dimensions of a frequency and for calculation purposes is taken as the characteristic frequency of the breaking bonds. Likewise ϵ_o is calculated as the sum of the bond dissociation energies. Thus for the case of the mercury dialkyls (R_2Hg) to which this approach was applied it was assumed that:

$$\epsilon_o = D(RM-R) + D(R-M).$$

To get agreement within an order of magnitude of the experimental k's, it was necessary to assume that s increases as the size of R. The possibility of s as great as 4 is explained by the several ways of breaking the two Hg-R bonds simultaneously. The idea for this approach was suggested in fact when it was observed that the activation energy for the dissociation of di-isopropyl mercury was very close to the sum of the bond dissociation energies for two isopropyl groups from mercury.

Steel (27) has based his approach to multiple critical oscillators on the assumptions of Kassel theory. He starts with an expression for the specific rate of a molecule with

energy ϵ, of the form:

$$k(\epsilon) = \lambda H_{s,z}(\epsilon, \epsilon_o),$$

where $H_{s,z}(\epsilon, \epsilon_o)$ is the probability that the total energy is in the range ϵ to $\epsilon+d\epsilon$, s refers to the total number of oscillators and z to the number of oscillators into which the critical energy ϵ_o must be concentrated. λ is the rate of interchange of energy within the molecule and is equated to a normal vibration frequency. The resulting integrated expression for the high pressure rate constant is:

$$k^{\infty} = \frac{\lambda(\epsilon_o/\underline{k}T)^{s-1}}{(z-1)!} \exp.(-\epsilon_o/\underline{k}T) \left[1 + \frac{z-1}{\epsilon_o/\underline{k}T} + \ldots \frac{(z-1)!}{(\epsilon_o/\underline{k}T)^{z-1}}\right]$$

It is obvious that this expression gives an increased A factor over the value of λ which is a vibration frequency when z is greater than 1. Steel (27) has indicated how the general rate constant k may be expressed in an analogous fashion but has not attempted to integrate the result. This approach is not of practical utility as far as correcting Kassel theory for the case of multiple critical oscillators is concerned. No attempt in this theory is made to actually calculate the A factor.

Steel (27) has shown that the phase relationship of the critical oscillators is also important. Not only must

the z oscillators possess the requisite energy but they must be undergoing extension at the same time. For z = 2, as a first approximation, the probability of their being in phase is $^1/_4$; for z = 3, it is $^1/_8$. Thus the calculated A's by whatever method must be multiplied by this factor.

Schlag (21) has applied multiple critical oscillator considerations to the quantum version of Kassel theory. He has considered the specific case of two critical oscillators and integrated the resulting equation for a case where s = 32 (number of oscillators), $h\nu/RT = 2.0$ ($h\nu$ being the energy in the critical oscillators, and ν a representative vibration frequency), and b = 40 (where $b = \epsilon_o/\underline{k}T$). The results show that compared to the treatment for a single critical oscillator the fall-off is shifted to a higher pressure region (i.e. fall-off occurs in a higher pressure region in the 2 critical oscillator case). The change in curvature is not greater than that which would be caused by an s change of one or two.

Thiele and Wilson (28) have considered the case of multiple critical oscillators from the Slater approach. They have attempted to explain the high pre-exponential factor for the decomposition of cyclobutane ($A = 4\times10^{15} sec^{-1}$) from the effect of two critical oscillators; Slater theory

predicts A between the highest and lowest vibrational frequency of the molecule, which would be impossible in this case. Using Slater terminology, they look for the critical distortion q_1^o of coordinate q_1 when another coordinate q_2 exceeds a value q_2^o. N^* is the number of times the critical configuration occurs during $0 \leq t \leq T''$. After converting N^* to an integral over t in the interval $0 \leq t \leq T''$, the frequency L^* is defined:

$$L^* = \int_0^1 \cdots \int_0^1 \frac{N^*}{T''} \, d\psi_1 \cdots d\psi_n,$$

by averaging N^*/T'' over a uniform distribution of phase angles ψ. An analogous expression for the high pressure rate constant to that of Slater (see sect.1.1.2) is then:

$$k_\infty^* = \int_0^\infty \cdots \int_0^\infty L^* \prod_{i=1}^{n} \frac{\exp.(-\epsilon_1/kT)}{kT} \, d\epsilon_i.$$

For the special case of equivalent simultaneous reaction coordinates:

$$q_1^o = q_2^o,$$

$$\bar{\nu}_1 = \bar{\nu}_2,$$

and

$$\alpha_1^2 = \alpha_2^2 = \sum_{i=1}^{n} \alpha_{1i}^2$$

Thus:

$$k_\infty^* = \left(\frac{kT}{\pi}\right)^{\frac{1}{2}} \frac{\bar{\nu}_1}{b_1} \exp.(-\epsilon_o/kT),$$

where: $$b_1^2 = \frac{\epsilon_o}{2}\left(1 - \frac{\alpha_{12}}{\alpha_1^2}\right),$$

and $$\alpha_{12} = \sum_{i=1}^{n} \alpha_{1i}\ \alpha_{2i}$$

By assuming approximate values of $\epsilon_o/\underline{k}T = 40$, and $b_1^2 = E_o/3$, they found the pre-exponential factor to have a value of $\bar{\nu}_1/6.5$ which could not explain the high value for cyclobutane.

Slater (29) has applied the last treatment to transition state theory and shown how an appropriate transmission coefficient can be calculated. His form results in a reduced k and A relative to the one critical oscillator version.

The more precise findings of Schlag (21), Thiele and Wilson (28), and Slater (29) seem to disagree with the general results of Pritchard (25) and Steele (27). The multiple critical oscillator approach gives reduced A factors in the case of cyclic compound decompositions.

1.2. The Thermal Reactions of Cyclopropanes

Elliott and Frey (40) have classified the thermal unimolecular isomerizations of cyclopropane and cyclopropane derivatives into five types:

(1) cyclopropane and alkylcyclopropanes, isomerize to give olefins,

e.g. $CH_3 \cdot \overline{CH \cdot CH_2 \cdot CH_2} \rightarrow CH_3CH = CH \cdot CH_3$.

(2) appropriately substituted dialkyl-cyclopropanes and also deuterocyclopropanes, undergo geometrical isomerization,

e.g.

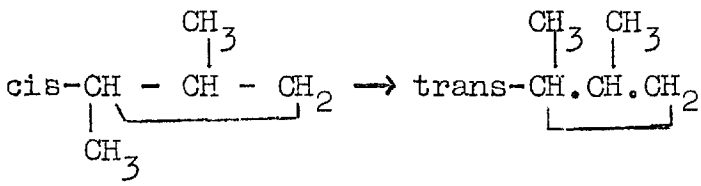

(3) Vinylcyclopropane and some substituted vinylcyclopropanes undergo a ring expansion to yield cyclopentenes,

e.g. $CH_2=CH-CH-CH_2-CH_2 \longrightarrow CH=CH-CH_2.CH_2.CH_2.$

(4) substituted methylene cyclopropanes undergo a ring shift,

e.g. ethylidene cyclopropane ⟶

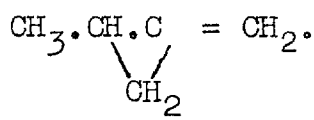

(5) substituted vinylcyclopropanes of the correct stereochemical configuration undergo a ring rupture simultaneous to H shift,

e.g. cis-$CH_3.CH-CH-CH = CH_2 \longrightarrow$ cis-$H_2C=CH-CH_2.CH=CH.CH_3$

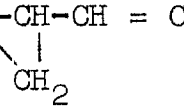

Typical of the type 1 reaction are a series of fluorinated hydrocarbon cyclopropanes which have been studied. Several fluorine substituted C_3 cyclopropanes have been studied (41,42) and also two CF_3 substituted

cyclopropanes (43). They all isomerize by a H shift to give a mixture of olefins. In table (1.2) the overall reaction high pressure constants in the Arrhenius equation are shown.

Recent work on fully fluorinated cyclopropanes has indicated that the reaction exemplified by perfluoro-cyclopropane:

$$\overline{CF_2\text{-}CF_2\text{-}CF_2} \longrightarrow CF_2 = CF_2 + :CF_2$$

is typical of fully fluorinated rings where an easier route is not possible. Almost simultaneous with the publication of initial data on the above reaction (44), Mitsch and Neuvar (45) published information concerning perfluoroallyl-cyclopropane which behaves in a similar fashion, i.e. decomposition by elimination of difluoromethylene. These reactions are found to be homogeneous and unimolecular; it thus seems justifiable to classify them as an additional type in the scheme of Elliott and Frey (40), although they are not strictly isomerizations. The more recent observation of Haszeldine and co-workers (146) that CF_2 is eliminated from fully halogenated chlorofluorocyclopropanes containing CF_2 (see sect.1.4.3) may lead to an even wider series of reactions of the same type.

Table 1.2

High Pressure Arrhenius Equation Constants for Reactions of Fluorinated Cyclopropanes

Compound	Temperature range studied(^{o}C)	A (sec^{-1})	E (k.cal)	Ref.
$FCH-CH_2-CH_2$	412 - 503	3.8×10^{14}	61.01	(41)
$CF_2-CH_2-CH_2$	401 - 495	1.1×10^{14}	56.35	(42)
$FCH-CF_2-CH_2$	317 - 369	2.7×10^{14}	50.52	(42)
$CF_2-CF_2-CH_2$	252 - 323	1.86×10^{15}	48.48	(42)
$CF_3.CH.CH_2.CH_2$	445 - 524	4.11×10^{14}	65.6	(43)
$CF_3.CH_2.CH.CH_2.CH_2$	406 - 542	2.4×10^{14}	63.6	(43)
$CF_2-CF_2-CF_2$	230 - 289	8.41×10^{14}	42.55	(this work)
$CF_2.CF = CF_2$ $CF-CF_2.CF_2$	196 - 250	6.3×10^{14}	42.7	(45)

1.3. The Chemistry of Perfluorocyclopropane

Perfluorocyclopropane (abbreviated c-C_3F_6) was first reported to be among the pyrolysis products of tetrafluoroethylene (C_2F_4) by Benning and Co. (50). This was later shown by Young and Murray (51) to be the isomeric perfluoropropene ($CF_3.CF = CF_2$). c-C_3F_6 was also reported by Harmon. (52) among the products formed by passing C_2F_4 over a platinum filiment heated to 1340°C, in another patent (53), and by Lewis and Naylor (144) to be among the products formed by the depolymerization of polytetrafluoroethylene. Again these observations were undoubtedly of $CF_3.CF = CF_2$.

The separate existence of a cyclic C_3F_6 compound was first clearly established by Atkinson (54), who found that c-C_3F_6 was formed as a byproduct in the Hg photo-sensitized reaction of C_2F_4. Atkinson (55) reported that the quantum efficiency of the formation of c-C_3F_6 increased with pressure of C_2F_4 over the range 1-35 cm. of Hg abs. He found the following properties:

b.p. - 33°C

m.p. - 80°C

vap.press.: $\log P_{(mm)} = 7.746 - \frac{1168}{T}$

$(T > -80°C)$

Several workers have reported c-C_3F_6 as a minor by-product in the pyrolysis of various fluorine containing halocarbons. Haszeldine (56) reacted C_2F_5I in the presence of C_2F_4 to give polymer and about 3% yield of c-C_3F_6. Serpinet (57) detected c-C_3F_6 in the pyrolysis products of $CF_2.Cl.H$. Small amounts of c-C_3F_6 are also found in the pyrolysis products of $C.ClF_3$ or polytetrafluoroethylene (58,59).

The original studies of Atkinson on the Hg photosensitized reaction of C_2F_4 have been extended by more recent work. Heicklen and co-workers (60,61,62,64,70,71) have confirmed that the formation of c-C_3F_6 in this reaction is unaffected by the presence of O_2 or N_2, and that the rate increases with pressure of C_2F_4 and temperature. Gozzo and Carnaggi (72) have also observed c-C_3F_6 in the photochemical oxidation of C_2F_4. Miller and Dacey (65) have reported trace amounts of c-C_3F_6 in theXe photosensitized reaction of octaflurocyclobutane. Andreades (66) exposed C_2F_4 and NOF to u.v. radiation and obtained about 6% yield of c-C_3F_6.

Various reactions involving stronger sources of radiation have been found to yield c-C_3F_6. Kevan and Hamlet (67) reported small amounts of c-C_3F_6 after exposing perfluoroethane (C_2F_6) to gamma rays. Cordischi et al.(68) found c-C_3F_6 in the gamma and x-ray induced oxidation of

C_2F_4. Ionizing radiation was also used by Site (69) in similar oxidation studies.

A number of compounds containing atoms other than carbon, hydrogen and halogen, have been synthesized, which under mild heating or u.v. radiation, generate difluoromethylene; under the right conditions substantial yields of c-C_3F_6 can be obtained. King (73) showed that the pyrolysis of perfluoromethyl iron-tetracarbonyl iodide at 100°C in the presence of C_2F_4 or ethylene produced the corresponding cyclopropane from the CF_2 produced. Mahler (74) synthesized tris-(trifluoromethyl) difluorophosphorine, which gave 80% c-C_3F_6 when heated at 120° for 24 hours. Other trifluoromethylphosphoranes ($(CF_3)_2PF_3$ and CF_3PF_4) behave in a similar fashion. Clark and Willis (75) obtained good yields of c-C_3F_6 when they pyrolized trimethyltrifluoromethyl tin at 150°C, either by itself or in the presence of C_2F_4. The same workers (76) obtained similar results when trifluoromethyltriiodo germane was pyrolyzed at 180°C. Ayscough and Emeleus (77) found c-C_3F_6 and C_2F_4 when they heated tris-(trifluoromethyl) arsine ($(CF_3)_3Sb$). More recently Mitsch (78,79) has synthesized difluorodiazirine 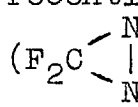 which decomposes to give N_2 and CF_2, the latter

of which adds to C_2F_4 to give c-C_3F_6 or to other olefins to give the corresponding cyclopropane. Difluorodiazirine is inconvenient to use due to its explosive nature.

The infrared spectrum of c-C_3F_6 was first studied by Haszeldine (80) in conjunction with Atkinson's early work in distinguishing the two C_3F_6 isomers. The compound identified by Atkinson as c-C_3F_6 was found to have a distinctively different infra-red from $CF_3.CF=CF_2$. Heicklen (63,81) has published infra-red absorption data for c-C_3F_6 along with partial assignments. Ito (82) has used both infra-red and Raman data to give a more complete vibrational analysis of c-C_3F_6. The information from this source is summarized in table 1.3.

Table 1.3

Fundamental Vibrations of Perfluorocyclopropane

Species	Vibration No.	Approx. mode of vibration	Spectral activites (D_{3h}) Raman	Infra-red	Freq. (cm^{-1})
A_1'	ν_1	ring deform.	a(P)	ia	
	ν_2	CF stretch.	a(P)	ia	735
	ν_3	CF_2 deform.	a(P)	ia	364
A_1''	ν_4	CF_2 twist.	ia	ia	
A_2'	ν_5	CF_2 wagg.	ia	ia	
A_2''	ν_6	CF stretch.	ia	a	1370
	ν_7	CF_2 rock.	ia	a	**
E'	ν_8	ring deform.	a(dP)	a	863
	ν_9	CF stretch.	a(dP)	a	1277
	ν_{10}	CF_2 deform.	a(dP)	a	495
	ν_{11}	CF_2 wagg.	a(dP)	a	
E''	ν_{12}	CF stretch.	a(dP)	ia	
	ν_{13}	CF_2 rock.	a(dP)	ia	
	ν_{14}	CF_2 twist.	a(dP)	ia	

note: the species notation is that of Herzberg (15). Under activities, the various symbols denote: a - active, a(P) - active polarized, a(dP) - active depolarized, and ia - inactive. Perfluorocyclopropane is assumed to have D_{3h} symmetry.

** Atkinson has shown that the 552 cm^{-1} fundamental assignment of Ito (82) cannot be rationalized as a CF_2 deformation from reasonable values of force constants. He gives this absorption an E' fundamental assignment. Some evidence also points to a wrong assumption for the 495 cm^{-1} line. The matter will be further considered.

1.4. The Chemistry of Difluoromethylene

1.4.1. The Electronic State and Spectral properties

The emission spectrum of CF_2 was first observed by Venkateswarlu (94) in the uncondensed transformer discharge of CF_4. A system of many headed bands in the region 2340 to 5000 Å, are partly attributed to non-linear CF_2, on the basis of vibrational analysis (114). Laird and co-workers (95) identified several of the same bands in their study of the absorption spectrum of CF_2, and on this basis concluded that the ground state was being observed in both studies. They found the CF_2 radical to have a half life of about one second under the conditions of their experiments. Simons and Yarwood (98) observed the same CF_2 obsorption bands as Laird and co-workers, in the pyrolysis of syn-tetrafluorodichloro acetone and 1,1,3-trichloro-trifluoroacetone. The length of duration of CF_2 absorption after the photolysis flash was evidence of the long life of CF_2 as compared to CH_2. They found evidence that the rate of disappearance of CF_2 was zero order confirming the suggestion (95) that CF_2 is removed by diffusion to the walls of the container. No C_2F_4 was found in the products.

Duchesne and Burnelle (96) conclude that the ground state of CF_2 is a singlet since an angle of 90 - 110° must

be assumed for F-C-F, in order to obtain reasonable values of force constants from the fundamental vibrations of the ground state. They argue that the high value of the valency force constant obtained suggests some hybridization of the SP^2 type in which the nonbonding pair at the carbon atom occupies an orbit which is more nearly s than otherwise.

Mann and Thrush (97) have studied the absorption spectrum of CF_2 from the flash photolysis of CF_2Br_2. The only electronic transition which occurs is found to have its origin at about 37,695 cm^{-1}. Nelson and Kuebler (115) observed most of the same lines in absorption for CF_2 produced by flash heating CF_4. Thrush and Zwolenick (133) have produced a more intense absorption spectrum of CF_2 from a d.c. pulse discharge in perfluoro-n-pentane. All observed transitions could be assigned purely in terms of excitation of the bending vibrations.

Simons and Yarwood (100) have reviewed the methods of producing CF_2 by photolysis and heating in order to carry out spectroscopic studies. Among halogenated methanes, CF_2 is produced with difficulty in the process:

$$CF_3 \cdot X \longrightarrow CF_2 + FX,$$

where X is Br or I, but more easily in the process:

$$X \cdot CF_2 \cdot Y \longrightarrow CF_2 + XY,$$

where X and Y are Br, Cl, or H, and X can be Y.

This is explained on energetic grounds. The primary process in any case is the production of the CF_2 radical. Other sources of CF_2 mentioned are CF_3COOH by photolysis and CF_4 (99) by pyrolysis.

Matthews (129) has studied the 2540 Å absorption spectrum of CF_2 produced by flashing chlorodifluoroethylene, and tabulated rotational constants from analysis of one of the individual bands.

The absorption spectrum of solid CF_2 has been studied by Bass and Mann (126). The products of a microwave discharge through a mixture of octafluorocyclobutane and argon were condensed on a liquid helium cooled surface and the ultra-violet absorption spectrum studied. They found some 13 bands in a single progression between 2300 and 2670 Å. Gas phase frequencies are slightly lower than those observed in this system.

Milligan and co-workers (132) obtained an infra-red spectrum of CF_2 from the flash photolysis of difluorodiazirine. The three vibration fundamentals of CF_2 in a matrix environment were observed at 668, 1102, 1122 cm^{-1}. The molecular angle of CF_2 was calculated to be 108°.

Powell and Lide (136) have observed the microwave spectrum of CF_2 generated by a weak radio frequency discharge in C_2F_3Cl, CF_4 and $(CF_3)_2$ CO. They have backed

up their assignments with a partial resolution of Stark effects on several transitions. The absence of fine structure and observeable Zeeman shifts in the spectrum confirm the expected singlet ground state of CF_2 generated in this way.

On the basis of wide differences in reactivity when produced by different methods, Heicklen and co-workers (116) have suggested that CF_2 may be present in its triplet state in the instances of enhanced reactivity. They still consider the singlet to be the ground state.

Simons (93) has tried to explain the finite activation energy of recombination of CF_2 radicals produced in flash photolysis. The slow decay of CF_2 concentration in these experiments indicated that the initial approach of two singlet CF_2's so produced was repulsive. It is assumed that C_2F_4 in its ground state correlates with 2 CF_2 ($^3B_1$).

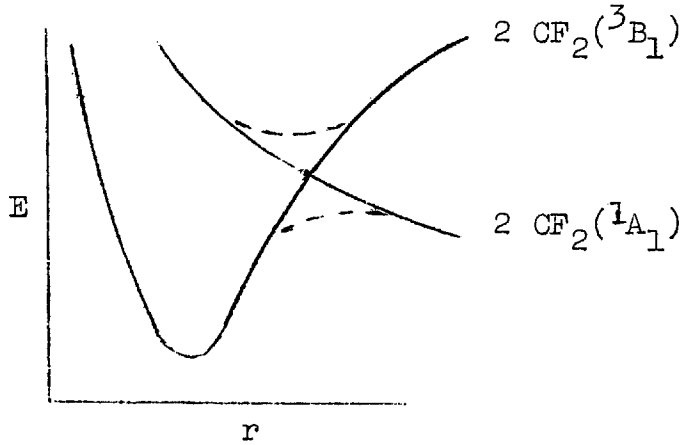

The potential energy curve for this dissociation crosses the repulsive potential energy curve for 2 CF_2 ($^1A_1$), and

makes it possible for two associating CF_2 ($^1A_1$) to go from one path to the other. This process will require an activation energy, the magnitude of which will depend on the height of the cross-over point.

Simons (127) has performed molecular orbital calculations for CF_2 in an effort to elucidate the nature of the electronic transition whose origin is 2650 Å (corresponding to an energy of 4.66 e.V.). He finds that of the possible excited states the only one with an energy value close to 4.66 has the electronic configuration $\cdots (4a_1)^1 (2b_1)^1$. This is the lowest excited singlet state of CF_2 and has B_1 symmetry. The transition is:

$$\ldots(4a_1)^1(2b_1)^1,\ {}^1B_1 \leftarrow \ldots(4a_1)^2,\ {}^1A_1;$$

the excited state B_1 has an energy approximately $\geq$ 4.2 e.V. above the ground state. Earlier work (94) proposed for this transition:

$$^1B_2 \leftarrow {}^1A_1.$$

1.4.2. Thermodynamic properties

A large number of papers have appeared concerning the elucidation of ΔH_f° (CF_2) from electron impact data; ionization and appearance potential data are obtained by mass spectral studies. Values that place limits like $\leq$ -17 k.cal./mole (83) and $\leq$ 54 k.cal./mole (84), to quote

extremes, have been published. Majer and Patrick (85) have suggested that such studies give uncertain data due to the excited nature of the fragments produced in the dissociation processes. Recent information obtained by Steele (86) from electron impact studies on CF_3H and CF_2H_2 (ΔH_f^o (CF_2) = -43 k.cal./mol) and by Pottie (87) on CF_2 from pyrolysis of C_2F_4 (ΔH_f^o (CF_2) = -37 k.cal./mol), are in greater agreement with data from other sources.

From the data of Farlow (88), who prepared C_2F_4 from CF_4 and graphite, Stull (89) has calculated $\Delta H_f^o = -46 \pm 5$ k.cal./mol. Wentink and Isaacson (90) have pointed out a slight error in the value of the former publication in the light of more recent information.

Gozzo and Patrick (91) estimate a value of ΔH_f^o (CF_2) $\leq$ -43 k.cal./mole from kinetic studies of the pyrolysis of CF_2HCl. In later work on this compound, Edwards and Small (92) found a value of -46.3. Simons (93) has assumed a value of ΔH_f^o (CF_2) less than approx. -40 k.cal./mole, calculated from this data. This value seems to agree as well as possible with the more recent electron impact data.

Modica and La Graff (106) have determined ΔH for the reaction:

$$C_2F_4 \rightleftharpoons 2CF_2$$

in shock wave studies on tetrafluoroethylene; they obtained ΔHr_{298} = 76.06 k.cal./mole. If this is combined with $\Delta Hf_{298}(C_2F_4)$ = -155.5 (107), they obtained $\Delta Hf_{298}(CF_2)$ = -39.7 ± 3 k.cal./mole.

Zeleznik and Huff (134) have tabulated coefficients for equations which express the dependence of heat capacity, enthalpy, and entropy on temperature in the range 150 - 6000°F for a large number of species including CF_2. They give a detailed description of a general computer program for chemical equilibrium calculations involving these species.

Wiederkehr (135) has tabulated thermodynamic data for CF_2 and a large number of other species observed in high temperature reactions. The range of applicability is above 1000°K. The information is tabulated as thermodynamic property vectors. This can be applied to the calculation of entropy, enthalpy and free energy of multicomponent systems as a function of composition and temperature by carrying out a few matrix operations.

Milligan and co-workers (132) have tabulated the thermodynamic properties of CF_2 from 273 - 3000°K. Their data are based on an infra-red spectral analysis of CF_2 and an assumption of 1.32 Å for the C-F bond distance.

1.4.3. The Generation of Difluorocarbene.

In discussing the chemistry of perfluorocyclopropane, methods of generating CF_2 in the gas phase were mentioned; when produced from these various materials, two CF_2 combine to give C_2F_4 or one CF_2 reacts with C_2F_4 to give $c\text{-}C_3F_6$.

Two such compounds were $CF_3Sn(CH_3)_3$ (75) and CF_3Ge I (76). The carbene elimination reaction of group IVA elements (silicon, germanium, tin and lead), containing a carbon chain with CF_2 next to the metal, is probably a general one. Haszeldine and Young (148) have shown that heating of (1,1,2-trifluoro-2-chloroethyl) trichlorosilicon gives:

$$Cl\cdot CHF\cdot CF_2\cdot SiCl_3 \longrightarrow CHF = CFCl + FSiCl_3,$$

by removal of the fluorine on the α carbon.

Analogous behaviour seems to be the case for the group VA metals. The decomposition of $(CF_3)_2PF_3$, $(CF_3)PF_4$, $(CF_3)_3PF_2$ (74) and $(CF_3)_3Sb$ (77) have already been mentioned.

Heating or u.v. light gives CF_2 from difluorodiazirine (78,79), i.e. $CF_2\cdot N_2$. The homolog of this compound, bis-(trifluoromethyl) diazomethane has been synthesized by Gale and co-workers (149) who trapped the carbene $(CF_3)_2C$: with benzene by heating the parent compound.

Other sources of CF_2 have already been mentioned. $CF_3Fe(CO)_4I$ (73) produces CF_2 by heating at relatively low temperatures while relatively high temperature pyrolysis of halogenated methanes and ethanes (100, 129, 136) has proven useful as a source of CF_2 for spectroscopic studies.

Tetrafluoroethylene has been found to produce CF_2 in its flash photolysis (48), mercury photosensitized reaction (54, 55, 60, 62) and shock wave decomposition (106, 128, 130). CF_4 is also a source of CF_2 (130) in shock waves.

Lenzi and Mele (47) have shown that CF_2 is produced in the thermal breakdown by tetrafluoroethylene oxide. They have observed both C_2F_4, the product of the combination of two CF_2's and c-C_3F_6 from the addition of CF_2 to C_2F_4.

More recently, Haszeldine and co-workers (146) have observed the elimination of CF_2 nearly quantitatively in the thermal decomposition of chlorofluorocyclopropanes:

$$\begin{array}{l} CF_2 - CX_2 \\ \quad\diagdown\diagup \\ \quad CX_2 \end{array} \xrightarrow{160\text{-}200^\circ} CF_2 + CX_2 = CX_2$$

where X = Cl or F.

This is an extension of the present work (44) and that of Mitsch and Neuvar (45) which has demonstrated

the elimination of CF_2 in the decomposition of perfluorocyclopropane and perfluoroallylcyclopropane.

$(CH_3)Sn\ CF_3$ is also found to give good yields of CF_2 in solution; Seyferth and co-workers (101) formed gem-difluorocyclopropanes in good yield from cyclohexene and tetramethylene by heating at 80°C in the presence of $(CH_3)\ Sn\ CF_3$, although they in fact suggest a CF_3 intermediate. Hine and Tanabe (109) have shown that chlorodifluoromethane reacted with potassium isopropoxide in dry isopropanol to give CF_2. This basic hydrolysis of $CF_2.Cl.H$ in alcohols has been the subject of a number of other studies (122, 123) and seems to be an example of a general reaction for the formation of dihalomethylenes.

Franzen (103) has reported the generation of CF_2 in solution by the action of organo-lithium compounds on CF_3Br; under the conditions used, the free radical has a half life of from 5×10^{-4} to 10^{-3} seconds. The CF_2 generated was trapped with cyclohexene. The same author (104) claims to have trapped the CF_2 generated in this way with triphenylphosphine as well. Speziale and Ratts(105) were unsuccessful with this method when they substituted chlorotrifluoromethane for CF_3Br. Birchall and co-workers (102) have trapped CF_2 with cyclohexene in the thermal breakdown of chlorodifluoroacetate.

1.4.4 The Reactivity of Difluoromethylene

Difluoromethylene has been found to be a surprisingly stable and unreactive free radical, especially compared to CH_2. Mahler (74), in his studies on the trifluorophosphoranes found that the generated CF_2 did not react with H_2 (100°C), BF_3, CO, NF_3, N_2O, PF_3, CS_2, SO_2 or CF_3I. He found that it did react with I_2 to give CF_2I_2, HCl to give HCF_2Cl, Cl_2 to give CF_2Cl_2 and O_2 to give CF_2O. It reduced the metal fluorides UF_6 and MoF_6 and produced CF_4 in the process. The same author (124) found that CF_2 generated in the same way added to hexafluoro-2-butyne once or twice to form respectively the mono and bicyclopropane of the original compound.

The simultaneous reactions of CF_2 with itself to form C_2F_4 or with C_2F_4 to form c-C_3F_6 have been the subject of a number of kinetic studies: Atkinson (55,111), Cohen and Heicklen (62), Lenzi and Mele (47). They have been part of the experimental studies associated with this thesis, preliminary results of which have already been published (44). The results of the other authors will be compared to the data of this thesis at a later stage.

Edwards and Small (92) in their kinetic studies on the pyrolysis of CF_2HCl estimated the following Arrhenius parameters for various reactions involving CF_2:

		A(l/mole sec)	E(k.cal.)
(1)	$CF_2HCl \longrightarrow CF_2+HCl$	$10^{13.84}$	55.8
(2)	$CF_2+HCl \longrightarrow CF_2HCl$	$10^{8.35}$	6.2
(3)	$2CF_2 \longrightarrow C_2F_4$	$10^{9.94}$	5.8
(4)	$C_2F_4 \longrightarrow 2CF_2$	$10^{16.66}$	70.4

The uncertainty in the activation energy for reaction (3) was considered to be as great as the value itself. Dalby (48) has determined the rate of recombination of CF_2 radicals from flash photolysis studies on C_2F_4; the expression he obtained was:

$$k = 2.82 \times 10^8 \exp.(-1740/RT).\ l./\text{mole sec}$$

Dalby's (48) studies further indicated that the reactivity of CF_2 towards olefins and oxygen to be low. He placed the following limits on the corresponding reactions at 25°C:

$CF_2 + C_2F_4 \longrightarrow C_3F_6$, $k < 3 \times 10^3$ l./mole sec.

$CF_2 + O_2 \longrightarrow CF_2O_2$, $k < 10^4$ l./mole sec.

$CF_2 + C_2H_4 \longrightarrow C_3H_4F_2$, $k < 3 \times 10^3$ l./mole sec.

perfluoropropene and carbonyl fluoride were observed respectively in the first two of these reactions, in small quantities.

CF_2 generated from halomethanes does not seem to react with oxygen if the latter is present (93). This is confirmed by Fielding and Pritchard (131) who found no evidence for reaction between CF_2 and O_2, H_2, CO, C_2H_4 and C_3H_8 at 250°C.

The reaction of oxygen with CF_2 is observed in the Hg photosensitized oxidation of C_2F_4 (60). The CF_2O product is explained by the reaction of electronically excited C_2F_4 produced by Hg^* quenching or by reaction of oxygen atoms produced in the Hg photosensitized reaction of O_2. In the latter case:

$$O + C_2F_4 \longrightarrow C_2F_4O \longrightarrow 2CF_2O + O.$$

This second step was not observed by Lenzi and Mele (47) in their studies of the thermal breakdown of tetrafluoroethylene oxide; at similar low temperatures:

$$CF_2 - CF_2 \;(\text{O bridge}) \longrightarrow CF_3.CF = O$$

The C_2F_4O produced from the O atom reactions may have sufficient energy to behave like tetrafluoroethylene oxide at higher temperatures (47):

$$CF_2 - CF_2 \;(\text{O bridge}) \longrightarrow COF_2 + CF_2$$

Difluoromethylene produced at higher temperatures such as by the pyrolysis of halomethanes seems to be more reactive under certain conditions. One patent (117) has claimed substantial yields of higher molecular weight fluorocarbons when CF_2 generated by the pyrolysis of CF_2HCl added to C_2F_4, $CF_3.CF = CF_2$ and $CF_3.CF_2.CF = CF_2$.

Pyrolysis of CF_2HCl by itself gave a yield of 89% C_2F_4 under certain conditions (118). Substantial yield of C_2F_4 has also been claimed in the pyrolysis of CF_4 (119).

Mitsch (108) has shown that CF_2 generated in the photolysis of difluorodiazirine undergoes the following reactions:

$$CF_2 + Cl_2 \longrightarrow Cl_2CF_2$$

$$CF_2 + I_2 \longrightarrow I_2CF_2$$

$$CF_2 + N_2O_4 \longrightarrow CF_2(NO_2)_2$$

$$CF_2 + ClNO_2 \longrightarrow ClCF_2NO_2 \qquad 15\%$$

$$\longrightarrow CF_2.Cl_2 \qquad 70\text{-}80\%$$

$$\longrightarrow CF_2(NO_2)_2 \qquad 1\text{-}2\%$$

The same author (49) has discussed the addition of CF_2 generated in the photolysis or pyrolysis of difluorodiazirine, to olefins; the stereospecific nature of the addition is evidence of the singlet character of the CF_2 so generated. He used a 5-10 molar excess of olefin to get the yields shown in the following table. C_2F_4 and $CF_2{=}N{-}N{=}CF_2$ (perfluoromaldazine) were the only side products in the photolysis experiments. $c\text{-}C_3F_6$ was also found in the products of the pyrolysis reactions.

Olefin	cyclopropane	Molar Ratio	Yield %	Technique
Isobutylene	$(CH_2)_2$-C-CH_2-CF_2	5	71	photolysis
1,3-butadiene	CH_2=CH.CH.CH_2.CF_2	10	71	pyrolysis for 60 hr., 135-145°C
trans-butene-2	trans-CH_3.C-CH.CH_3 (CF_2)	15	33	photolysis
cis-butene-2	cis.CH_3.C-CH.CH_3 (CF_2)	8	83	pyrolysis for 2 hr., 175-185°C
1,1-difluoro-2-vinylcyclopropane	CF_2.CH_2.CH.CH.CH_2.CF_2	1	15	pyrolysis for 60 hr., 135-145°C

Neuvar and Mitsch (147) have fitted data for the thermal unimolecular breakdown of difluorodiazirine to N_2 and CF_2, to the following Arrhenius expression

$$0.68\ k^{\infty} = k_{200\ mm} = 10^{13.1} \exp.(-32{,}200/RT)\ sec^{-1}.$$

Mastrangelo (125) has found C_2F_4 in the warm up products of trapped CF_2's produced from a radio frequency discharge in c-C_4F_8; the CF_2 trapped in this way also was found to react with Cl_2 or Br_2 to give CF_2X_2 or $(CF_2X)_2$.

The observation of CF_2 in shock waves and study of resulting reactions is only beginning to be exploited. Modica and Le Graff (106,130), have found CF_2 in shocked C_2F_4-Ar, CF_4-Ar and C_2F_4-N_2 mixtures, and studied the reaction of CF_2 in the temperature range 1200-1800°K. At higher temperatures (above 2600°K) Modica (128) has studied the reaction:

$$CF_2 \longrightarrow CF + F$$

2. EXPERIMENTAL

2. EXPERIMENTAL

2.1. The Apparatus

A vacuum system was ordinarily used in carrying out the experimental work. This system consisted of a vacuum producing section, storage and handling section, analysis and preparative section and reaction section. Construction was exclusively of pyrex glass, using standard Quickfit Quartz fittings where necessary. Facilities for temperature and pressure measurement and control have been incorporated with the reaction section.

The vacuum system was designed so that reaction starting materials and products could be handled and stored free from atmospheric contamination. The reaction and analysis sections were incorporated into the system in such a way that reactions were carried out and samples put into the chromotograph, again under stringent air free conditions.

2.1.1. Vacuum Producing Section

A vacuum was maintained on the main line by means of an Edwards 'Speedivac' Model ED 35 two stage gas

ballast rotary pump, backing an Edwards Model 1M 2C two stage mercury vapor diffusion pump. The rated capability of this combination is a vacuum of better than 10^{-6} torr.

A trap between the main line and the pump system was kept cooled in liquid nitrogen to prevent reactive materials passing through the pumps. The stopcock arrangement permitted the mercury diffusion pump to be bypassed if desired. The gas ballast system of the backing pump allowed condensible material collected in the trap to be pumped to atmosphere outside the building when required, without danger of contaminating the pump oil. Stopcocks and joints in this section were made reasonably large to facilitate quick production of low pressure on the main line.

A McLeod gauge was connected to the main line and was used to determine semi-quantitatively the nature of the vacuum e.g. less than 10^{-4} or 10^{-6} m.m. The mercury level was controlled with a separate rotary oil pump.

2.1.2. Storage and Handling Section

The gas handling section, to which all other parts of the vacuum system were directly connected, consisted of a pair of traps (shown A in fig. 2.1). Any part of

Scheme of Storage & Handling Section.

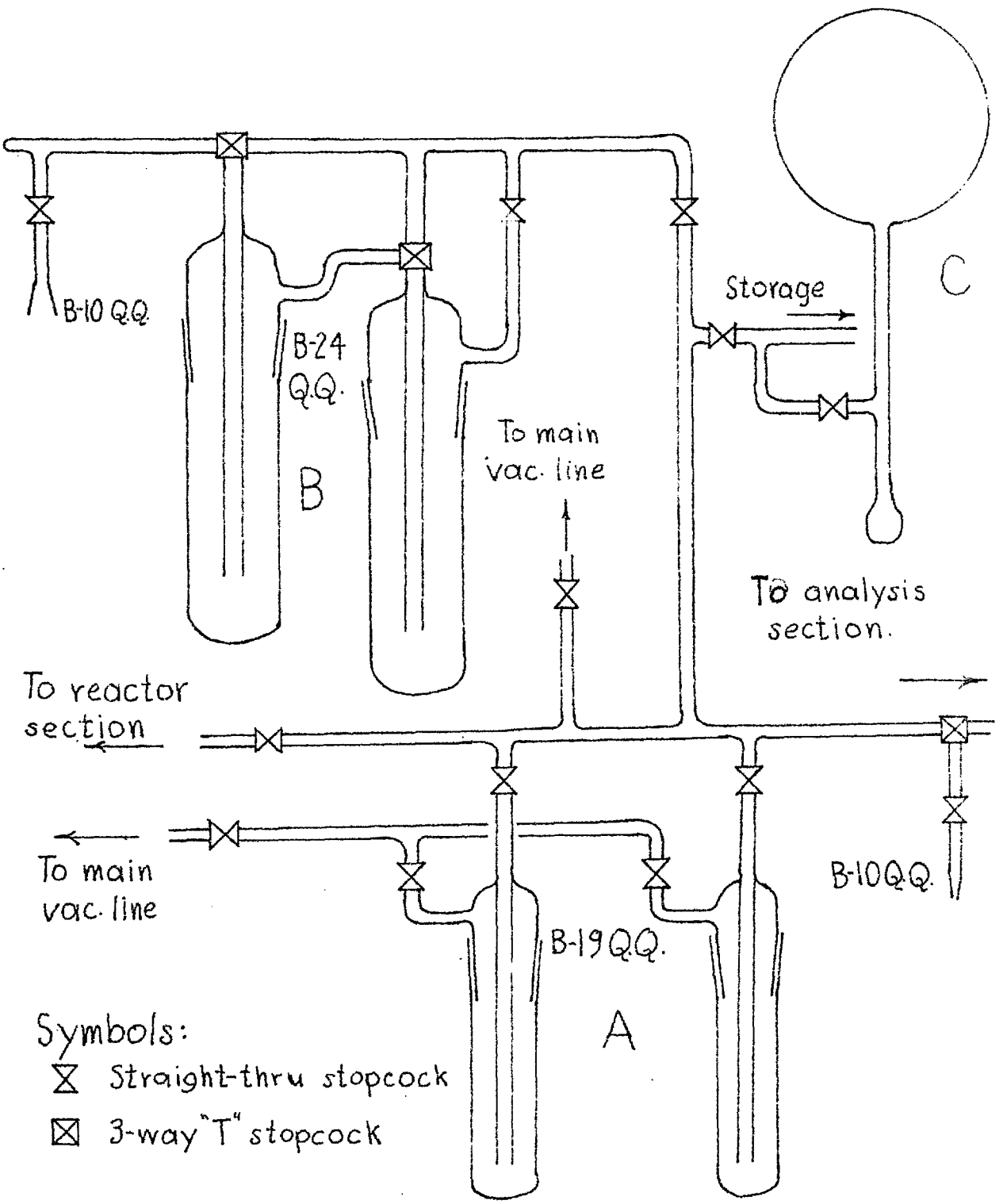

Figure21.

the storage, reaction, or analysis section could be pumped through these traps to the main line. The traps in A were about 50 c.c. total volume each.

The traps B in fig. 2.1 were of larger capacity (about 200 c.c. total volume). They were used for trap to trap distillations of large volumes of material and for collecting product from the photochemical apparatus which will be described later.

Gases were stored in a series of globes of one and two litre capacity. Their location relative to the other parts of the vacuum system is shown as C in fig. 2.1. All globes were covered with black paint; the most frequently stored material was tetrafluoroethylene which polymerizes slowly in the presence of light and traces of mercury. In addition the globes were covered with cellotape to minimize the effects of any implosion.

2.1.3. Analysis and Preparative Section

Analysis and purification of the gases used were performed on a Pye 'Panchromatograph'. The instrument is designed for the injection of samples by syringe; however it was adapted so that samples could be injected directly from the vacuum system into the columns. This

was effected by means of the pair of four-way stopcocks shown in fig. 2.2. Metal-to-glass connectors of Pye design (see fig. 2.3) were used to connect the steel capillary piping supplying carrier gas, to the glass tubing of the sampling device and column inlet. The metal-to-glass connector effects the seal against the inside of the glass tube at the rubber washer. Screwing down the thumb screw forces the plastic spacer against the rubber washer, flaring it out between the spacer and the brass nozzle. The washer also presses against the outlet end of the connector running through the centre of the washer, and creates a seal there as well.

In usual operation of a Panchromatograph the carrier gas would flow from the $^{1}/_{32}$ in. steel pipe via the metal-to-glass connector directly into a packed glass column in the chromatograph. The illustrated arrangement allows a sample to be taken (A and B of fig. 2.2) from the vacuum system and then injected into the chromatographic column (C of fig. 2.2). As the column inlet pressure was about 30 lb. gauge, spring loaded stopcocks were used; frequent regreasing was required in order to allow production of a reasonable vacuum in the sample loop.

Sampling Device.

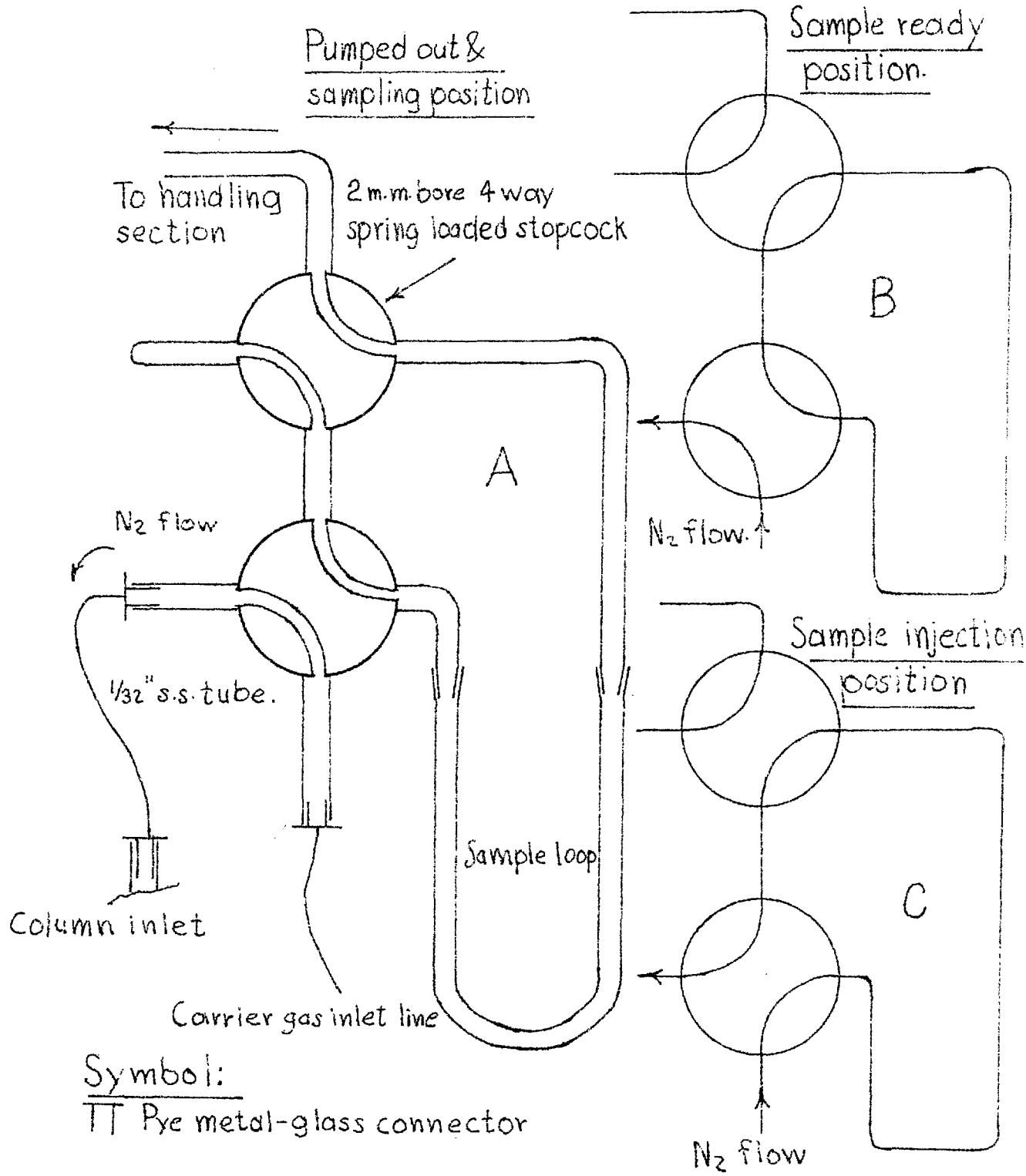

Figure 2.2

Pye Metal-to-Glass Connector.

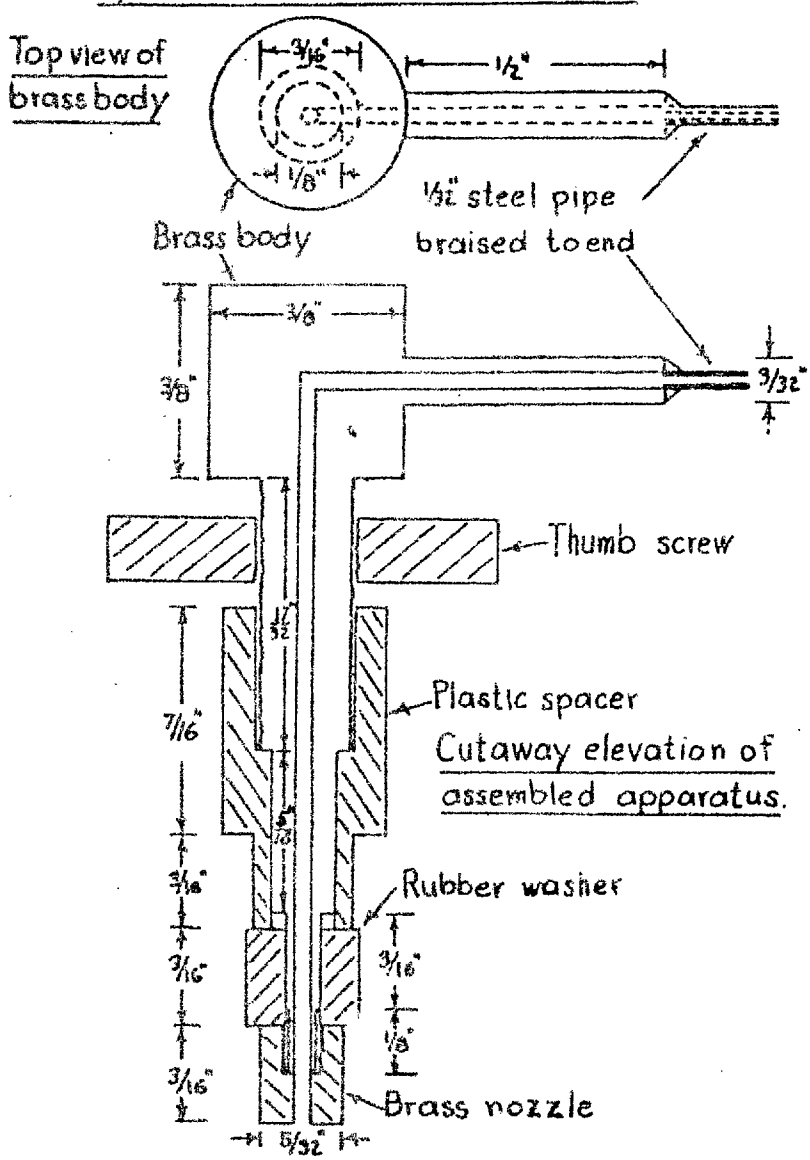

Figure 2.3

Thermal conductivity and hydrogen flame detectors were both used in conjunction with the Panchromatograph. The thermal conductivity detector (Pye Cat. No. 12220) was a Gow-Mac hot wire device Type 9285-D with a four filiment bridge, each arm being a code W2 tungsten filiment. This was used in conjunction with a Gow-Mac Instrument Co. regulated D.C. power supply Model 9999-CS (Pye Cat.No. 12293). The design of the detector was such that it was unsuitable for analytical work when nitrogen carrier gas was used; the sensitivity was low and the detector produced negative peaks at low concentrations of sample in carrier gas. Rather than resort to the use of more expensive helium, argon or hydrogen with this detector, it was found convenient to permanently connect it to the outlet of the preparative column of the chromatograph. All quantitative analyses were performed with a hydrogen flame detector (Pye Cat. No. 12353) and Decade Voltage Supply (Pye Cat. No.12363). The stream splitting device supplied with the Panchromatograph enabled a small fraction (e.g. 1/300) of a sample injected to be taken to the highly sensitive flame detector if required. All calibrations were however made with a direct flow of column effluent gas to the detector.

A Honeywell Model Y1530 Y855 recorder and Model S158-2-HB integrator were used to measure detector output. The recorder was provided with a switch and terminal box. Six sets of twin terminals were provided, any pair of which could be selected as recorder input; another switch provided a selection of the 1 or 10 m.v. range of the recorder. The integrator maximum count rate of 600 counts/min. at full scale deflection was invariably used; the four digit counter was the only facility employed to determine integrator output. The separate pen trace for integrator output which can be purchased causes interference with the main trace.

The Panchromatograph is provided with a thermostated oven with place for two glass columns. A separate oven holds the thermal conductivity detector, and can be thermostated at a different temperature. The operating range in both ovens is 50-250°C. During most of the work, only two columns were used: one a column for preparative work and one for analysis. They were kept connected respectively to the thermal conductivity and hydrogen flame detectors.

The preparative column was a 9 ft. long 1 cm. i.d. glass coil packed with 100/120 mesh silica gel. The analytical column was a 9 ft. long 5 m.m. i.d. trombone

shaped glass column packed with 60/80 mesh silica gel. The analytical column packed with the finer material did not give adequate flow rates (i.e. at least 50 c.c./ min. of carrier gas) to be of practical use. Green and Wachi (112) have described the use of silica gel to separate fluorocarbons. In a column similar to the analytical column of this work and programming from room temperature to 180°C over one hour, they obtained good separation of the following substances which were eluted in the order mentioned: air, CF_4, C_2F_6, C_2F_4, C_2F_2, C_3F_8, c-C_3F_6, $CF_3.CF{:}CF_2$, octafluorocyclobutane, C_4F_8-2, i-C_4F_8, C_4F_8-1.

Both of the columns used in this work were packed by drawing a vacuum on one end and causing the column to vibrate using a Burgess Prods. Ltd. Model UT62 'Vibro-Tool' usually used for engraving metal. After purging with N_2 at 250°C for several hours, it was found that the columns had to be 'topped up' with packing.

Nitrogen was used exclusively as the carrier gas in both preparative and analytical work. Outlet pressure from the cylinders was controlled with standard British Industrial Gases two stage regulators. The flow to the columns and to the column simulator used in conjunction with the thermal conductivity detector were controlled

with Edwards vacuum needle valves. Four rotameters in the chromatograph monitored inlet flows; bubble flow meters were used to measure the flows directly where possible and to calibrate the rotameters. Two stage regulators on the hydrogen and air cylinders were the only control on the supply of these gases to the flame detector. A molecular sieve packed dryer was placed on the air line; traces of moisture in the gas supply to the detector causes eratic behavior. It was found necessary to regenerate this dryer about every nine months. The oxygen free nitrogen is known to be moisture free.

When preparative work was being done the outlet of the thermal conductivity detector, which took the entire column flow was connected via 1/32 in. metal piping and a metal-to-glass connector, to the apparatus shown in Fig.2.4. A single fraction could be separated from the bulk sample using this four way stopcock arrangement. The device is cooled in liquid nitrogen to collect the materials used in these studies; it can easily be connected to the vacuum system by the B-10 joint to transfer the separated fractions to the vacuum system.

A device similar to that described by Stockwell (110) is connected to the vacuum line as part of the

Sample Collecting Device.

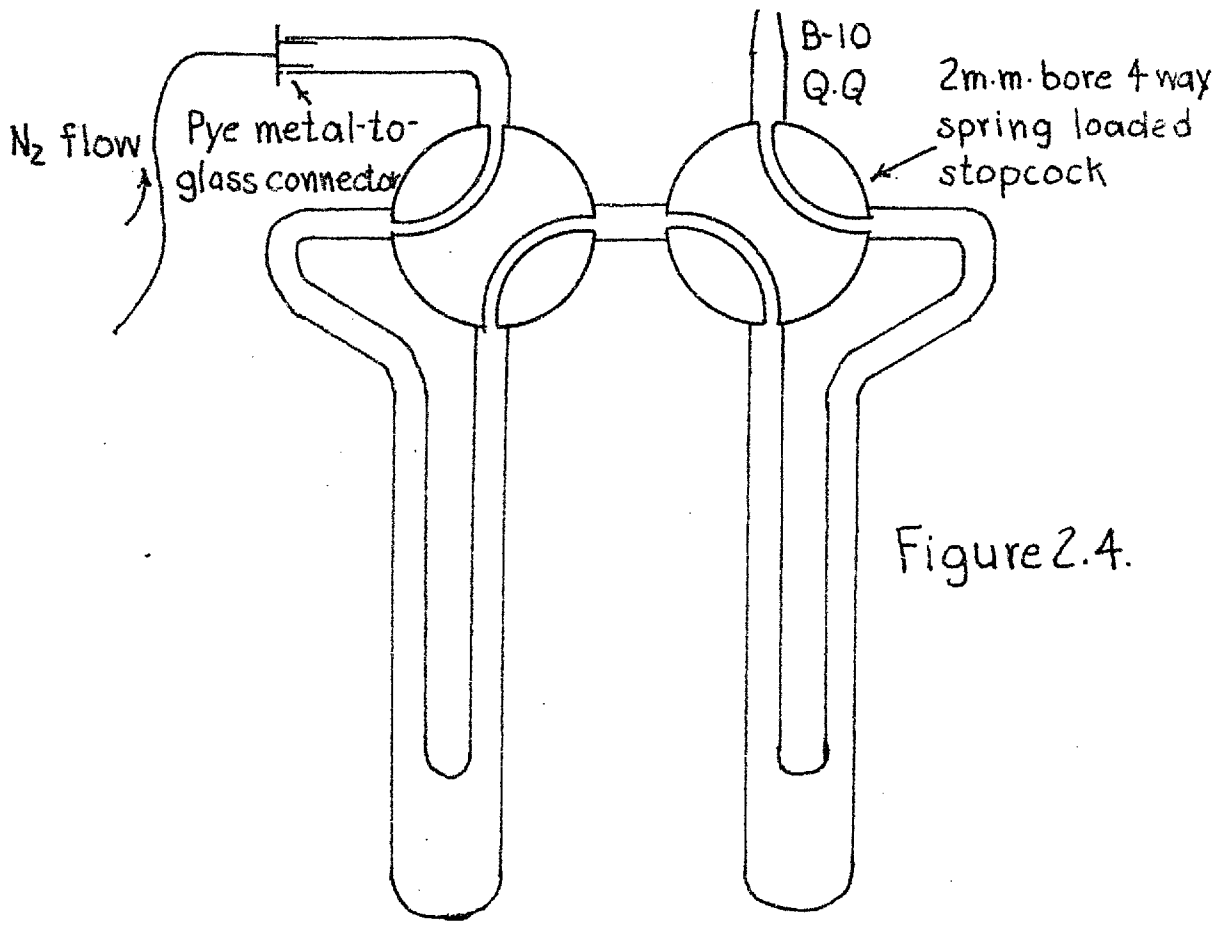

Figure 2.4.

Sample Mixing Device.

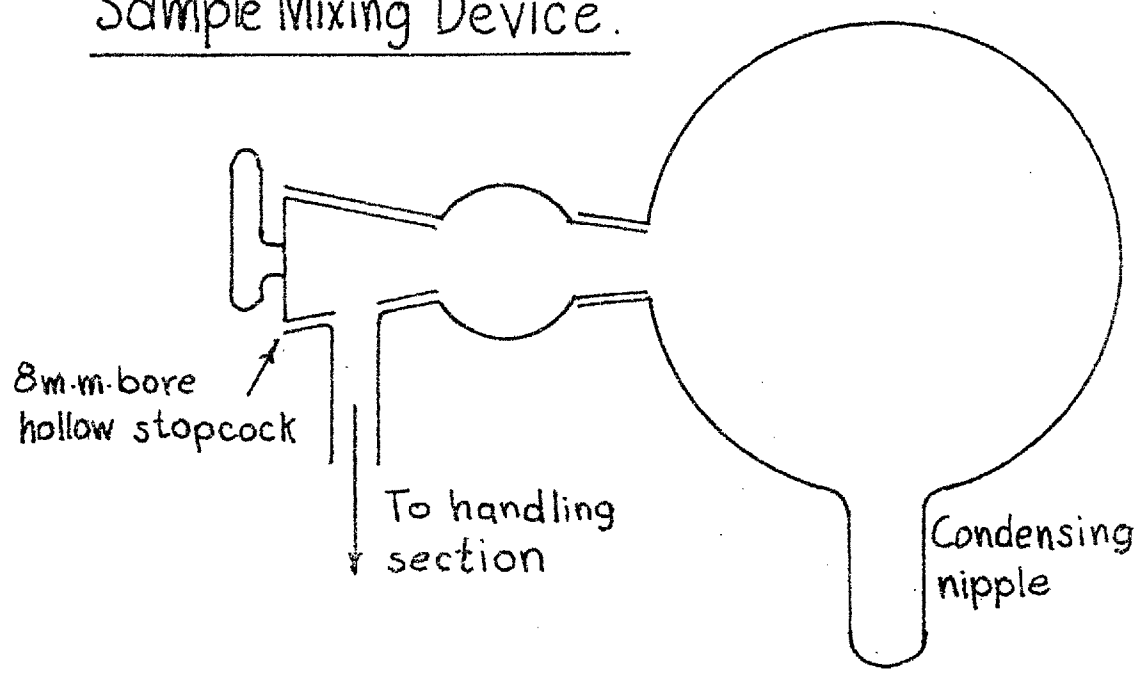

Figure 2.5

analytical section (fig. 2.5). It is used to get a well mixed sample for analysis. The hollow stopcock helps provide a freedom from dead zones which prevent attainment of a homogeneous mixture in a short time.

2.1.4. Reaction Section

The reaction section of the vacuum system consisted of a cylindrical pyrex reaction vessel, greaseless stopcock inlet assembly, pressure measuring device and a wide bore manometer. The arrangement and associated equipment is depicted in fig. 2.6; it should be noted that different parts of this sketch are not to scale.

Two cylindrical pyrex vessels were used: one empty except for a thermowell and the other packed with pyrex glass rods and also having a thermowell. The external dimensions of each were about 2 in.o.d. and 5 in. long. The thermowell extended $3\frac{1}{2}$ in. into the reactor. To minimize dead space the reactor inlet was constructed of 2.5 m.m.i.d. capillary pyrex tubing. The unpacked reactor had a free volume of about 205 c.c., the packed reactor 131 c.c; these figures were estimated by weighing quantities of pure tetrafluoroethylene whose pressure and temperature in the reactor were known. The uncertainty is about 1.5 c.c.

The dead space volume was determined in a similar fashion. The reactor was cut from the capillary lead one inch from the reactor; the rest was assumed to be dead space. The line was sealed at this point and the dead space volume from the greaseless stopcock determined by weighing quantities of C_2F_4 whose pressure and temperature in the unknown volume were measured; the initial value was 2.84 $\pm$ .03 c.c. and later 3.75 $\pm$ 0.1 c.c.

The packed reactor was estimated to have a surface area exposed to reagent of 6·7 times that in the unpacked reactor; this was estimated by taking the dimensions of the various pieces of glass and calculating the surface areas. Reactors were aged overnight with C_2F_4 at about 10 cm pressure and at the reaction temperature before being used for reactions. If the hot reactor had been in contact with oxygen and not then seasoned in this fashion, significantly different rates of reaction were observed.

Springham high vacuum greaseless stopcocks (2 m.m. bore, glass body, Viton A fluorocarbon rubber diaphragm) were used on the reactor inlet. These have the advantage over ordinary greased taps of being dependable under high (10^{-6} torr) vacuum at elevated

(up to 450°F): temperatures. The particular design of the assembly employing two of these stopcocks (see fig 2.6) was selected to enable a reasonable pressure of involatile material to be put into the reactor. A sample of the substance could be condensed into the nipple between the greaseless stopcocks, the stopcock heater brought up to a suitable temperature, and the substance then admitted to the reactor. This facility was only used for runs with $(CH_3)_3 SnCF_3$ and not with hexafluorocyclopropane.

The greaseless stopcock heater is shown in greater detail in fig. 2.7. It consisted essentially of a length of copper pipe split into halves. The protruding section at one end fitted snugly into the silica pipe holding the reactor, thus preventing any strain on the stopcock heater being transmitted to the fragile capillary inlet of the reactor. Heating was by three 175 watt strip mica heaters attached to the bottom half of the copper pipe heater assembly. A variac was used to regulate the mains supply to the heating elements which were connected in series.

In later work the device shown in fig. 2.8 was incorporated with the greaseless stopcock on the reactor side in order to increase the speed of opening and

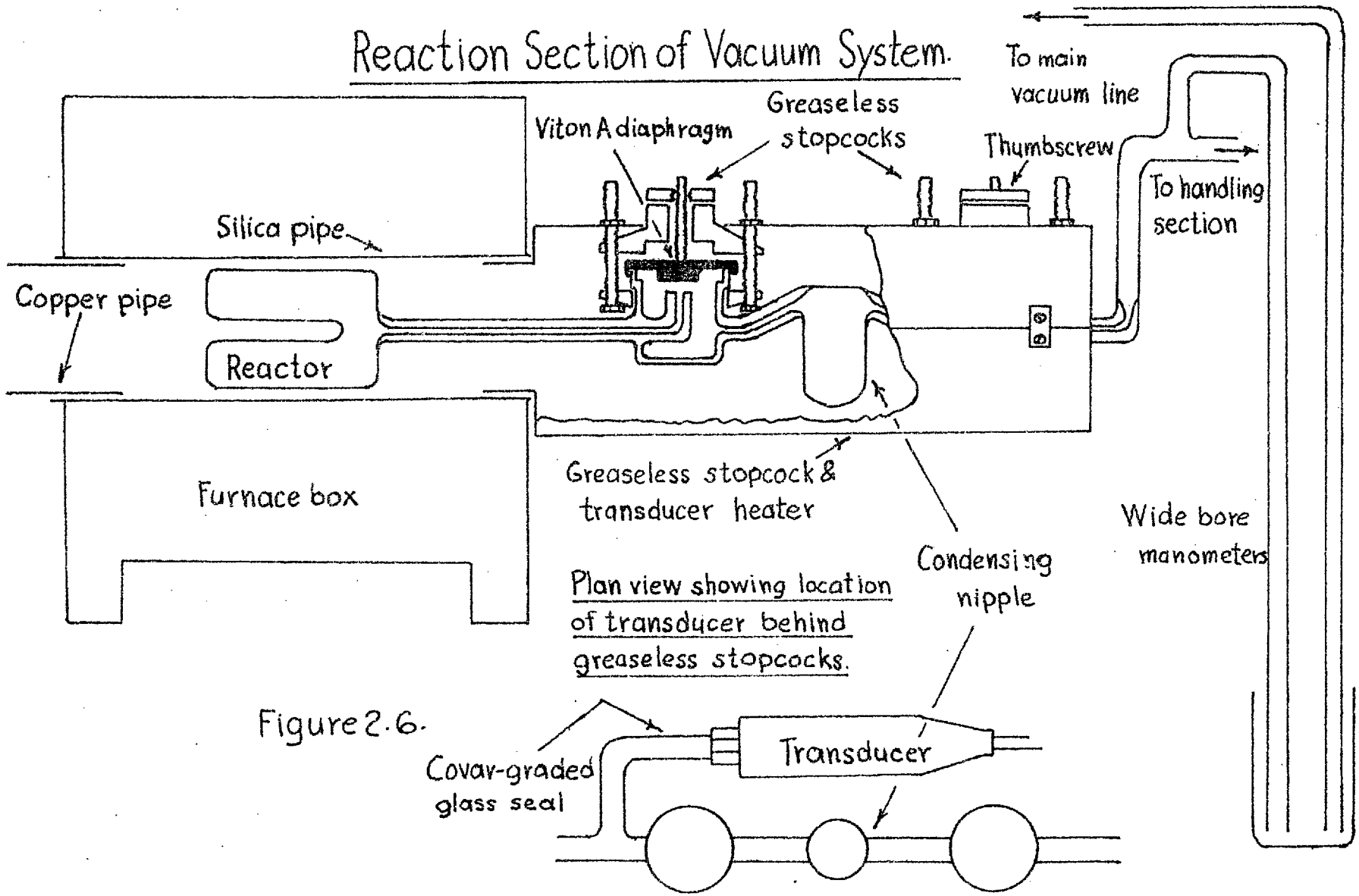
Reaction Section of Vacuum System.
To main vacuum line
Greaseless stopcocks
Viton A diaphragm
Thumbscrew
To handling section
Silica pipe
Copper pipe
Reactor
Furnace box
Greaseless stopcock & transducer heater
Condensing nipple
Wide bore manometers
Plan view showing location of transducer behind greaseless stopcocks.
Transducer
Covar-graded glass seal

Figure 2.6.

Greaseless Stopcock Heater

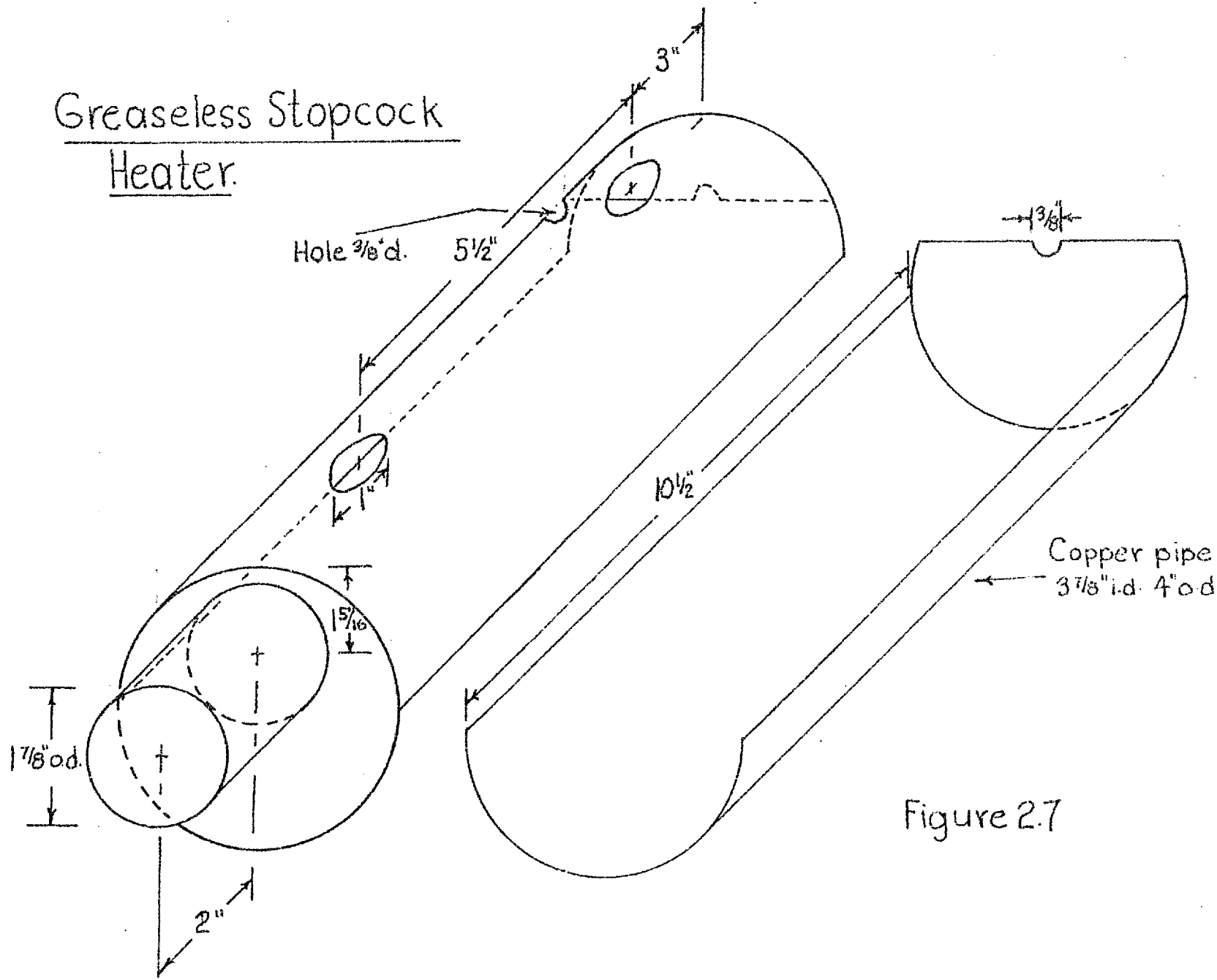

Figure 2.7

Greaseless Stopcock Quick Acting Handle.

Top View.

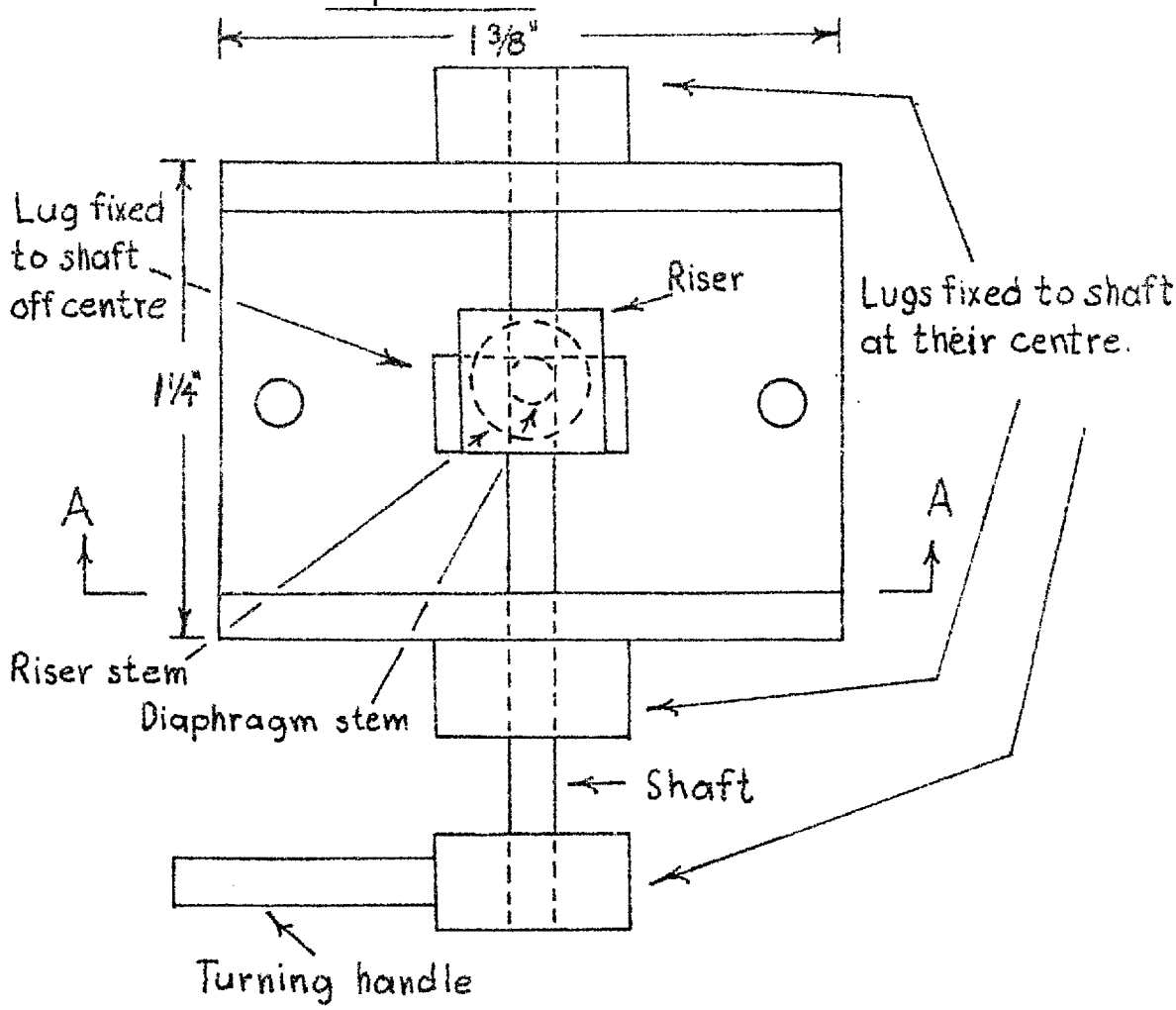

Scale : 2 × f.s.

Figure 2.8a

Greaseless Stopcock Quick Acting Handle.

Side View at Sect A-A.

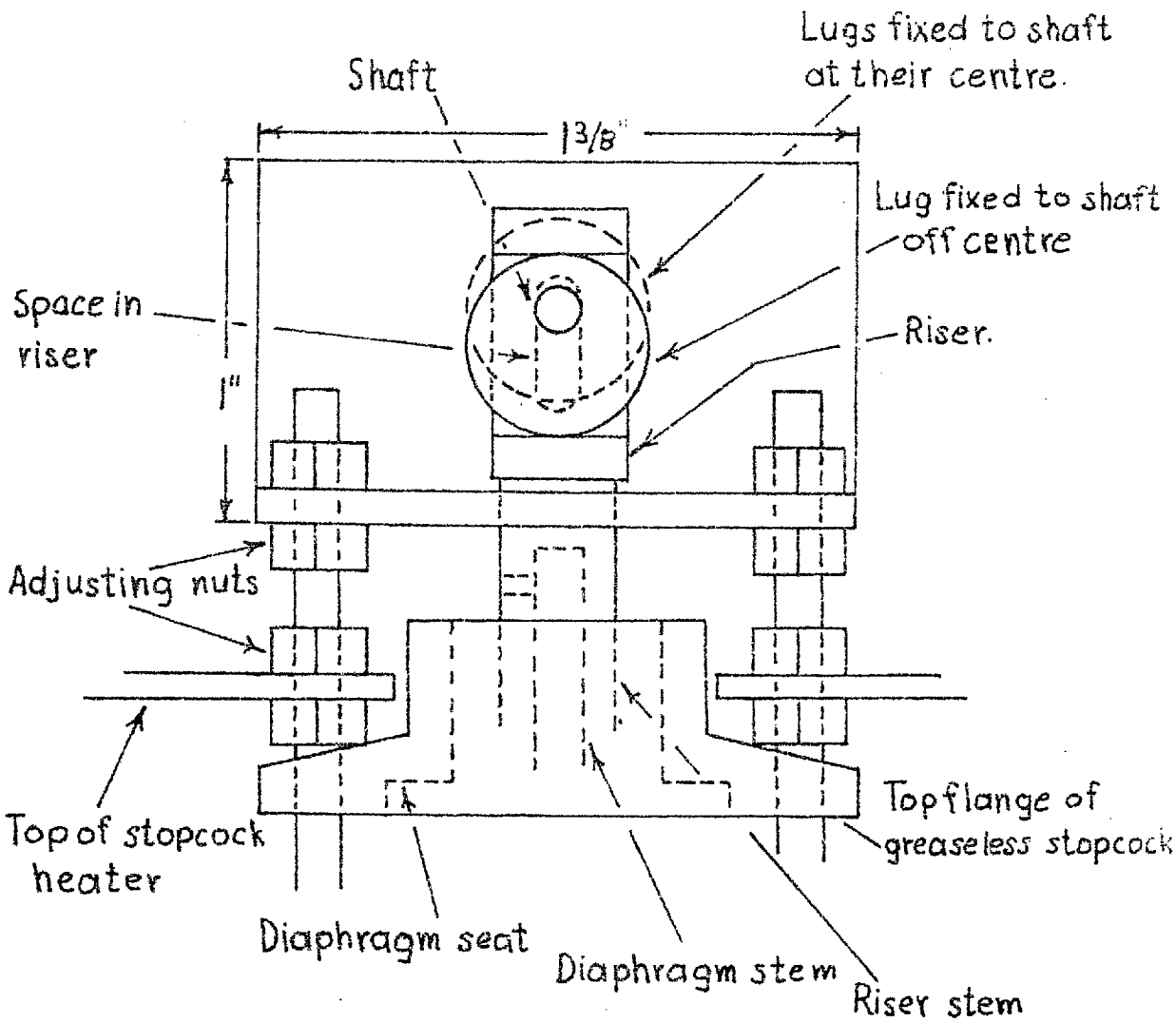

Scale: 2×f.s.

Figure 2.8b

closing the stopcock. One drawback of this type of stopcock is that repeated opening and closing of the stopcock quickly wears out the threaded stem attached to the diaphragm. This is inconvenient to replace. In normal operation of these stopcocks (see fig. 2.6), turning the thumbscrew moves the flexible centre of the diaphragm onto and off the capillary seat. The device described in fig. 2.8 moves a riser which is attached to the moving diaphragm stem. This up and down motion is effected by means of a circular lug which is attached eccentrically to a shaft which can be conveniently turned (fig. 2.8-a). The eccentrically attached lug fits snugly into an extension of the riser stem which however permits the lug to turn inside it and by the motion of turning to raise and lower it (fig. 2.8-b). The frame holding the arrangement can be adjusted to the proper position with a number of adjusting nuts which move on the same bolts used to attach the stopcock to the heater assembly. To put the device in place the thumbscrew must be removed from the upper flange of the greaseless stopcock; when in place the riser stem is tightened against the diaphragm stem using an Allen screw and this causes it to move with it. The vacuum seal is not affected since this is still

brought about by tightening the flanges of the stopcock around the diaphragm which seats against the top edge of the glass body (see fig. 2.6).

Pressure measurements during the runs were effected by means of a Consolidated Electrodynamics Model 4-326 low range sealed gauge pressure transducer; its location is indicated in fig. 2.6. The output of the device was found to be eratic if the stopcock heater was not in place; air currents in the lab caused noise on the recorder used to measure the output. Accordingly the transducer was maintained at 44 $\pm$ 1°C during all runs and calibrations, by means of the stopcock heater. Calibrations performed at 38°C in the most sensitive range (10 volt input) were found to give indistinguishable results.

The measuring side of the pressure transducer is provided with a $^1/4$ in. B.S.P. cone fitting. A suitable socket was brazed to the covar side of an approximately 0.1 in. i.d. covar-glass graded seal and connected to the transducer. The glass side of the tube was in turn connected to the reactor inlet line as shown in fig. 2.6.

2.1.5 Pressure Transducer Measurements and Calibrations

The pressure transducer incorporates an unbonded strain gauge sensing element balanced by an unspecified reference pressure of dry, non-corrosive gas. Pressure variations are indicated by the variation in resistance of one arm of a Wheatstone Bridge. A regulated maximum of 12^{V} D-C or A-C is supplied to the bridge and the inbalance can be measured by suitable potentiometric methods.

The control circuitry for the transducer is described in fig. 2.9. It has a facility for 'backing off' a portion of the output signal using a constant voltage Malloy cell (1.3505 volts), so that the full range of the recorder used to indicate pressure changes during runs may be made a suitable small fraction of the transducer range.

Runs and calibrations were performed using 2, 3.05, and 10 volt regulated D-C input. This was provided by Ether transformer-rectifier modules taking 230 volt A-C mains supply. The units are described as follows:

Unit	Nominal Output
Model XBH 10/30	10^{V}, 30 m.a. D-C
Type EB.01	3^{V}, 10 m.a. D-C
Type EB·01 + 175 ohm resistor	2^{V}, 30 m.a. D-C

Transducer Zeroing & Backing-Off Circuit.

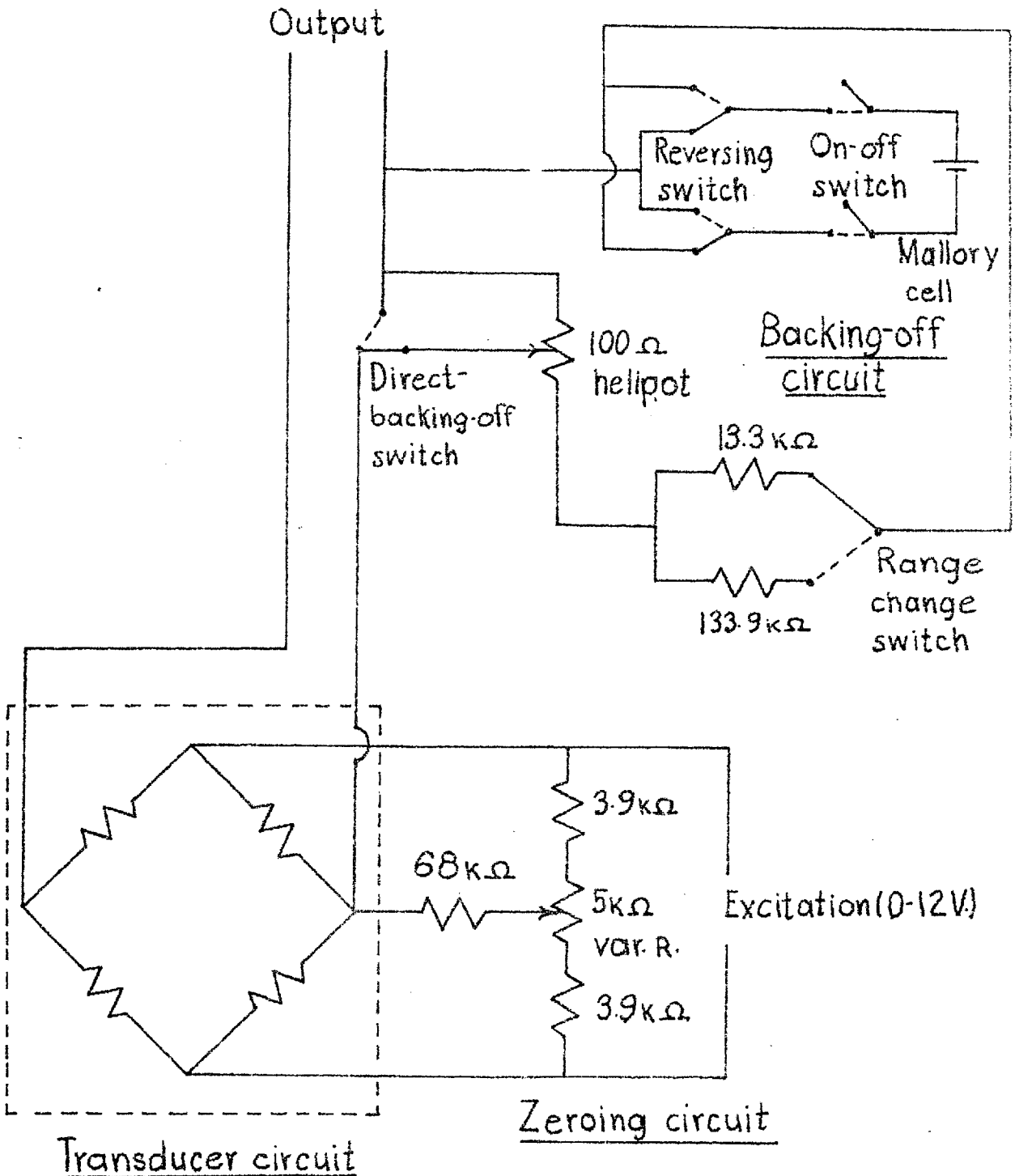

Figure 2.9.

The output of these modules could be adjusted within a fraction of a volt of the nominal value. The output was checked using a Universal precision potentiometer (Pye Cat. No. 7565) and a voltage division arrangement as follows:

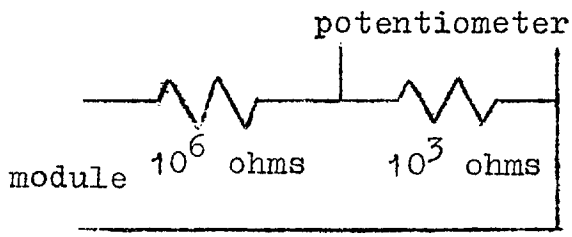

The resistances were provided by decade resistance boxes with accuracy better than 0.1%.

A correction had to be applied to the transducer output measured on the Honeywell recorder due to the current drawn by its 10K ohm bridge. For the 1 m.V. full scale range of the recorder this correction is 10.43 chart inches per m.V. Thus a recorder reading in inches divided by this figure gives the true reading in m.V.

The sensitivity of the transducer for a given input was found not to vary with pressure. The calibration figures used to calculate the results are as follows:

Input volts	Sensitivity cm./m.v.	Std. Deviation (No. of trials)	Range Covered cm.
2.000	5.738	0.009 (5)	29.4 - 58.4
3.000	3.770	0.012 (15)	10.5 - 71.0
10.000	1.144	0.014 (28)	0.5 - 18.9

Sensitivities are expressed in cm. of H_ε absolute per m.v. of transducer output. They are not linearily related to input. The normal variation of the Ether module outputs (less than .01 volt) had an insignificant effect on the results; it was necessary to allow 3-4 hours connection to the mains for this output to stabilize however. The above sensitivities compare well with the manufacturer's calibration:

> 45.10 m.v. output for 10 p.s.i. pressure with 10 volt excitation at 25°C (equiv. to 1.147 cm./mv.)

The calibration figures were checked periodically along with the voltage of the Mallory cell. The pressure 'backed off' with the mallory cell was controlled with a 100 ohm helipot (see fig. 2.9) having 10 main divisions, each with 100 sub-divisions. The sensitivity of this arrangement was 1.042 cm./main division. The recorder calibration was periodically

checked by determining the signal for a known pressure on the transducer.

Calibrations of the transducer were made using oxygen free nitrogen from the supply to the chromatograph, put into the vacuum system with the sampling device of the analysis section (see fig. 2.2). The known pressures indicated on the 1 cm.i.d. wide bore manometers whose relative location are shown in fig. 2.6, were read with a cathetometer to 0.01 cm.; these figures were compared to the transducer output read on the precision potentiometer. This instrument was used with a galvanometer modulator (Pye Cat.No. 11353), amplifier indicator (Pye Cat. No. 11343) and standard (cadmium) Weston cell (Pye Cat. No. 8655/T).

2.1.6. Temperature Measurement and Control

The reactor arrangement of fig. 2.6 shows the furnace used to keep the reactor at the desired temperature. The pyrex reactor itself was placed near the centre of a 24 in. long, 2 1/8 in. i.d. silica pipe on which were wound the heating coils of the furnace. The pipe was first covered with three layers of asbestos paper and then the main heating coil of 4.14 ohms/yd. nicrome resistance wire was wound on as described

in A of table 2.1. The pipe was then covered with about a 1/8 in. thick layer of cement made from about 40% chopped asbestos paper and 60% alumina cement. The tube was left to dry for about four hours before an electric heater was turned on beside it. After several hours of this drying with repeated turning to face the heater, the pipe was left overnight until the cement was firm enough to put on the auxiliary heating coils. After covering the pipe again with several layers of asbestos paper, further coils of resistance wire were wound on as described in B of Table 2.1. The rate of coiling for each of the main and auxiliary heater elements is the same at each end of the pipe. A piece of thin Platinum wire (for use as a thermometer) of total resistance about 10 ohms and length about 1 yd., was coiled onto the centre 3 in. of the pipe as indicated in C of Table 2.1. The whole was again covered with a thickness of about 1/8 in. of asbestos-alumina cement and the tube left overnight to dry. The bulk of the remaining moisture was then driven off with an electric heater and the whole baked in a glass annealing oven at about 600°C for several hours.

The pipe was then placed in a furnace box $11\frac{1}{2}$ in. wide, 12 in. high, and 24 in. long (see fig. 2.6) and

Table 2.1. Location of Heating and Platinum Resistance Thermometer Coils

Coil Rate	Distance from end of Silica Tube (inches)														
	0	1	2	3	4	5	6	7	8	9	10	11	12	13	14
A: main heater (turns/in.)	0	0	7	6	5	4	3	3	3	3	3	3			
B: Aux. heater (turns/in.)			1	2	2	2	1								
C: Pt.resist. therm. (turns)												1	1	1	

packed around with ceramic bricks. Spaces were filled with brick powder, asbestos rope, or asbestos wool. The ends of the Pt resistance wire were brazed to tungsten rods which were passed through holes in the bricks on top of the pipe. The tungsten rods were in turn connected with low resistance nickel wire to brass connectors on the side of the furnace box. Similar brass connectors were provided separately for the main and auxiliary heating coils.

The circuitry of the heating and temperature control system is shown in fig. 2.10. The controller is an A.E.I. Type R.T.3. Resistance Thermometer device and the variac a Phillips type E401 AE080, 8 amp transformer. The main coil has a resistance of 86 ohms and thus a maximum output of about 615 watts. The auxiliary coil has a resistance of 26 ohms; thus when connected in series with the main coil the maximum output is 470 watts or in parallel 2650 watts.

Control is effected when the R.T.3 device periodically bypasses the 50 ohm rheostat. The setting of the rheostat is adjusted to give a suitable ratio of the 'mark/space' current to the heater coil.

The temperatures required during the experiments were relatively low (less than 325^{o}C) and only the main

Furnace Heating Circuit.

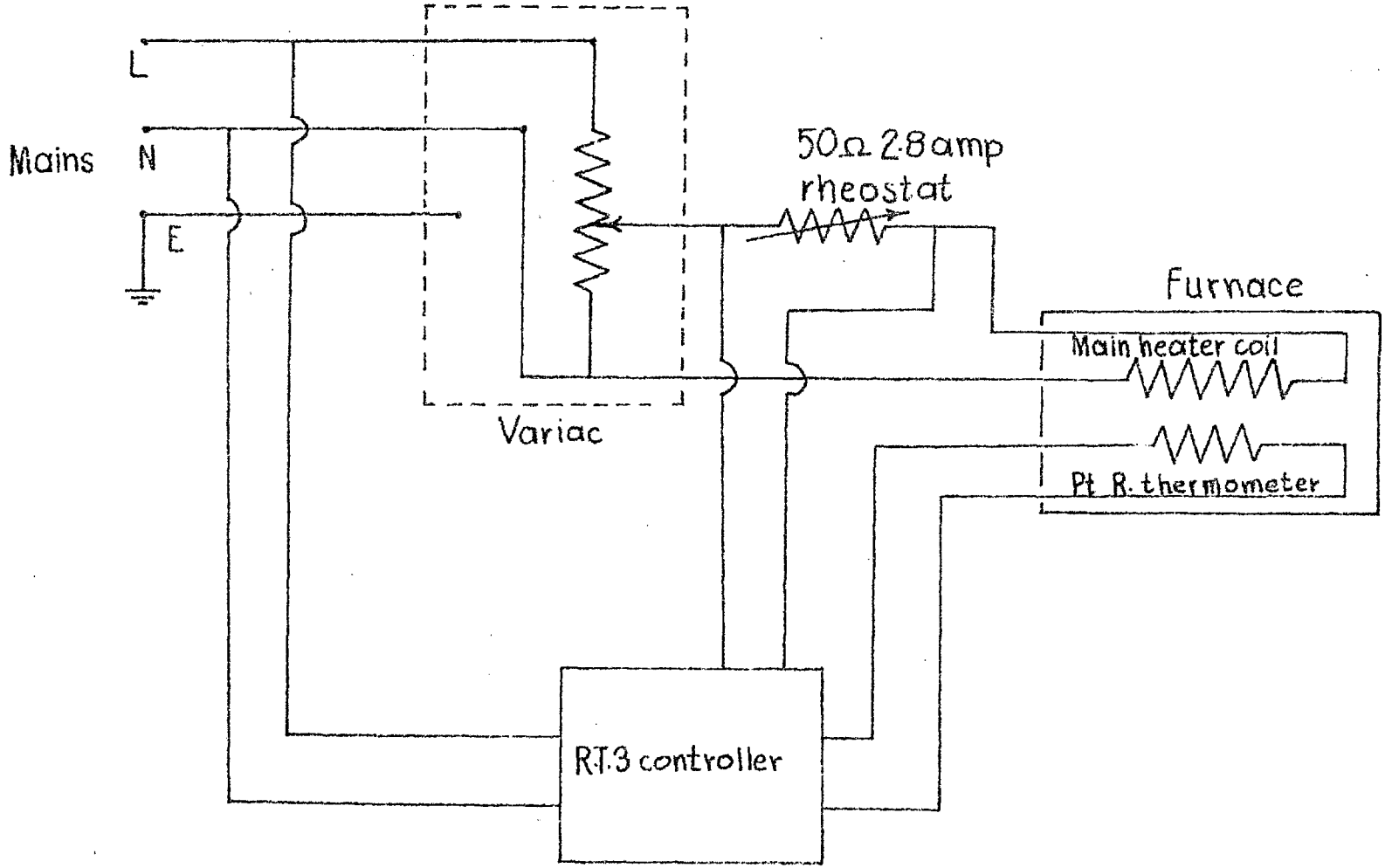

Figure 2.10

heating coil was used. It was found necessary to compensate for the heat losses through the copper pipe greaseless stopcock assembly by placing a piece of copper pipe in the other end of the silica pipe (see fig. 2.6); this evened out the heat losses at either end and a constant temperature zone could be found for the reactor.

With the reactor in place in the silica pipe, two thermocouples were placed in the thermowell: one at the end of the well and one near the inlet about $^{1}/_{2}$ in. inside the well. The remaining space inside the silica pipe was then stuffed with asbestos wool.

Three chromel-alumel thermocouples designated (A, B and C) were calibrated for use in the experimental work; the results of the calibrations are as follows:

Calibration	Melting Point °C	Thermocouple Output (m.v.)		
		A	B	C
Tin	231.9	9.425 ± .002	9.425 ± .002	9.421 ± .002
lead	327.4	13.311 ± .005	13.322 ± .0025	13.331 ± .001
zinc	419.4	17.155 ± .004	17.165 ± .004	17.213 ± .004

The calibrations were obtained using 'Analar' tin, lead and zinc; the cold ends were kept in an ice packed thermos bottle. Each result is from several measurements both heating and cooling the sample. Outputs were measured with the precision potentiometer. From the results of these calibrations the following relationships were derived assuming a straight line variation of m.v. output with temperature:

Thermocouple A: $T = 24.575 \times (m.v.) + 0.20$

Thermocouple B: $T = 24.505 \times (m.v.) + 0.90$

These equations relate the observed m.v. reading to the temperature T (^{o}C) between 231.9 and 327.4, the two calibration points used to derive the equations. All quantitative runs were done with thermocouples A and B and in the range 230 - 320^{o}C. For convenience the straight line equations were plotted on graph paper so that the temperature could easily be read to 0.1^{o}C. When literature values for chromel-alumel thermocouples (150, P.E48) were plotted on these graphs, they appeared closely scattered about the lines; there is no curvature indicated by the literature points and no such correction was applied.

Since 0.004 m.v. represents about 0.1^{o}C, the combined uncertainty from the calibrations and melting

points of the calibration materials should not be greater than 0.15°C. The control arrangement was found to give good temperature stability, even over the longest runs (60 min.). A greater cause of uncertainty in the measured reaction temperature was due to cooling by starting material when entering the reactor. In figures 2.11 and 2.12, some temperature readings from the thermocouple at the end of the thermowell for a series of experiments at low and high temperatures are given. The absolute temperature is not known with the accuracy depicted; however the potentiometer can be read precisely to 0.0005 m.v. so that changes of about 0.01°C should be observable. In figure 2.11 the readings from the early part of the runs (up to 3 minutes) have been plotted on a different scale compared to the later readings. The later results indicated the degree of stability for the longest runs used; the run at 22.91 cm. was the worst stability observed. The other runs are typical of the usual variation. In both figures 2.11 and 2.12 the readings have been extrapolated to the time when reaction was terminated. The reading at time zero is taken just before reactant is admitted to the reactor.

The results are a bit difficult to interpret when

Variation of Thermocouple Reading with Time.

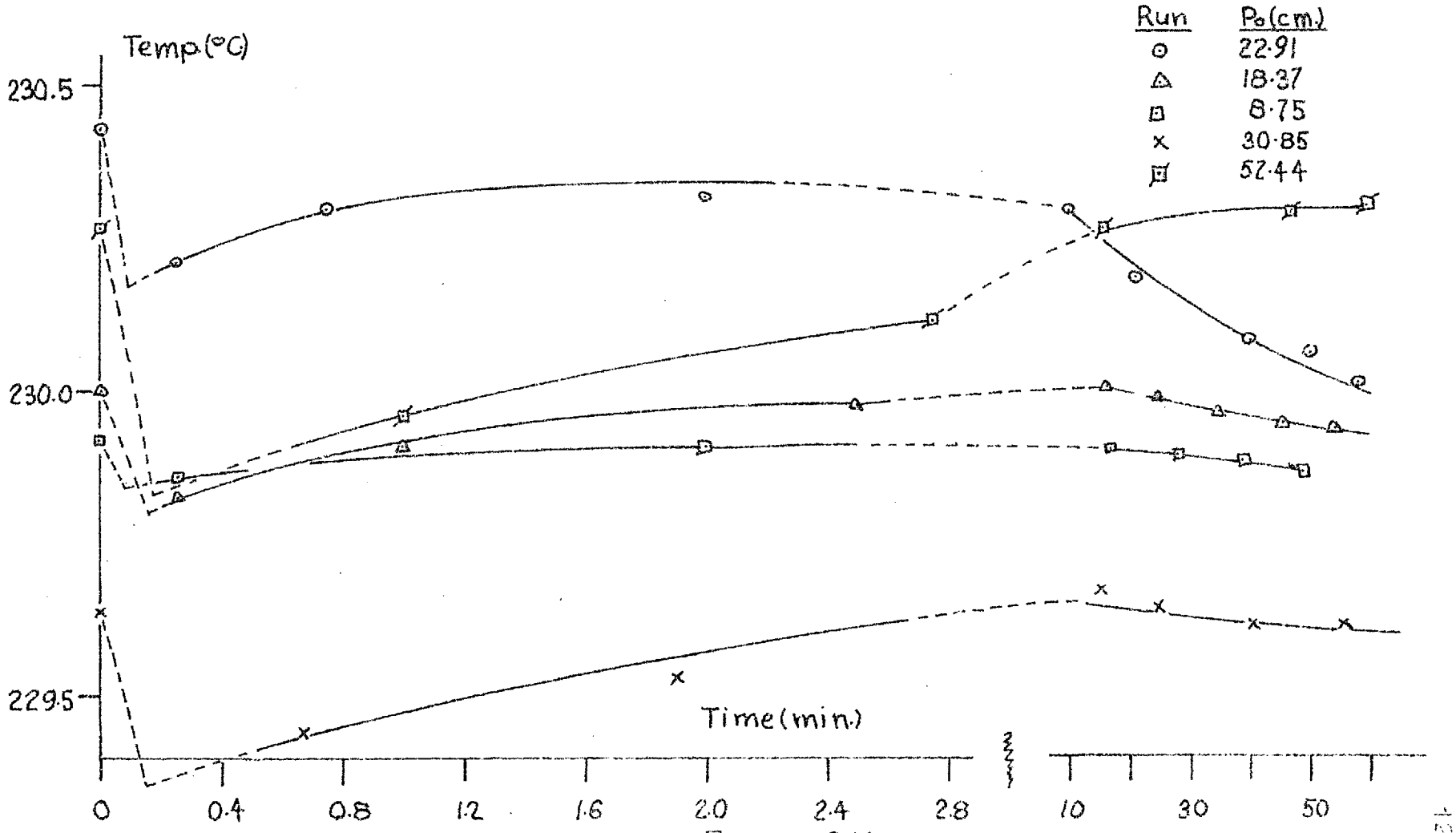

Figure 2.11.

Variation of Thermocouple Reading with Time.

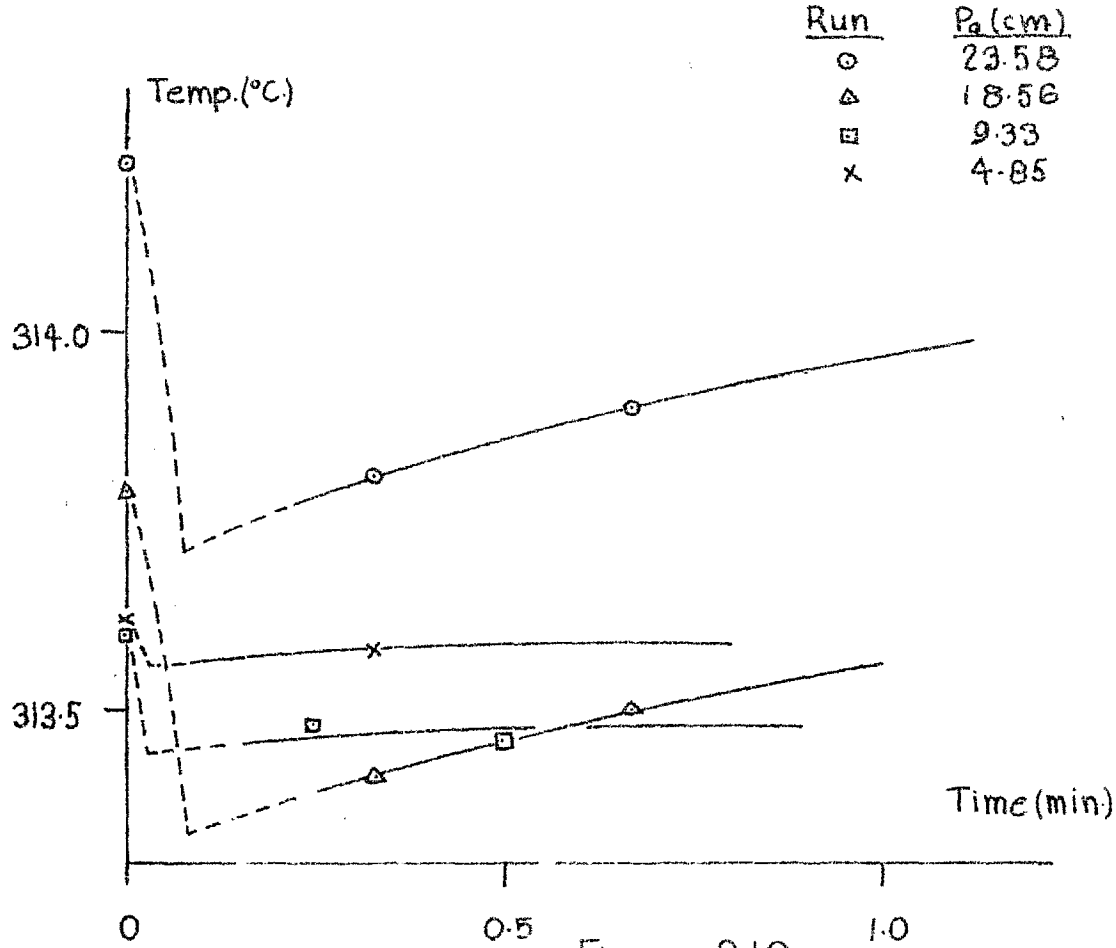

Figure 2.12

it is uncertain how well the thermocouple represents the reactor temperature at the instant a reading is taken. The tip of the thermocouple is up against the glass but sitting in the stagnant air of the thermowell. The glass of the thermowell itself is a good insulating material. However it is apparent that above 10 cm. pressure a significant drop in temperature is observed. At the higher temperatures the time (perhaps 15 sec.) to come to temperature equilibrium is significant, and the uncertainty in the average reaction temperature may be as high as several degrees. At temperatures and pressures where the time required to come to equilibrium is not significant, the combined uncertainties in the reaction temperature should not be greater than $0.3^{\circ}C$. This takes into account the maximum observed difference between the two thermocouple readings ($0.2^{\circ}C$); an average of the two readings is usually taken.

2.1.7. Low Pressure Experiments

For experiments below 0.5 cm. it was not practical to use the potentiometric recorder to obtain a continuous record of pressure changes during a run. Below 0.5 cm. the output from the transducer with the maximum input of 10 volts was too small for accurate measurement with the

recorder on its most sensitive (1 m.v.) range. It was found to be better in the range 0.5 - 0.05 cm. to measure the output of the transducer directly with the potentiometer. Results in this range and at lower pressure could be obtained by terminal analysis of products.

The reactor arrangement used at high pressure was found unsuitable for use below 0.05 cm. pressure. The size of sample which was obtained for analysis was found to be too small even if the entire products were injected into the chromatograph. The capillary inlet to the reactor offered such a constriction that only a minor part of the reaction products would be condensed out after a reaction. In one run at a starting pressure of 0.033 cm., pressure transducer measurements indicated that after 30 seconds open to a liquid nitrogen cooled trap at the end of the run, only 43% of the material in the reactor had been condensed out.

The furnace which was in use permitted using reactors of greater length only. A reactor of twice the volume was installed but found to have such a large temperature drop across it (about 10°C) to be of no practical use; the furnace has a constant temperature zone of only about 7 in.

A new furnace was brought into use which permitted

the use of larger reactors and shorter inlet lines. The furnace was machined from an aluminium block about 6 x 6 x $8^1/2$ in. long. Blocks $1^1/2$ in. thick were cut from each end and a cylindrical hole 5 x $3^1/4$ in. machined in the remaining centre portion. The result is sketched in figure 2.13. Grooves about $^5/16$ in. deep and $4^3/4$ in. long were machined into the corners of the outside of the centre portion to facilitate the winding on of heating coils. After covering the outside with asbestos paper, about 44 ohms of 2.5 ohms/yd. nichrome wire was wound on and the whole covered with alumina cement. A groove was cut on the inside of the centre portion to position a Pt resistance thermometer for use with the temperature controller. The block which formed the back end of the furnace had a hole cut in it to pass the Pt-resistance thermometer and another in the middle as a thermocouple inlet. The block at the front end was cut in half so that it could be easily removed to change reactors. It has a hole in the centre which is for the reactor inlet. The three portions are held together by four 9 in. long stainless steel bolts. Four horizontal holes in the end blocks were cut near the surface to hold heating wire coils. About 20 ohms of heating wire was placed in each end.

Aluminium Furnace

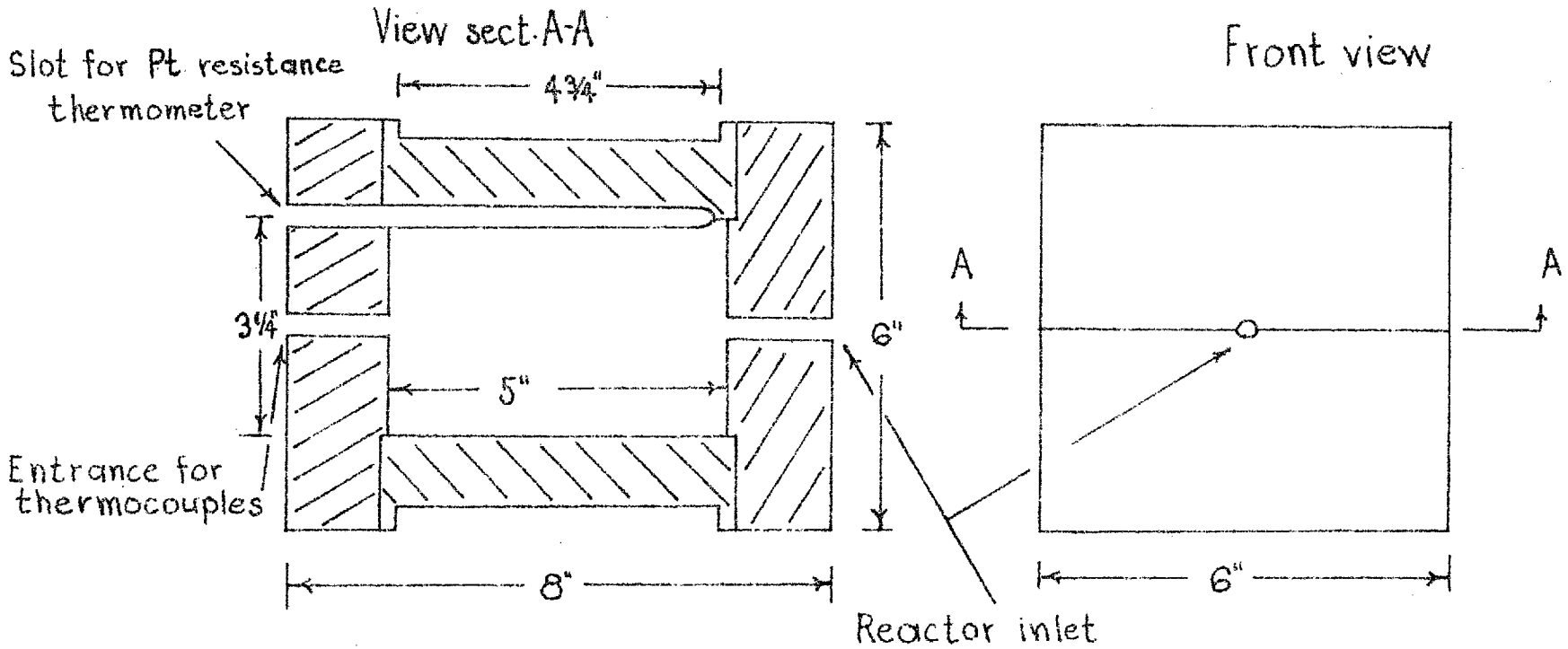

Figure 2.13

The heating wire from each section was run to separate connections on the box containing the furnace. This box was 12 in. wide, 12 in. high and 15 in. long; construction was of sindanyo board. The furnace was attached to a metal frame in order that it could be placed in the centre of the furnace box. The box was divided into two sections by a piece of sindanyo just behind the front end block of the furnace. The section behind this board and around the furnace was filled with alumina powder. The front end of the box was cut into two halves for easy removal while a reactor was in place; the section of the box in front of the dividing board was packed with asbestos wool which is not inconvenient to handle when a reactor is being replaced.

The furnace box was found to give quite insufficient insulation; at an operating temperature of 250°C the outside of the box was quite hot to touch. These losses undoubtedly contributed to the temperature variation in the reactor zone which was worse than expected. The cylindrical reactor which was made for use with this furnace was as large as possible; its external dimensions were 11 cm. long and 6.8 cm. diameter. An inlet line consisting of 3 cm. of 4.5 m.m bore tubing next to the reactor was connected to 12 cm. of 2 m.m. bore

tubing and then to a 2 m.m bore stopcock. Connection to the vacuum system was at the same location as the old reactor. A thermowell 7.5 cm. in length was constructed in the reactor and entered the middle of the back end. Thermocouples were placed in the thermowell in the middle of the reactor and just inside the entrance of the thermowell. A difference in reading from 0.4 - 0.6°C was experienced with the two thermocouples in runs at 230 and 253°C. The hotter temperature of the thermocouple in the middle of the reactor was always taken as the reactor temperature since it was uncertain how well placed the other thermocouple was.

The starting pressure of a reaction was achieved by expansion of reactant pressures, measured with the cathetometer, from the vacuum line into the reactor. The volume of the reactor was determined by weighing some purified C_2F_4 whose pressure and temperature in the reactor were known; the value found was 426.6 c.c., of which 0.135% was estimated to be dead space. Volumes of various sections of the vacuum system were determined in the same way so that several expansions could be carried out if a lower pressure was required. Because of the size of the reactor capillary inlet, thermal transpiration must be taken into consideration in

determining the true pressures.

Temperature stability was found to be as good at $\pm$ 0.15° over a day. It was necessary to achieve this degree of control as each run where final analysis results were used required several runs at the same starting pressures and temperatures but different reaction times.

It was found at low pressures (below 0.1 cm.) that as much as 25% of the sample collected from the reactor would not be condensed into the sample injection device (see fig. 2.2) even if the stopcocks were regreased frequently and the system well evacuated. Continual small leakage of N_2 from the carrier gas flow could not be avoided. To improve the 'efficiency' of getting the reaction products into the reactor, the spare connection on the left hand side of the upper stopcock of this device was connected to the main vacuum line. A stopcock was placed in this connecting line just by the sampling device. Thus when most of the sample had condensed into the sample loop from the gas handling section, the loop could be pumped through to get as much of the material as possible from the line frozen in.

2.2 Preparation of Reagents

Tetrafluoroethylene was purified from the pyrolysis products of polytetrafluoroethylene. Perfluorocyclopropane was prepared by the mercury photosensitized reaction of tetrafluoroethylene. Preparative scale chromotography was found to be the best method of purifying these substances. The procedures for preparing, purifying and analyzing the materials under study are described.

2.2.1. Preparation of Tetrafluoroethylene

Polytetrafluoroethylene waste turnings were pyrolized to produce C_2F_4. These were placed in a pyrex tube about 6 in. long and $^3/_4$ in. diameter which was connected to the vacuum system at the B-10 joint of A, fig. 2.1. A hand torch without pressurized air or oxygen was used to heat the tube; a bunsen flame was found to be too hot as it softened the tube. Products of pyrolysis were collected in a liquid nitrogen cooled trap of the handling section (see fig. 2.1); the trap was pumped through continueously to collect the products, to eliminate any non-condensables. It is important that the pressure be kept low in the system as above 150 m.m.

a significant increase in $CF_3 \cdot CF = CF_2$ produced is known to occur (53), and the dimerization of C_2F_4 to $c\text{-}C_4F_8$ is encouraged.

The pyrolysis products of the polymer were found to contain about 5% $CF_3 \cdot CF = CF_2$, 1% $c\text{-}C_4F_8$ and trace quantities of perfluorobutenes in the main product C_2F_4. There is chromotographic evidence from the analysis of a concentrated C-3 fraction that trace quantities of $c\text{-}C_3F_6$ are also present. The impurities can be substantially removed by trap to trap distillation using melting pentane. However, trace quantities of $CF_3 \cdot CF = CF_2$ invariably remained. This is concentrated in the photochemical reaction and as it was desirable to have completely $CF_3 \cdot CF = CF_2$ free $c\text{-}C_3F_6$ (the former is a possible product of the latter's decomposition), preparative chromatography was used.

In preparing pure C_2F_4 chromatographically, the preparative column was operated at 150°C with a carrier gas flow rate of 60 c.c. N_2/min. Approximately one gram samples of crude C_2F_4 at a time were condensed into the sample loop (see fig. 2.2), and injected into the column. The last impurities are removed from the column in about one hour. $CF_3 \cdot CF = CF_2$ concentration is reduced below detectable limits using the hydrogen flame detector. A

typical chromotogram from this procedure is shown in fig. 2.14. In fig. 2.15, a chromotogram of concentrated residues from the purifications by trap to trap distillation is given.

2.2.2. The Mercury Photosensitized Reaction of C_2F_4

The main product of this reaction is polytetrafluoroethylene with c-C_3F_6 a substantial side product. Atkinson (55, 111) has shown that the rates of both reactions increase with temperature, and pressure of C_2F_4; the polymer formation increases with its accumulation.

Several apparatus similar to that shown in fig. 2.16 were constructed to carry out the reaction on a large scale. The globe shown had a capacity of one litre and the heated asbestos pipe could be operated with two of the apparatus in place at once. Each was constructed of pyrex glass with a silica window which passed the 2537 Å light from the mercury lamp. Under typical operating conditions, an apparatus was filled to about 35 cm. with starting material C_2F_4 after connection to the vacuum system and evacuation. It was then placed in the asbestos pipe holder and left for about ten days at 80°C. The apparatus was then reconnected to the

Chromatogram of Products from Polytetrafluoroethylene Pyrolysis on Preparative Column.

Conditions:

Column: 1 cm. id. pyrex 9 ft. long
packing: 100/120 mesh silica gel
temp: 150 °C

Detector: thermal conductivity
temp: 125 °C
bridge current: 120 m.a.
column simulator flow: 45 c.c./min. (N_2)
sensitivity: 10%

Carrier gas: N_2
flow: 60 c.c./min.

Recorder: 10 m.v. range

Sample size: approx: 1.0 gm.

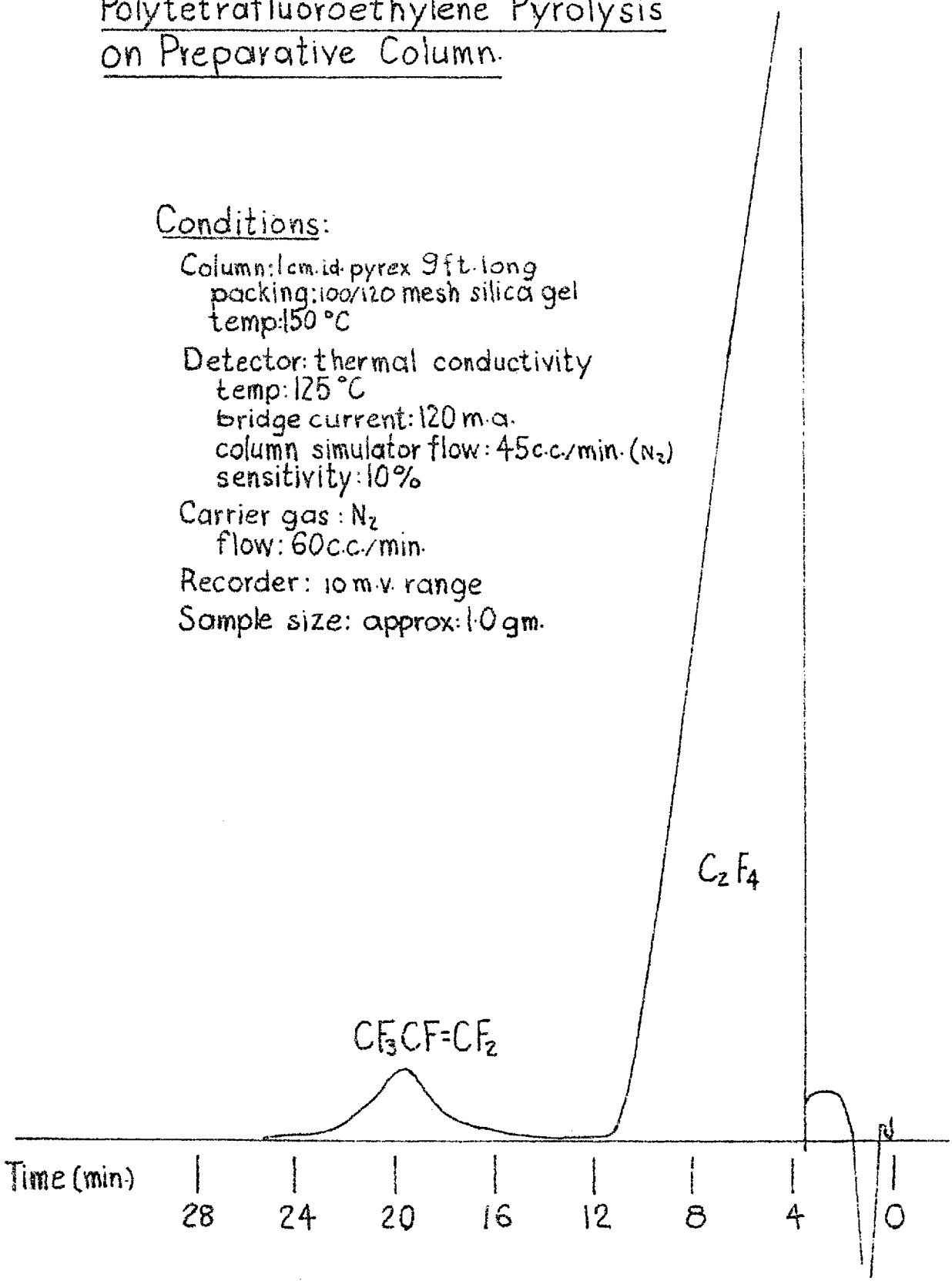

Figure 2.14

Chromatogram of Residues from Purification of C_2F_4 in Polytetrafluoroethylene Pyrolysis Products.

Conditions:
as in fig. 2-14

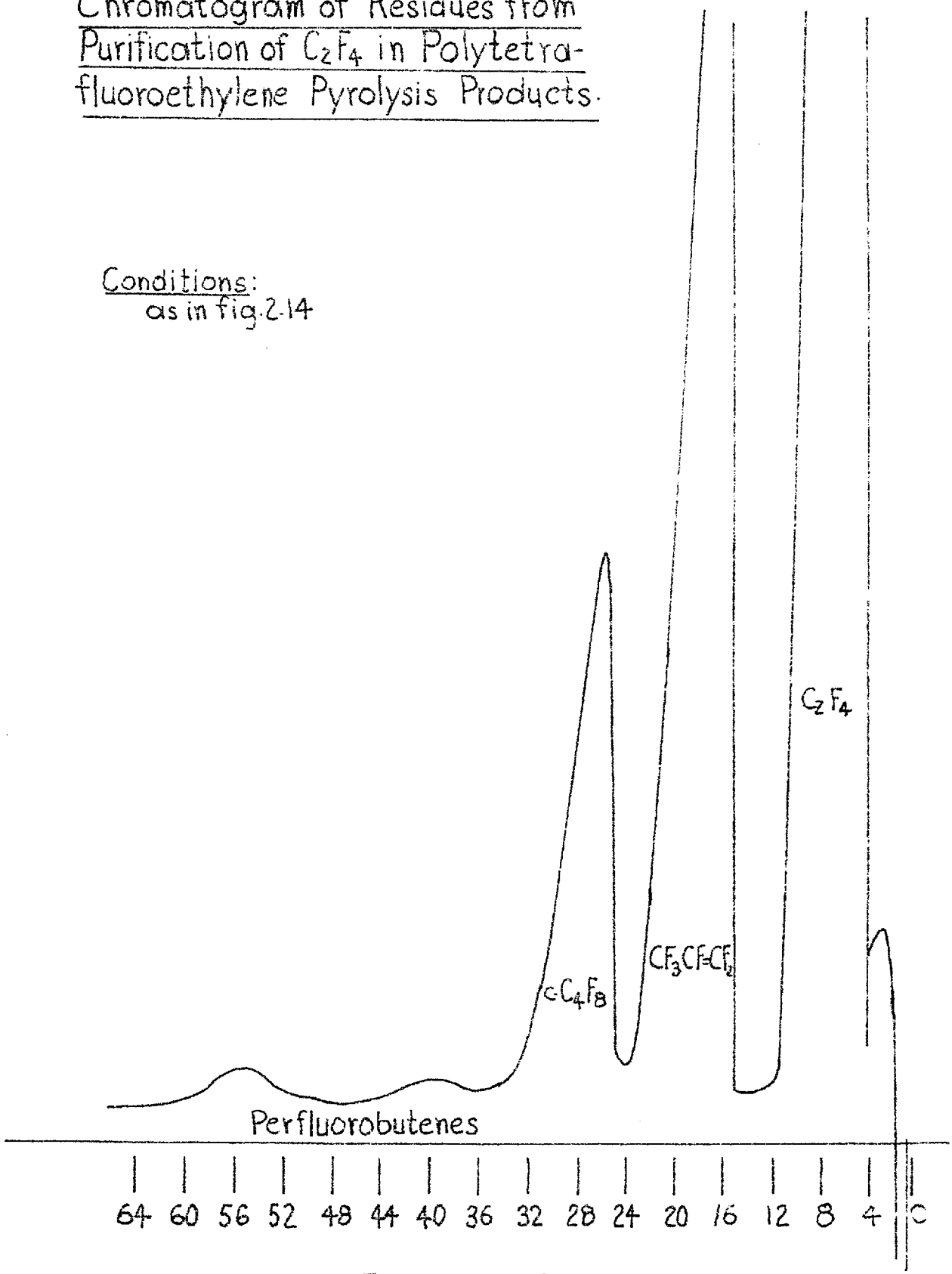

Figure 2-15

Apparatus for Photolysis of C_2F_4.

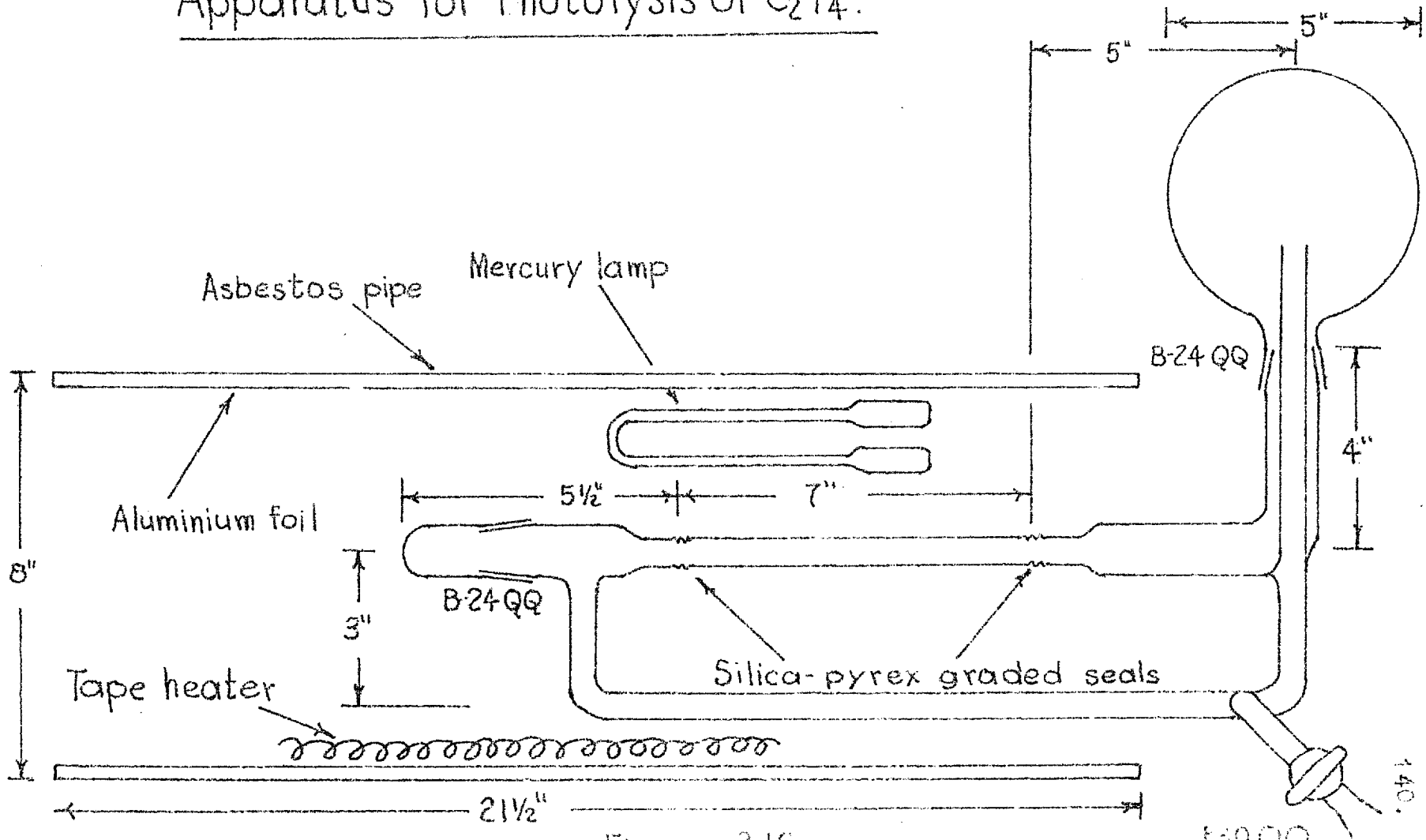

Figure 2-16

vacuum line and volatile products collected. The silica window was then scraped clean of accumulated polymer and the cycle repeated.

C_2F_4 was recovered from the volatile products and reused. It was observed that yields of c-C_3F_6 improved after a time with continued recycling of unreacted C_2F_4. This was associated with a build up of an impurity in the recovered C_2F_4 which had a retention time just greater than C_2F_4 on both the analytical and preparative columns. No more than a semi-quantitative study of the effect was made but results are illustrated by two typical runs shown in table 2.2.

Table 2.2

Photolysis of C_2F_4 at 80°C.

	Starting press (cm. of C_2F_4)	Reaction time (hrs.)	C_2F_4 Reacted (%)	Yield on C_2F_4 % to polymer	Reacted % to c-C_3F_6
Pure C_2F_4 Starting Material	35	230	84	83	17
Starting with 0.2% impurity	25	170	78	45	55

The impurity was freed of C_2F_4 by allowing one photochemical reaction to proceed for about four weeks. The absence of C_2F_4 was confirmed by chromotographic analysis. An infra-red analysis performed on the material is shown in fig. 2.17. This was done on a Perkin-Elmer 'Infracord' machine using a fast scan. The cell had NaCl windows and a 10 cm. path length. Gas pressure in the cell was about 1 cm. The calibration absorptions are from polystyrene film. The nature of the impurity was not elucidated from the infrared analysis. The chromatographic retention time is however unquestionably that of a C_2 compound. A single peak is obtained on the analytical column at 125°C. When passed through the preparative column at 75°C, a chromatogram of at least four different nearly equal sized peaks is obtained.

2.2.3. Purification of $c\text{-}C_3F_6$.

$c\text{-}C_3F_6$ was isolated from the volatile products of the photochemical reaction using the preparative column. A typical chromatogram is shown in fig. 2.18. Operation was at 125°C until the C_2F_4 had been eluted and then at 150°C in order to speedily remove the octafluorocyclobutane ($c\text{-}C_4F_8$) which was found in trace quantities in the photochemical products. $c\text{-}C_4F_8$ is eluted from about

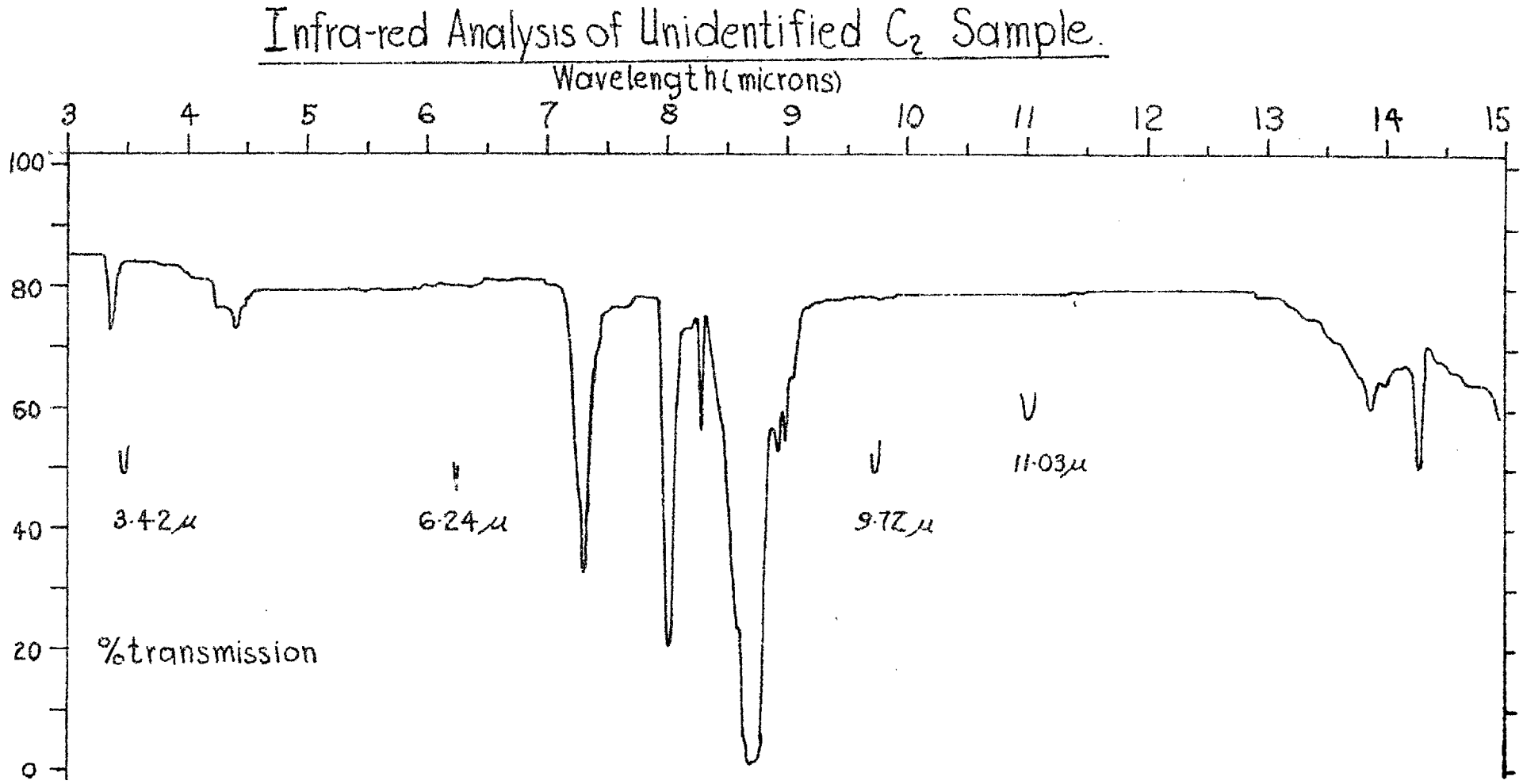
Infra-red Analysis of Unidentified C_2 Sample.
Wavelength (microns)
3
4
5
6
7
8
9
10
11
12
13
14
15
100
80
60
40
20
0
3·42μ
6·24μ
9·72μ
11·03μ
%transmission

Figure 2.17

Chromatogram of Products from Photochemical Reactor on Preparative Column.

Conditions:

Column: 9ft. long 1cm. id. pyrex
packing: 100/120 mesh silica gel
temp: 125-150°C.

Detector: thermal conductivity
temp: 125°C.
bridge current: 120 m.a.
column simulator flow: 10 cc./min (N_2)
sensitivity: 10%

Carrier gas: N_2
flow: 60 cc/min.

Recorder range: 10 m.v.

Sample size: 0.1 gm.

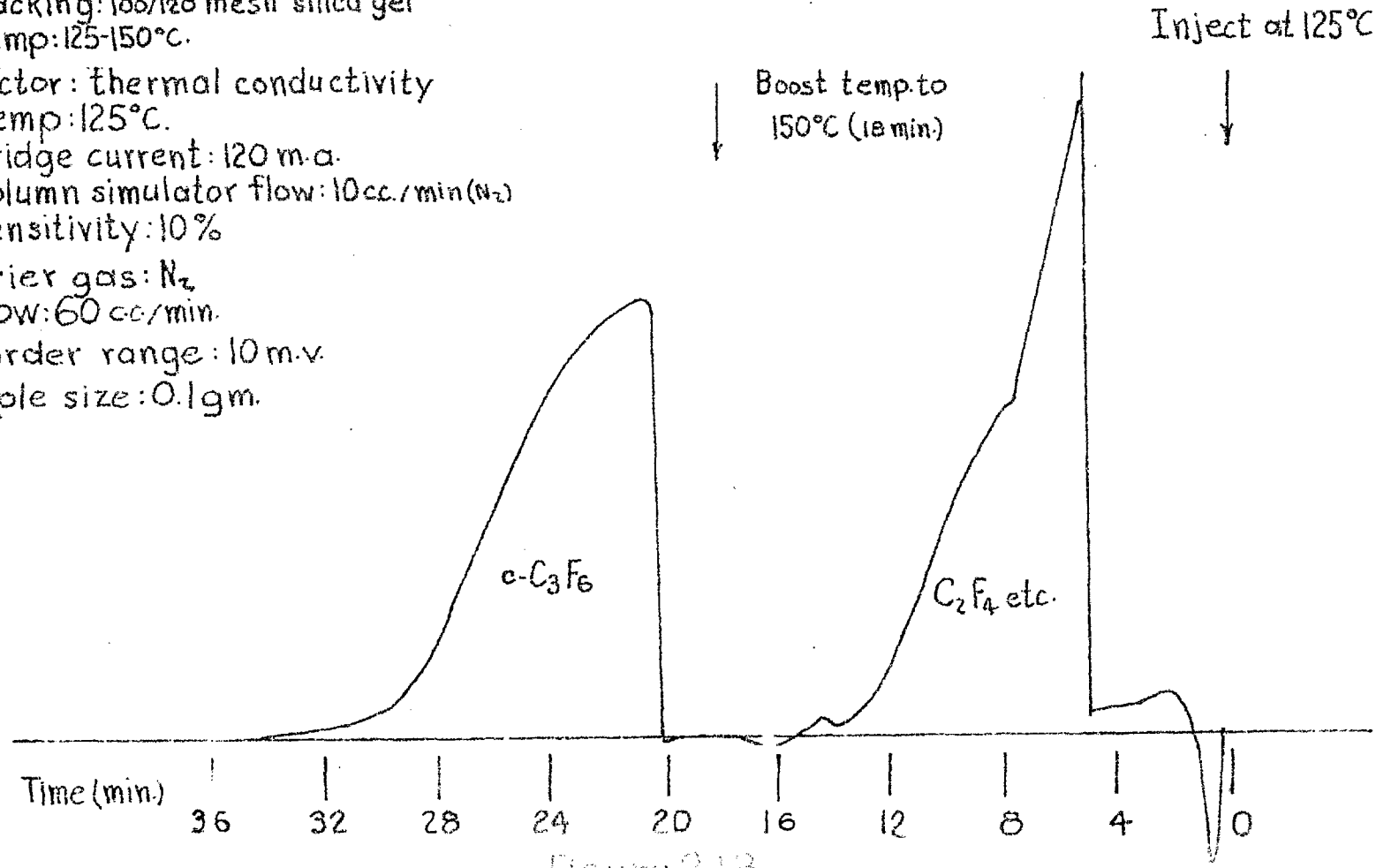

Figure 2.13

36 - 42 min. under the conditions used. The c-C_3F_6 could never be completely freed of C_2F_4, probably due to slight decomposition of the c-C_3F_6 on the column. However the level of C_2F_4 was less than 0.1% which was tolerable.

Trace quantities of $CF_3.CF = CF_2$ were found in the pyrolysis products of c-C_3F_6; this had to be removed before the unreacted c-C_3F_6 could be used in further reactions. After removing the main product C_2F_4 from the pyrolized c-C_3F_6 using conditions identical with the treatment of the photochemical products (fig. 2.18), $CF_3.CF = CF_2$ was removed chromatographically. As the retention time of $CF_3.CF = CF_2$ is only slightly greater than c-C_3F_6, reduced carrier gas flow was employed and considerably smaller samples injected. The series of successive injections of the chromatogram fig. 2.19 illustrate the procedure followed. About 50 cm. gas pressure in the approximately 10 c.c. sample loop was the maximum tolerable sample size before overloading of the column would hinder separation.

It should be pointed out that the retention times of the various substances are reduced under the same operating conditions, with the passage of time. The problem is only slightly alleviated by purging the

Preparative Chromatogram for Removal of Traces of $CF_3CF{=}CF_2$ from c-C_3F_6.

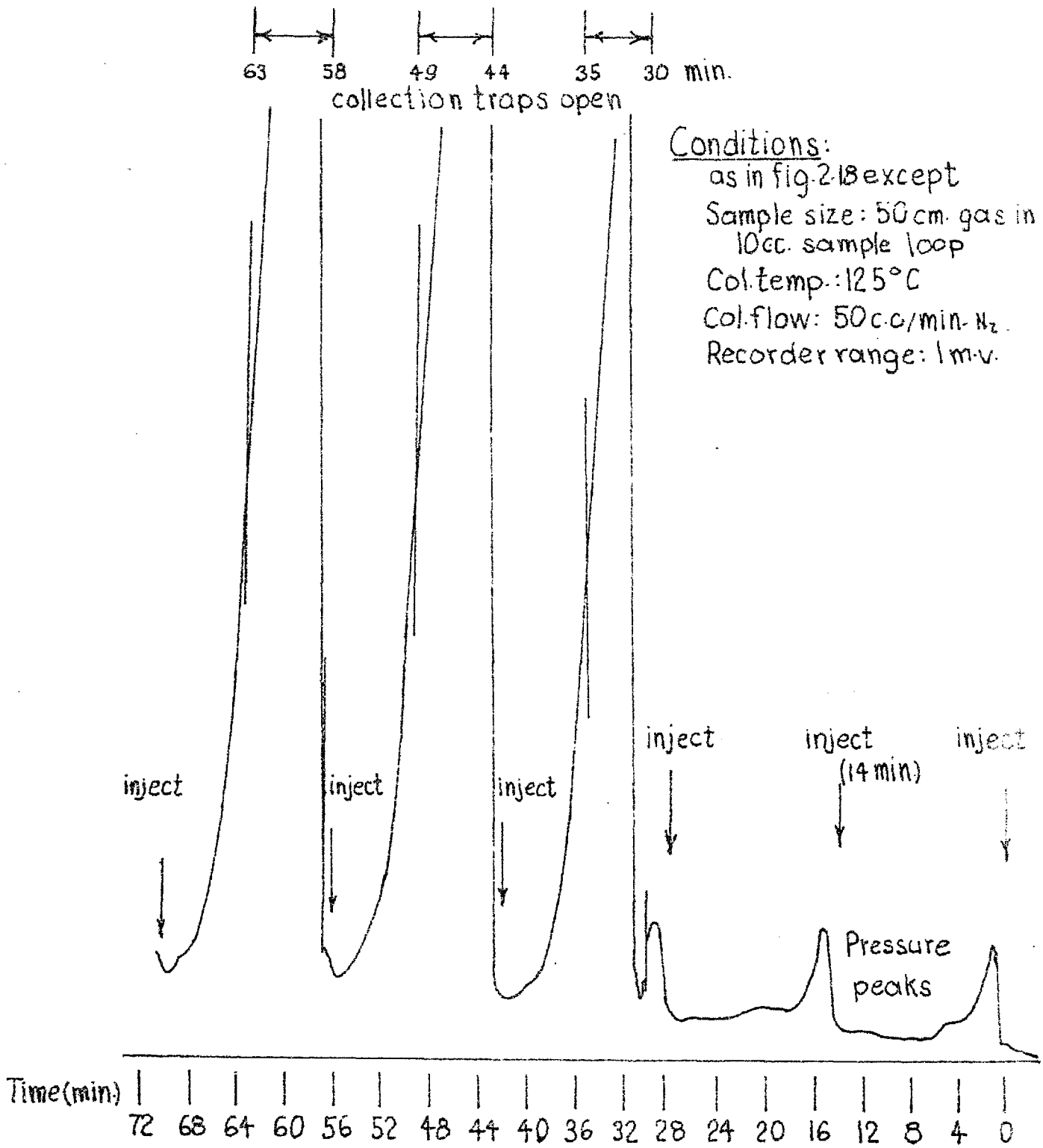

Figure 2.19

column at high temperature. Eventually the packing must be replaced.

2.2.4. Preparation of $CF_3Sn(CH_3)_3$.

Clark and Willis (75) have reported the formation of $c\text{-}C_3F_6$ in the pyrolysis of trimethyltrifluoromethyl tin either alone or in the presence of C_2F_4. The reaction may be described by the following sequence:

$$CF_3Sn(CH_3)_3 \longrightarrow CF_2 + F\,Sn(CH_3)_3$$

$$2\,CF_2 \longrightarrow C_2F_4$$

$$CF_2 + C_2F_4 \longrightarrow c\text{-}C_3F_6$$

as one route to the synthesis of $c\text{-}C_3F_6$, the procedure recommended by these authors was followed:

$$\text{(i)}\quad CH_3I \xrightarrow{Mg} CH_3I.Mg.$$

The Grignard is carried out in n-butyl ether

$$CH_3.I.Mg + SnCl_4 \longrightarrow (CH_3)_4\,Sn + MgCl + MgI$$

an excess of the Grignard is employed and the $(CH_3)_4Sn$ isolated by fractional distillation.

(ii) $3(CH_3)_4Sn + Sn\,Br_4 \xrightarrow{\Delta} 4(CH_3)_3\,Sn\,Br$

a slight excess of $Sn\,Br_4$ is used and $(CH_3)_3\,Sn\,Br$ is recovered by distillation.

(iii) $(CH_3)_3\,Sn\,Br \xrightarrow{Na} Na\,Br + (CH_3)_3\,Sn.Sn\,(CH_3)_3$

the reaction is carried out in liquid NH_3 and the hexmethyl ditin isolated by vacuum sublimation.

(iv) $(CH_3)_3\,Sn.Sn\,(CH_3)_3 + CF_3I \longrightarrow CF_3Sn(CH_3)_3 + (CH_3)_3Sn\,I.$

the reaction is carried out in a Carius tube which was left about 15 hours exposed to a Hg lamp. The tube was cooled in ice and the volatile products collected in the vacuum system.

When examined chromatographically, the products of reaction (iv) contained a large number of different substances. A middle boiling fraction was isolated from the products and a small amount of the principal constituent isolated by preparative chromatography; a 9 ft. long,

1 cm. i.d. column packed with di-octyl sebacate on celite was used at 75°C, with a N_2 flow of 70 c.c./min. Sample injections of about 0.2 c.c. were made and $(CH_3)_3$-$SnCF_3$ had a retention time of about 16 min. The identity of the substance as $(CH_3)_3$-$SnCF_3$ was confirmed by infra-red gas absorption analysis. Chromatographically the isolated substance seemd to be pure; no extraneous infra-red absorptions were observed. However the vapor pressure was higher than that published by Kaesz (139); for example a vapor pressure of 39 m.m. compared to 28 m.m. at 20°C was obtained. Small amounts of volatile impurities may still have been present. No further purification was attempted.

A reaction was carried out with some of the isolated $(CH_3)_3$ $SnCF_3$. The material was condensed into the nipple between the two greaseless stopcocks. The stop-cock heater was brought up to 41° before opening to the reactor which was at 152°C. The pressure in the reactor fell from an initial value of 5.53 cm. to 4.29 cm. after 15 minutes when the products were removed for analysis.

The products were largely unreacted $(CH_3)_3SnCF_3$. The volatile constituents were isolated and analysed. This fraction contained about 65% C_2F_4, 10% c-C_3F_6, and about 20% of an unknown substance which eluted before

C_2F_4. This unknown product was not reported by Clark and Willis. Larger yields of c-C_3F_6 could have been expected at higher pressures. This preparative procedure was not pursued since the photochemical reaction seemed simpler and less expensive.

2.3. Chromatographic Calibrations

Calibrations were performed on mixtures of perfluorocyclopropane and tetrafluoroethylene. Samples were prepared by measuring the pressure of each pure constituent in the sampling device (fig. 2.5) with the cathetometer. $CF_3.CF = CF_2$ had a different sensitivity than perfluorocyclopropane in the H_2 flame detector and could not be used to do the calibrations. The conditions used with the analytical column were as follows:

H_2 regulator outlet pressure: 8 lb.g.

Air regulator outlet pressure: 15 lb.g.

N_2 regulator outlet pressure: 30 lb.g.

N_2 flow: 60 c.c./min.

Column temp.: 125°C

Detector voltage: 50 V.

Recorder range: 10 m.V.

The identities of the peaks or chromatographic retention times of all the substances found in analysis were confirmed by injection of pure samples. The order of elution conformed with the observations of Greene and Wachi (112).

The relative sensitivity of the constituents in the calibration was found to vary considerably with sample size for the same sample. This had to be treated as a variable. A series of analyses were performed on each sample of known concentration using a wide range of sample size. A plot could then be made of peak area concentration against total area measured. On the final calibration graph which was a plot of peak area concentration against actual concentration a series of curves were drawn at intervals of total area selected from the curves drawn for each sample.

The output of the amplifier to the recorder could be attenuated by selection of the appropriate detector current range. The most sensitive range was 10^{-10} amps and the other available ranges were 3×10^{-10}, 10^{-9}, 3×10^{-9}, 10^{-8}, 3×10^{-8}, 10^{-7}, 3×10^{-7} and 10^{-6} amps. Peak area in the calibrations was expressed as the equivalent value at 10^{-10} amps by multiplying the peak area by the ratio of the actual current range to 10^{-10}.

One important fact which was observed for a large number of injections of the same sample at different attenuations was that within the uncertainty of the calibration figures this conversion procedure was found to give consistent results regardless of attenuation.

Details from the preparation of the samples used are presented in the following table:

Sample	Reagent Pressures (cm.)		Reagent Concentrations (%)	
	C_2F_4	$c\text{-}C_3F_6$	C_2F_4	$c\text{-}C_3F_6$
A	8.103	11.668	41.0	59.0
B	15.077	9.809	60.5	39.5
C	17.767	6.056	74.6	25.4
D	7.740	6.255	55.3	44.7
E	4.010	12.308	24.6	75.4
F	5.393	6.956	43.6	56.4

Since the individual pressures are accurate to about 0.01 cm. the accuracy of the concentrations should be known to at least $\pm$ 0.15%.

The integrator was used to measure the peak areas and the results for all the trial samples injected are plotted as total equivalent area at 10^{-10} amps against peak area % $c\text{-}C_3F_6$ in figs. 2.20 to 2.24. The spread of individual points around the curves drawn through them

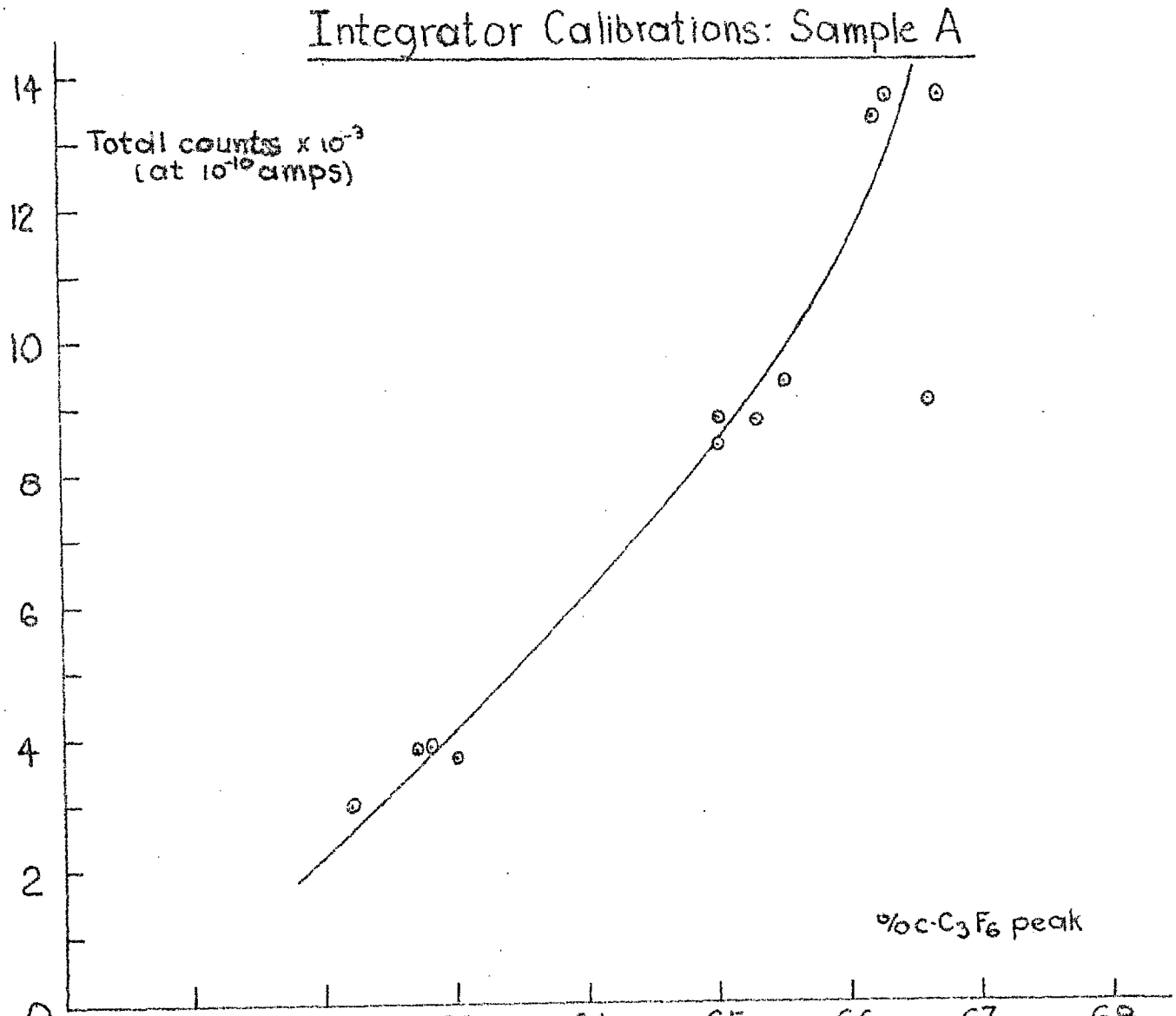
Integrator Calibrations: Sample A
Total counts x 10^{-3} (at 10^{-10} amps)
14
12
10
8
6
4
2
0
61
62
63
64
65
66
67
68
% c-C_3F_6 peak

Figure 2.20

Integrator Calibrations: Sample C

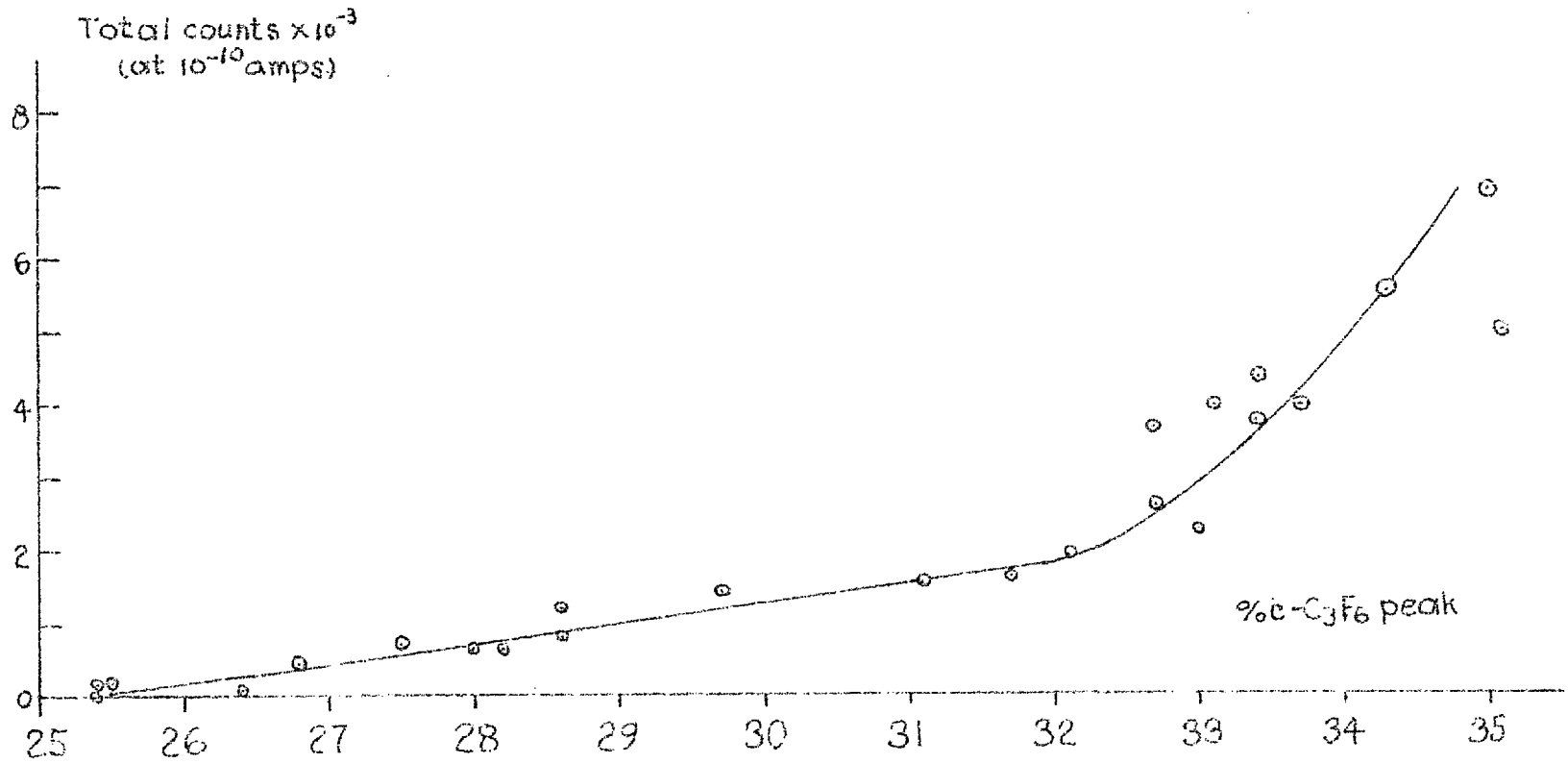

Figure 2.21

Integrator Calibrations: Sample D

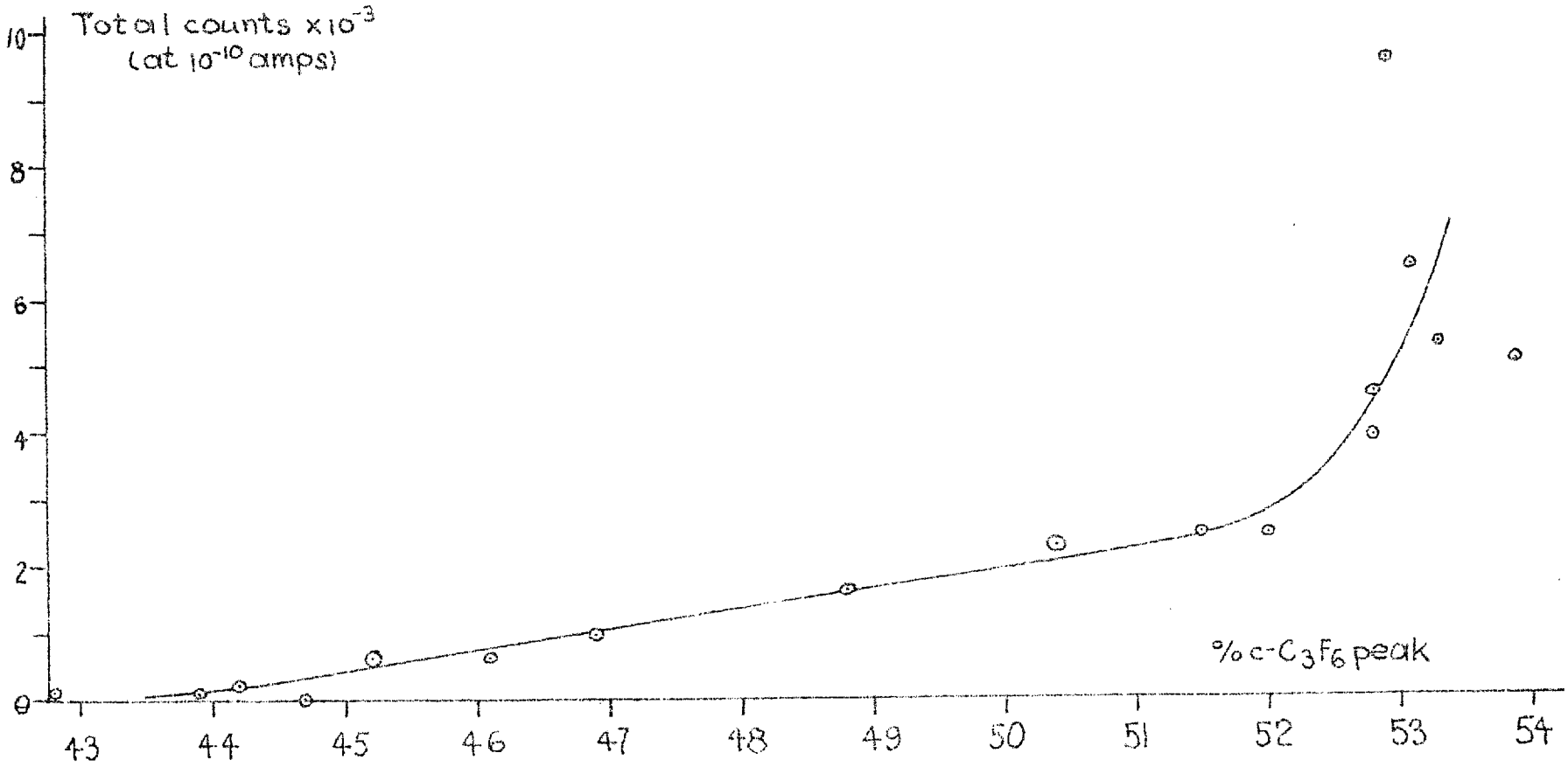

Figure 2.22

Integrator Calibrations: Sample E

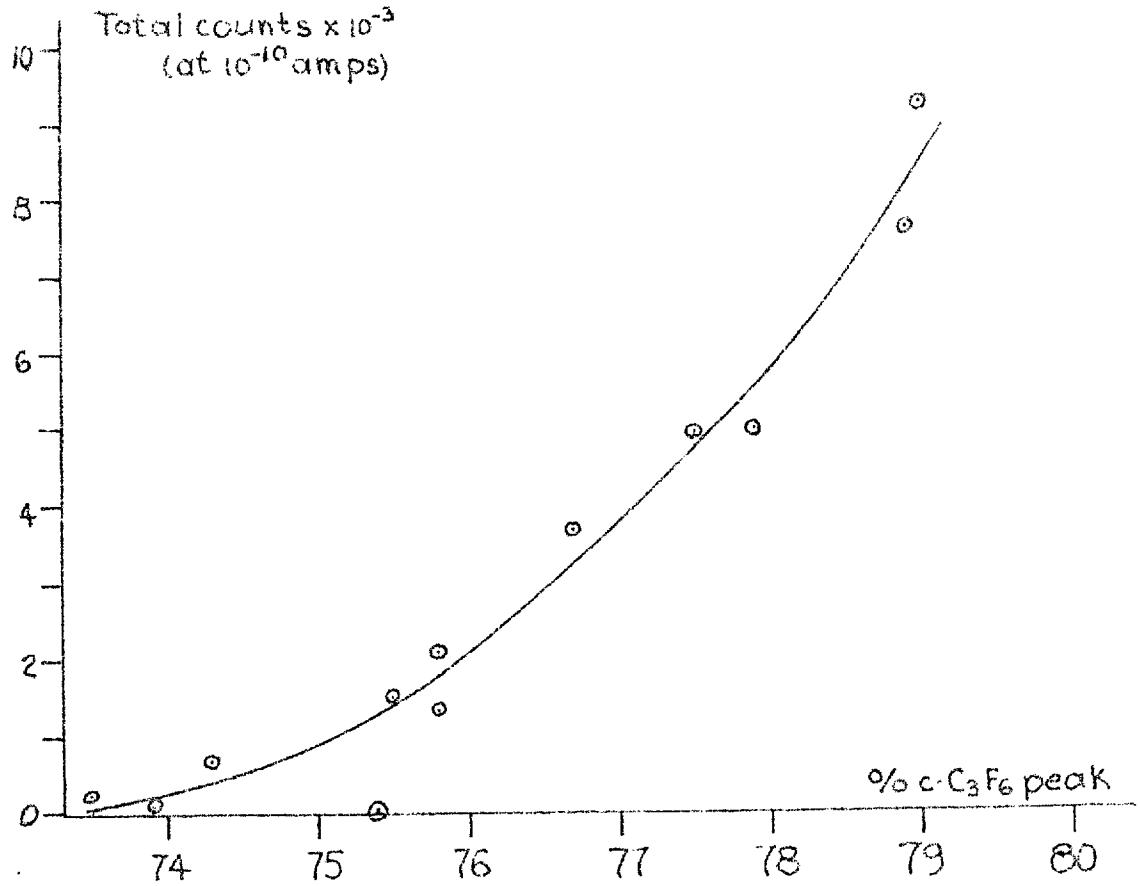

Figure 2.23

Integrator Calibrations: Sample F

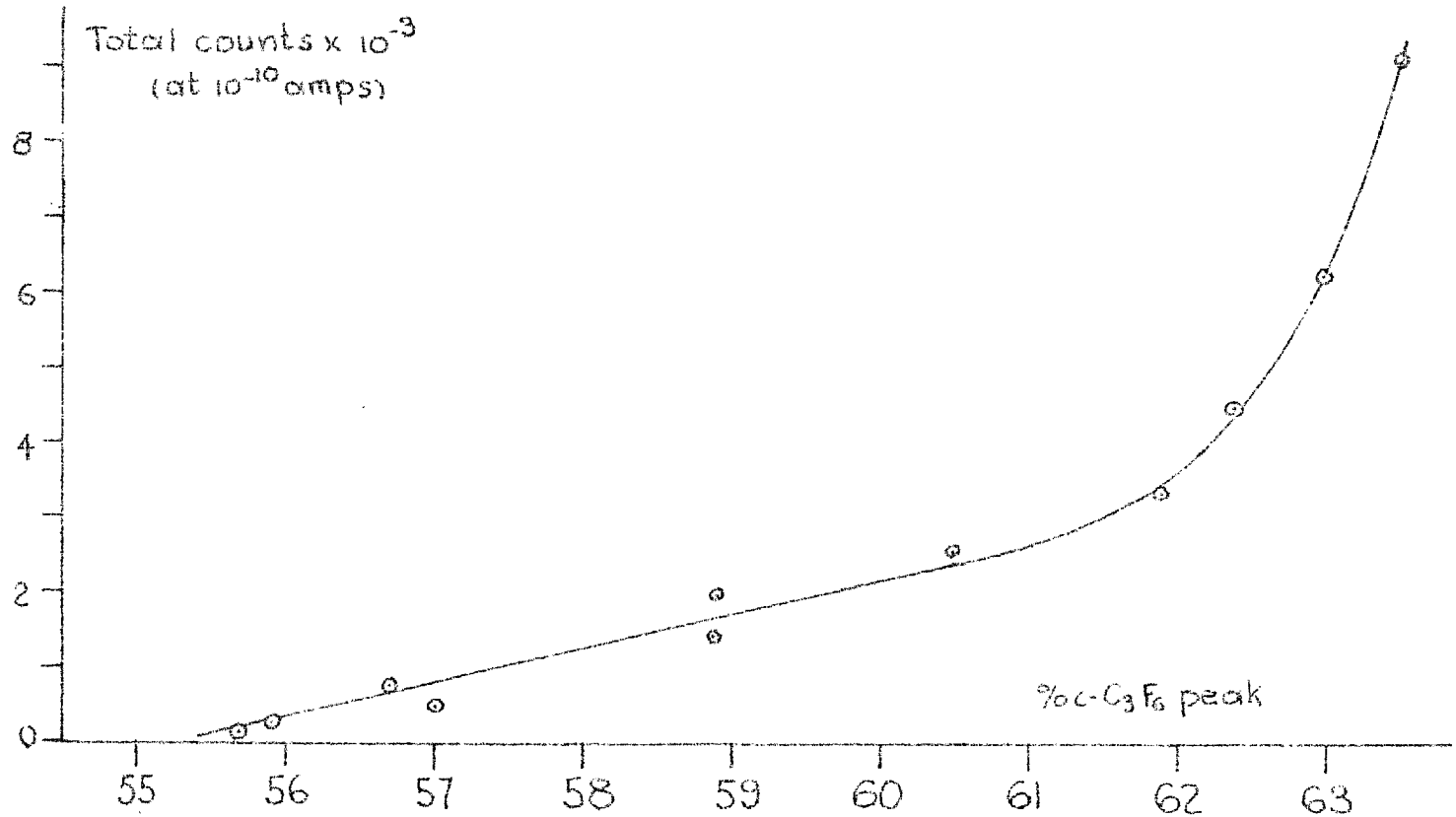

Figure 2.24

is about ± 1% and accuracy within these limits should be expected in the calibration range. The accuracy of the calibrations is limited to this degree by the count rate of the integrator. The number of samples of B injected was too few to make such a plot but it was used as a check on the other calibrations in the same region. The results from these graphs were then plotted as peak area % c-C_3F_6 against partial pressure % c-C_3F_6 at various suitable intervals of total area as indicated in fig. 2.25.

It should be noted from the curves for particular samples that as sample size increases the observed peak area % seems to approach a constant value, although large enough samples to confirm this behavior were never injected (overloading of the column becomes a consideration above the region studied).

The products of some runs performed before these calibrations, were analyzed using samples considerably larger than in the calibrations; in addition the integrator had not been used. In order to apply material balances to these runs the calibration peak areas were measured by the 'peak ht. x width at half height' method and the results are presented in figures 2.26 - 2.31. The curves were extrapolated to high total area values

Integrator Calibrations
Correlation of Integrator & True Conc.

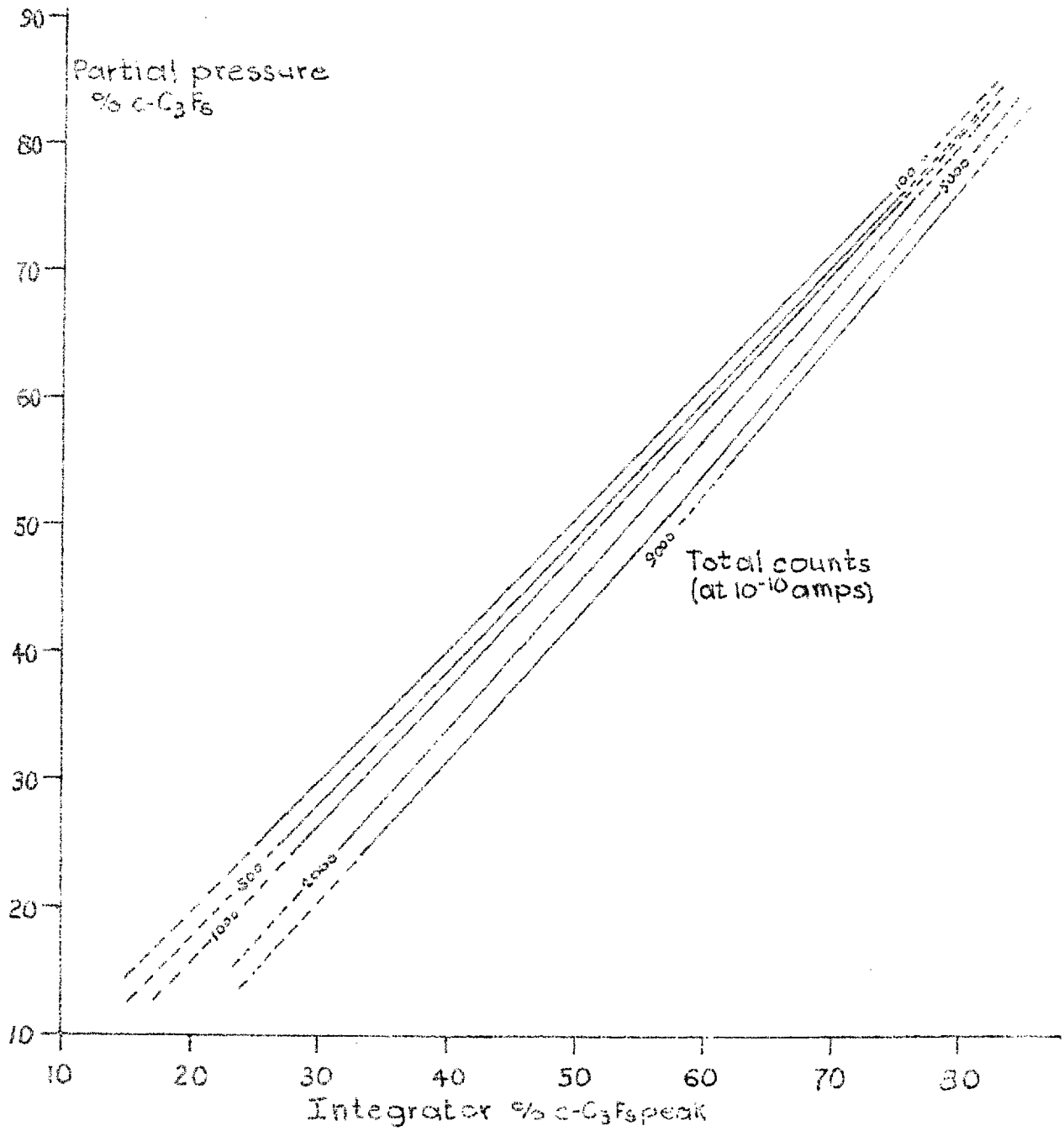

Figure 2.25

Triangulation Calibrations: Sample A

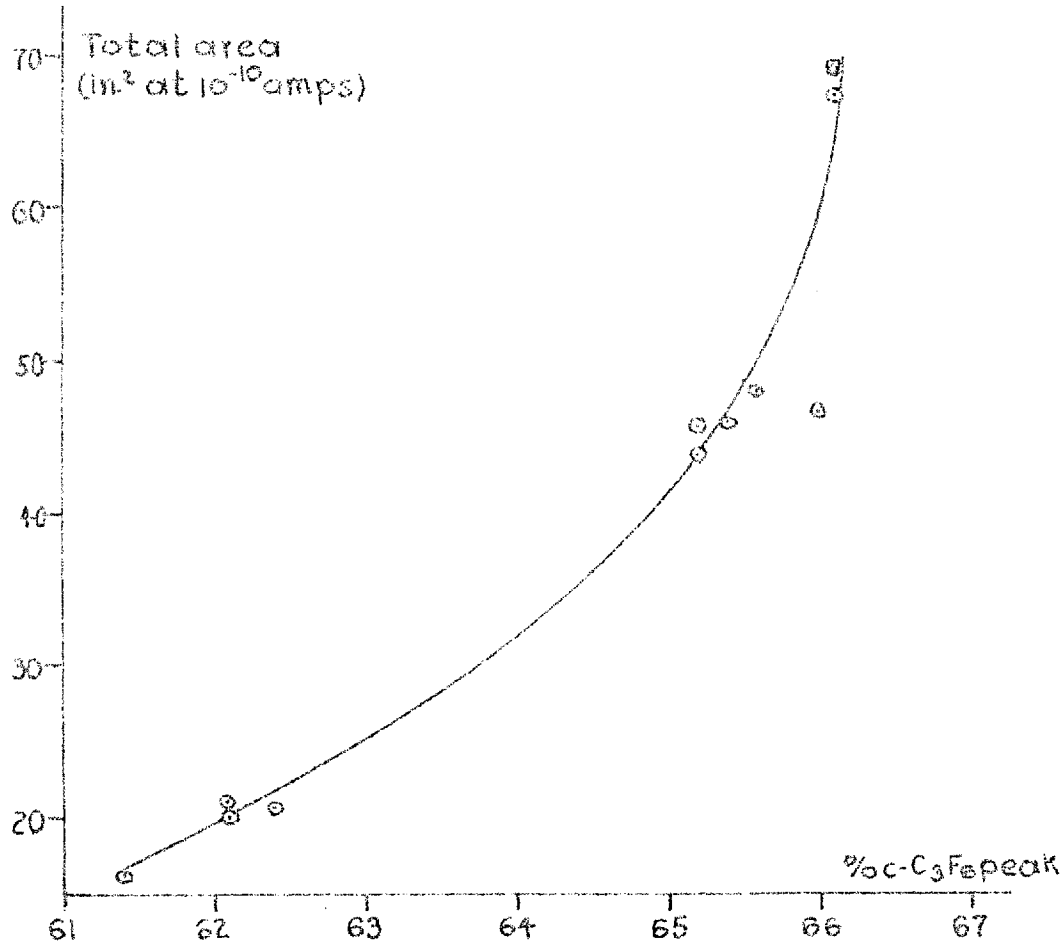

Figure 2 26

Triangulation Calibrations: Sample C

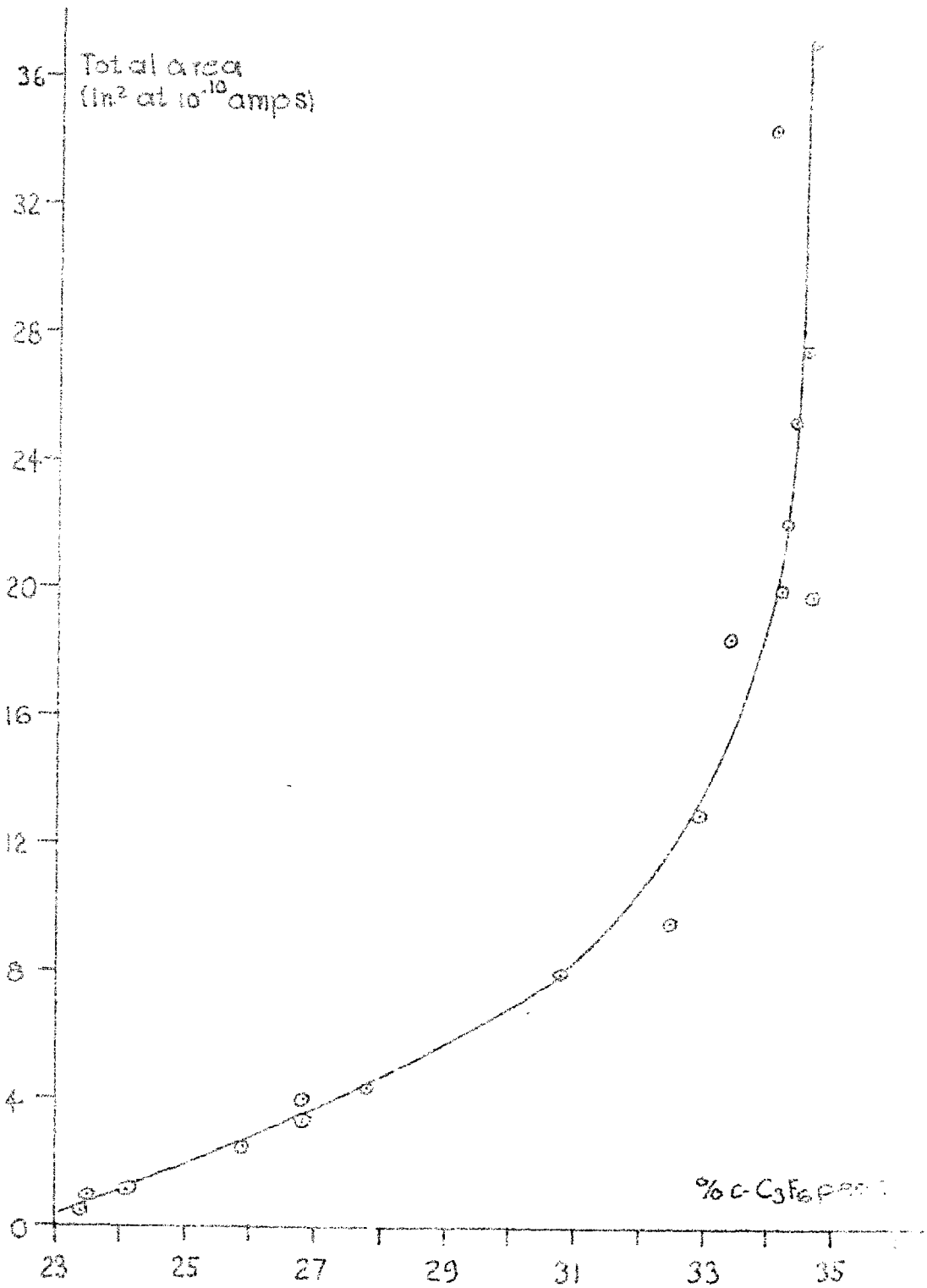

Figure 2·27

Triangulation Calibrations: Sample D

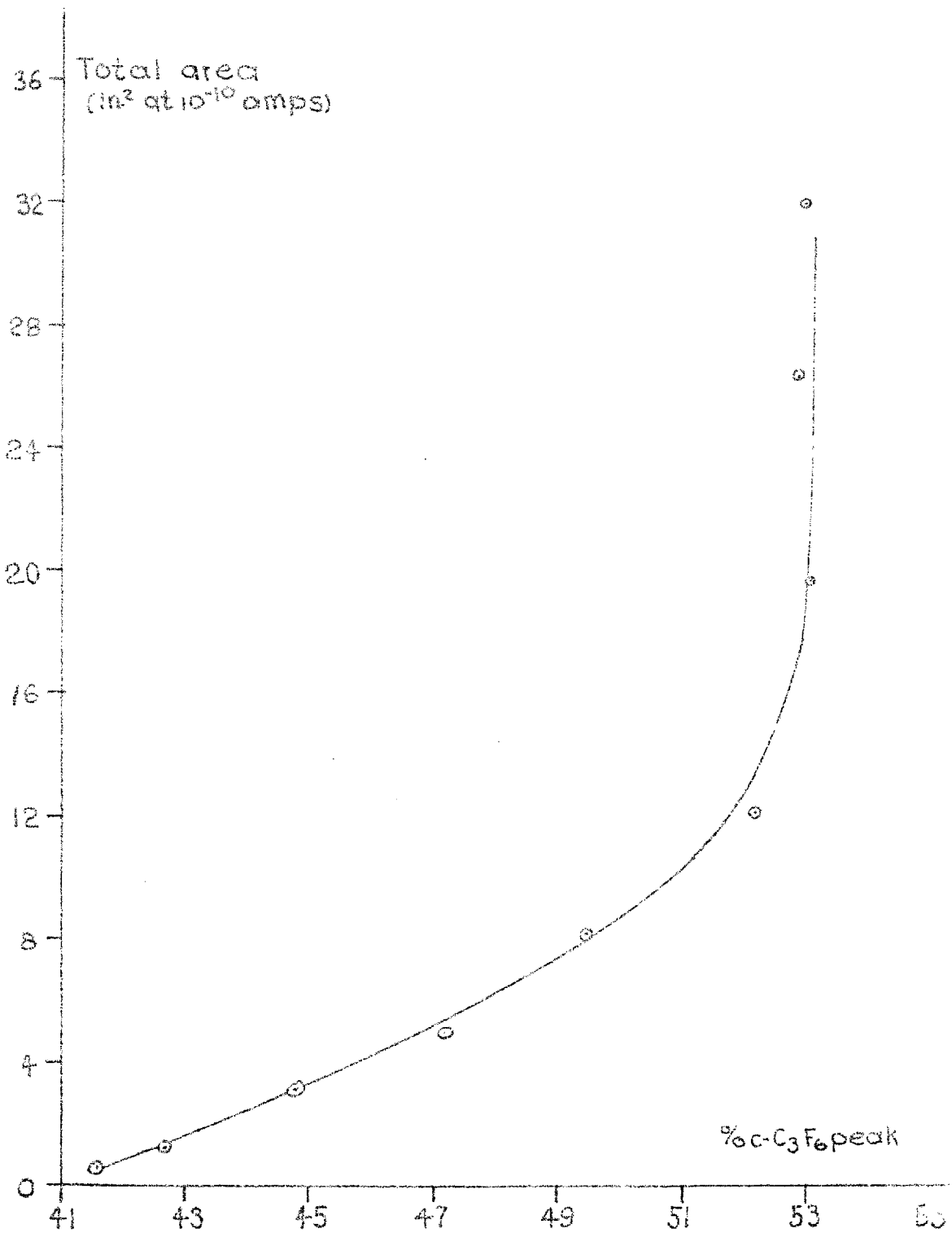

Figure 228

Triangulation Calibrations: Sample E

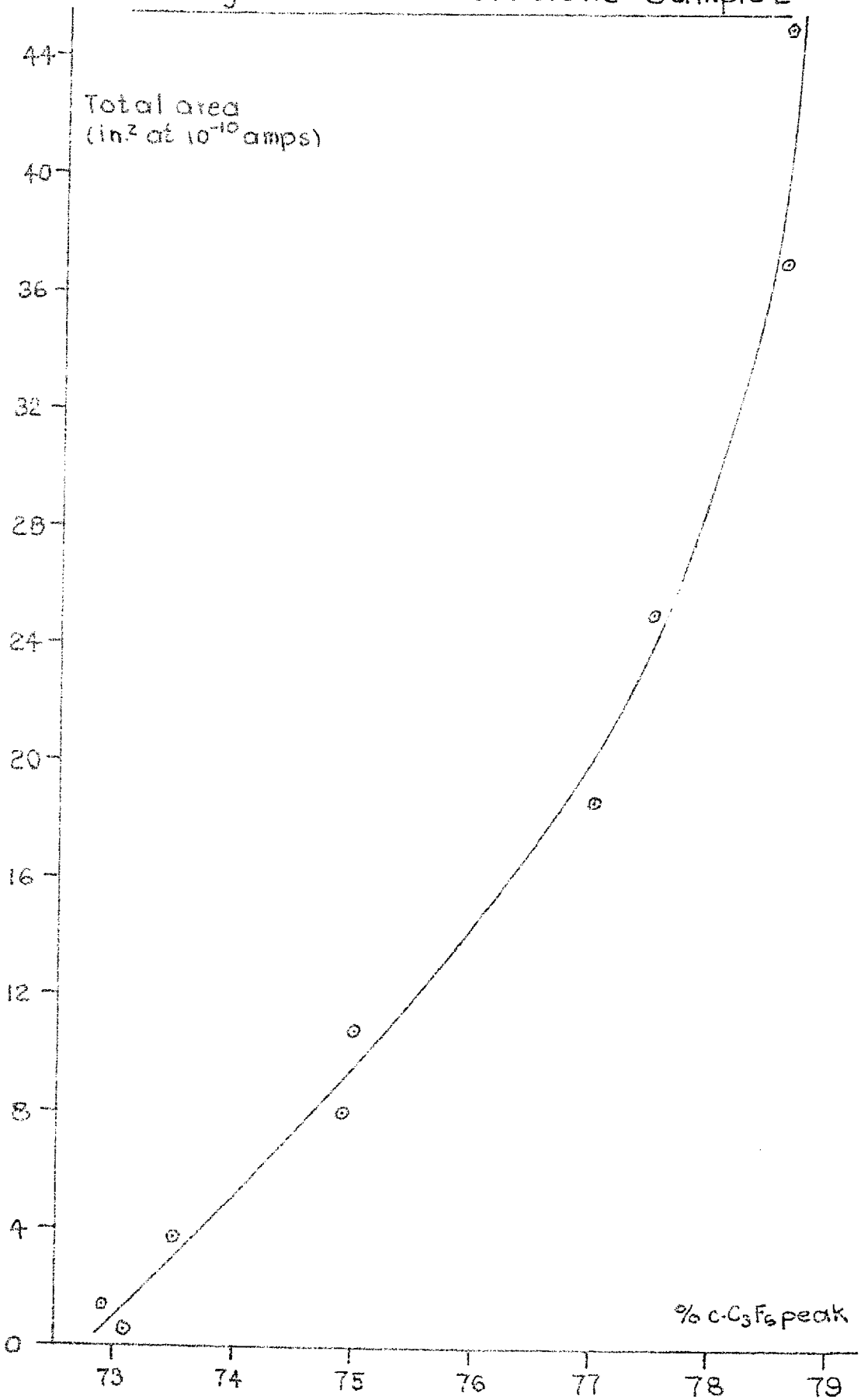

Figure 2.29

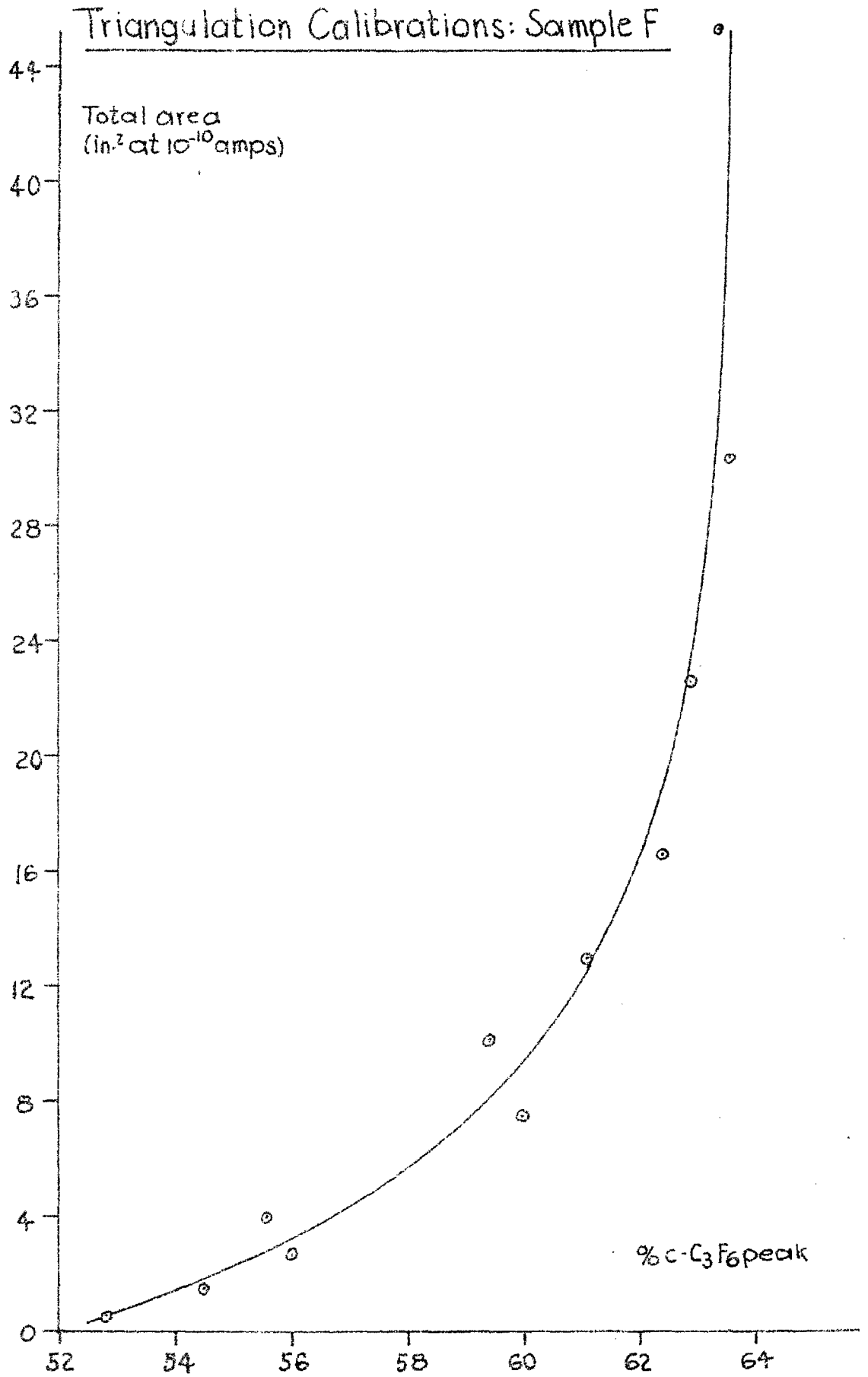
Triangulation Calibrations: Sample F
Total area
(in.² at 10⁻¹⁰ amps)
44
40
36
32
28
24
20
16
12
8
4
0
52
54
56
58
60
62
64
% c-C₃F₆ peak

Figure 2.30

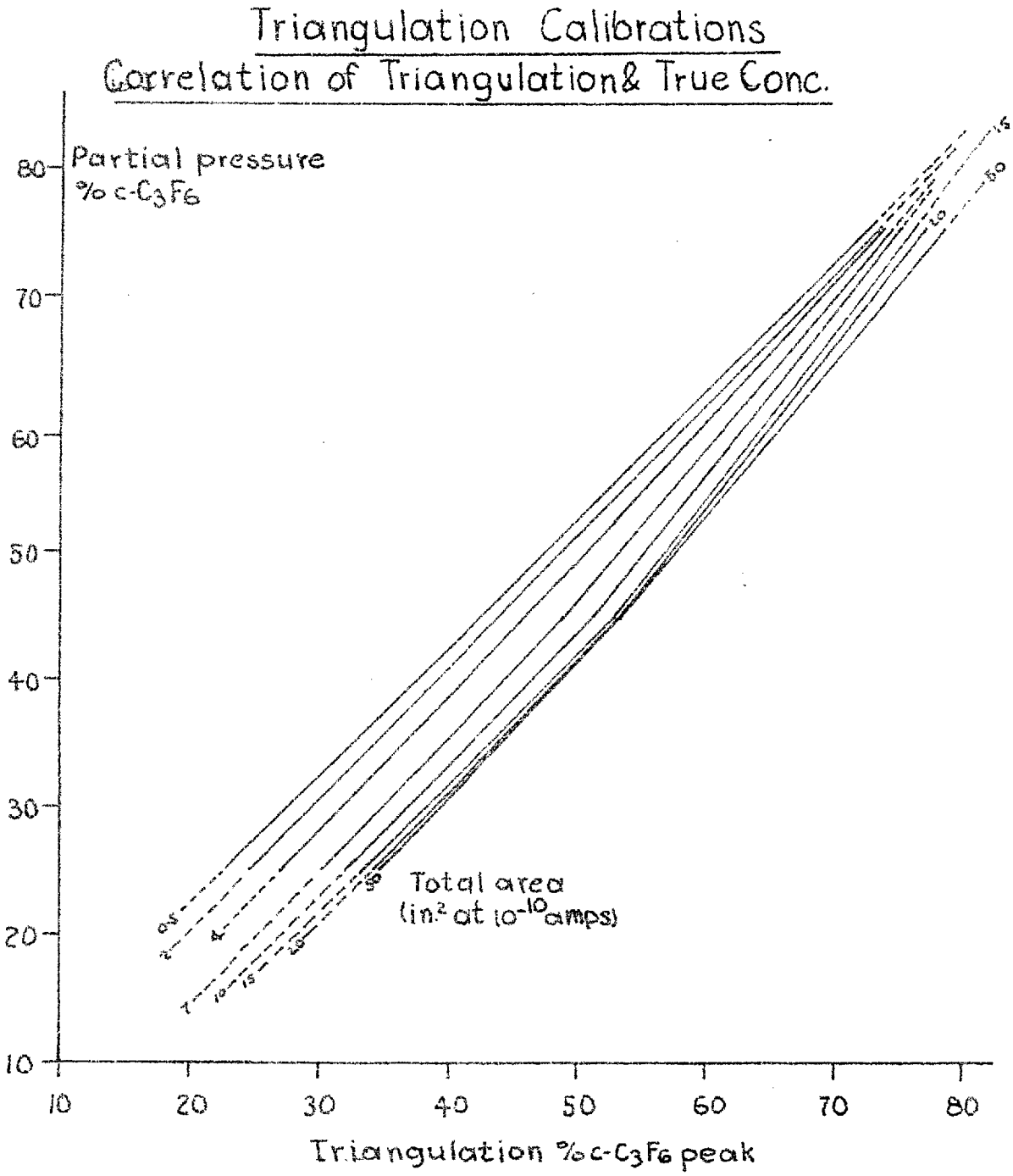
Triangulation Calibrations
Correlation of Triangulation & True Conc.
Partial pressure
% c-C3F6
80
70
60
50
40
30
20
10
0.5
2
4
7
10
15
20
30
50
Total area
(in.² at 10⁻¹⁰ amps)
10
20
30
40
50
60
70
80
Triangulation % c-C3F6 peak

Figure 2.31

and all runs above 50 in.^{2} were estimated using this calibration line or extrapolations to this region. As indicated in the material balance figures (sect. 3.1.1.), these calibrations did not give results which differed substantially from the results covered by the calibrations. This is some indication that the extrapolations were not far wrong. These latter area calibrations would be more accurately described as peak height ones since a constant width of 0.115 in. for the C_2F_4 peak and 0.30 in. for the c-C_3F_6 peak were assumed. At the chart speed invariably used (20 in. per hr.) the peaks are very narrow and slight variations in width give large variations in resulting peak area which are not indicative of concentration differences. This particular circumstance makes the triangulation method less reliable than the integrator approach. However, with increased chart speeds comparable or improved reliability might be expected with the triangulation method.

2.4. Infra-Red Analysis

Infra-red analysis was used for identification of compounds and to determine if impurities were present when chromatographic analysis was not considered sufficient.

For rough work a Perkin-Elmer 'Infracord' model 137 was used, which covered the range 3 - 15 μ. If greater sensitivity and higher resolution were desired then a Grubb-Parsons Spectromaster was used. This covered the range 1 - 25 μ. The cell which was usually used had a B-10 cone connection so that it could be connected to the vacuum system for putting in samples. The cell had Na Cl windows and a 10 cm. path length. Where calibrations were performed in the 3 - 15 μ range, polystyrene film was used.

3. RESULTS

3. RESULTS

3.1 The Pyrolysis of Perfluorocyclopropane

Some initial pyrolysis reactions of perfluorocyclopropane were carried out in order to establish the nature of the reaction and the temperature range over which studies could be suitably carried out. In these and later more careful experiments the course of the reaction was studied by observing pressure changes and by terminal analysis of products. The differential equation describing the pressure changes during the reaction has been integrated with a computer. The rate constant for the unimolecular decomposition of perfluorocyclopropane has been determined in both the high pressure and falloff regions.

3.1.1 The Initial Experiments

An initial series of experiments was carried out in a pyrex reactor of about 75 c.c. capacity. Pressure changes were monitored with the pressure transducer; unregulated battery d.c. input to the transducer was used. Individual calibrations were performed for each run using a narrow bore manometer, with which accuracy

of better than 1 m.m. could not be expected. Analysis of reaction products was carried out using the H_2 flame detector but conditions were not rigorously maintained and were not necessarily the same as those specified in the experimental section. No particular care about seasoning the reactor was taken other than to leave a few centimeters of C_2F_4 in the reactor for an hour or so before a reaction.

In the first experiment (TR-1) a mixture of C_3F_6 isomers analyzing 29% $CF_3 \cdot CF = CF_2$ and 71% $c\text{-}C_3F_6$ by chromatographic peak area was placed in the reactor to a starting pressure of 24.4 cm. Pressure changes were not studied. After five hours at 374°C, the material was removed from the reactor for analysis. In the first column below the % of total chromatographic peak area (measured as height times width at half height) is given; this figure is converted to % equivalent C_3F_6 in the second column by multiplying the fraction in the product by the ratio of the component's molecular weight divided by 150 (the molecular weight of C_3F_6), and converting to %.

component in product	% in product	% equiv. C_3F_6
C_2F_4	2·7	1.45
c-C_3F_6	0	0
$CF_3 \cdot CF = CF_2$	22·0	17·7
octafluorocyclobutane	75·4	80·7
other C_4 fluorocarbons	trace	0

An infra-red analysis was carried out on the products; all observed absorptions could be attributed to octafluorocyclobutane, $CF_3 \cdot CF = CF_2$ or C_2F_4. The characteristic absorption of c-C_3F_6 at 11.6μ was absent. These analyses show the decomposition of all the c-C_3F_6 and possibly some of the $CF_3 \cdot CF = CF_2$ with the formation of C_2F_4 and octafluorocyclobutane.

In TR-2 , the same starting material was put into the reactor at 237·5°C to a pressure of 22.0 cm. After 62·5 min the pressure had risen to 25·2 cm and the product was removed for analysis. This gave:

	% in product	% equiv. C_3F_6
C_2F_4	45·0	35·3
c-C_3F_6	33.9	39·8
$CF_3 \cdot CF = CF_2$	21·2	24·9
C_4 fluorocarbons	0	0

If the pressure changes are considered on the basis that $CF_3 \cdot CF = CF_2$ does not react and the following reaction alone takes place:

$$2c\text{-}C_3F_6 \longrightarrow 3C_2F_4 \ ,$$

then the following final analysis would be expected:

	% in product	% equiv. C_3F_6
C_2F_4	38.1	29.1
$c\text{-}C_3F_6$	36.5	41.8
$CF_3 \cdot CF = CF_2$	25.3	29.0

These results indicate that $c\text{-}C_3F_6$ decomposes to C_2F_4 although C_2F_4 may dimerize to octafluorocyclobutane under the right conditions; $CF_3 \cdot CF = CF_2$ reaction is still indicated.

In TR-3 the same mixture of C_3F_6 isomers was put into the reactor to a pressure of 6.05 cm. and at a temperature of 285°C. The time of the run was 5 min. 5 sec. An analysis of poorer quality than for the other runs was obtained (too small a sample), which resulted in the following:

	% in product	% equiv. C_3F_6
C_2F_4	71.0	59.5
c-C_3F_6	10.3	14.4
$CF_3.CF = CF_2$	18.6	26.0
C_4 fluorocarbons	0	0

The initial and final pressures were 6.03 and 7.74 cm. respectively. On the basis of the above mentioned simple scheme the following analysis should have resulted:

	% in product	% equiv. C_3F_6
C_2F_4	66.3	56.8
c-C_3F_6	11.1	14.2
$CF_3.CF = CF_2$	22.6	29.0

The behaviour at 237.5°C and that at 285°C are observed to be similar, with no definite conclusions regarding the $CF_3 \cdot CF = CF_2$ possible.

From a study of the pressure changes indicated by the transducer during TR-3 , a plot of $\log(\triangle P/\triangle t)$ against log Pr (where P is the total pressure and Pr the pressure of c-C_3F_6) was made. Calculations were based on an initial concentration of 29% $CF_3.CF = CF_2$, treated as an inert diluent and the stoiciometry: $2c\text{-}C_3F_6 \longrightarrow 3C_2F_4$. The slope of the

resulting plot gave an order of reaction of 2.07 in $c\text{-}C_3F_6$.

In TR-4 the same starting material was left for 10 minutes at 251·1°C. The pressure rose from 8·01 to 9·15 cm. over this period. The analysis gave the following results:

	% in product	% equiv. C_3F_6
C_2F_4	37·0	28·1
$c\text{-}C_3F_6$	38·0	43·2
$CF_3 \cdot CF = CF_2$	24·4	27·8
octafluorocyclobutane	0	0
$CF_3 \cdot CF \cdot CF_2 \cdot CF_2$	0·7	1·02

The identity of the trifluoromethyl substituted cyclopropane was not established until later. It was found at the time to have a retention time greater than $c\text{-}C_4F_8$ and to be clearly separated from it under the chromatographic conditions used. The same peak was also identified in the products of a series of photochemical reactions for the preparation of $c\text{-}C_3F_6$ in which successive reactions were carried out by adding new C_2F_4 to the product of the previous one; the $CF_3 \cdot CF = CF_2$ concentration had built up to a significant level (about 33% in the C_3 fraction).

On the basis that the following reactions were taking place:

$$2c\text{-}C_3F_6 \longrightarrow 3C_2F_4$$

$$c\text{-}C_3F_6 + CF_3\cdot CF = CF_2 \longrightarrow C_2F_4 + CF_3\cdot \overline{CF - CF_2\cdot CF_2} \ ,$$

the product analysis predicted by the pressure changes is given in the following table:

	% in product	% equiv. C_3F_6
C_2F_4	38·1	29·1
$c\text{-}C_3F_6$	36·5	41·7
$CF_3\cdot CF = CF_2$	24·6	28·1
$CF_3\cdot \overline{CF\cdot CF_2\cdot CF_2}$	0·7	1·06

The calculations are based on 0·7% trifluoromethylperfluorocyclopropane and the $CF_3\cdot CF = CF_2$ inert except for the reaction to form the C_4 product. As in the previous reactions, the product analysis seems to conform fairly closely to that predicted by the pressure changes on the basis of the exclusive reaction of $c\text{-}C_3F_6$ to form C_2F_4. When the pressure changes for this reaction were treated as in TR-3 and the side reaction to $CF_3\cdot \overline{CF\cdot CF_2\cdot CF_2}$ ignored, an order of 2.78 in $c\text{-}C_3F_6$ resulted.

In TR-6 a sample of $CF_3 \cdot CF = CF_2$ free $c\text{-}C_3F_6$ was left in the reactor at 257·9°C for 25 min. The pressure rose from 8·30 to 10·22 cm. in this time. The actual analysis and pressure predictions are tabulated below:

	% in product	Press. predicted %
C_2F_4	55·5	56·4
$c\text{-}C_3F_6$	44·5	43·6
$CF_3 \cdot CF = CF_2$	0	0
C_4 fluorocarbons	0	0

The order of the reaction determined from the pressure changes as before was found to be 4·2.

In one experiment, a careful material balance was performed. 0.32874 g. of chromatographically purified perfluorocyclopropane was weighed by difference in a gas holder using a precision balance. As much as possible of this material was expanded into a reactor of 526·5 c.c. capacity whose average temperature during the run was 253·3°C. The starting pressure in the reactor was estimated to be 14·92 cm. 0.03932 gm. of reagent which did not enter the reactor were recovered from the vacuum system. After twenty minutes the products of the reaction were condensed out and

found to weigh 0.28877 gm. This compared to 0.28942 gm. reacted, left 0.00065 gm. unaccounted for which represents a loss of 0.02%.

Chromatographic calibrations were performed at a late stage in the work primarily for the study of the reaction at low pressure. These could however be used to do material balances on runs for which a terminal analysis had been performed. The calibrations give concentration figures for $c\text{-}C_3F_6$ and C_2F_4 in mixtures of the two; small quantities of octafluorocyclobutane and perfluoropropene in the product were estimated by their peak area measured as height x width at half height. In correcting the calibration figures for comparison with the starting and final pressure, it was assumed that these impurities came from the starting material or the tetrafluoroethylene produced from it. Corrections were applied as follows. If the calibration gave a value z' for fraction of $c\text{-}C_3F_6$, then the corrected concentration z for an observed fraction q of octafluorocyclobutane (assumed produced by dimerization of C_2F_4) is:

$$z = \frac{z'}{1+2q}$$

If in addition a fraction r of $CF_3 \cdot CF = CF_3$ is observed (assumed produced directly from $c\text{-}C_3F_6$), then the corrected value z is:

$$z = \frac{z' + r}{1 + r + 2q}$$

Thus a value of z which is indicative of the fraction of $c\text{-}C_3F_6$ in the product assuming all reaction to C_2F_4, can be determined. From the stoiciometry of the reaction:

$$2\ c\text{-}C_3F_6 \longrightarrow 3C_2F_4,$$

the ratio of the initial pressure (P_o) to the final pressure (P_f) can be determined from the relation

$$\frac{P_o}{P_f} = \frac{z+2}{3}$$

The pressure results give values of P_f and P_o directly. The observed P_f must be corrected for octafluorocyclobutane if present, and a value of P_o can be calculated from the analysis using the ratio P_o/P_f. This P_o is compared to the pressure value to

determine if material has been lost or gained.

In Table 3.1, the results where the integrator was used during the analysis of the reaction products are presented. The calibrations are only strictly valid for an equivalent count at 10^{-10} amps of up to 5000 from 25-75% c-C_3F_6 or up to 9000 from 55-75% c-C_3F_6. The total count is indicated in the table to show where extrapolated calibration lines have been used.

The 'loss' in run G-4 can be explained by the high temperature of the run where the time required to get the products out of the reactor (about $\wedge^{1/4\ min.}$) is important relative to the total reaction time (1.08 min.). Some further reaction occurs during the sampling process so that the analysis shows a value of z less than that which corresponds to the P_f value at 1.08 min. (If z is smaller so is P_o/P_f and the P_o predicted from the analysis - hence the apparent loss).

The other results show a fairly consistent gain. The uncertainty due to the analysis should not indicate more than $\pm$ 0.3% loss; the corrections for $CF_3 \cdot CF = CF_2$ and octafluorocyclobutane are not so large as to make a great difference unless their sensitivities in the detector are vastly different from c-C_3F_6 and C_2F_4. The discrepancies although not large, cannot be explained.

Table 3.1: Material Balance Results from Integrator Analysis

Exper.	Total Peak Area at 10^{-10} amps. (Counts)	Temp. °C	Prod. impurities		Anal. Predictions		Actual P_o loss	
			%$CF_3.CF{=}CF_2$	%c-C_4F_8	P_o/P_f	P_o(cm.)	(cm.)	(%)
D-9	3720	230.2	0	0.32	0.910	52.5	52.44	-0.1
D-11	4830	229.8	0	0.27	0.909	41.1	40.82	-0.1
D-12	3750	229.7	0	0.35	0.904	31.2	30.85	-1.0
D-13	4180	230.5	1.09	0	0.866	2.795	2.763	-1.6
D-14	4050	230.5	1.50	0	0.821	1.003	0.995	-0.8
D-15	2020	230.3	0	0	0.831	0.199	0.195	-2.1
A-29(i)	1900	253.3	0	0	0.737	0.0820	0.0834	1.7
A-29(ii)	1157	253.3	0	0	0.699	0.0786	0.0779	-0.9
A-30(i)	906	253.2	0	0	0.697	0.1706	0.1700	-0.3
A-30(ii)	3906	253.1	0	0	0.751	0.1702	0.1709	0.4
A-30(iii)	3980	253.1	0	0	0.821	0.1688	0.1695	0.5
A-35(i)	2630	253.2	0	0	0.840	0.1394	0.1378	-1.4
A-35(ii)	1612	253.1	0	0	0.777	0.1312	0.1272	-3.1
A-35(iii)	663	253.1	0	0	0.727	0.1333	0.1365	2.4
A-35(iv)	801	253.0	0	0	0.686	0.1252	0.1278	2.0
G-4	6420	302.2	0.07	0.93	0.711	23.9	24.22	1.2

A larger number of runs are available where the peak area as measured by height x width at half height could be used, although some large calibration extrapolations had to be assumed. Above an equivalent total area at 10^{-10} amps of 40 in.^{2} and outside the range 25-75% c-C_3F_6 the calibration is uncertain. Results are presented in table 3.2. Similar behavior to the integrator studies are apparent.

For example in Run D-13 the analysis figures corrected for $CF_3.CF = CF_2$ gave z = 0.600 which showed a gain of 1.6%. In order to predict the starting pressure from the final pressure a value of z = 0.568 would have been necessary. This discrepancy of 3.2% is greater than the 1% expected with the analysis figures.

The conclusions which can be drawn from these results are several. The principal product of the thermal decomposition of c-C_3F_6 is C_2F_4. The occurrence of octafluoracyclobutane at the higher temperatures can be explained by the dimerization of C_2F_4(143). The side reaction

$$c\text{-}C_3F_6 \longrightarrow CF_3.CF{=}CF_2$$

occurs at a very slow rate which seems to be somehow

Table 3.2: Material Balance Results from Triangulation Analysis

Exper.	Total Peak Area at 10^{-10} amps. ($in.^2$)	Temp. (^oC)	Prod. impurities $\%CF_3.CF{=}CF_2$	Prod. impurities $\%c\text{-}C_4F_8$	Anal. Predictions P_o/P_f	Anal. Predictions P_o(cm.)	Actual P_o (cm.)	loss (%)
E-2	52.3	240.5	0	0.33	0.770	1.86	1.829	-1.6
E-3	36.05	240.8	0	0.46	0.798	6.29	6.229	-1.0
E-4	104.2	240.7	0	0.49	0.790	4.01	3.957	-1.3
E-5	39.3	240.6	1.15	0.41	0.840	12.22	12.01	-1.7
E-6	49.6	240.4	0.13	0.79	0.839	23.35	23.19	-0.6
E-7	47.7	240.4	0.10	0.62	0.834	18.18	18.11	-0.4
G-2	27.8	302.4	0.06	0.26	0.688	5.61	5.782	2.9
G-3	27.3	302.4	0.10	0.27	0.699	8.15	8.331	2.2
G-5	31.8	302.3	0.14	0.91	0.711	18.51	18.57	0.3
G-6	30.9	302.4	0.11	0.51	0.704	11.23	11.41	1.6
G-7	22.4	302.5	0.05	0	0.685	1.624	1.657	1.8
B-3	373.	265.9	0.10	0.31	0.824	24.1	23.61	-2.1
B-4	375.	265.9	0.10	0.34	0.813	18.55	18.09	-2.5
B-5	333.	265.9	0.10	0.38	0.786	12.50	12.14	-2.9
B-6	326.	266.3	0.03	0.49	0.750	5.94	5.777	-2.8
B-7	218.	266.3	0.09	0.20	0.741	4.09	4.065	-0.6
B-8	297.	266.2	0.10	0.15	0.745	1.982	1.938	-2.3
B-9	295.	266.2	0.13	0.09	0.739	0.967	0.942	-2.7
F-3	261.	290.0	0.12	0.49	0.717	8.42	8.327	-1.1
F-4	220.	289.9	0.43	0.11	0.721	3.67	3.616	-1.4
F-5	202.	289.7	0.55	0.07	0.710	1.80	1.803	0
F-6	170.	289.7	0.09	0.02	0.704	0.824	0.831	0.9
F-7	299.	288.4	0.03	0.40	0.767	19.25	18.74	-2.7
F-8	277.	288.4	0	0.27	0.754	12.54	12.08	-3.7
D-4	42.3	230.1	0	0.33	0.885	22.9	22.91	0
D-5	35.2	229.9	0	0.16	0.887	18.45	18.37	-0.4
D-6	71.0	229.9	0	0.01	0.876	8.74	8.75	0
D-7	33.9	229.7	0	0	0.883	3.23	3.171	-1.21
D-8	43.3	229.6	0	0	0.879	5.24	5.216	-0.5
A-9	19.6	253.5	0	1.26	0.751	22.4	23.5	4.7
C-8	32.4	277.0	0.10	0	0.695	11.65	12.41	6.1

dependent on the nature of the reactor surface. After a long series of runs, only small quantities of polymer were observed in the reactor. This supports the conclusion from the material balance studies that significant polymerization or formation of heavier than C_4 compounds was not taking place. Octafluorocyclobutane was the only C_4 fluorocarbon observed in the reaction products of pure $c\text{-}C_3F_6$ starting material.

The observation of only small quantities of perfluoropropene in the products concurs with evidence from other studies that somewhat higher temperatures are required to break C-F bonds in fluorocarbons. It seemed likely that some scheme involving difluoromethylene would explain what was going on. Its presence in the system was confirmed by a series of semiquantitative experiments. A mixture of about 10% $c\text{-}C_3F_6$ and 90% $CF_3.CF{=}CF_2$ was pyrolized. A new chromatographic peak appeared which was not present in the starting material; it had a retention time greater than that of octafluorocyclobutane but less than those of the perfluorobutenes found in the teflon pyrolysis products. About 0.9% of this compound was observed in the product when 10.2 cm. of the above mixture was pyrolized for 25 minutes at 253°C.

A peak having a similar retention time and a concen-

tration of about 0.7% was observed in the products of run TR-4 (see above) when the starting material contained 71% c-C_3F_6 and 29% $CF_3.CF=CF_2$.

A 50-50 mixture of C_2F_4 and $CF_3.CF=CF_2$ was irradiated with light of wavelength 2537Å in the presence of Hg and at 80°C. $CF_3.CF=CF_2$ is known to react at a negligible rate at these temperatures in the presence of Hg and 2537Å light. The products removed from the photochemical reactor analysed as follows:

C_2F_4	10.3%
c-C_3F_6	0.7%
$CF_3.CF=CF_2$	87.5
Octafluorocyclobutane	0.6
$CF_3.\underline{CF.CF_2}.CF_2$	0.8

A small amount of the last substance was isolated from this product by preparative chromatography; the infrared spectrum showed a 6.60μ peak. Mitsch (78) observed an absorption at 6.55 μ for $CF_3.\underline{CF.CF_2}=CF_2$. The infrared done on this sample is shown in figure 3.1. This employed a pressure of about 1 m. m. in the 10 cm. path NaCl window cell and was done on the "Infracord" machine. In order to specify the absorptions more carefully the same sample was run on the "Spectramaster" and the

Infra-red Analysis of Perfluoromethylperfluorocyclopropane.

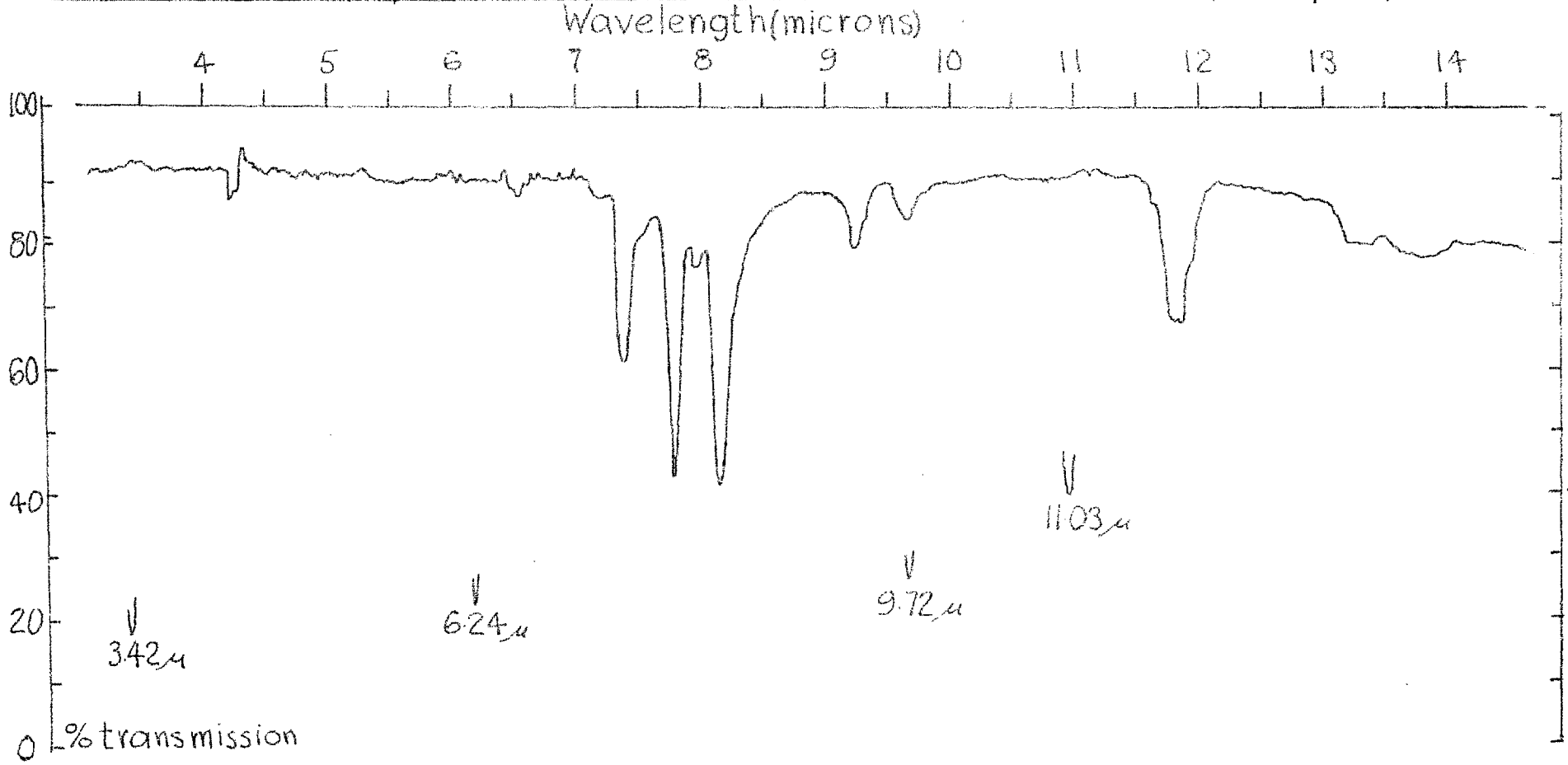

Figure 3.1

Infra-red Analysis of Perfluoromethylperfluorocyclopropane.

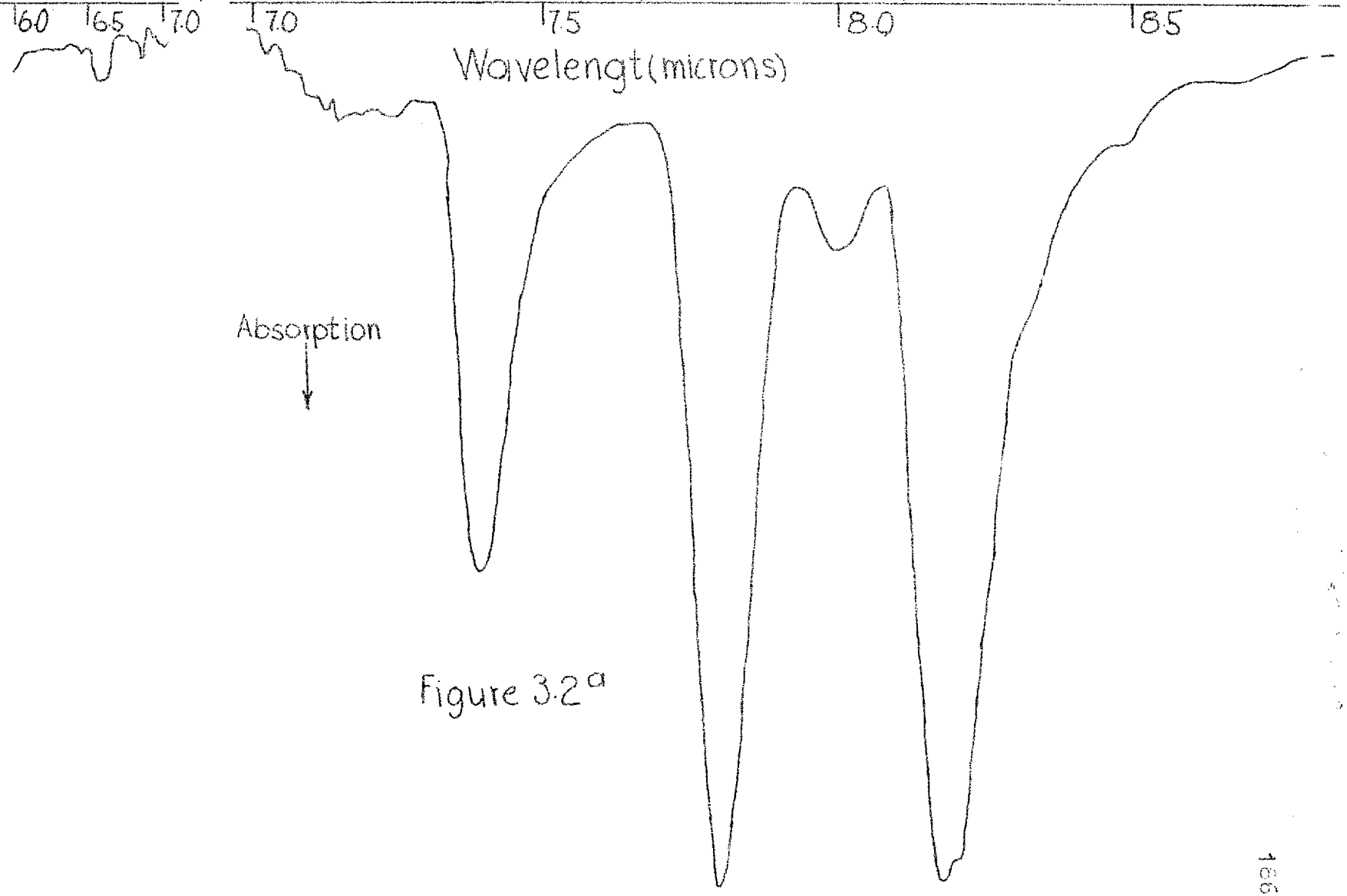

Figure 3.2[a]

Infra-red Analysis of Perfluoromethylperfluorocyclopropane.

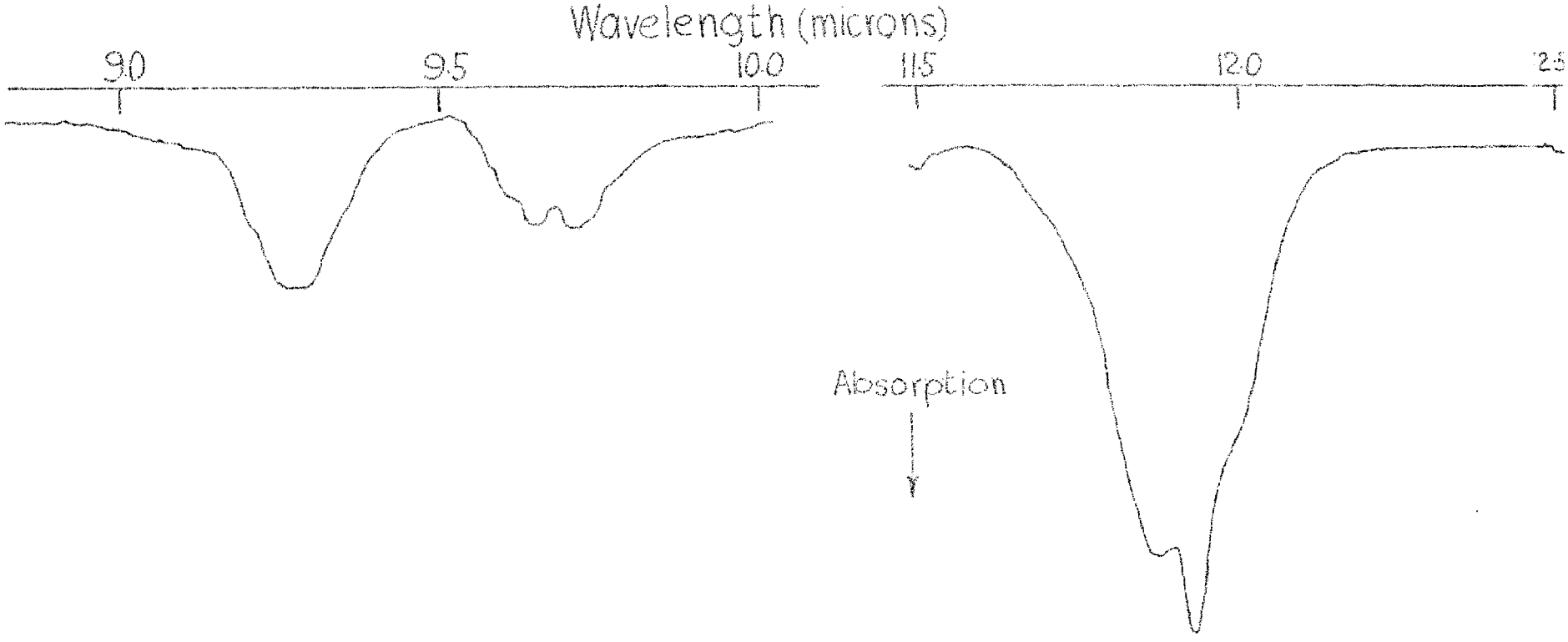

Figure 32b

results are traced in figures 3.2a and b. The following table summarizes the absorptions observed.

Infra-red Absorptions of $CF_3.\underline{CF}.\underline{CF_2}.CF_2$ (microns)

6.60	W
7.39	S
7.81	S
8.01	M
8.18	S
8.34	W (shoulder)
8.49	W (shoulder)
9.28	M
9.66	M
9.72	M
11.87	S
11.93	S
11.98	M (shoulder)

The apparent absorption at 4.2μ in figure 3.1 was not observed with the higher resolution apparatus.

The chromotographic retention time is some evidence of it being the substance suggested; it is known that cyclic compounds are eluted before olefinic ones of the same molecular weight. This is confirmed in the examples

of $c\text{-}C_3F_6$ before $CF_3.CF{=}CF_2$ and $c\text{-}C_4F_8$ before perfluorobutenes. This material also precedes the perfluorobutenes. The occurrence of the reaction:

$$CF_2 + CF_3.CF = CF_2 \longrightarrow CF_3.\overbrace{CF.CF_2.CF_2}$$

in the presence of pyrolizing $c\text{-}C_3F_6$ is confirmed.

The decomposition of $c\text{-}C_3F_6$ was also carried out in the presence of about 90% C_2H_4 at 253°C for two hours, to decompose all the $c\text{-}C_3F_6$. A small amount of material having a retention time slightly but unmistakeably greater than $c\text{-}C_3F_6$ was found when chromotographic analysis of the products was performed. Hydrocarbons are expected to have slightly greater retention times, under the conditions used, than related fluorocarbons (confirmed in the case of C_2H_4 and C_2F_4). $\overbrace{CF_2.CH_2.CH_2}$ would not have been expected to decompose under the reaction conditions (42). It seems likely that the reaction:

$$CF_2 + C_2H_4 \rightarrow \overbrace{CF_2.CH_2.CH_2}$$

was observed even if sufficient quantities to confirm the presence of the cyclic compound by infra-red analysis, were not formed.

The following reaction scheme was suggested to explain the results:

$$c\text{-}C_3F_6 \xrightarrow[k_2]{k_1} CF_2 + C_2F_4 \qquad (1)$$

$$2CF_2 \xrightarrow{k_3} C_2F_4 \qquad (2)$$

$$CF_2 + C_2F_4 \longrightarrow c\text{-}C_3F_6 \qquad (3)$$

Difluoromethylene is known to react with C_2F_4 to give $c\text{-}C_3F_6$ and to combine with another CF_2 to give C_2F_4 from studies on other systems where CF_2 is present. The experimental evidence does not give support to other mechanisms. The process:

$$2c\text{-}C_3F_6 \longrightarrow 3C_2F_4$$

would result in a reaction order of 2, which is not observed. Chain processes involving CF_2 are unlikely since it is readily consumed by reactions (2) and (3).

Evidence has been obtained that there are no unidentified impurities in the starting material or in the reaction product. A sample of $c\text{-}C_4F_8$ free $c\text{-}C_3F_6$ was found to contain 0.014% C_2F_4 and 0.022% $CF_3.CF{=}CF_2$ by peak area when analysed at low temperature (60 c.c. N_2/min. carrier gas at 75° for 29 min. and then at 125° for 19 more min.) to give more complete resolution of any impurities. This material was pyrolized for 4½ hours at 253° and analysed by running the column at 75°C with 60 c.c. N_2/min. carrier gas flow. The peak area concentrations and retention times of the products were as follows:

C_2F_4	92.0 %	10.0 min.
c-C_3F_6	3.42	35.2
$CF_3.CF=CF_2$	0.35	39.2
c-C_4F_8	4.48	49.6

The retention times under normal operating conditions (60 c.c./min. N_2 and 125°C) are as follows:

C_2F_4	4.8 min.
c-C_3F_6	12.1
CF_3-$CF=CF_2$	14.5
c-C_4F_8	22.4

No evidence of other peaks in either the starting material or the reaction product above the detectable limit (about 0.03%) was obtained. This excludes the presence of C_2 and C_3 hydrocarbons which may have been present as a result of the photochemical reaction and which may have been building up in the unreacted starting material. It also excludes unidentified side products of the reaction.

3.1.2 <u>The Differential Equation Describing the Kinetics</u>.

The reaction scheme suggested above was:

$$c\text{-}C_3F_6 \xrightarrow{k_1} CF_2 + C_2F_4 \qquad (1)$$

$$2CF_2 \xrightarrow{k_2} C_2F_4 \qquad (2)$$

$$CF_2 + C_2F_4 \xrightarrow{k_3} c\text{-}C_3F_6 \qquad (3)\ .$$

Let P_r, P_T and P_m represent respectively the partial pressure in cm. of H_g of $c\text{-}C_3F_6$, C_2F_4 and CF_2, and assume in reaction (2) that: $\frac{dP_T}{dt} = \frac{k_2 P_m^2}{RT}$, then:

$$\frac{dP_r}{dt} = -k_1 P_r + \frac{k_3 P_m P_T}{RT} \qquad (4)$$

$$\frac{dP_m}{dt} = k_1 P_r - 2\frac{k_2 P_m^2}{RT} - \frac{k_3 P_m P_T}{RT} \qquad (5)$$

$$\frac{dP_T}{dt} = k_1 P_r + \frac{k_2 P_m^2}{RT} - \frac{k_3 P_m P_T}{RT} \qquad (6)$$

If it is assumed that the level of difluoromethylene concentration is steady, then $dP_m/dt = 0$ and subtracting (5) from (6):

$$\frac{dP_T}{dt} = \frac{3k_2 P_m^2}{RT} \qquad (7)$$

From the overall stoiciometry of the reaction, realizing that P_m is much less than P_r or P_T:

$$P_T = \frac{3}{2}(P_o - P_r) \qquad (8)$$

where P_o is the initial P_r for pure starting material.

Then $\frac{dP_T}{dt} = -\frac{3}{2}\frac{dP_r}{dt}$, and from (7)

$$\frac{dP_r}{dt} = -\frac{2k_2P_m^2}{RT}$$

or $$P_m = \left(-\frac{dP_r}{dt}\frac{RT}{2k_2}\right)^{1/2} \qquad (9)$$

Substituting (9) in (4):

$$\frac{dP_r}{dt} = -k_1P_r + \frac{k_3}{RT}\left(\frac{-dP_r}{dt}\frac{RT}{2k_2}\right)^{\frac{1}{2}}\frac{3}{2}(P_o-P_r)$$

or $$\frac{dP_r}{dt} + k_1P_r - a(P_o-P_r)\left(-\frac{dP_r}{dt}\right)^{\frac{1}{2}} = 0 \qquad (10)$$

$$\text{where } a = \frac{3k_3}{2}\left(\frac{1}{2k_2RT}\right)^{\frac{1}{2}}$$

The differential equation (10) cannot be integrated exactly and numerical methods must be used to carry out the integration and to determine a and k_1 from experimental data. In order to do this, it is convenient to rearrange equation (10):

$$\frac{P_r}{P_o} = \frac{-\frac{1}{P_o}\frac{dP_r}{dt} + a\left(\frac{-dP_r}{dt}\right)^{\frac{1}{2}}}{k_1+a\left(\frac{-dP_r}{dt}\right)^{\frac{1}{2}}}, \text{ or}$$

$$\frac{P_r}{P_o} = \frac{\alpha X^{\frac{1}{2}} + X}{\alpha X^{\frac{1}{2}} + 1} = Y$$

$$\text{where } X = \left(\frac{-dP_r}{dt}\right)\frac{1}{P_ok_1} \qquad (11)$$

$$\alpha = a\left(\frac{P_o}{k_1}\right)^{\frac{1}{2}}$$

or solving for X and taking only the positive quadratic root:

$$X = \left[\frac{(\alpha Y-\alpha) + [(\alpha-\alpha Y)^2 + 4Y]^{\frac{1}{2}}}{2}\right]^2 \qquad (12)$$

Integration of the differential equation (10) is effected by selecting a particular combination of α and k_1; the X corresponding to a series of Y can be calculated from equation (12). The area under the curve of a 1/X against

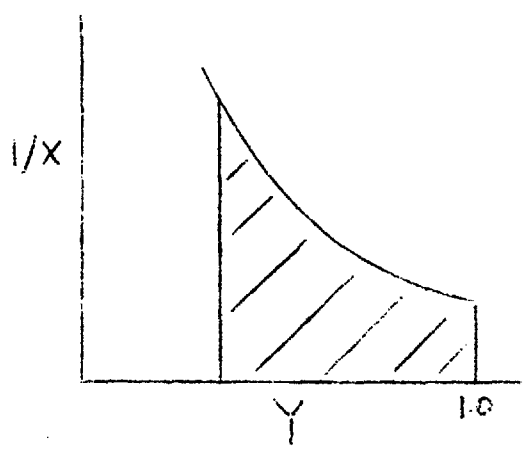

Y plot is the value of $k_1 t$. Thus from the assumed k_1, the t corresponding to various Y are found.

3.1.3. Treatment of Experimental data.

During an experiment, a total pressure-time record is obtained. The treatment of the raw data to get the true pressure variations has been considered in section 2.1.5. This information must be corrected for dead space to

determine the changes taking place at the reaction temperature. The value of P_r is related to the total pressure P and its initial value P_o by the relation:

$$P_r = 3P(P_o/P)^{1/b} - 2P$$

where $1/b = (V_h + V_c T_h/T_c)(1/V_h)$

V_h = Vol. of reactor at T_h, the reactor temp.

V_c = Vol. of reactor at T_c, the dead space temp.

The derivation of this expression due to Allen (46), is given in Appendix I.

The dead space temperature was estimated from the following formula:

$$T_c = \frac{T_h - \left(\frac{T_h - 317}{2}\right) + 317}{2},$$

where the temperature of the greaseless stopcock assembly is 44^oC or 317^oK. Greater weight is given to the temperature in the region of the greaseless stropcock and pressure transducer connection where a more significant proportion of the dead space is found. Thus T_c is an average between 44^oC and an estimate of the temperature half way to the reactor. An error of several degrees in T_c does not significantly effect the value of b and even

less the overall dead space correction.

The experimental results for variation of Y with t may now be compared with the variation calculated by numerical integration of equation (10). The values of k_1 and α which best predict the experimental results are selected by trial and error.

To simplify this fitting process, a program was written in Fortran IV for use with the I.B.M. 1401-7090 tandem of the Imperial College Computing Section, to carry out the graphical integrations. Simpson's rule was used to approximate the areas under the curves. The program is given in Appendix III. The integration was in fact carried out for a large number of k_1 and α at equal Y intervals. Print out was arranged as follows for example:

α	Y	.80	.78	.76
5.25		.4158	.4976	--
-		.4260	-	-
-		-	values of $k_1 t$	

For each Y a graph of $k_1 t$ against α was plotted.

To determine the best fit of the experimental data from the computer information, a series of trial k_1's were selected. The corresponding $(k_1 t)$'s were then calculated using the experimental t's at a series of Y values. The corresponding α's were then determined

from the appropriate graph of $k_1 t$ against α. For each value of Y a graph of trial k_1 against α was plotted. The results of the technique are illustrated for a typical run B-7 in figure 3.3[a], where values of Y from 0.9 to 0.3 in steps of 0.1 were selected. In theory all the lines for different Y should intersect at the same point indicating the k_1 and α which apply over the range of experimental data. In practice k_1 and α must be selected from a region of line intersections; a little experience makes the "weighting" of particular Y curves and intersections a quicker process. The fit may be tested by determining $k_1 t$ values from the α of the fitting process, using the $k_1 t$-α curves; the predicted t's are then found from these values and the k_1 from the fitting process, and then compared to the appropriate experimental t's. From figure 3.3[a] values of $k_1 = 0.27$ and $\alpha = 1.0$ were selected as the best fit for run B-7 and the resulting comparison is shown in the following table:

Y	Predicted $k_1 t$	Predicted t (min.)	Experimental t (min.)
.9	0.111	0.41	0.40
.8	0.250	0.925	0.91
.7	0.429	1.59	1.59
.6	0.666	2.46	2.46
.5	1.00	3.70	3.71
.4	1.50	5.55	5.54
.3	2.35	8.70	8.86

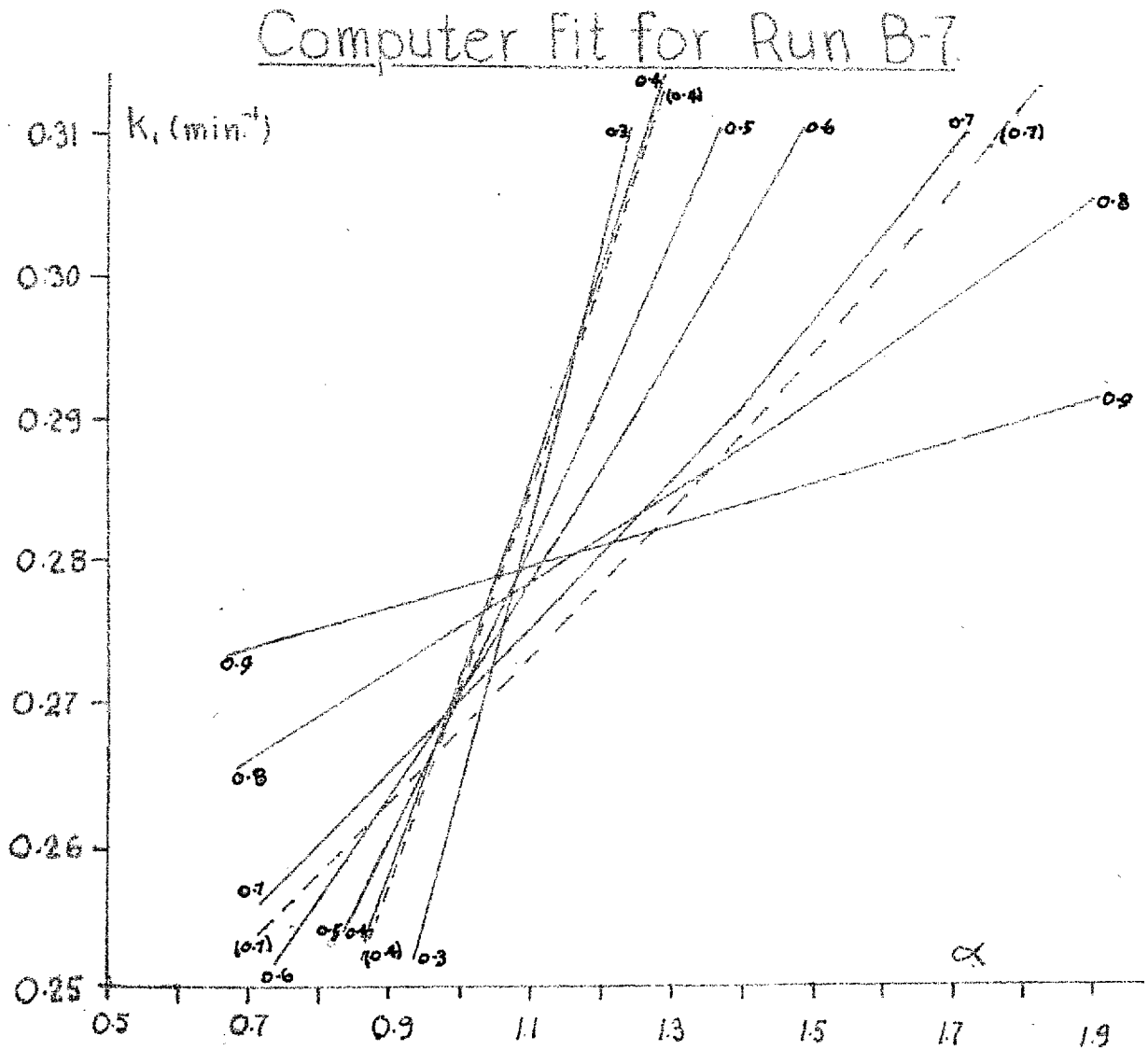
Computer Fit for Run B-7
k, (min⁻¹)
0.31
0.30
0.29
0.28
0.27
0.26
0.25
0.5
0.7
0.9
1.1
1.3
1.5
1.7
1.9
α
0.4
(0.4)
0.3
0.5
0.6
0.7
(0.7)
0.8
0.9
0.9
0.8
0.7
(0.7)
0.6
0.5
0.4
(0.4)
0.3

Figure 3.3[a]

In the product of run B-7 removed at $t = 10$ minutes, 0.2% octafluorocyclobutane was found. If the pressures at 9 min. are corrected by assuming this material to be C_2F_4, the time to reach $Y = 0.3$ is 8.66 min., bringing the figure for this Y into line. With chart speeds of 120 in. per hr., uncertainties of up to 0.5 sec. in the times of observed pressures can be expected; but the variations in pressure at later stages in the run are so small that uncertainties of up to 2-3 seconds can be expected so that the fit for run B-7 is representative within experimental error.

The computer program has been checked by the more tedious method of manual graphical integration. The validity of the results may be illustrated by the application of this procedure to run B-7. For $\alpha = 1.0$, values of X were calculated in equation (12) for Y from 0.9 to 0.3 in steps of 0.1. A plot of $^1/X$ against Y was made as shown in figure 3.3b, and $k_1 t$ evaluated at each Y by counting off squares on the graph origional. The results evaluated using $k_1 = 0.27$ are compared to the observed t's in the following table:

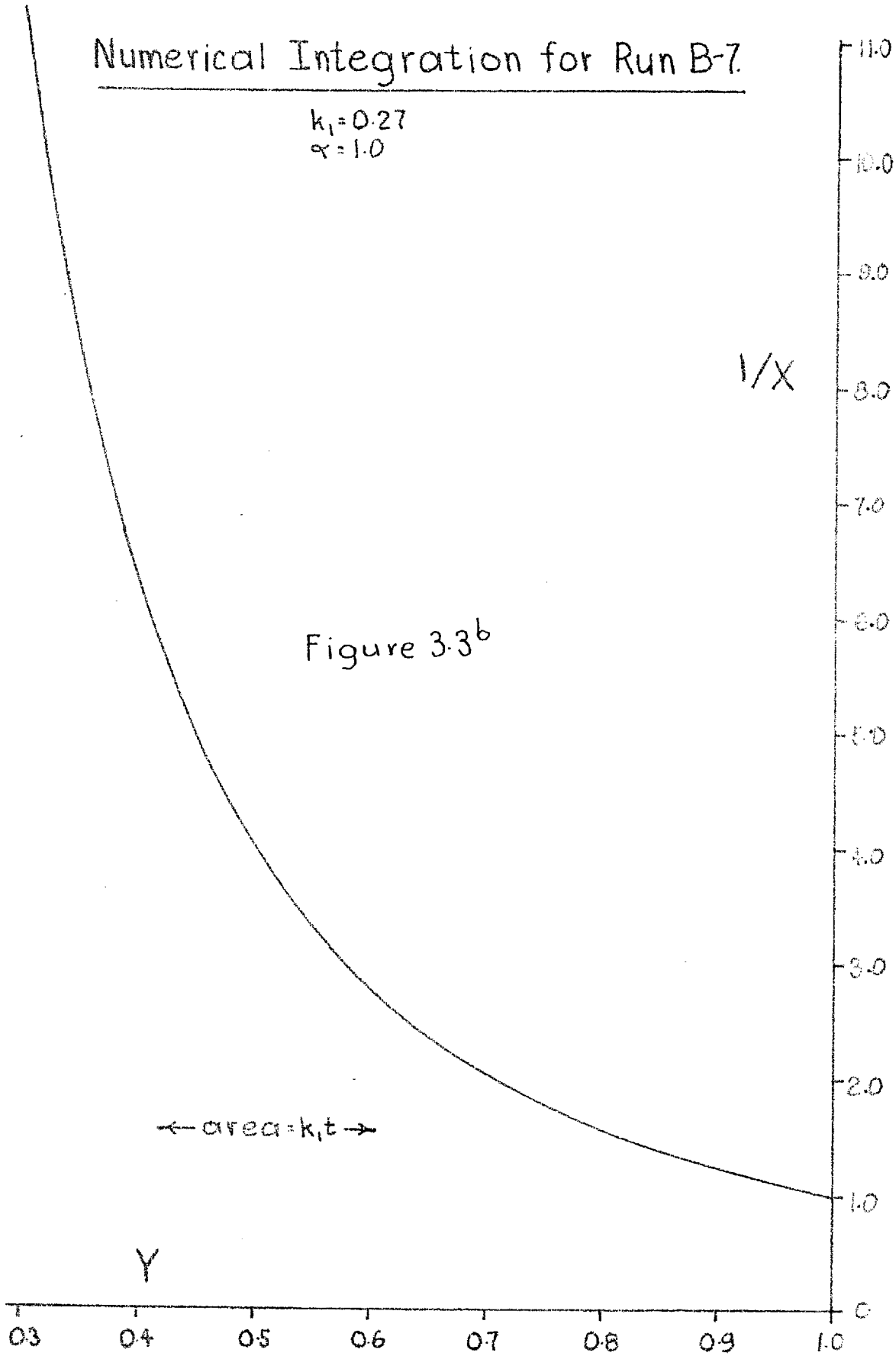
Numerical Integration for Run B-7.
$k_1 = 0.27$
$\alpha = 1.0$
1/X
11.0
10.0
9.0
8.0
7.0
6.0
5.0
4.0
3.0
2.0
1.0
0
← area = $k_1 t$ →
Y
0.3
0.4
0.5
0.6
0.7
0.8
0.9
1.0

Figure 3.3b

Y	Predicted $k_1 t$	Predicted t (min.)	Experimental t (min.)
.9	0.110	0.407	0.40
.8	0.248	0.919	0.91
.7	0.425	1.575	1.59
.6	0.661	2.45	2.46
.5	0.992	3.68	3.71
.4	1.501	5.56	5.54
.3	2.335	8.64	8.86

The results of the computer have been verified at suitable other values of the constants used to ensure that error has not been brought in by various program changes.

The fit for run B-7 whose temperature was 266.1°C is typical for the runs from 240-300°C. The lines in figure 3.3^a for $Y = 0.4$ and 0.7 are representative of the fit since they intersect at $\alpha = 1.0$ and $k_1 = 0.27$. If the t's for these lines are increased by 0.5 sec., then the curves are displaced as shown by the dotted lines of figure 3.3^a. This represents a fit at $\alpha = 0.97$ and $k_1 = 0.2665$. Generally speaking, the uncertainties in k_1 and α when a fairly large number of Y curves are drawn is not greater than 2% in k_1 and 5% in α.

The same is not true at higher temperatures as is illustrated in figure 3.4 for run H-9 at 321.1°C. A fit of $k_1 = 9.8$ and $\alpha = 0.26$ was assumed. If the t's for $Y = 0.2$ and 0.4, which intersect at this k_1 and α, are increased by 0.5 sec. then the curves are displaced as shown by the dotted lines of figure 3.4; the intersection is at $k_1 = 9.25$ and $\alpha = 0.25$. The increased uncertainty in k_1 (about 6% in this case) is typical of runs at this temperature. Uncertainties in α are usually increased correspondingly. At such temperatures reaction times are so short that the Y-t data becomes less certain than at lower temperatures. The times involved are illustrated in the following table where figures for the half life of $c\text{-}C_3F_6$ have been given for typical high temperature runs:

Run	Temp.	P_o (cm.)	half-life of $c\text{-}C_3F_6$ (sec.)
H-4	320.7	1.561	6.0
H-8	320.5	8.71	4.8
H-10	320.9	22.63	4.3
I-5	313.5	3.22	6.6
I-4	313.5	9.33	7.1
I-2	313.9	23.58	9.1
G-7	302.5	1.657	15.6
G-3	302.4	8.331	15.0
G-4	302.2	24.22	17.6

Computer Fit for Run H-9.

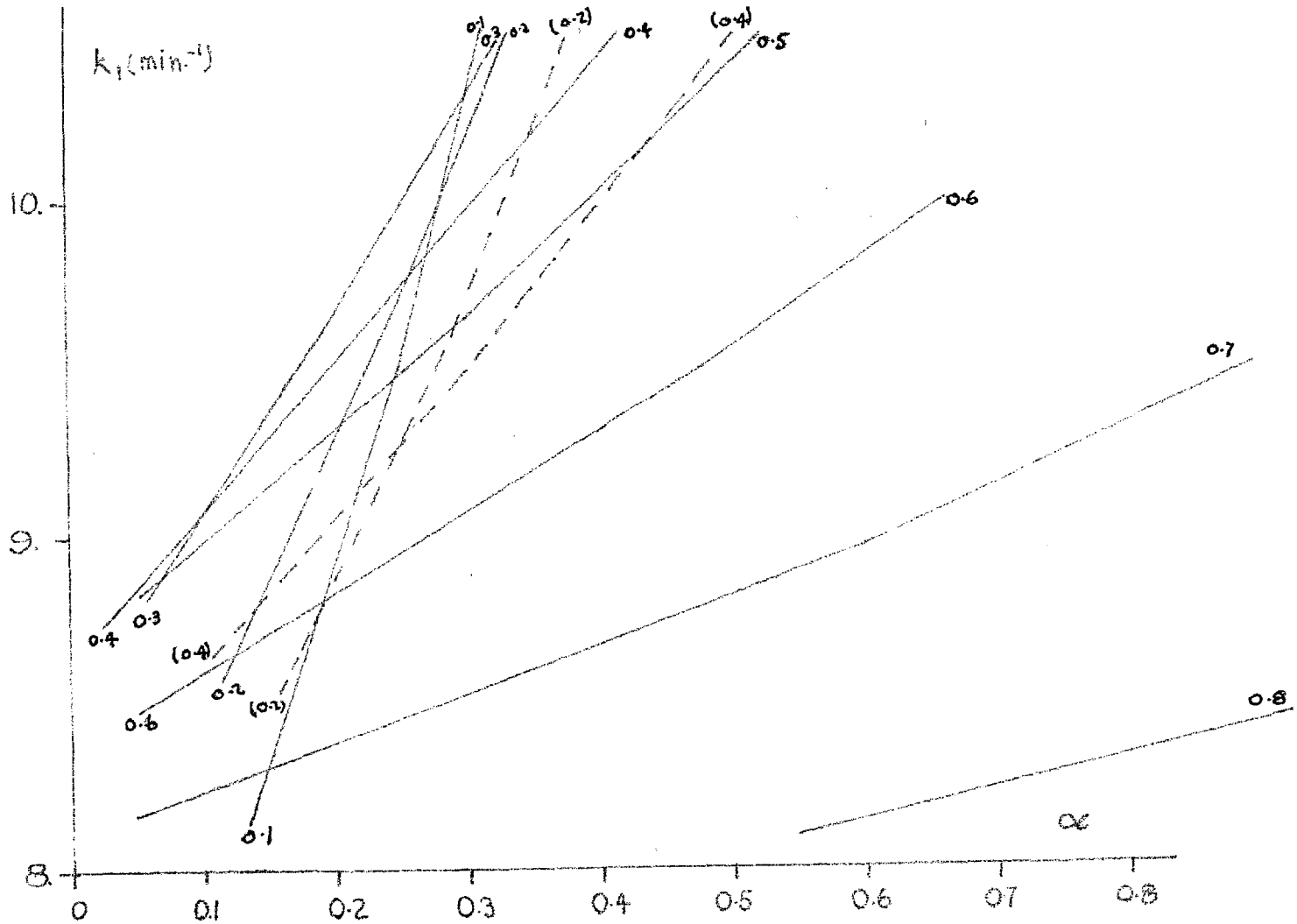

Figure 3.4

The fitting process again increases in uncertainty below 240°C. Typical conversions at 240° are about 50% while for high pressure runs at 230° they are only 20-30% It is obvious from figures 3.3[a] and 3.4 that a higher conversion will give Y lines of widely differing slopes and hence more precise intersections. With low conversions most of the Y lines do not differ greatly in slope and the uncertainties increase.

The factor a in equation (10) was calculated from the α and k_1 of the computer fit and the known P_o in the expression (11) for α. The value of $k_3/k_2^{1/2}$ could then be determined from equation (10).

Octafluorocyclobutane has been observed in the products of most of the reactions as indicated by the results from a number of runs in tables 3.1 and 3.2, of section 3.1.1. Higher pressures encourage the dimerization of C_2F_4 as would be expected. In the discussion of the fitting process done for run B-7 it was shown that allowance for $c\text{-}C_4F_8$ gave a shorter time for Y = 0.3 bringing it into line with the computer fit. In runs where $c\text{-}C_4F_8$ was greater than 0.3% in the product the α against P_1 plot for a Y curve evaluated from an experimental t late in the run would be abnormally displaced to the right (see figure 3.3[a]). It would not

intersect the other Y curves in the region where most of the lines were meeting. If such was the case this Y curve was neglected in determining the fit. In most cases as with B-7, the curve could be brought into line by making the correction for $c\text{-}C_4F_8$. In practice reaction times were determined by the amounts of $c\text{-}C_4F_8$ whose formation could be roughly predicted from the concentrations in earlier runs.

The only side product of the reaction other than $c\text{-}C_4F_8$ which has been confirmed is $CF_3.CF=CF_2$. Terminal analysis was carried out on the products of most of the reactions mainly to determine the level of $c\text{-}C_4F_8$ reached at the particular temperature and pressure. However on estimate of the perfluoropropene content which was usually small could also be obtained. Under the analysis conditions used this substance comes out as a shoulder peak about two and a half minutes after perfluorocyclopropane. No calibrations were performed and peak area was used to estimate the mole per cent. In analysis of starting material, perfluoropropene content is usualy 0.1% or less. Because of the excessive tailing of the large $c\text{-}C_3F_6$ peak in these analyses the uncertainty is about $\pm$ .03%. If the concentration was less than 0.01% this would be confirmed by the smoothness

of the $c\text{-}C_3F_6$ tailing and the perfluoropropene content was assumed to be zero.

The uncertainty in the analysis of the products depends on a number of factors. For the runs at 230 and 240°C the same uncertainty as in starting material analysis applies since with from 20-60% reaction the $c\text{-}C_3F_6$ content in the sample is still large. This applies for reactions with starting pressures above about 0.1 cm. where the sample size is sufficient to see small concentrations of the impurity. Below this pressure the uncertainty increases with decreasing sample size to about $\pm$ 0.15% at the lowest pressures studied. At higher temperatures the accuracy of product analysis improves since the $c\text{-}C_3F_6$ content is lower. A fair estimate of the accuracy for the runs above 250°C is about $\pm$ 0.015%. This uncertainty increases with decreasing sample size below 0.1 cm run pressure as with the lower temperature runs.

The product analyses for perfluoropropene content where meaningful results were obtained are presented in Table 3.3. The results were arranged in the order in which the runs were performed in an attempt to correlate the perfluoropropene content with reactor history. Careful consideration of the experimental records gives

Table 3.3 Pyrolysis of c-C_3F_6

Chromotographic Analysis by Peak Area for $CF_3.CF = CF_2$

Results in Temporal Order

Run	Temp. °C	P_o cm.	Reaction time min.	$CF_3.CF = CF_2$ % initial	final
D-1	230.4	11.69	135.0	0	0
D-2	229.8	23.97	120.0	0	0
E-1	240.3	11.79	52.0	0	0
F-1	289.4	12.17	4.0	0	0.08
F-2	289.5	6.06	2.5	0	0
C-2	274.0	5.83	5.0	0	0
G-1	303.4	5.51	1.5	0	0.16
H-1	323	6.17	1.2	0	0.16
I-1	314	6.29	1.2	0	0.12
C-3	277.6	12.27	5.0	0.06	0.10
C-4	277.4	24.02	5.0	0.12	0.10
C-5	274.9	18.96	5.0	0	0.07
C-6	274.0	9.41	5.0	0	0.05
C-7	276.8	18.72	6.0	0.1	0.1
C-8	277.0	12.41	6.0	0.1	0.1
C-9	276.9	3.08	8.0	0.1	0.16
C-10	277.0	1.431	8.0	0.1	0.15
C-11	277.3	0.594	8.0	0.1	0.18
A-9	253.5	23.50	30.0	0	0
A-10	253.5	12.08	30.0	0	0.10
A-11	253.5	6.085	30.0	0	0.10
A-20	253.3	41.2	18.0	0	0

Table 3.3 Pyrolysis of c-C_3F_6

Run	Temp. ^oC	P_o cm.	Reaction time min.	$CF_3.CF = CF_2$ % initial	final
A-23	252.5	35.54	20.0	0	0
A(P)-24	253.3	6.103	30.0	0.10	0.40
A(P)-25	253.3	2.017	30.0	0.10	0.71
A(P)-26	253.1	8.535	20.0	0.10	0.08
H(P)-2	321.6	6.253	1.3	0	0.10
D(P)-3	230.6	6.08	60.0	0	0
F-3	290.0	8.327	3.0	0	0.12
F-4	289.9	3.616	2.0	0	0.43
F-5	289.7	1.803	2.0	0	0.55
F-6	289.7	0.831	2.0	0	0.09
F-7	288.4	18.74	1.8	0	0.03
F-8	288.4	12.08	1.9	0	0
B-3	265.9	23.61	6.0	0.48	0.56
B-4	265.9	18.09	7.0	0.48	0.57
B-5	265.9	12.14	9.0	0.48	0.55
B-6	266.3	5.777	13.0	0	0.03
B-7	266.3	4.065	10.0	0	0.09
B-8	266.2	1.938	10.0	0	0.10
B-9	266.2	0.942	10.0	0	0.13
E-2	240.5	1.829	69.3	0	0
E-3	240.8	6.229	60.0	0	0
E-4	240.7	3.957	60.1	0	0
E-5	240.6	12.01	45.0	0	1.15
E-6	240.4	23.19	55.0	0	0.13
E-7	240.4	18.11	50.0	0	0.10

Table 3.3 Pyrolysis of c-C_3F_6

Run	Temp. °C	P_o cm.	Reaction time min.	$CF_3.CF = CF_2$ % initial	final
G-2	302.4	5.782	1.1	0.02	0.37
G-3	302.4	8.331	0.9	0.02	0.09
G-4	302.2	24.22	1.1	0.02	0.07
G-5	302.3	18.57	1.1	0.02	0.09
G-6	302.4	11.41	1.1	0.02	0.10
G-7	302.5	1.657	1.0	0.02	0.25
H-3	320.8	1.649	0.8	0	0.02
H-5	320.6	9.55	0.8	0	3.33
H-6	320.6	2.430	0.7	0	0.15
H-7	320.6	5.007	0.8	0	0.02
H-8	320.5	8.71	0.7	0	0.01
H-9	321.1	8.93	0.8	0.18	1.23
H-10	320.9	22.63	0.9	0.18	0.31
H-11	321.1	2.943	0.8	0.18	0.62
I-2	313.9	23.58	1.1	0.18	0.19
I-3	313.5	18.56	1.0	0.18	0.25
I-4	313.5	9.33	0.9	0.18	0.34
I-6	313.6	4.851	0.8	0.18	0.20
D-4	230.1	22.91	60.0	0	0
D-5	229.9	18.37	60.0	0	0
D-6	229.9	8.75	50.0	0	0
D-7	229.7	3.171	45.0	0	0
D-8	229.6	5.216	45.0	0	0

Table 3.3 Pyrolysis of c-C_3F_6

Run	Temp. ^oC	P_o cm.	Reaction time min.	$CF_3.CF = CF_2$ % initial	final
A-29(ii)	253.3	0.078	40.0	0	0
A-30(i)	253.2	0.017	37.4	0	0
A-31	253.1	0.034	28.0	0	0
A-32	253.0	0.014	45.0	0	0
A-35	253.0	0.132	40.0	0	0
D-9	230.2	52.44	60.3	0.08	0.10
D-11	229.8	40.82	60.0	0.1	0.1
D-12	229.7	30.85	65.0	0.1	0.1
D-13	230.5	2.763	60.0	0.1	1.09
D-14	230.5	0.995	45.0	0.1	1.50
D-15	230.3	0.195	65.2	0.1	0.1
A-36(i)	253.3	0.0235	6.2	0.03	0.21
A-36(ii)	253.3	0.0240	12.2	0.03	0.32
A-36(iii)	253.3	0.0240	22.2	0.03	1.87
A-36(iv)	253.3	0.0241	35.2	0.03	5.32
A-37(i)	253.0	0.0092	20.2	0.03	1.61
A-37(ii)	253.0	0.0090	30.2	0.03	0.86
A-37(iii)	253.3	0.0089	40.2	0.03	1.45
A-37(iv)	253.3	0.0090	10.2	0.03	0.29
A-36(v)	253.3	0.0240	45.2	0.03	0.22
D-17(ii)	230.4	0.0053	70.2	0	0

no evidence that perfluoropropene formation was enhanced by a reactor which might not have been properly seasoned. On some occasions the reactor was left under vacuum for several days between reactions, on others with a pressure of from 5-20 cm. of tetrafluoroethylene. If air had leaked into the heated reactor it was seasoned with tetrafluoroethylene. But there seems to be no reason to believe that this treatment causes increased perfluoropropene formation. Substantially greater than normal quantities were occasionally formed in one run of a sequence on the same day.

If any trend can be deduced from these analysis results it is that higher temperature and lower pressure encourage perfluoropropene formation; this trend is observed in the majority of cases although the reverse is also observed. Enhanced perfluoropropene content was observed in the runs in the packed reactor at 253°C (designated P in brackets after the letter of the run number). Normal results were however obtained in the packed reactor runs at 320 and 230°C. The lack of consistency over a large number of runs when pressure, temperature, and condition of starting material were known indicates that the history of the reactor is of

some significance in the formation of perfluoropropene.

In most cases high concentration of $CF_3-CF_2 = CF_2$. occurs at high temperature. The possible effect on the fitting process can be misleading when it is realized that pressure changes only during about the first $^1/_3$ of the total reaction time are used to calculate results. In run I-4 for instance, 0.82% $c-C_4F_8$ and 0.16% $CF_3.CF = CF_2$ can be assumed to have formed in the reaction. But the total reaction time was 54 seconds and the latest line used in the fitting process was for $Y = 0.2$ which was at $t = 19.3$ seconds. In run H-5 where 0.98% $c-C_4F_8$ and 3.33% $CF_3.CF = CF_2$ were formed, the latest line used was at $Y = 0.2$ for which $t = 14.1$ sec.; the total run time was 48.5 sec. Thus at these temperatures the impurities in the product are not representative of impurities present during the useful pressure changes.

At lower temperatures occasional concentrations of 1-1.5% $CF_3.CF = CF_2$ are observed. Thus at later stages in the reaction a true concentration of $c-C_3F_6$ less than that indicated by the pressure changes is in fact present, since no pressure change is observed for the reaction:

$$c-C_3F_6 \longrightarrow CF_3.CF = CF_2 \ .$$

In run D-14, 1.5% $CF_3.CF = CF_2$ was found in the product. The latest Y used was Y = 0.7 for which the t found was 39.3 min. This line did not agree too well with that for earlier lines and was neglected in the fitting process which predicted $t_{.7}$ at 36.6 min. If 1.5% $CF_3.CF = CF_2$ is assumed at 39.3 min an approximate corrected value of 37.5 min. is obtained. This falls within the uncertainty of estimating Y times at the pressure (1.0 cm.) of this reaction.

Thus in the cases where observable quantities of $c\text{-}C_4F_8$ or $CF_3.CF = CF_2$ are found the quantities are either too small to have an effect within the uncertainties of the fitting process or can explain anomalies in individual fittings within experimental error.

The ability of the integrated expression for pressure changes to predict the observed shape of the pressure time curve strongly supports the validity of the mechanism suggested.

3.2. Quantitative Measurements of Reaction Rate in the Region 0.5 - 55. cm. Pressure

In this section it will be shown that both k_1 and the ratio $k_3/(k_2)^{1/2}$ vary significantly with pressure in a range from 0.5 cm. upwards. Values of k_1 and $k_3/(k_2)^{1/2}$ at theoretical infinite pressure are determined by plotting appropriate functions against the reciprocal of starting pressure and extrapolating to $^1/P = 0$. Chromatographically purified perfluorocyclopropane containing less than 0.15% tetrafluoroethylene, less than 0.1% perfluoropropene and no octafluorocyclobutane was used as starting material.

3.2.1 The k_1^∞ Results

A large number of runs were carried out at two temperatures in order to establish with some certainty the nature of the variation of k_1 above 0.5 cm. The results for the A series of runs at 253.0°C are collected in table 3.4 and for the C series in table 3.5. The curve fitting procedure of section 3.1.3 was used to obtain the values shown. The constants for the A series have been plotted as $1/k_1$ against $^1/P_o$ in figure 3.5 and k_1 against P_o in figure 3.6. The corresponding

Table 3.4 Dissociation of Perfluorocyclopropane

Results at 253°C

Exper.	Temp. °C	P_o (cm.)	time (min.)	k_1 (min^{-1})	k_1 (253.0°C) (min^{-1})	a (cm. min.)$^{-1/2}$	a(253.0°C) (cm. min.)$^{-1/2}$
A-9	253.5	23.50	30.0	0.112	0.108	0.254	0.252
A-10	253.5	12.08	30.0	0.113	0.109	0.259	0.257
A-11	253.5	6.085	30.0	0.105	0.101	0.245	0.243
A-12	253.5	3.974	30.1	0.106	0.102	0.242	0.241
A-13	253.5	3.127	30.0	0.098	0.094	0.236	0.234
A-14	253.4	1.664	30.0	0.090	0.087	0.231	0.230
A-15	252.2	0.627	30.0	0.072	0.077	0.173	0.175
A-16	252.4	1.126	30.0	0.086	0.090	0.210	0.212
A-17	252.4	3.899	25.0	0.096	0.101	0.239	0.241
A-18	252.5	8.385	29.2	0.101	0.105	0.257	0.259
A-19	252.5	0.834	30.0	0.084	0.088	0.201	0.202
A-20	253.3	41.24	18.0	0.114	0.112	0.258	0.257
A-21	251.7	1.855	20.0	0.087	0.097	0.232	0.236
A-22	251.8	1.077	18.0	0.077	0.085	0.219	0.222
A-23	252.5	35.54	20.0	0.108	0.112	0.268	0.270
A-24(P)	253.3	6.103	30.0	0.114	0.111	0.249	0.248
A-25(P)	253.3	2.017	30.0	0.101	0.099	0.226	0.225
A-26(P)	253.1	8.535	20.0	0.112	0.111	0.255	0.255
A-27(P)	253.5	1.201	30.0	0.099	0.095	0.192	0.191
A-28(P)	253.8	0.610	30.0	0.091	0.085	0.186	0.185

Table 3.5 Dissociation of Perfluorocyclopropane

Results at 277°C

Exper.	Temp. °C	P_o (cm.)	time (min.)	k_1 (min^{-1})	k_1 (277.0°C) (min^{-1})	a (cm. min.)	a(277.0°C) $(cm.\ min.)^{-1/2}$
C-8	277.0	12.41	6.0	0.600	0.600	0.356	0.356
C-9	276.9	3.077	8.0	0.594	0.598	0.348	0.348
C-10	277.0	1.431	8.0	0.529	0.529	0.285	0.285
C-11	277.3	0.594	8.0	0.494	0.484	0.219	0.218
C-12	273.8	1.965	8.0	0.448	0.560	0.327	0.340
C-13	276.8	1.075	8.0	0.508	0.516	0.282	0.283
C-14	276.7	12.42	5.0	0.622	0.635	0.343	0.343
C-15	276.6	9.28	6.0	0.608	0.623	0.346	0.346
C-16	276.6	6.14	6.0	0.617	0.632	0.371	0.372
C-17	276.8	1.966	5.0	0.570	0.578	0.269	0.270
C-18	276.8	1.117	7.9	0.532	0.540	0.241	0.242
C-19	276.8	1.200	8.0	0.541	0.549	0.209	0.209
C-20	276.7	12.52	7.0	0.605	0.619	0.312	0.313
C-21	276.7	6.25	7.0	0.610	0.624	0.347	0.347
C-22	279.7	1.957	5.8	0.683	0.563	0.307	0.299
C-23	279.6	0.955	6.0	0.615	0.510	0.253	0.246

Variation of $1/k_1$ with $1/P_o$ for A Series of Experiments. T=253.0°C

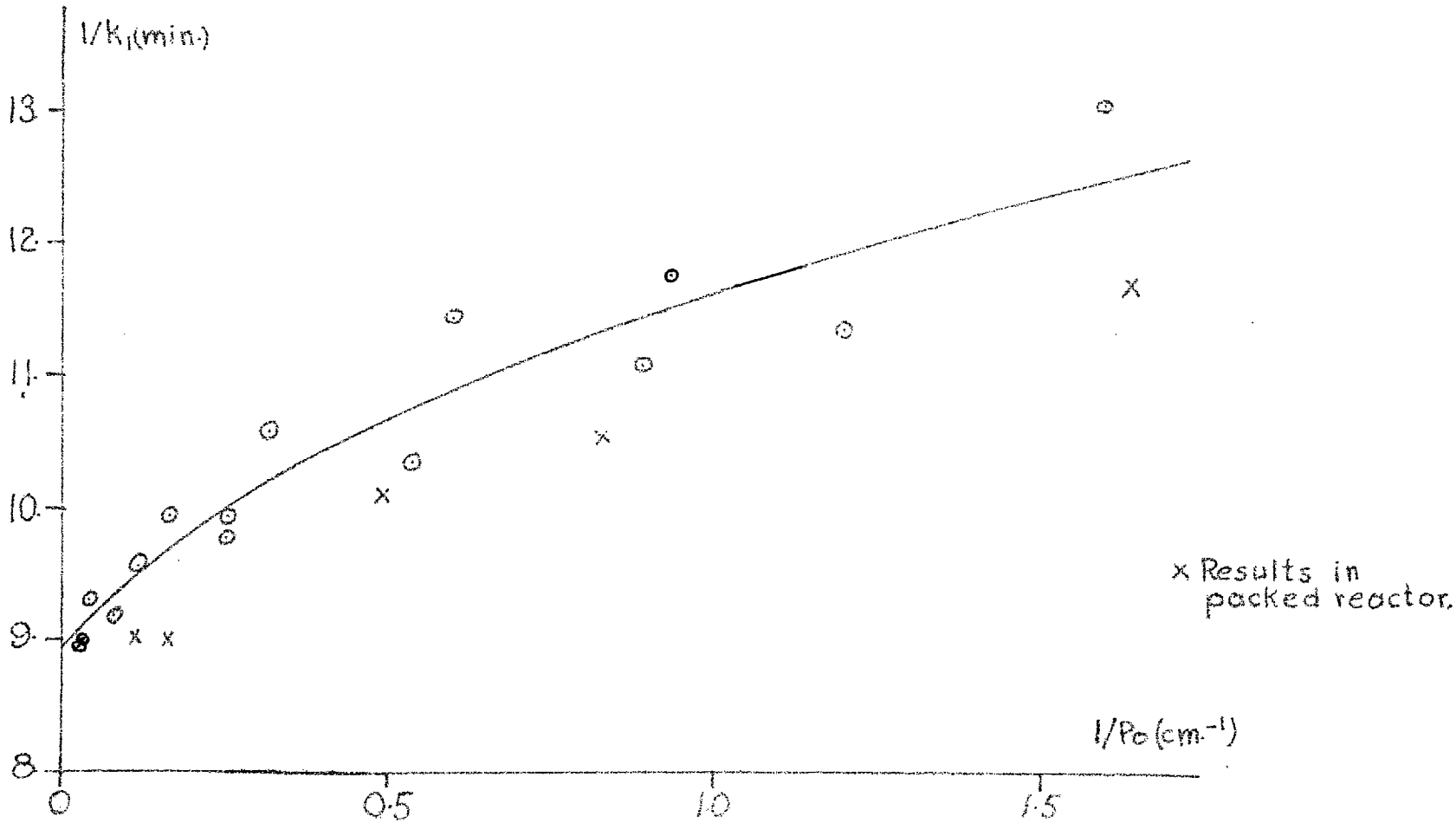

Figure 3.5

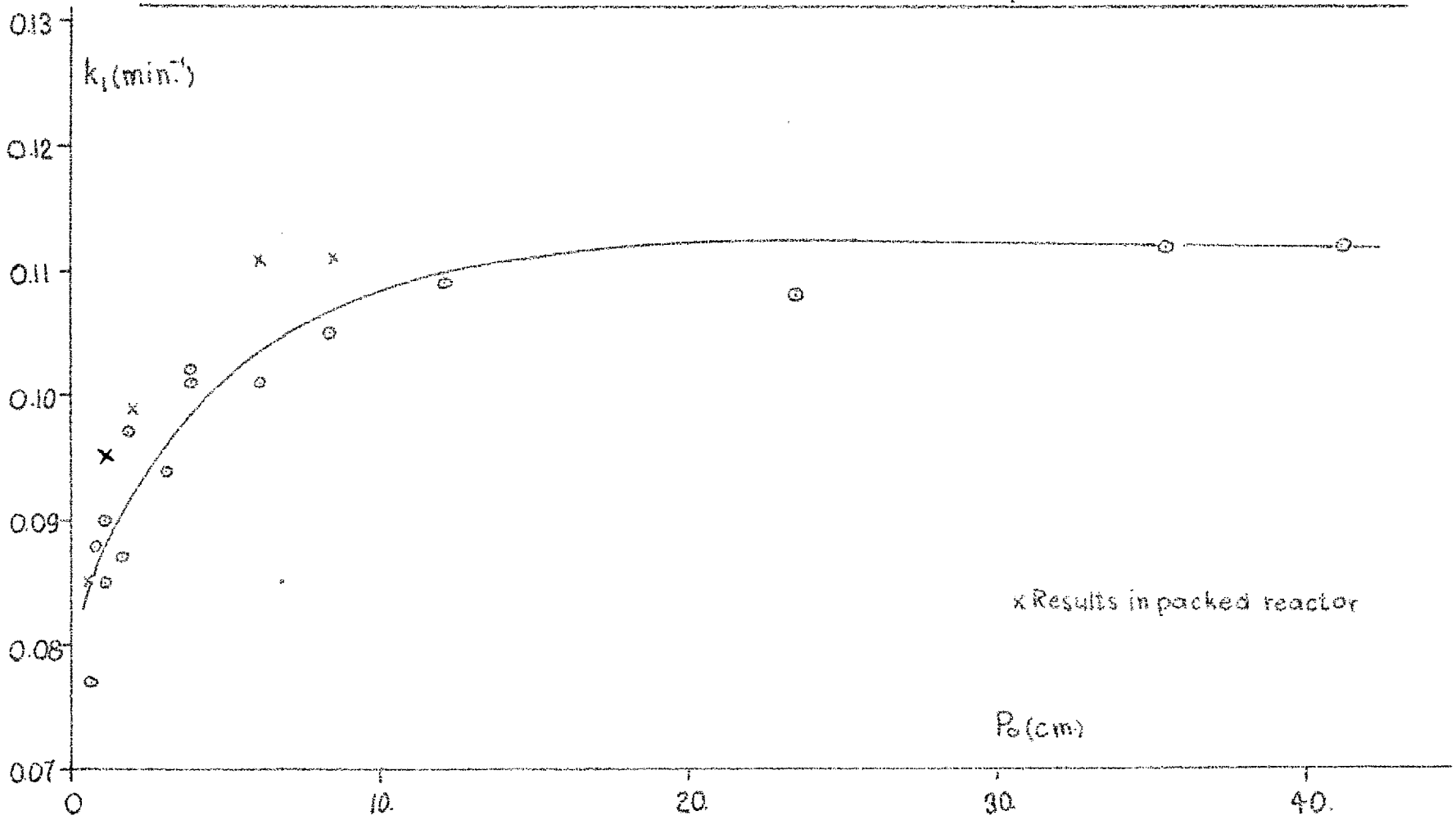
Variation of k_1 with P_o for A Series of Experiments. T=253.0°C.
0.13
k_1(min.$^{-1}$)
0.12
0.11
0.10
0.09
0.08
0.07
0
10.
20.
30.
40.
x Results in packed reactor
P_o(cm.)

Figure 3.6

figures for the C runs are figures 3.7 and 3.8. The $k_1 - P_o$ plots indicate a detectable fall off at about 8-12 cm. It is not really certain which is the best method for determining k_1^∞ by extrapolation. In the two series of runs under consideration either method gives the same results within experimental error. However since in subsequent series of runs many fewer actual runs were done it was deemed best to use the $1/k_1 - 1/P_o$ plots since being more nearly a straight line they would be safer to extrapolate with a smaller number of points; in addition the scatter in the more important higher pressure runs is reduced by using the reciprocal pressure scale.

The uncertainty of the k_1^∞ values determined from these plots can be estimated from the spread of points about the line drawn through them. By this means uncertainties of 3.6% for the A series and 2.7% for the C series of runs have been placed for the value of k_1^∞. This is about what would be expected for a large number of runs and the uncertainty due to the fitting process (see previous section).

The value of k_1^∞ can also be found from the initial slope of the pressure-time record. At time zero:

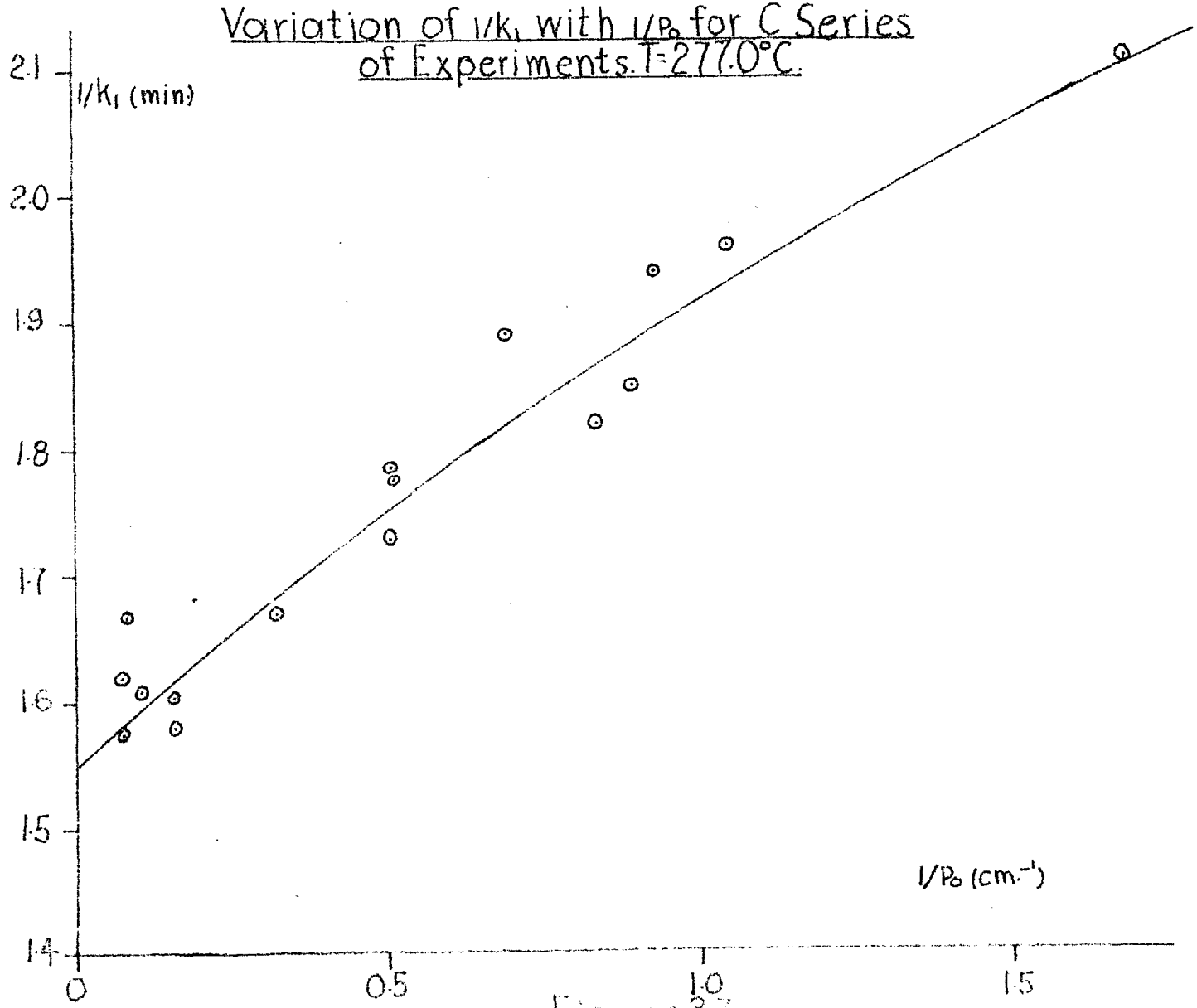
Variation of 1/k1 with 1/P0 for C Series of Experiments. T=277.0°C.
1/k1 (min)
2.1
2.0
1.9
1.8
1.7
1.6
1.5
1.4
0
0.5
1.0
1.5
1/P0 (cm.⁻¹)

Figure 37.

Variation of k_1 with P_o for C Series of Experiment. T=277.0°C.

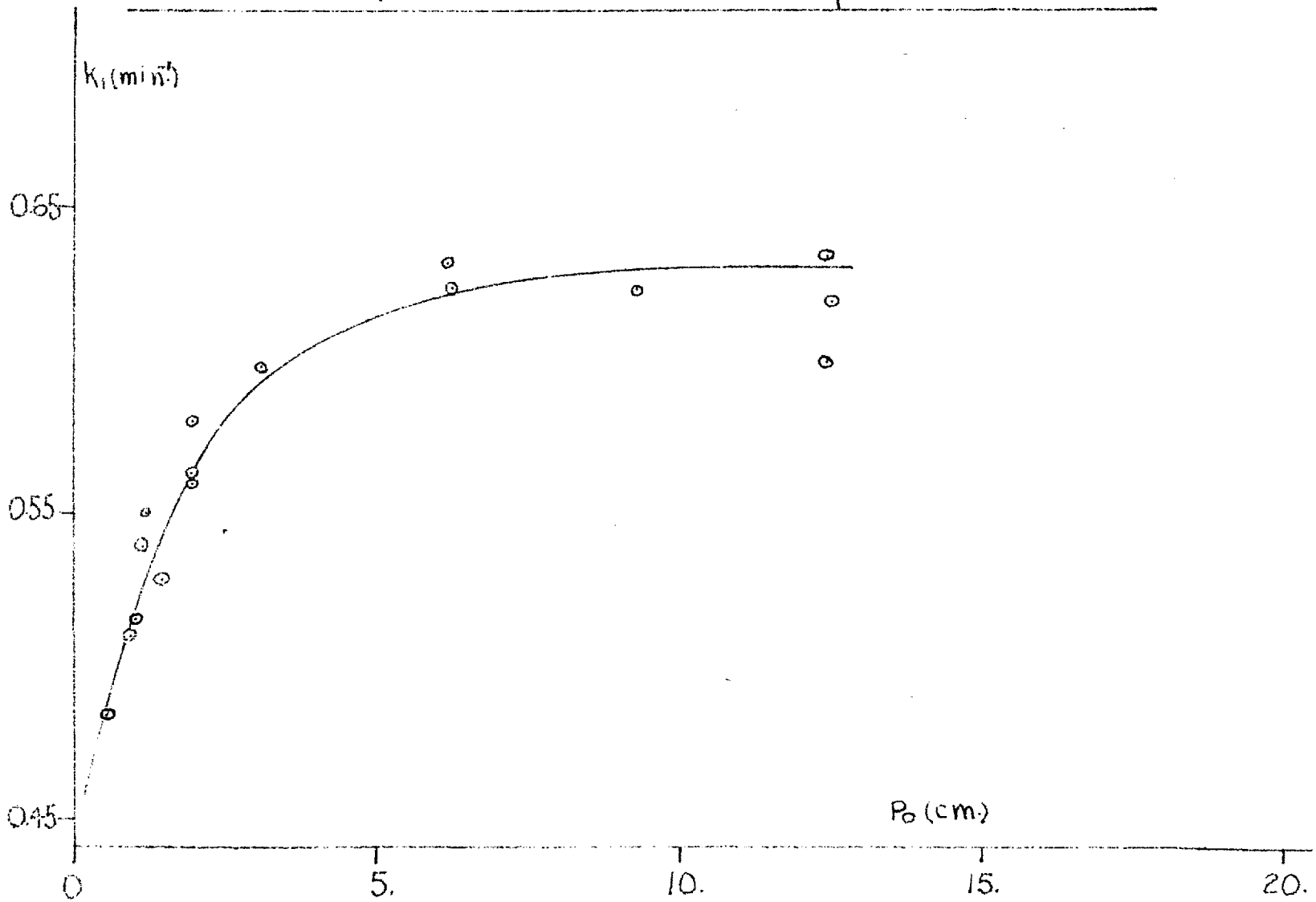

Figure 3.8

$$\left(\frac{dP_r}{dt}\right)_o = -k_1 P_o$$

The value of P_r at any time is given by:

$$P_r = 3P(P_o/P)^{1/b} - 2P \quad \text{(see appendix I)}$$

whence

$$\frac{dP_r}{dt} = (1 - \frac{3}{b}) \frac{dP}{dt}$$

and $k_1 = \frac{1}{P_o}(\frac{3}{b} - 1)(\frac{dP}{dt})_o$

This has been done for the A series of runs and the results plotted as $^1/k_1$ against $^1/P_o$ in figure 3.9. If this graph is placed over that of figure 3.5, the curves from the two methods coincide allowing for the spread of the points although greater scatter is found from the initial slope method. The method of determining k_1^{∞} from the fitting process is further vindicated. The uncertainty in determining the initial slope explains the scatter in figure 3.9. Upon reexamination of the results from a number of runs the k_1 from the

Initial Slope Variation of $1/k_1$ with $1/P_o$ for A Experiments. T = 253.0°C.

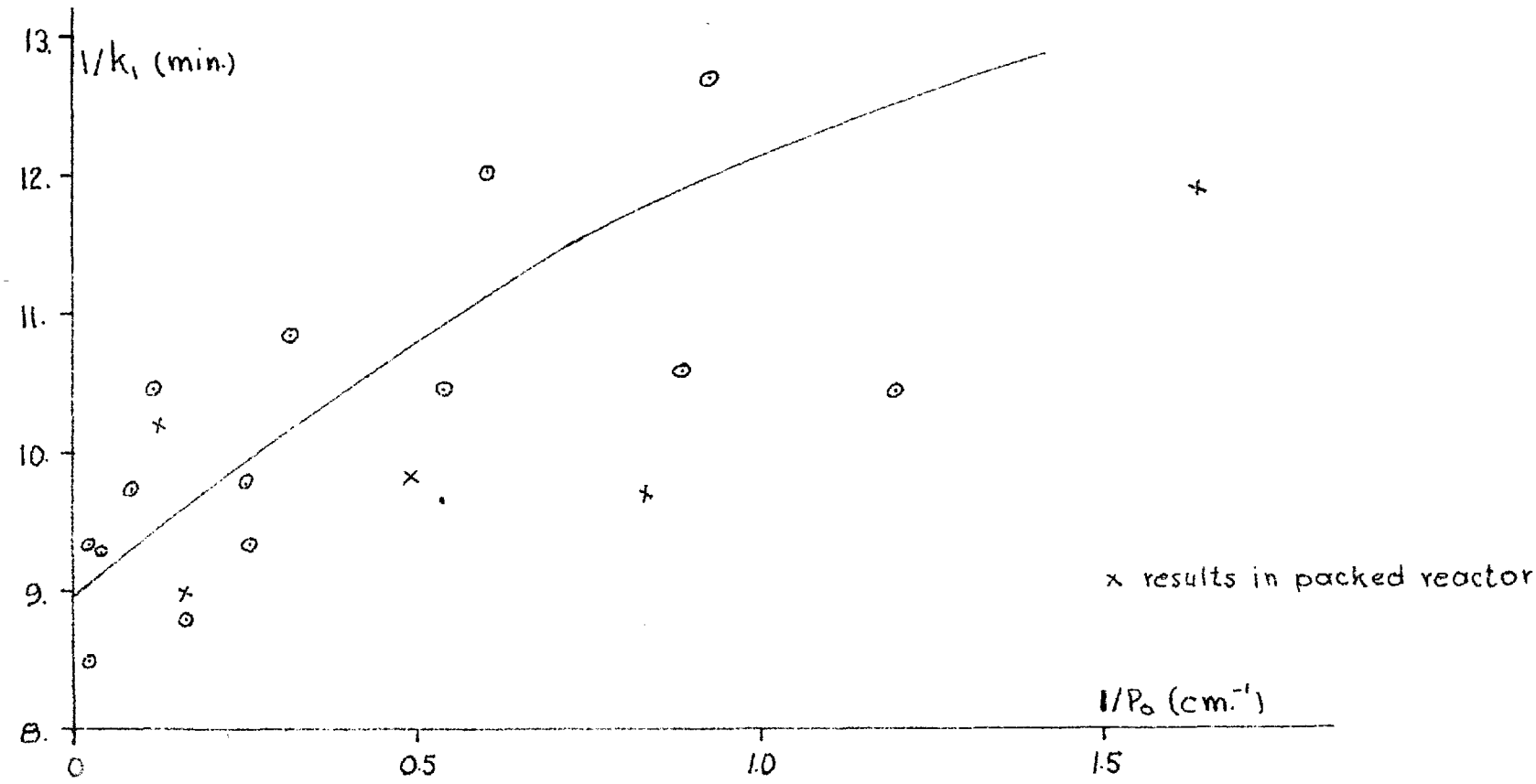

Figure 3.9

computer fitting process could be used to determine $(dP/dt)_o$ and was nearly always within the spread of possible $(dP/dt)_o$. The initial slope method was not applied to other run series.

Because of the variation in pressure during a run the question arises whether k_1 varies during a run. As a consequence of the rise in pressure a higher k_1 might be expected in the later stages of the run. In the following table, three runs which are representative of figure 3.5 have been taken. Values of k_1 for the experimental initial and final pressure have been read from the line through the points of figure 3.5.

Run	Initial Values		Final Values	
	P_o (cm.)	k_1 (min.$^{-1}$) (fig.3.5)	P_F (cm.)	k_1 (min.$^{-1}$) (fig.3.5)
A-9	23.50	0.1098	29.48	0.1120
A-11	6.085	0.103	8.03	0.1055
A-15	0.627	0.0798	0.860	0.084

For A-9 and A-11 the expected change in k_1 is about equal to the uncertainty of the fitting process; this is however not to be interpreted as the cause of it. For runs below 1 cm. (e.g. A-15) the method of using the recorder to follow the pressure changes indicated by the transducer is approaching the limit of its usefulness. Uncertainty in the fitting process of

greater than 2% is to be expected and changes such as that indicated by the above table would not be resolved. Although there is undoubtedly some variation in k_1 during a run if the curves of figures 3.5 to 3.9 are to be believed, the determination of k_1^{∞} is not thus affected, since as seen in figures 3.6 and 3.8, the results at the highest pressures are very close to those expected at infinite pressure.

Runs were performed at nine different temperatures in the range 230-320°C. In the series not already discussed, fewer actual runs were performed but a similar shape of the $^1/k_1 - {}^1/P_o$ plots was assumed. The results are presented in Tables 3.6 to 3.12. and figures 3.10 to 3.13. c-C_3F_6 dissociation of greater than 80% was always obtained above 300°, since the material could not be removed from the reactor quickly enough for the degree of reaction to be lower. At lower temperatures the conversions studied were limited by the formation of c-C_4F_8; dissociation was usually not allowed to proceed past the point where the pressure time curves could not be fitted due to the noticeable effect of c-C_4F_8 . This meant greater than 50% conversion at 10 cm. or less in the temperature range 240-290°C, and 30-40% conversion in the same

Table 3.6 Dissociation of Perfluorocyclopropane

Results at 230°C

Exper.	Temp. °C	P_o (cm.)	time (min.)	k_1 ($min.^{-1}$)	k_1 (230.0°C) ($min.^{-1}$)	a (cm. min.)	a(230.0°C) $(cm.\ min.)^{-1/2}$
D-3(P)	230.6	6.08	60.0	0.0158	0.0150	0.173	0.172
D-4	230.1	22.91	60.0	0.0158	0.0157	0.182	0.182
D-5	229.9	18.37	60.0	0.0164	0.0166	0.199	0.199
D-6	229.9	8.75	50.0	0.0157	0.0159	0.198	0.198
D-7	229.7	3.171	45.0	0.0138	0.0141	0.164	0.164
D-8	229.6	5.216	45.0	0.0140	0.0145	0.164	0.164
D-10	229.4	54.44	60.0	0.0154	0.0162	0.207	0.208
D-11	229.8	40.82	60.0	0.0146	0.0148	0.189	0.189
D-12	229.7	30.85	65.0	0.0146	0.0150	0.194	0.195
D-14	230.5	0.995	45.0	0.0119	0.01140	0.149	0.148

Table 3.7 Dissociation of Perfluorocyclopropane

Results at 240.5°C

Exper.	Temp. °C	P_o (cm.)	time (min.)	k_1 ($min.^{-1}$)	k_1 (240.5°C) ($min.^{-1}$)	a (cm. min.)	a (240.5°C $(cm.\ min.)^{-1/2}$
E-2	240.5	1.829	69.3	0.0333	0.0333	0.184	0.184
E-3	240.8	6.229	60.0	0.0378	0.0366	0.209	0.208
E-4	240.7	3.957	60.1	0.0355	0.0348	0.192	0.192
E-5	240.6	12.01	45.0	0.0381	0.0377	0.216	0.216
E-6	240.4	23.19	55.0	0.0387	0.0391	0.227	0.227
E-7	240.4	18.11	50.0	0.0375	0.0379	0.214	0.215

Table 3.8 Dissociation of Perfluorocyclopropane

Results at 266°C

Exper.	Temp. °C	P_o (cm.)	time (min.)	k_1 (min^{-1})	k_1 (266.0°C) (min^{-1})	a (cm. min.)$^{-1/2}$	a(266.0°C) (cm. min.)$^{-1/2}$
B-3	265.9	23.61	6.0	0.295	0.297	0.305	0.305
B-4	265.9	18.09	7.0	0.290	0.292	0.305	0.305
B-5	265.9	12.14	9.0	0.287	0.289	0.288	0.288
B-6	266.3	5.777	13.0	0.282	0.276	0.281	0.279
B-7	266.3	4.065	10.0	0.270	0.264	0.258	0.257
B-8	266.2	1.938	10.0	0.261	0.257	0.279	0.278
B-9	266.2	0.942	10.0	0.240	0.236	0.247	0.247

Table 3.9 Dissociation of Perfluorocyclopropane

Results at 302.4°C

Exper.	Temp. °C	P_o (cm.)	time (min.)	k_1 (min^{-1})	k_1 (302.4°C) (min^{-1})	a (cm. min.)$^{-1/2}$	a(302.4°C) (cm. min.)$^{-1/2}$
G-2	302.4	5.782	1.1	3.22	3.22	0.421	0.421
G-3	302.4	8.331	0.9	3.49	3.49	0.427	0.427
G-4	302.2	24.22	1.1	3.26	3.31	0.356	0.357
G-5	302.3	18.57	1.1	3.25	3.27	0.320	0.320
G-6	302.4	11.41	1.1	3.35	3.35	0.417	0.417
G-7	302.5	1.657	1.0	2.81	2.80	0.267	0.267

Table 3.10 Dissociation of Perfluorocyclopropane

Results at 289.0°C

Exper.	Temp. °C	P_o (cm.)	time (min.)	k_1	k_1 (289.0°C)	a	a(289.0°C)
				$(min.^{-1})$	$(min.^{-1})$	(cm. min.)	$^{-1/2}$
F-3	290.0	8.327	3.0	1.42	1.33	0.360	0.356
F-4	289.9	3.616	2.0	1.45	1.36	0.279	0.276
F-5	289.7	1.803	2.0	1.28	1.22	0.312	0.309
F-6	289.7	0.831	2.0	1.10	1.05	0.230	0.229
F-7	288.4	18.74	1.8	1.53	1.59	0.400	0.402
F-8	288.4	12.08	1.9	1.59	1.66	0.337	0.339

Table 3.11 Dissociation of Perfluorocyclopropane

Results at 320.7°C

Exper.	Temp. °C	P_o (cm.)	time (min.)	k_1	k_1 (320.7°C)	a	a(320.7°C)
				$(min.^{-1})$	$(min.^{-1})$	(cm. min.)	$^{-1/2}$
H-2(P)	321.6	6.253	1.3	10.0	9.66	0.917	0.911
H-3	320.8	1.649	0.8	7.34	7.30	0.0253	0.0253
H-4	320.7	1.561	0.8	7.68	7.68	0.0998	0.0998
H-5	320.6	9.55	0.8	10.4	10.5	0.480	0.480
H-6	320.6	2.430	0.7	9.40	9.45	0.0787	0.0787
H-7	320.6	5.007	0.8	10.8	10.9	0	0
H-8	320.8	8.71	0.7	9.36	9.31	0.197	0.197
H-9	321.1	8.93	0.8	9.80	9.65	0.272	0.272
H-10	320.9	22.63	0.9	10.3	10.2	0.128	0.128

Table 3.12 Dissociation of Perfluorocyclopropane

Results at 313.5°C

Exper.	Temp. °C	P_o (cm.)	time (min.)	k_1 (min^{-1})	k_1 (313.5°C) (min^{-1})	a (cm. min.)	$a(313.5^{\circ}C)^{-1/2}$
I-2	313.9	23.58	1.1	6.86	6.72	0.593	0.591
I-3	313.5	18.56	1.0	6.80	6.80	0.330	0.330
I-4	313.5	9.33	0.9	6.60	6.60	0.261	0.261
I-5	313.5	3.22	0.9	6.50	6.50	0.249	0.249
I-6	313.6	4.85	0.8	6.00	5.97	0.690	0.689

Variation of $1/k_1$ with $1/P_o$.

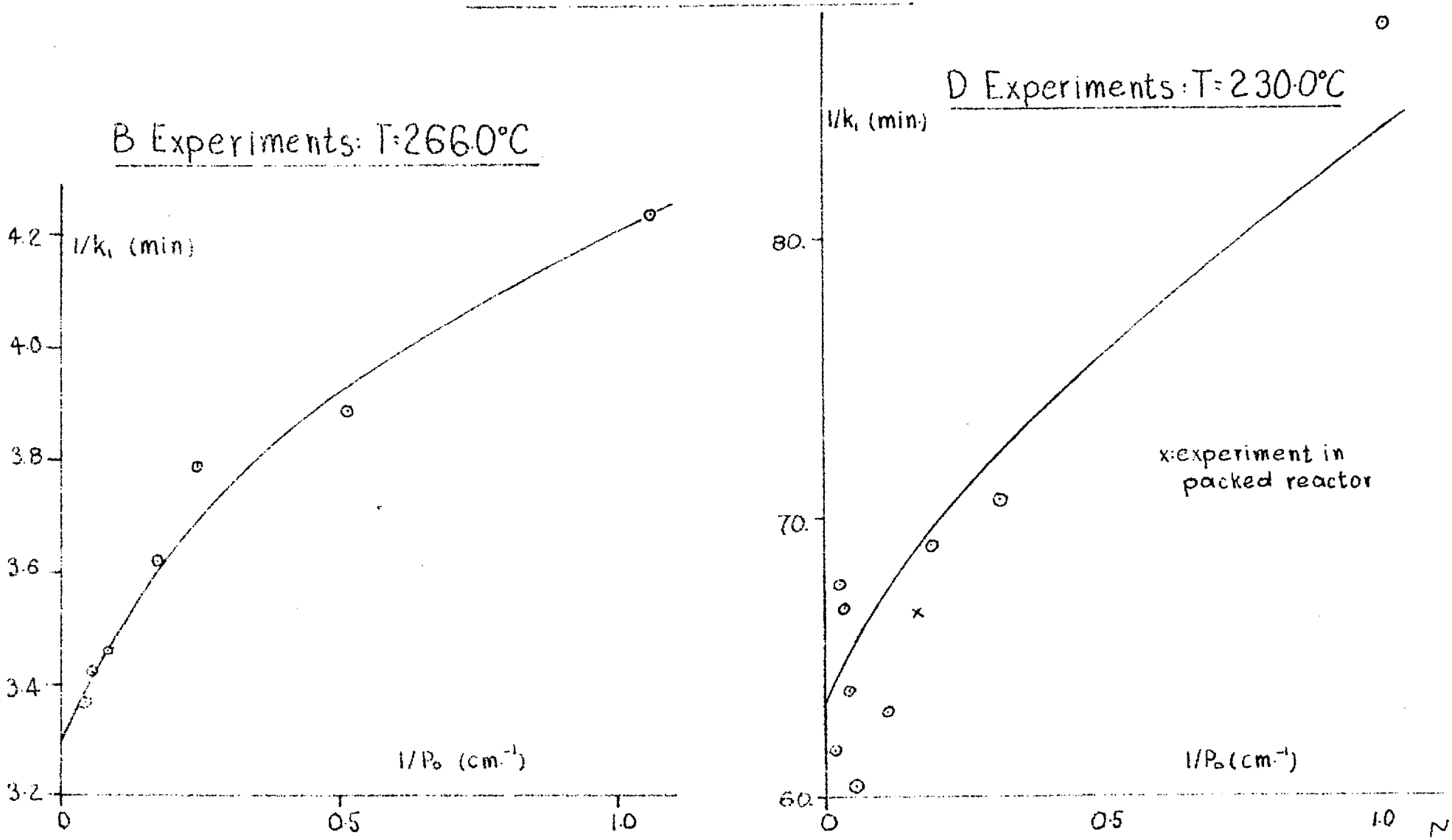

Figure 3.10

Variation of $1/k_1$ with $1/P_0$

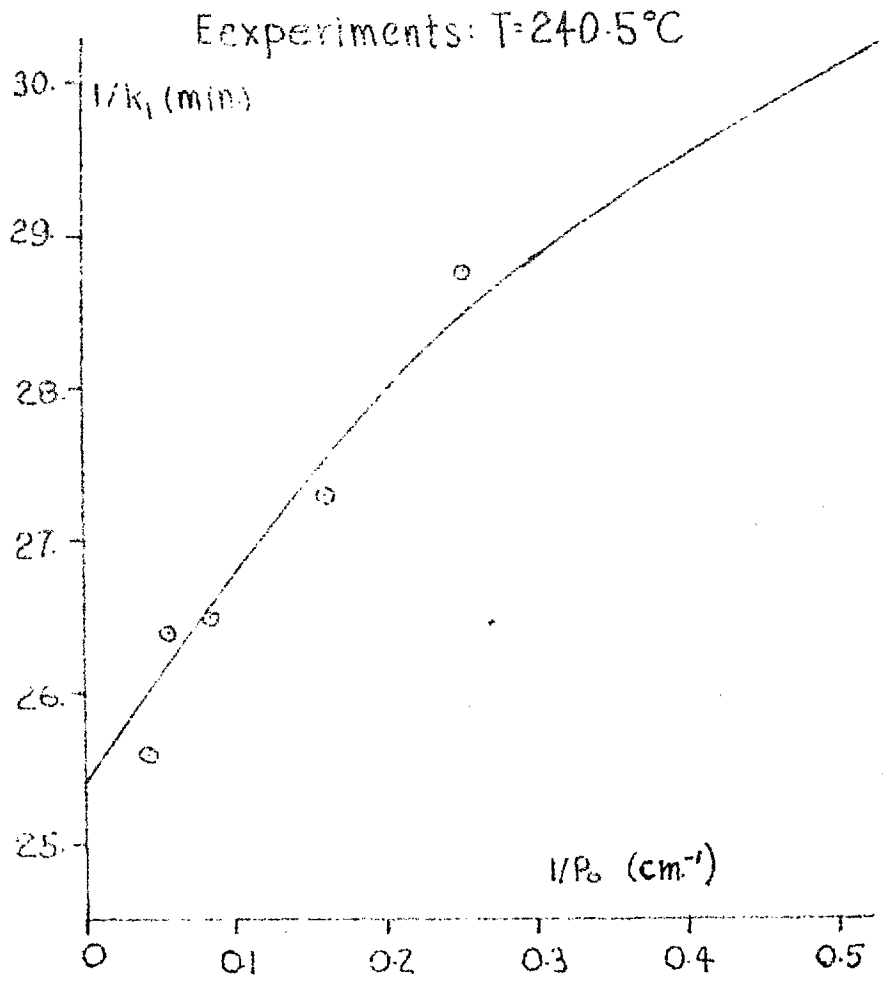

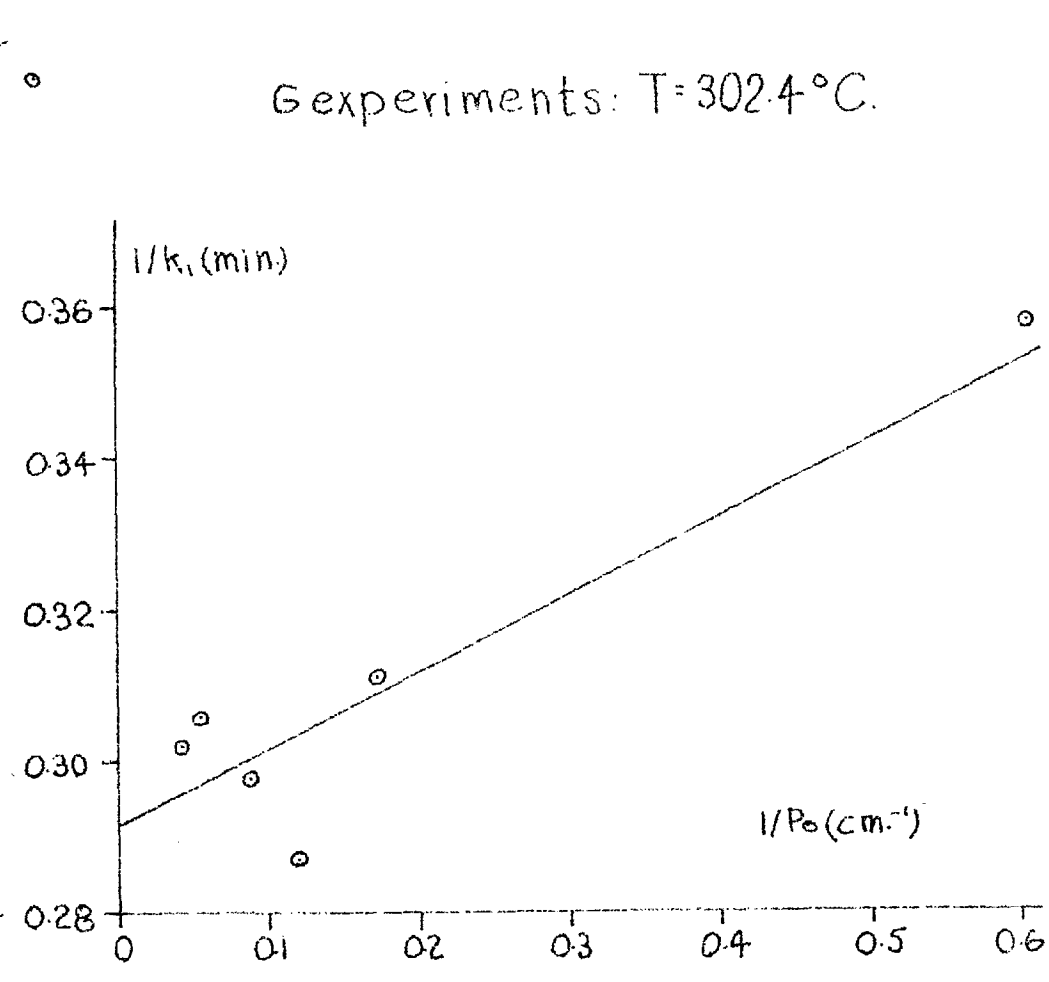

Figure 3.11

Variation of $1/k_1$ with $1/P_o$ for F Experiments. T=289.0°C.

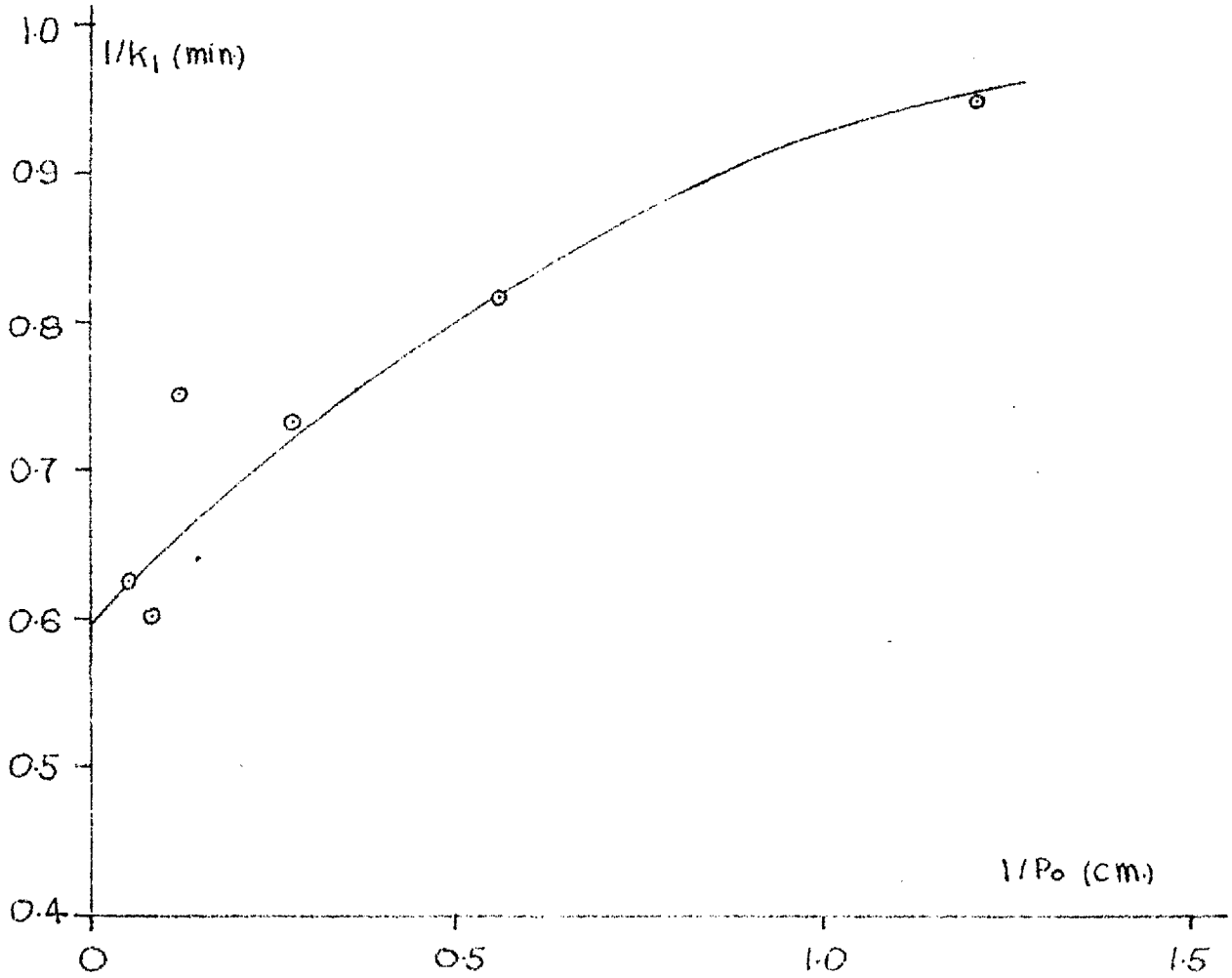

Figure 3.12.

Variation of $1/k_1$ with $1/P_o$

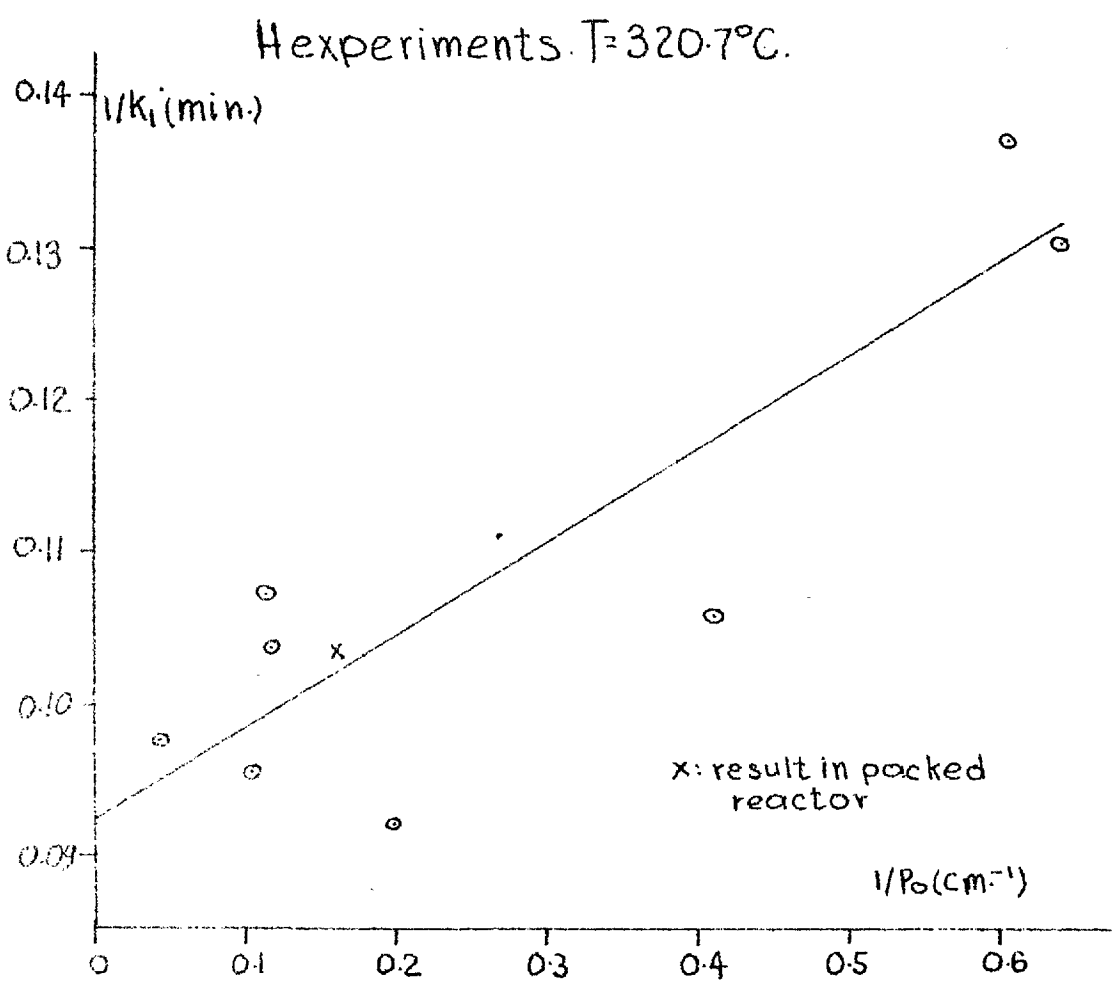

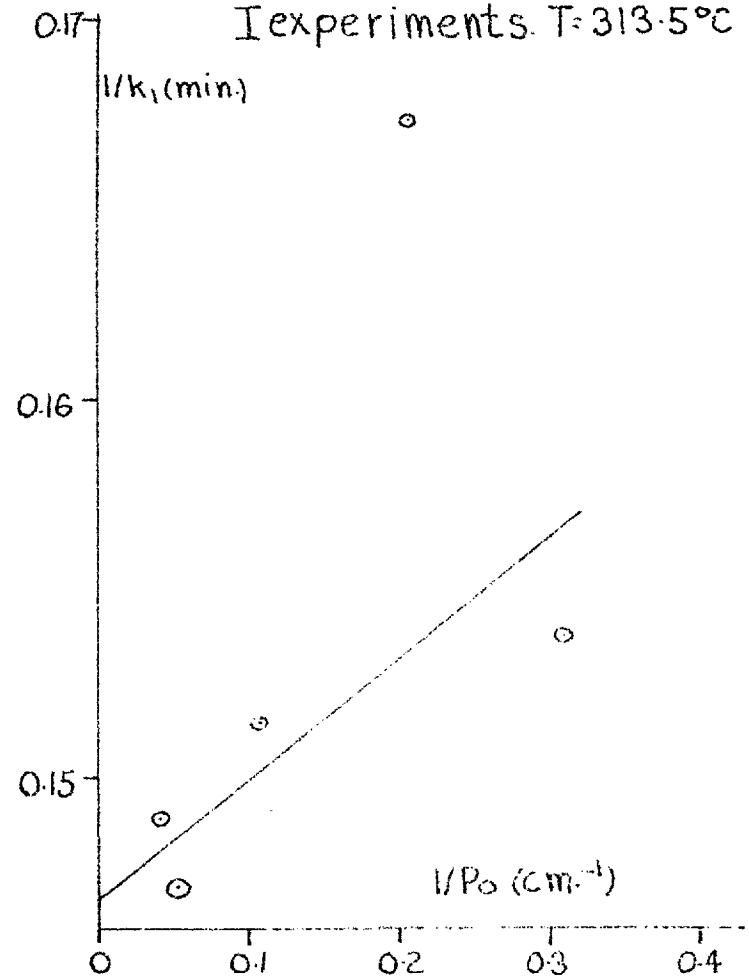

Figure 3·13

pressure range at 230°C. Above 15 cm. at 230°, only 20-25% dissociation could be used. Diminished accuracy in the fitting process can be expected with lower degree of dissociation.

The values of k_1^{∞} for each temperature obtained by extrapolation of the $^1/k_1 - {}^1/P_o$ plots to $^1/P_o = 0$ are presented in table 3.13 along with uncertainties estimated from the spread of points about the line drawn through them. A plot of these results in Arrhenius form is given in figure 3.15. The results were fitted to the following equation assuming straight line behaviour, by the method of least squares:

$$k_1^{\infty} = 8.41 \times 10^{14} \exp(-42,550/RT). \qquad (13)$$

This line has been drawn on the graph of figure 3.15. Uncertainties in the A and E factors have been estimated from the most probable error (156, p.500) in the slope and intercept of the straight line equation to be:

$$A = 10^{14.925 \pm 0.12} \text{ sec}^{-1}$$

$$E = 42,550 \pm 305 \text{ cal./mole.}$$

Table 3.13 Infinite Pressure Values of k_1

Run Series	Temp. ^{o}C	k_1 $sec.^{-1}$	Uncertainty %
D	230.0	2.60×10^{-4}	6.2
E	240.5	6.56×10^{-4}	0.8
A	253.0	1.86×10^{-3}	3.6
B	266.0	5.04×10^{-3}	1.5
C	277.0	0.0107	2.7
F	289.0	0.0266	6.0
G	302.4	0.0570	10.5
I	313.5	0.113	10.0
H	320.7	0.180	7.5

Variation of k_1 with P_o for Dexperiments. T=230.0°C.

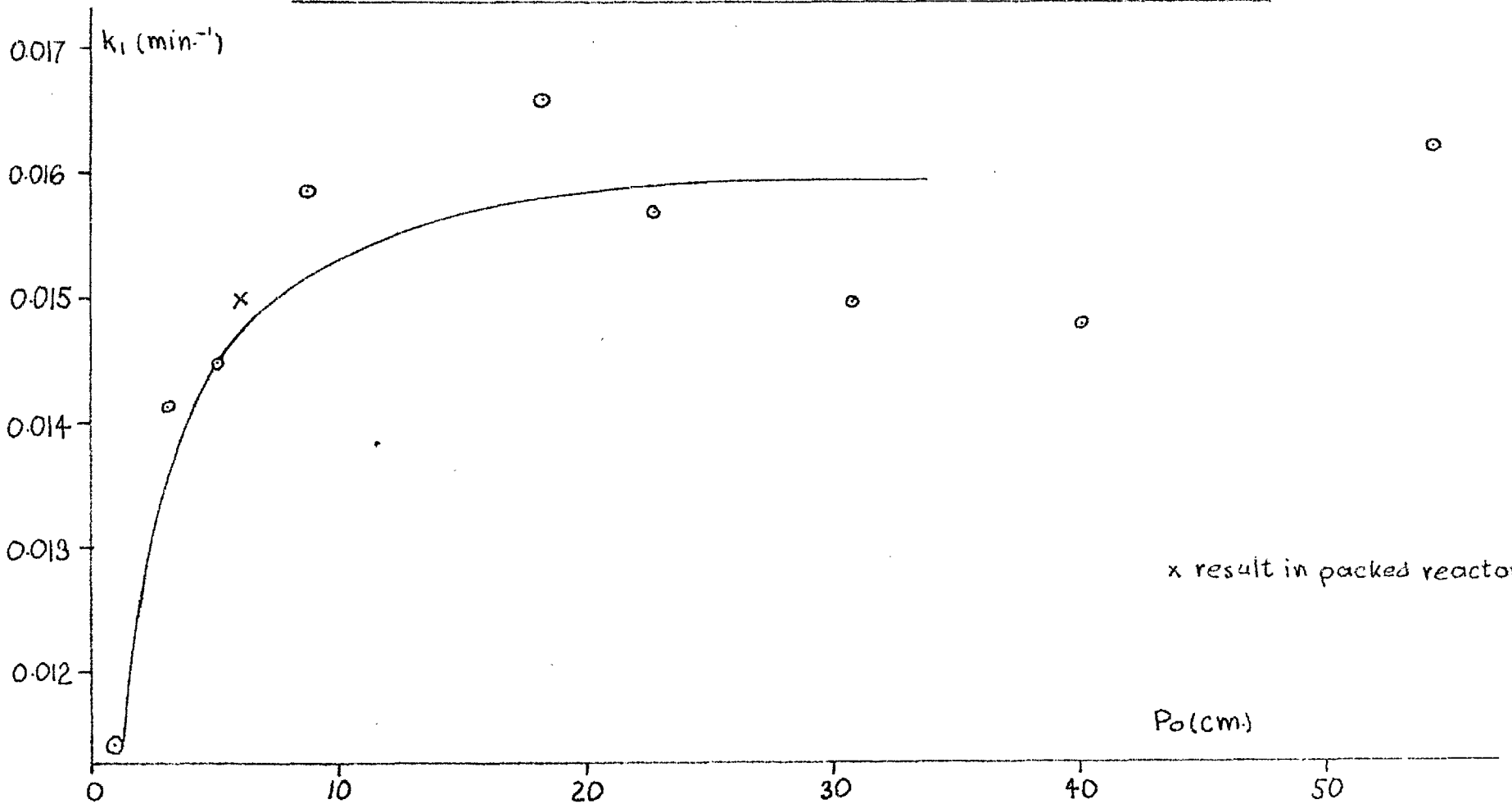

Figure 3.14

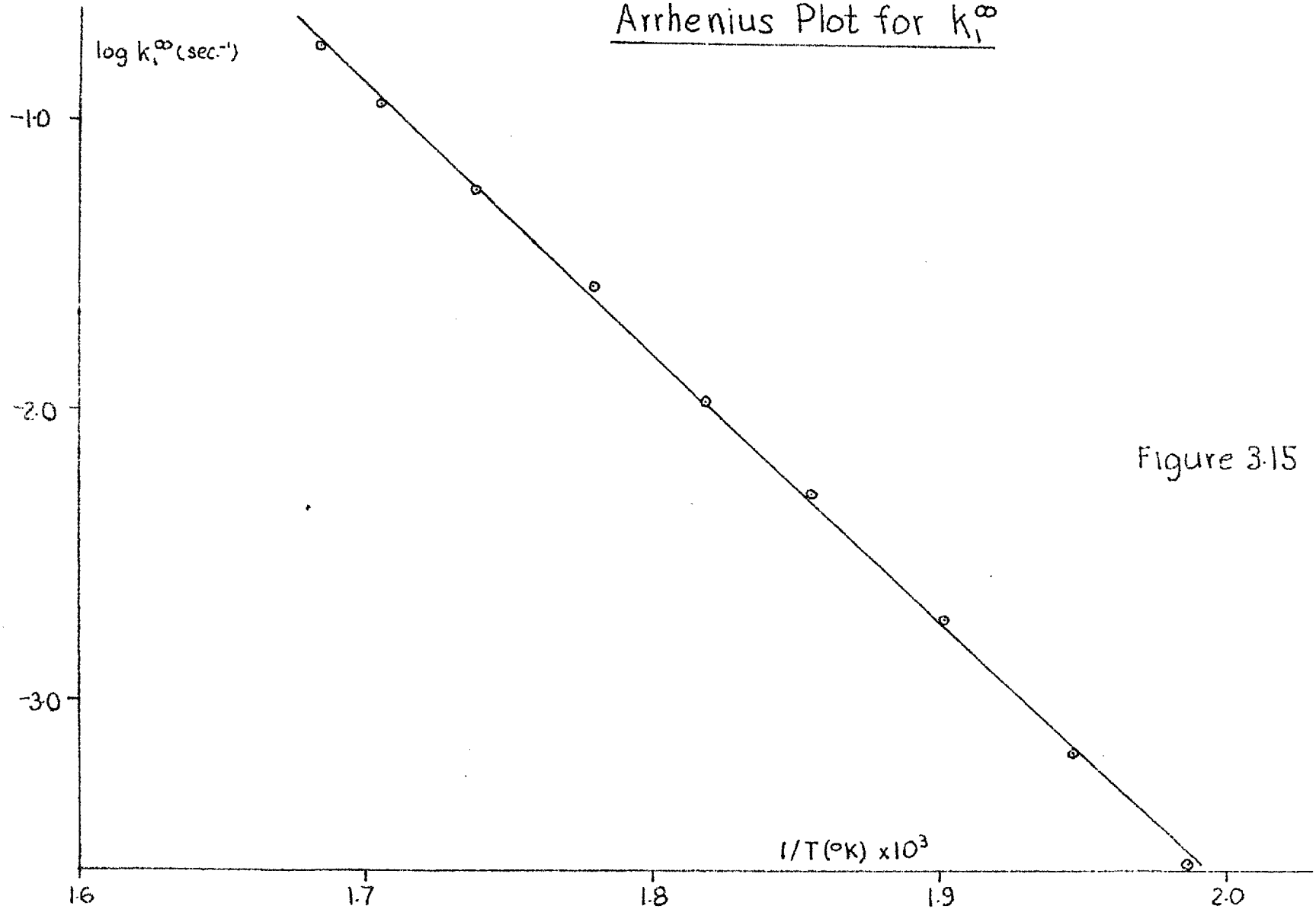
Arrhenius Plot for k_1^∞
log k_1^∞ (sec.$^{-1}$)
-1.0
-2.0
-3.0
1/T (°K) x10^3
1.6
1.7
1.8
1.9
2.0

Figure 3.15

The k_1 results for all experiments presented in tables 3.4 to 3.12 have been corrected to the run series temperature using expression (13).

The homogeneity of the reaction has been established by the results of a number of runs in the packed reactor at 230.0, 253.0 and 320.7°C. These runs are desginated by a (P) after the run number in tables 3.4, 3.6 and 3.11, and by an x in figures 3.5, 3.6, 3.9, 3.10, 3.13 and 3.14. Within experimental error no effect is observed on k_1 determined in the reactor with a larger surface area. The packed reactor had a surface area about 6.7 times that of the unpacked reactor.

Most of the reactions carried out to determine k_1^∞ were performed at starting pressures less than 25 cm.

A number of reactions were carried at higher pressure to determine the behavior of k_1 with pressure in this region. The maximum pressure which could be obtained in the reactor by expansion from the vacuum system was about 55 cm. In order to conserve the limited stock of perfluorocyclopropane it was decided to work at a low temperature (230°C) to get results with a minimum conversion. This would enable a greater number of runs to be performed. Above 45 cm. the recorder was not used as the signal from the transducer was outside the range of the calibrated backing off circuit (see fig. 2.9). No significant variation in transducer calibration was found up to 60 cm., the maximum pressure reached in these studies. The transducer output was read directly using the potentiometer, and readings extrapolated graphically to zero time to get the initial pressure. The results of these runs are gathered with the other D runs in table 3.6 and figure 3.10. The D run results are also presented as a $k_1 - P_o$ plot in figure 3.14.(page 236) Unfortunately there is a high degree of uncertainty in the determination of k_1 since only low conversions could be used, but within experimental error the value of k_1 is constant from about 14–55 cm. These results were confirmed by several runs at 253.0°C (A series) where k_1

is constant from about 12-41 cm. (see figure 3.6).

3.2.2. The Determination of $(k_3/k_2^{1/2})^{\infty}$

The high pressure value of the ratio of rate constants is determined from the high pressure value of a, where:

$$a = \frac{3k_3}{2} \frac{1}{(2\ k_2\ RT)^{1/2}}$$

A plot of a against $^1/P_o$ was made for each series of runs and extrapolated to $^1/P_o = 0$ to obtain a^{∞}. The figures for individual runs appear in tables 3.4 to 3.12. The results are plotted in figures 3.16 to 3.20 for the runs up to 289°; above this temperature results are too scattered to be meaningfully represented on an a against $^1/P_o$ plot.

The shape of the a-$^1/P_o$ plots was first established by the results of the A(253°C) and C(277°C) series in which a large number of runs were performed. Similar shapes were assumed for other series in which experimental points do not establish a clear line. Such plots give good results for a^{∞} if a small number of points are used to obtain the extrapolation to theoretical

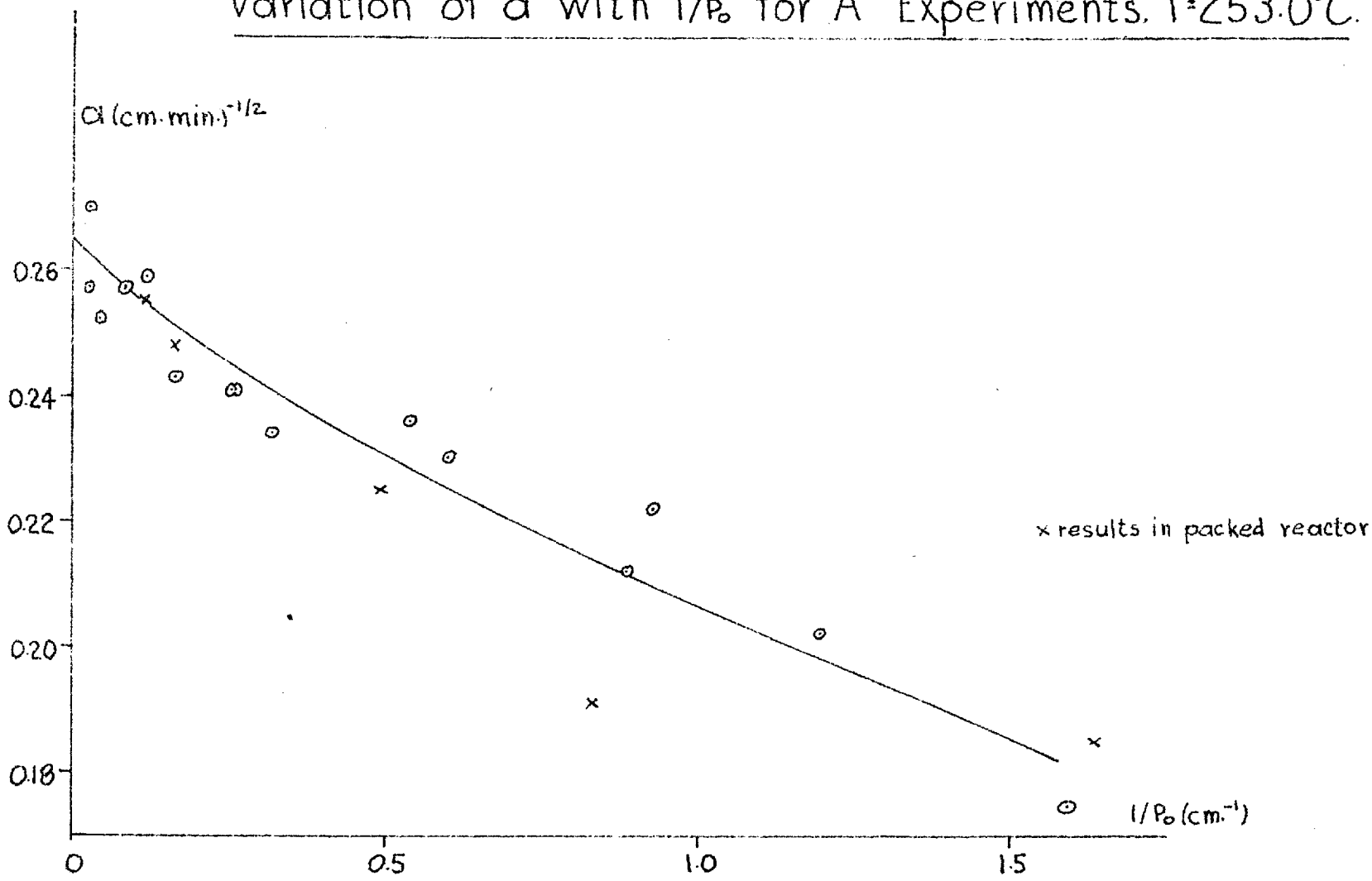
Variation of a with 1/P₀ for A Experiments. T=253.0°C.
a (cm.min.)^-1/2
0.26
0.24
0.22
0.20
0.18
0
0.5
1.0
1.5
1/P₀ (cm.^-1)
× results in packed reactor

Figure 3.16

Variation of a with $1/P_o$ for C Experiments. T = 277.0°C.

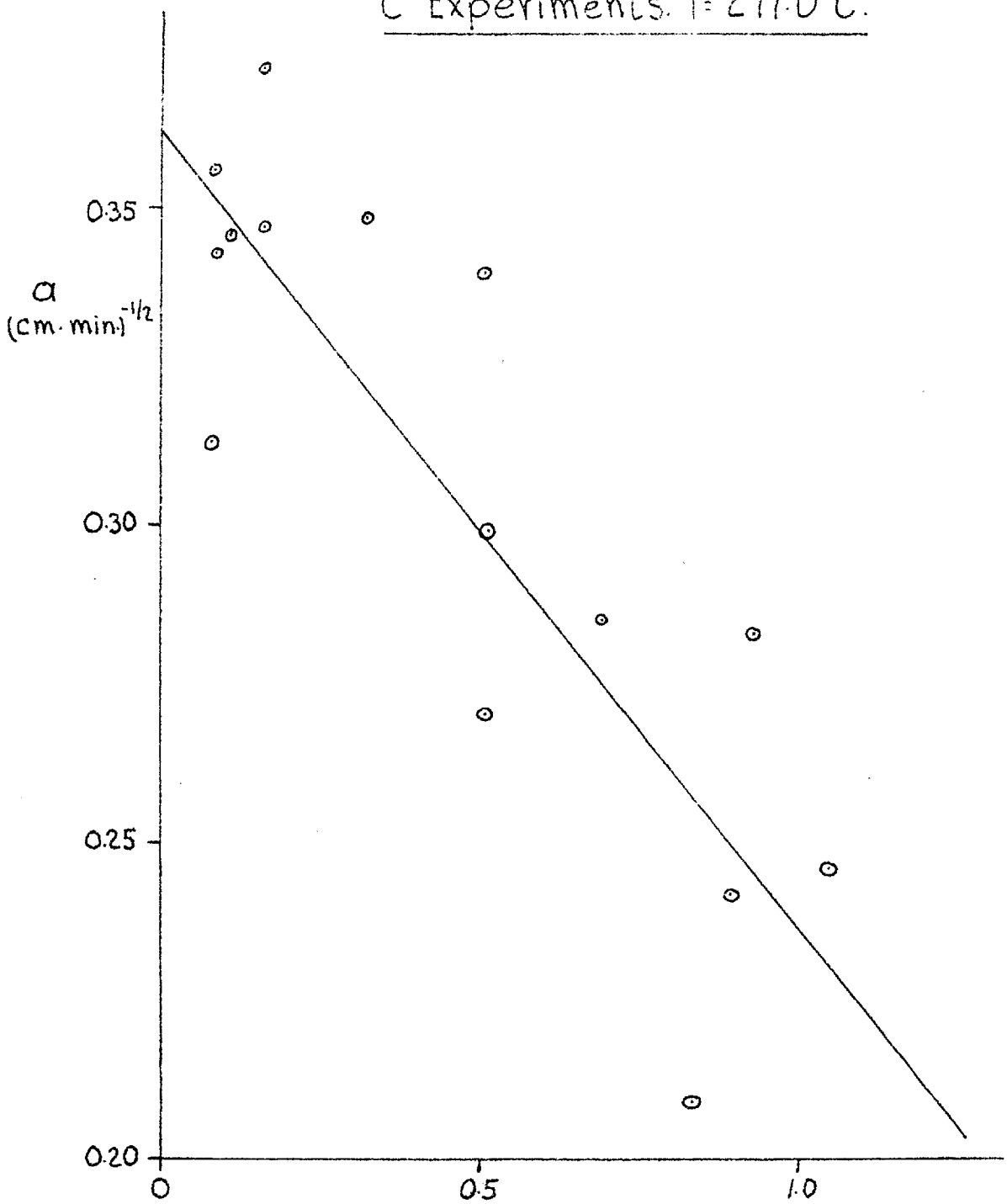

Figure 3.17

Variation of a with $1/P_o$.

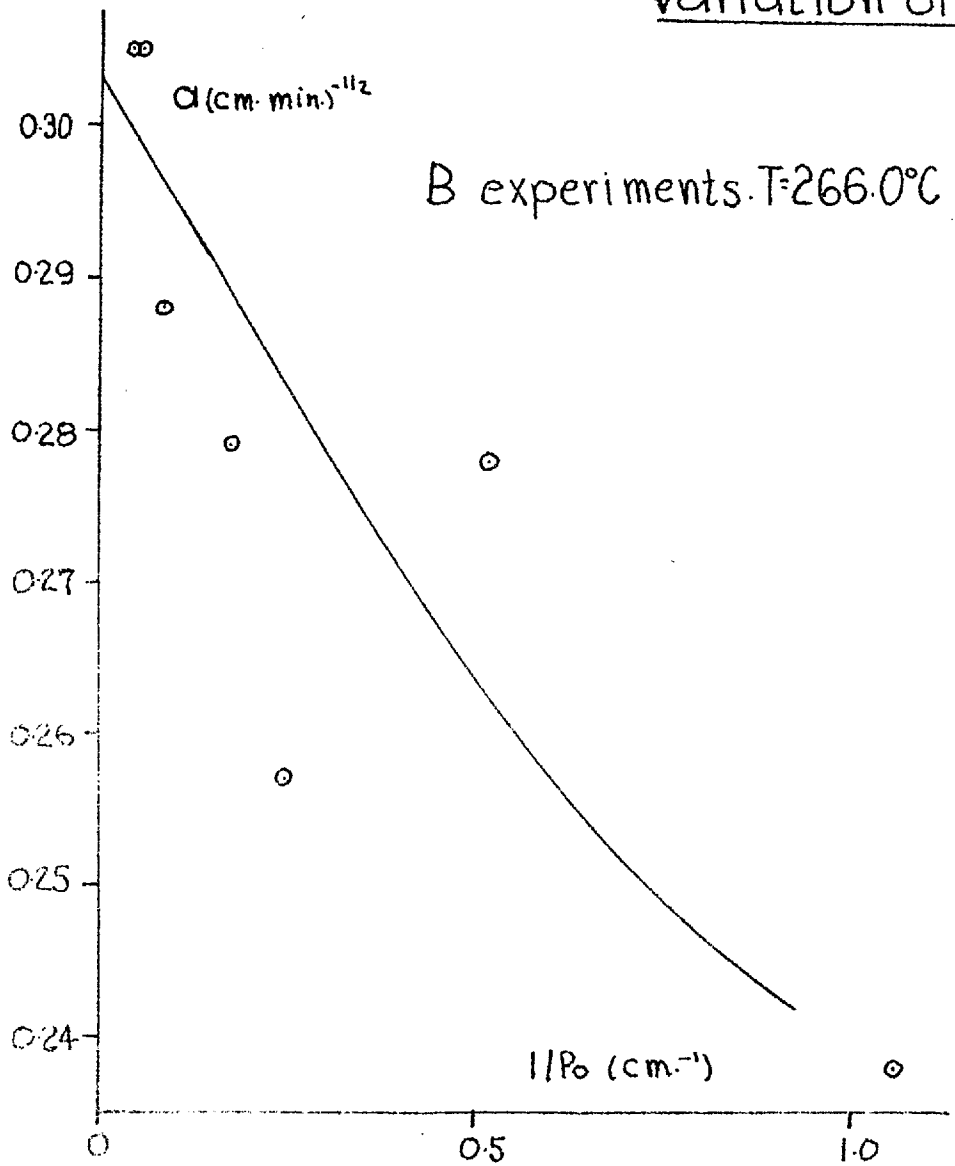

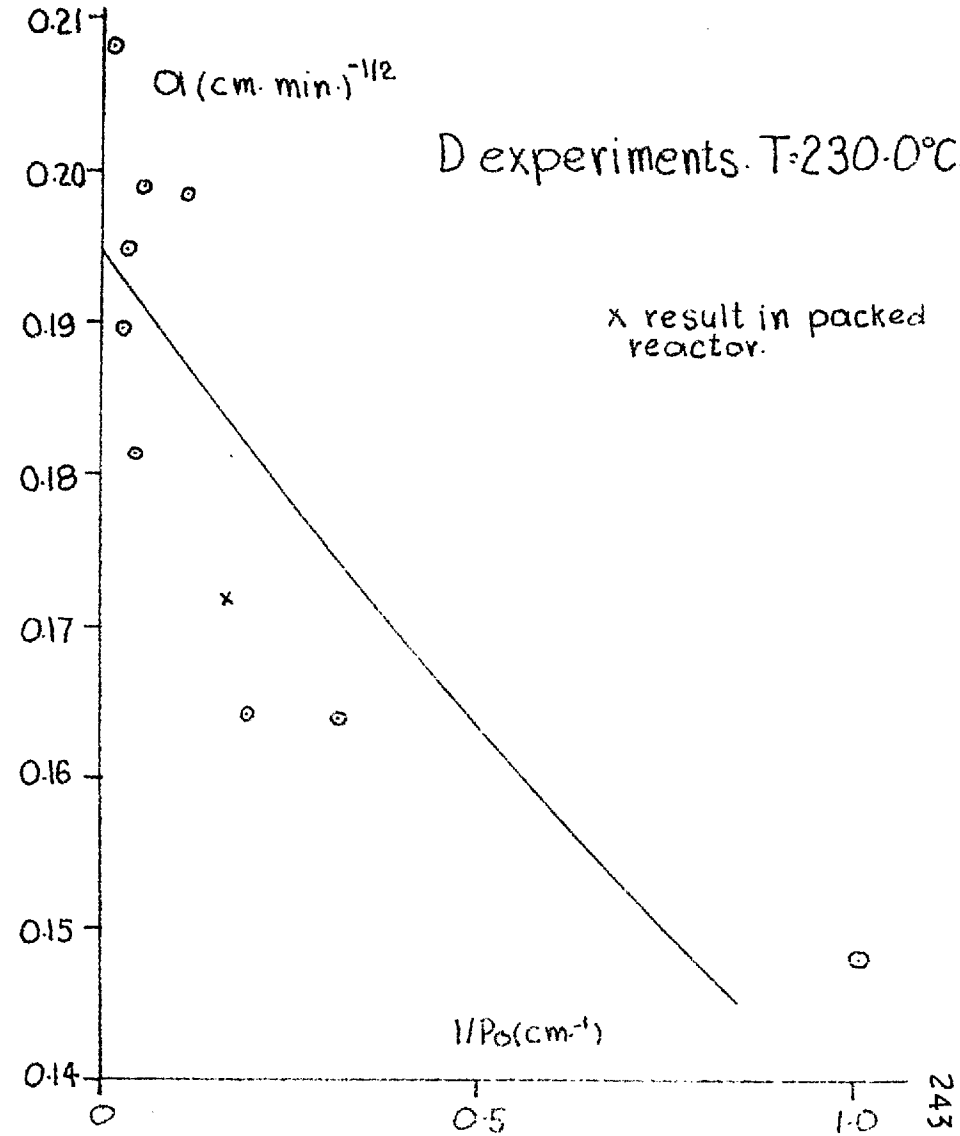

Figure 3.18

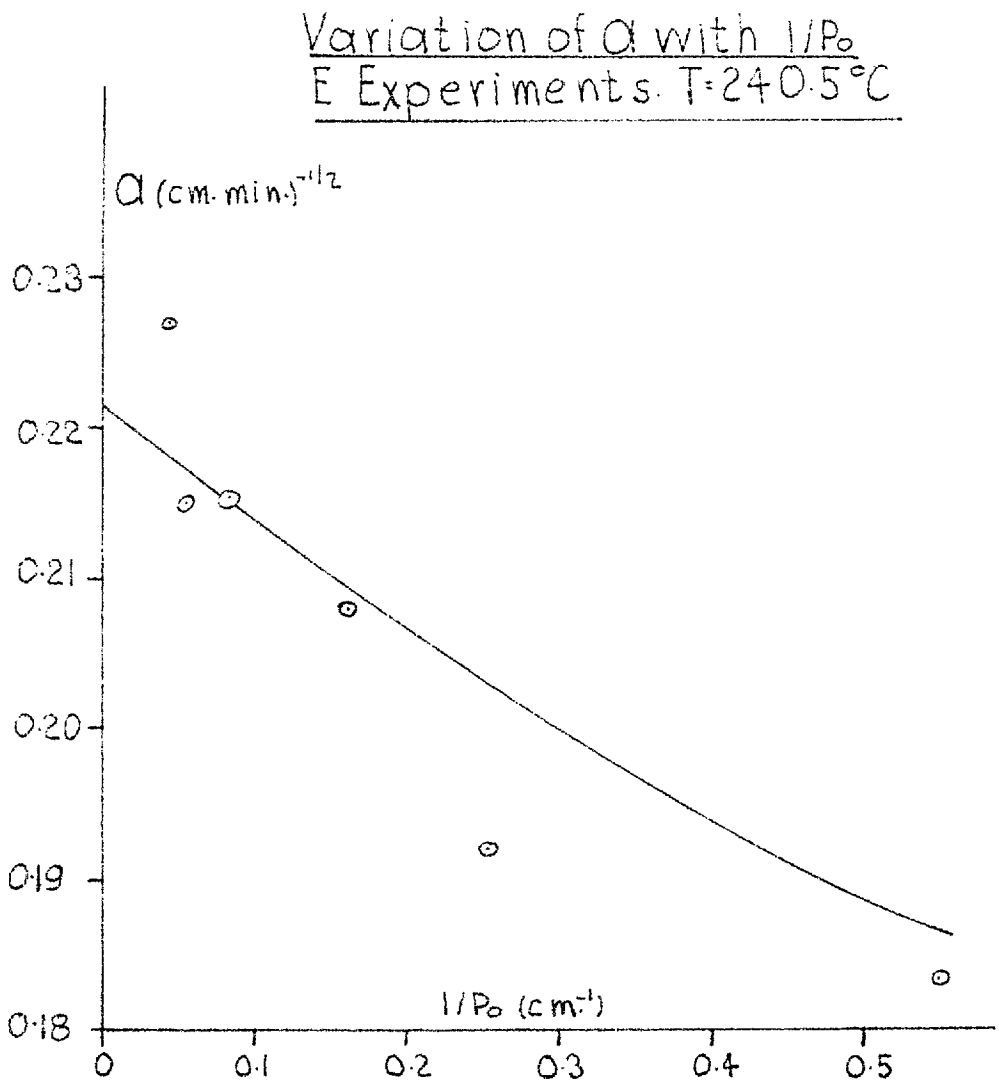
Variation of a with 1/P₀
E Experiments. T=240.5°C
a (cm. min.)^-1/2
0·23
0·22
0·21
0·20
0·19
0·18
1/P₀ (cm⁻¹)
0
0·1
0·2
0·3
0·4
0·5

Figure 3·19

Variation of a with 1/Po

F Experiments. T=289.0°C.

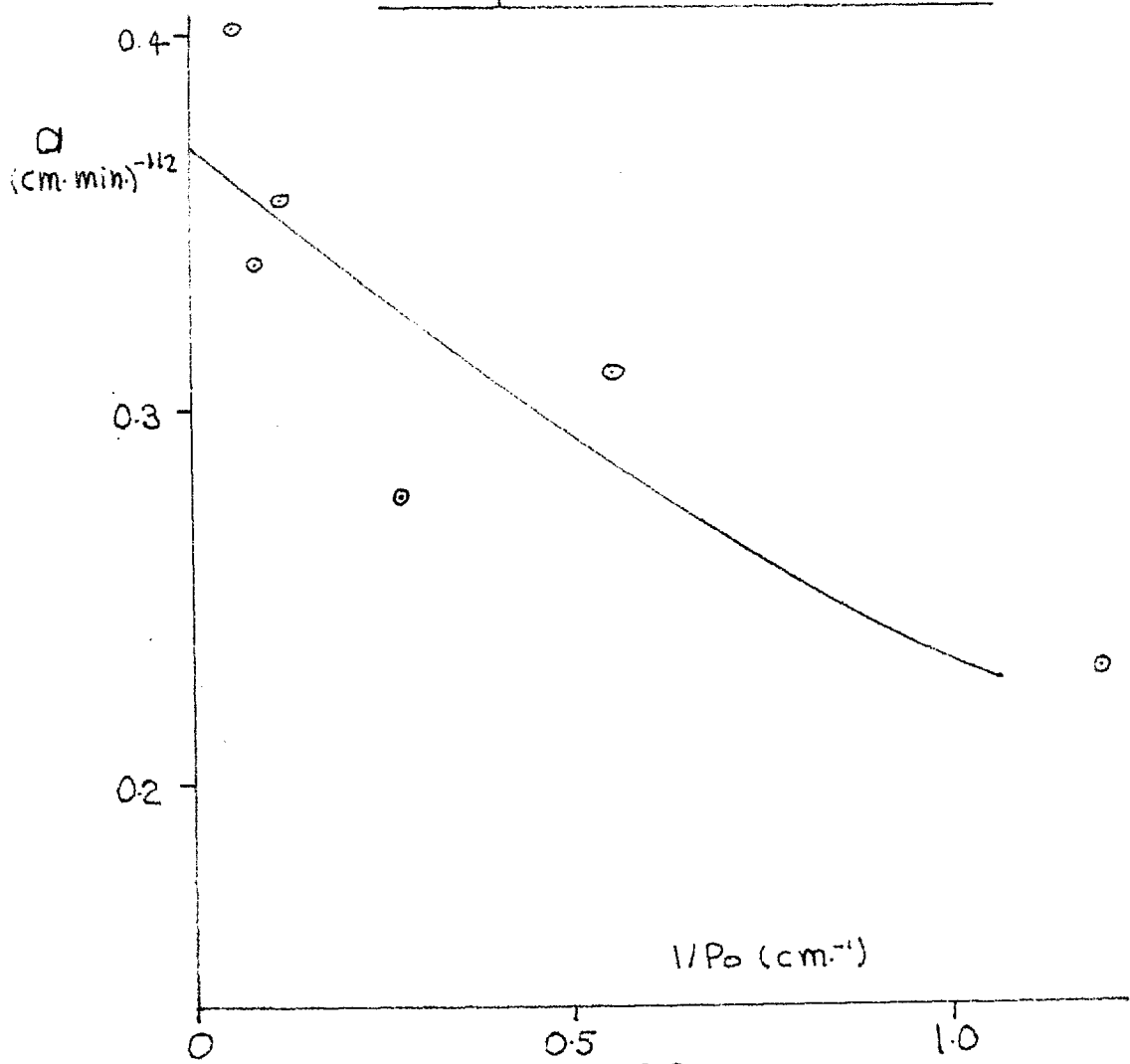

Figure 3.20

Arrhenius Plot for $(k_3/k_2^{1/2})^{\infty}$

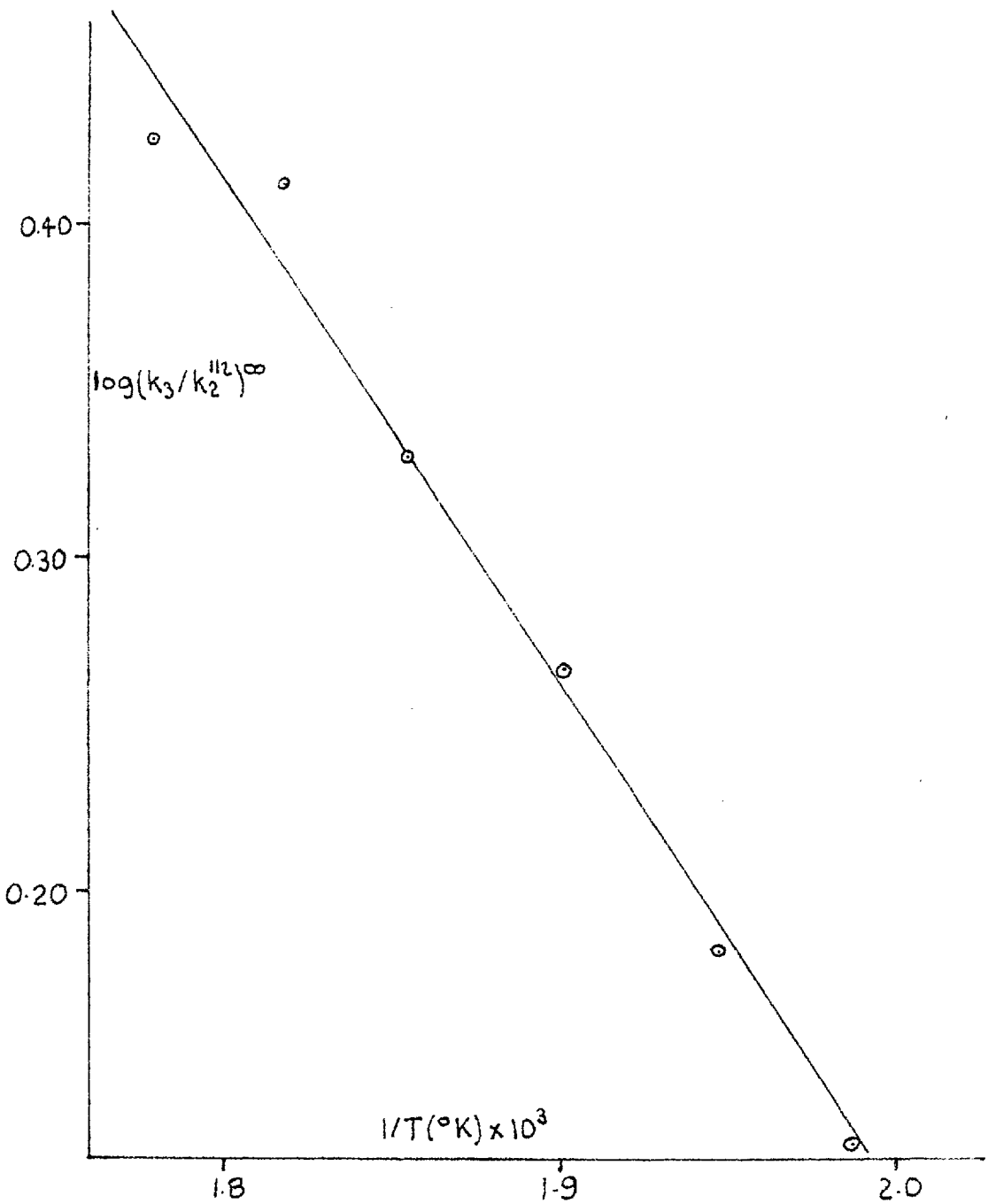

Figure 3.21

Variation of a with P_o for D Experiments. T=230.0°C.

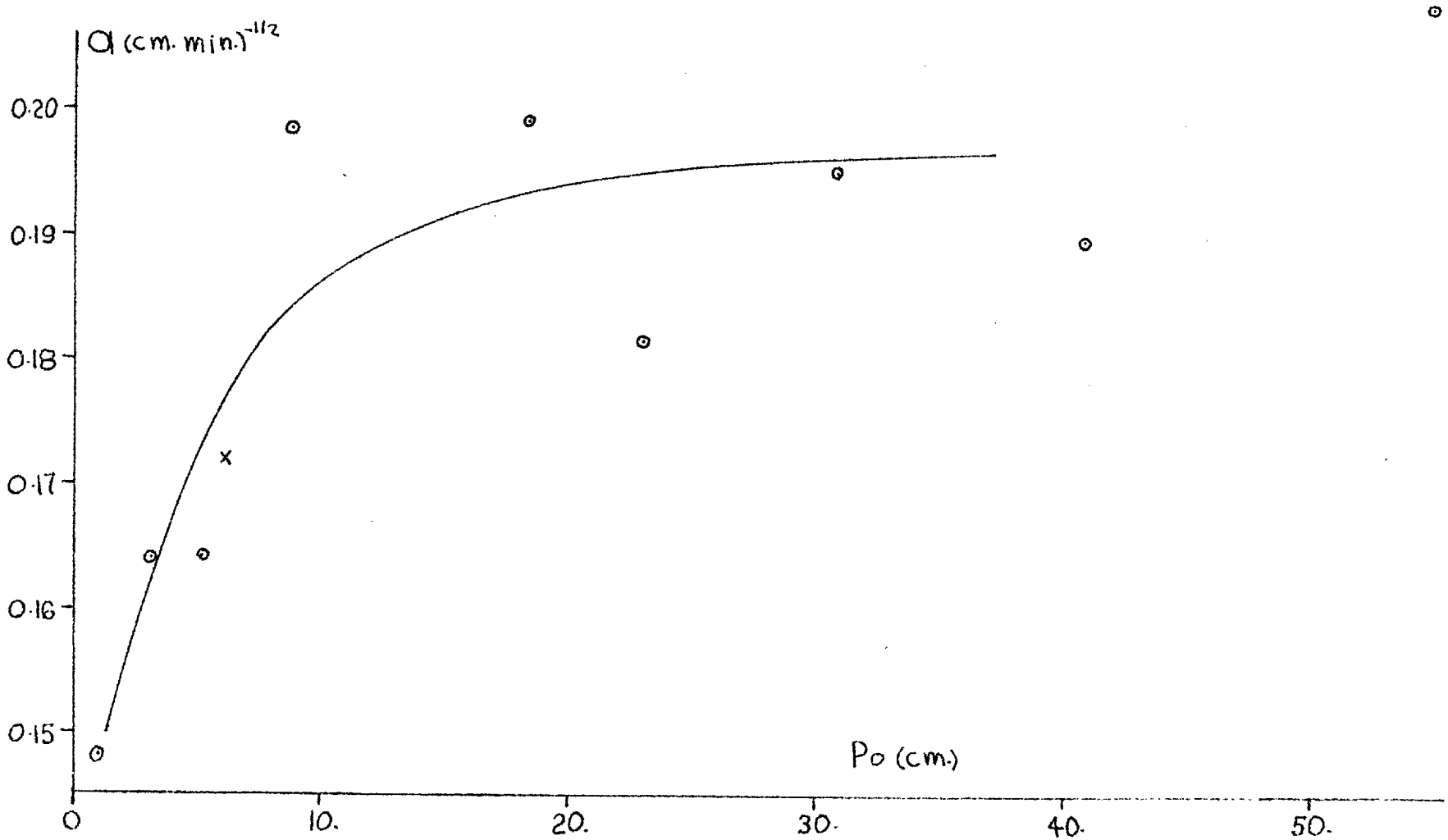

Ficure 3.22

infinite pressure.As shown in figure 3.22 for the D series, an $a-P_o$ plot gives essentially the same value of a^∞ (compare fig. 3.18).

The constant which results from the fitting process is α which is related to a by the relation:

$$\alpha = a\left(\frac{P_o}{k_1}\right)^{1/2} .$$

As mentioned in section 3.1.3., the determination of α is subject to greater uncertainty than k_1 . The value of a varies relatively little with temperature so that at higher temperature (hence higher k_1) and lower pressure, α is relatively low. The range of α which is covered by the various curves of an individual fit (see figs. 3.3^a and 3.4) does not vary greatly between runs. In run B-7 at 266.3°C and 4.065 cm. starting pressure, values of α varying from 0.96 to 1.1 are covered by the various Y plots; for run H-9 at 321.1°C and 8.93 cm. the fitting process gives α from 0.1 to 0.3. In run D-12 at 229.7°C and 30.85 cm. the range of α for the fit is from 8.6-9.0. Thus the absolute uncertainty in α changes very little but at temperatures over 300 the percentage uncertainty is high. This is especially reflected in the spread of a values in the G,

H and I series (302, 321, 314°C respectively).

The values of $(k_3/k_2^{1/2})^{\infty}$ which result from the extrpolation of the a^{-1}/P_o plots to $^1/P_o = 0$ are presented in Table 3.14. These do not include results above 300°C since they are too uncertain.

Table 3.14 Infinite Pressure Values of $(k_3/k_2^{1/2})$

Run Series	Temp. °C	a $(cm.min.)^{-1/2}$	Uncertainty %	$(k_3/k_2^{1/2})^{\infty}$ $(l./mol.sec.)^{1/2}$
D	230.0	0.195	4.1	1.33
E	240.5	0.221	2.6	1.52
A	253.0	0.265	3.5	1.85
B	266.0	0.303	2.0	2.14
C	277.0	0.362	6.0	2.58
F	289.0	0.370	9.5	2.67

The uncertainties in Table 3.14 have been estimated from the spread of points about the a^{-1}/P_o plots. The results of $(k_3/k_2^{1/2})^{\infty}$ have been fitted to a straight line equation of the Arrhenius form to give:

$$\left(\frac{k_3}{k_2^{1/2}}\right)^{\infty} = 10^{3.18\pm0.12} \exp.\left(\frac{-7030\pm295}{RT}\right) (liters/mole\ sec.)^{1/2} \quad (14)$$

The uncertainties have been estimated from the slope and intercept of the straight line equation (156, P.500). The straight line has been plotted in figure 3.21 along with the experimental points (page 246).

In order to correct rate constants for different runs in the same series to the same temperature, the expression (14) was converted to the equivalent expression in a . Thus:

$$a = \frac{4969}{T^{1}/2} \exp.(-7030/RT),$$

where a is in $(\text{cm. min.})^{-1}/2$

3.2.3 Low Pressure Results

Below 0.5 cm. the pressure changes indicated by the transducer were followed directly with the potentiometer, and the initial pressure determined by extrapolation to zero time. Accurate transducer calibrations could not be performed in this range; the output which is linear from 20 cm. down to 0.5 was assumed to be so in the region down to 0.05 cm. in which pressure transducer studies were done. Comparison of transducer figures with those calculated from the ideal gas law for expansion, in table 3.15, indicate the transducer calibration is

Table 3.15 Comparison of Transducer Indicated and Expansion Calculated Initial Pressure Values

Run	Transducer Indication cm.	Expansion Calculation cm.	% Deviation from Transducer
A-29(i)	0.083	0.079	-5.4
(ii)	0.078	0.076	-2.4
(iii)	0.075	0.074	-2.1
A-30(i)	0.170	0.171	+0.8
(ii)	0.171	0.170	-0.7
(iii)	0.170	0.168	-0.7
A-34	0.225	0.224	-0.4
A-35(i)	0.138	0.135	-2.4
(ii)	0.127	0.133	+4.2
(iii)	0.137	0.133	-2.9
(iv)	0.128	0.130	+1.5

linear in this region.

Results were also obtained by analysis in the range 0.5 to 0.001 cm. When the reactor arrangement for the high pressure studies was used, a correction had to be applied to the analysis for the dead space. In most cases about one half of the material in the reactor was removed for analysis. All of the material in the dead space could be assumed to be in this sample and hence a significant effect on the actual analysis in the section at the reaction temperature had to be accounted for. These corrections are described in Appendix II. The majority of the analytical results were obtained with the reactor in the aluminium furnace. The dead space in this case was estimated to be only about 0.14% of the total volume and no correction was applied for runs in this reactor. In this case equation (8) of Appendix II, for $V_h'' = V_h$ and $b = 1$, reduces to:

$$z = \frac{q(P_o/P) - 1}{q - 1}$$

Since $q = 1.5$ and $P = \frac{3}{2}(P_o - P_r) + P_r$,

$$z = \frac{2}{\frac{3P_o}{P_r} - 1} = \frac{3P_o}{P} - 2 \qquad (15)$$

This last expression relates the measured concentration to the pressure ratios in the reaction section when the dead space can be neglected. In the case where equation (8) of the appendix is used the determination of P_o/P is indirect since z is expressed as a function of P_o/P. In practice a number of points were calculated for the experimental conditions and the $z - P_o/P$ relation for particular runs were read from a plot of these figures.

As discussed previously, as pressure is reduced, the α determined in the fitting process is also lower since it is proportional to the square root of pressure (see equation (11) section 3.1.2.). At pressures below 0.5 cm. the fitting process is more uncertain than at higher pressures. In some runs it appeared that the best fit for the Y line intersections would be at a negative α. It is concluded that in such cases α is nearly zero and that within experimental error the kinetics are first order. Thus:

$$\frac{dP_r}{dt} = -k_1 P_r .$$

A plot of ln Pr against time gives a straight line. The fitting process was applied to runs between 0.5 and 0.05 cm. but a results are too scattered to be meaningful. Below 0.05 cm. α is always undetectably different from zero. These observations are illustrated by the following comparison in run A-34 of experimental times and times predicted for $k_1 = 0.0568$ and $\alpha = 0$.

Y	$k_1 t$	Predicted t min.	Experimental t min.
0.9	0.105	1.86	1.9
0.8	0.223	3.92	4.0
0.7	0.359	6.31	6.4
0.6	0.510	9.0	9.2
0.5	0.693	12.2	12.2
0.4	0.915	16.1	16.0

Run A-34 had an initial pressure of 0.225 cm.

As discussed in the experimental section, low pressures of $c\text{-}C_3F_6$ starting material were obtained in the reactor by expansions of vacuum line pressures measured by the cathetometer. The final expansion is from room temperature into the heated reactor and since a narrow capillary has been used on the reactor inlet to minimize dead space, thermal transpiration effects

must be taken into account. This subject and the method of correction is dealt with in Appendix IV.

Corrections were only applied to the results from the new reactor. At 0.05 cm. the correction is found to be about 0.5%. Since no runs were performed in the old reactor below 0.05 cm. and it had a larger capillary (2.5 m.m compared to 2.0 m.m.) corrections were neglected.

Each result at low pressure from analysis is obtained from a number of experiments at the same temperature and starting pressure but different reaction times. The entire reaction product is put into the chromatograph and the analysis gives a value of P_r/P_o (see equation (15) above), appropriate to the reaction time. The average starting pressure is used to calculate a value of P_r for each experiment and a plot of $\ln P_r$ against t gives k_1 from the slope. The pressure of the series of experiments is taken as the arithmetic average of the average initial pressure and the final pressure of the longest experiment. The latter is calculated from the appropriate P_r/P_o and the average initial pressure. Each initial pressure determined by expansion from the vacuum system is corrected with the appropriate thermal transpiration factor. The temperature of the group of experiments was taken as the average for the individual experiments.

It is observed with unimolecular reactions that as pressure is reduced the rate of falloff of the apparent first order rate constant with pressure increases until true second order behavior is obtained. The possibility of detectable variations in k_1 during the course of a run must be considered. A value of k_1 can be determined from the product analysis of an individual experiment assuming first order kinetics. Thus:

$$k_1 = \frac{- \ln (P_r/P_o)}{t}$$

For a group of experiments where only the time of reaction was changed, individual values of k_1 could be obtained at different average pressures due to different degree of reaction. Such calculations were performed for all the low pressure A(253°C) experiments. Individual experiments were corrected to the same temperature and the average pressure calculated from the starting pressure of the particular experiment; small variation in temperature and starting pressure between experiments under the same conditions was unavoidable. Although variation of k_1 with pressure was observed in the various groups of experiments no trend with pressure

could be implied so that within experimental error, k_1 is constant.

Because of the length of time which is required to get a sample from the reactor, low pressure experiments were only done at low temperatures where sampling time (up to 30 sec.) would be less significant. Results at 253° are presented in Table 3.16 and at 230° in Table 3.17 along with the thermal transpiration corrections used. Although the activation energy is known to be lower for quasi-unimolecular reactions in the falloff region the maximum deviation from the run temperatures was 0.4° and the high pressure activation energy was used to correct the individual runs to 253 and 230°. The results are plotted as $\log(k_1/k_1^{\infty})$ against log(average pressure) in figures 3.23 and 3.24. The analysis and pressure transducer results for the A runs show good agreement in the pressure range 0.5-0.05 cm.

The uncertainty in the individual rate constants is difficult to access for the analysis results. Values of k_1 calculated from individual analysis during a run gave a spread of up to 15% about the value obtained from the best straight line of the $\ln P_r$-t plot. The uncertainty of this averaged value is probably somewhat

Table 3.16 Low Pressure Runs at 253.0°C

Run	Method*	k_1 at 253°C $min.^{-1}$	Average Pressure cm.	Press. Corr. Factor
A-15	P	0.0765	0.732	1.0
19	P	0.0878	0.979	1.0
22	P	0.0848	1.235	1.0
28(P)	P	0.0852	0.730	1.0
29(i)	P	0.0376	0.0821	1.0
29(ii)	P	0.0514	0.100	1.0
29(iii)	P	0.0406	0.097	1.0
29	a	0.0454	0.100	1.0
30(i)	P	0.0581	0.189	1.0
30(ii)	P	0.0566	0.184	1.0
30(iii)	P	0.0571	0.188	1.0
30	a	0.0556	0.189	1.0
34	P	0.0568	0.255	1.0
35(iii)	P	0.0447	0.160	1.0
35(iv)	P	0.0545	0.153	1.0
35	a	0.0576	0.153	1.0
36	a	0.0186	0.0270	1.017
37	a	0.0123	0.0106	1.076
38	a	0.0089	0.00403	1.220

* P indicates results from pressure transducer and a from chromotographic analysis.

Table 3.17 Low Pressure Runs at 230.0°C

Run	Method	k_1 at 230.0°C min^{-1}	Average Pressure cm.	Press. Corr. Factor
D-14	P	0.01140	1.067	1.0
15	P	0.00930	0.217	1.0
16	a	0.00525	0.0305	1.011
17	a	0.00357	0.00638	1.144
18	a	0.00306	0.00354	1.200
19	a	0.00278	0.00213	1.225

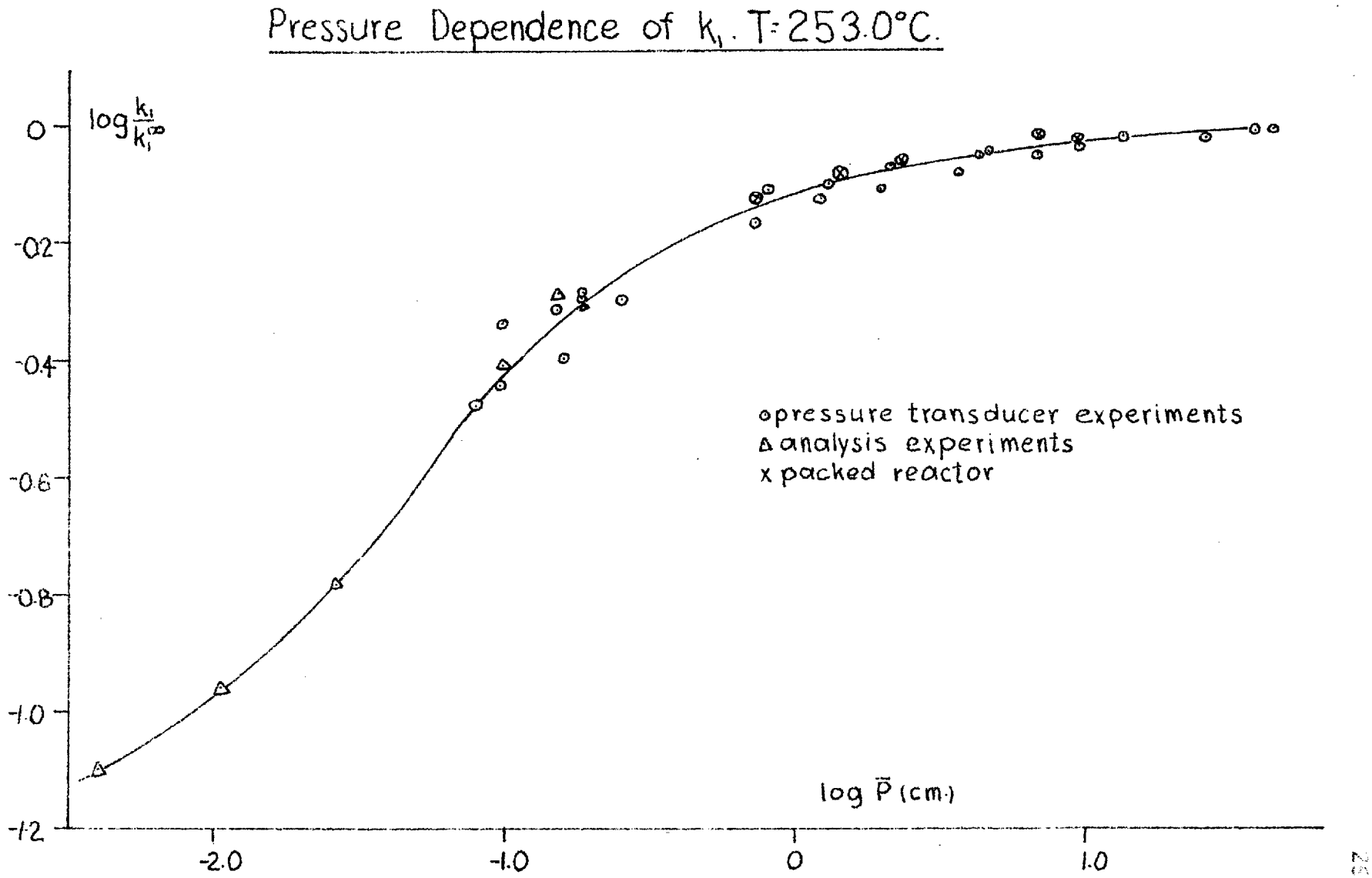
Pressure Dependence of k_1. T=253.0°C.
$\log \frac{k_1}{k_1^{\infty}}$
0
-0.2
-0.4
-0.6
-0.8
-1.0
-1.2
-2.0
-1.0
0
1.0
log $\bar{P}$ (cm.)
o pressure transducer experiments
Δ analysis experiments
x packed reactor

Figure 3.23

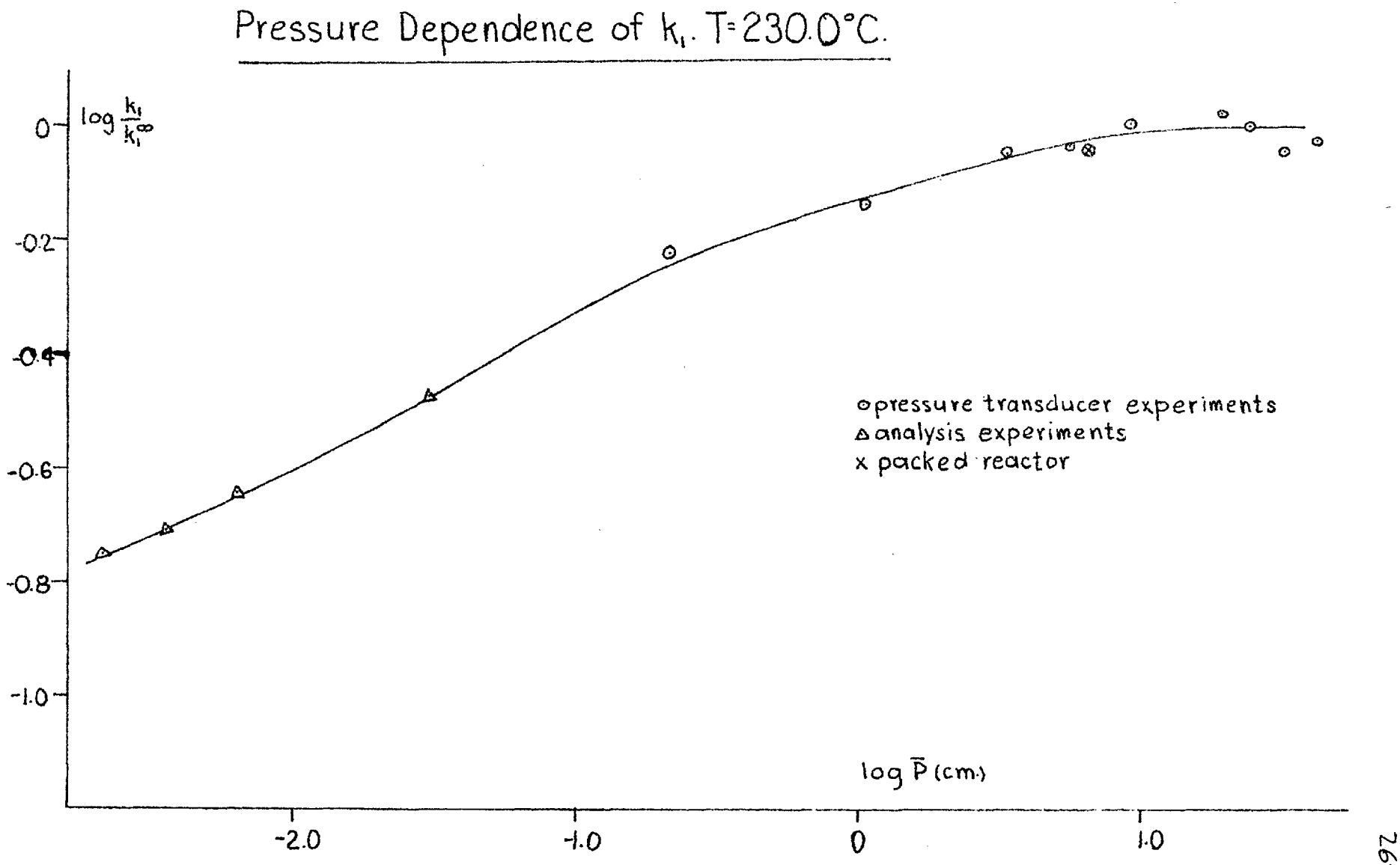
Pressure Dependence of k_1. T=230.0°C.
$\log \frac{k_1}{k_1^\infty}$
0
-0.2
-0.4
-0.6
-0.8
-1.0
o pressure transducer experiments
Δ analysis experiments
x packed reactor
$\log \bar{P}$ (cm.)
-2.0
-1.0
0
1.0

Figure 3.24.

less than this. The thermal transpiration correction is another uncertainty since the expression used involves a lot of approximation. For points on the curves of figures 3.23 and 3.24 the combined uncertainty is probably about 15% for pressures below 0.05 cm. Between 0.5 and 0.05 cm. the agreement between analysis and pressure transducer results is good and thermal transpiration effects are negligible so the uncertainty is probably about 10%.

Octafluorocyclobutane was not observed in the products of reactions below 0.5 cm. This is partly due to the size of sample for analysis which is available. Between 0.5 and 0.05 cm. 1% and between 0.05 and 0.001 cm. 3% is about the lower limit detectable. The results of Table 3.3 show unusually large quantities (up to 5%) of perfluoropropene in several A runs. Within experimental error correction for the effect of this impurity would have a negligible effect on the rate constant.

4. DISCUSSION

4. DISCUSSION

High pressure rate constants obtained in this study have been combined with published results for the rate of combination of difluoromethylene radicals to yield the equilibrium constant and heat of reaction of perfluorocyclopropane decomposition. The heat of formation and strain energy have also been determined for the perfluorocylopropane molecule. The unimolecular rate constant results have been interpreted in terms of various approaches to unimolecular reaction theory.

4.1. The High Pressure Rate Constants

4.1.1. Determination of High Pressure Constants for Unimolecular Reactions

If variation of unimolecular rate constant is observed with lowering of pressure a suitable method must be found to determine its value at high pressure if it is not found to be constant over a reasonable range of the higher pressures studied. One common method used is to make a plot of $1/k$ against $1/p$ and extrapolate to $1/p = 0$. This suggestion is based on the origional Hinshelwood mechanism which predicts that such a plot will be a straight line for a unimolecular reaction. In practice this plot is a curve whose slope increases as $1/p$ decreases. If as in the present study the data is near the high pressure region the extrapolation gives essentially the same value of k^{∞} predicted by a k - p plot as shown in figures 3.5 to 3.8. If however the data is not so close to the high pressure region there is a danger that the straight line through the experimental points will have a slope less than that applicable to the transition to high pressure behavior and a low value of k^{∞} will result.

Another commonly used method is to plot $1/k$ against $1/p^{\frac{1}{2}}$ and extrapolate the latter to zero. This has the effect of giving a straighter line than the $1/k$ - $1/p$ plot, by "compressing" the pressure axis in the region where the variation of $1/k$ with $1/p$ is decreasing (at lower pressure). When the two methods are compared it is obvious that

$$\text{for } p > 1, \qquad 1/p^{\frac{1}{2}} > 1/p$$

$$\text{and for } p < 1, \qquad 1/p^{\frac{1}{2}} < 1/p$$

If the pressure scale selected is such that 1 on the pressure scale is far from zero a somewhat greater value of k^{∞} will be predicted from the $1/p^{\frac{1}{2}}$ plot. Such a choice would more likely be made if the data available was near the high pressure region so that this method should not be used in such a case.

The difference between the two types of plot is illustrated in figure 4.1. for the results of the E series of experiments. A value 4·5% higher for k^{∞} is predicted by the $1/k$ - $1/p^{\frac{1}{2}}$ plot.

Extrapolation to k_1^{∞} for E Experiments. T=240.5°C.

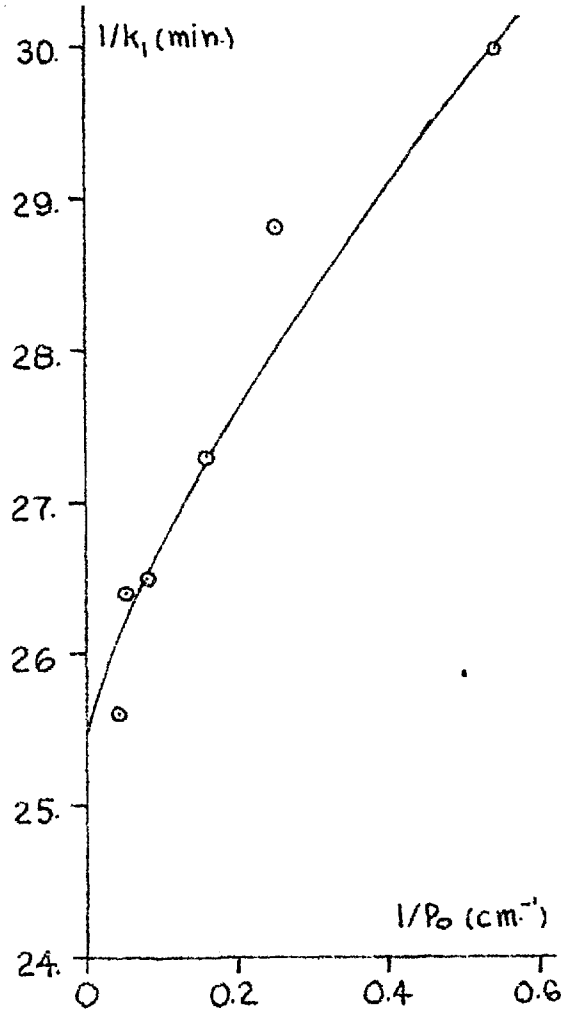

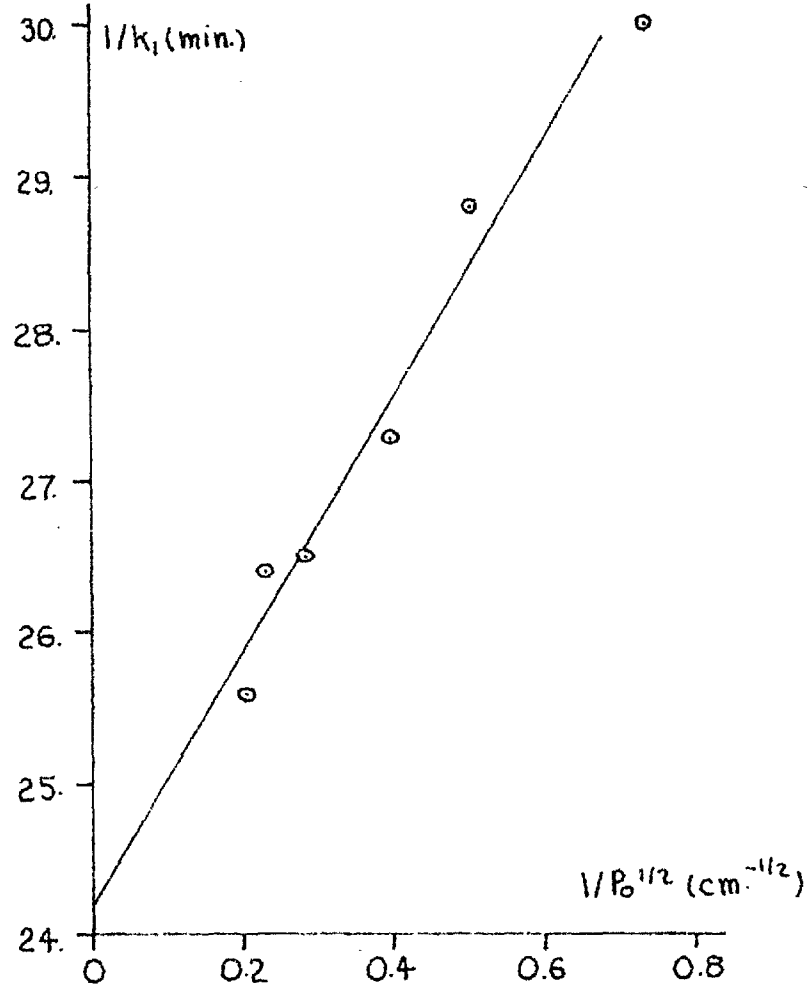

Figure 4-1

4.1.2. Limits on the Determination of the Rate Constants

It would be useful to summarize the limits which the experimental and calculation procedures have placed on the rate constants measured in the present studies. The computer fitting process which was applied to all results above 0·5cm. starting pressure, depends on the simultaneous determination of k_1 and α where α is related to the ratio of rate constants by the expression :

$$\alpha = \frac{3}{2} \left(\frac{k_3}{2 k_2 RT}\right)^{\frac{1}{2}} \times \left(\frac{po}{k_1}\right)^{\frac{1}{2}}$$

Generally speaking a good fit can be obtained if the variation in reagent pressure can be measured accurately over a reasonable range of decomposition as shown in figures 3·3[a] and 3·4. At early stages in the run Y curves are nearly horizontal and at later stages nearly vertical. At high pressures the formation of c-C_4 F_8 is more important and the degree of reaction which can be studied using the fitting procedure is limited to small conversions of reagent. At high temperatures the decomposition takes place so quickly that the placing of Y curves for the early stages of the run is highly uncertain; only the nearly vertical lines can be relied upon to give good results.

This fitting procedure is also dependent on the actual magnitude of α. Its role can be best illustrated by considering the rate expression in the following form :

$$X = \left[\frac{\alpha(Y - 1) + (\alpha^2(1 - Y)^2 + 4Y)^{\frac{1}{2}}}{2}\right]^2,$$

where $X = \left(-\frac{dp_r}{dt}\right) \times \frac{1}{p_o k_1}$

$$Y = \frac{p_r}{p_o}$$

The quantity X is in effect the ratio of the rate of change of p_r to that at the start of the run since :

$$\left(\frac{-dp_r}{dt}\right)_o = k_1 p_o$$

X starts at 1 and decreases during a run.

Under conditions where α is nearly zero the first expression for X reduces to :

$$X = Y$$

and the rate expression is that for the simple first order reaction. High temperature, that is high k_1, and low pressure make α approach zero. This explains why such scatter in α and k_1 is to a certain extent obtained in the high temperature runs. It is also obvious from the above

expression that for Y near one, that is a low degree of reaction, X is only slightly different from one and the $\alpha - k_1$ plots which are drawn for the fitting process will not have sufficiently differing slopes to give a region of intersection with very high certainty.

4.1.3. The Rate Constant k_1^{∞}

In preliminary work already published (44) somewhat different paramaters, in the Arrhenius expression for k_1^{∞} were indicated. At the time the accuracy and number of the experiments was not sufficient to show the variation of k_1 with pressure. Of the three temperatures considered in this early study the results at only one were nearly high pressure and so a different slope of the Arrhenius plot in the final results could be expected. In fact a lower activation energy and preexponential factor were found.

Almost simultaneous with this publication, Mitsch and Neuvar (45) published results for the homogeneous unimolecular decomposition of perfluoroallylcyclopropane :

$$CF_2 = CF - CF_2 - \overbrace{CF - CF_2 - CF_2} \longrightarrow$$

$$CF_2 + CF_2 = CF - CF_2 - CF = CF_2,$$

for which $k = 10^{14.8 \pm .2} \exp(-42{,}700 \pm 500/RT)$.

It is interesting to compare this result to that of the present study where for :

$$\underbrace{CF_2 - CF_2 - CF_2} \longrightarrow CF_2 + CF_2 = CF_2,$$

$$k_1 = 10^{14\cdot92 \pm \cdot12} \exp.\ (-42{,}550 \pm 305/RT)$$

The abnormally high (greater than 10^{14}) preexponential factors of these reactions conform with similar observations in other C_3 and C_4 ring compounds (see Tables 1.1 and 1.2.).

Some curvature of the Arrhenius plot is apparent for perfluorocyclopropane. The deviation from this straight line is such that lower E and A constants could be expected at higher temperatures. The effect is not particularly obvious in figure 3.15 but does appear in the least square analysis if points at high or low temperature rate constants are taken. To confirm the apparent trend a larger number of points would be needed, since a larger uncertainty in the rate constants exists at the high and low temperatures than in the intermediate range (see sect. 4.1.2). Without further experiment definite conclusions cannot be made in this regard.

4.1.4. The Ratio of Rate Constants $(k_3/k_2^{\frac{1}{2}})^{\infty}$

The simultaneous reactions of CF_2 with itself to form $CF_2 = CF_2$ and with $CF_2 = CF_2$ to form $c\text{-}C_3F_6$ have also been studied in other systems. Atkinson (55) in his study of the mercury photosensitized reaction of

C_2F_4 obtained a value

$$\frac{k_3}{k_2^{\frac{1}{2}}} = 0{\cdot}01012 \ (1./_{\text{mole sec.}})^{\frac{1}{2}}$$

at 30°C. Cohen and Heicklen (62) studied this reaction over the temperature range 21 - 224°C and obtained :

$$\frac{k_3}{k_2^{\frac{1}{2}}} = 395 \exp.(-\ 6700/RT) \ (1./_{\text{mole sec.}})^{\frac{1}{2}}$$

Lenzi and Mele (47) have observed the ratio of rate constants in their study of the decomposition of tetrafluoroethylene oxide. They obtained :

$$\frac{k_3}{k_2^{\frac{1}{2}}} = 0{\cdot}154 \ (1./_{\text{mole sec.}})^{\frac{1}{2}}$$

at 126°C.

These results may be compared to the ratio of rate constants between 230 and 289° obtained in the present study :

$$\frac{k_3}{k_2^{\frac{1}{2}}} = 1510 \exp.(-\ 7030/RT) \ (l./_{\text{mole sec.}})^{\frac{1}{2}}$$

The results of the three separate studies havd been plotted together in figure 4.2. Cohen and Heicklen's results predict a somewhat lower rate constant ratio than the other results. They have not allowed for the variation of this rate constant ratio with pressure

Arrhenius Plot for $k_3/k_2^{1/2}$

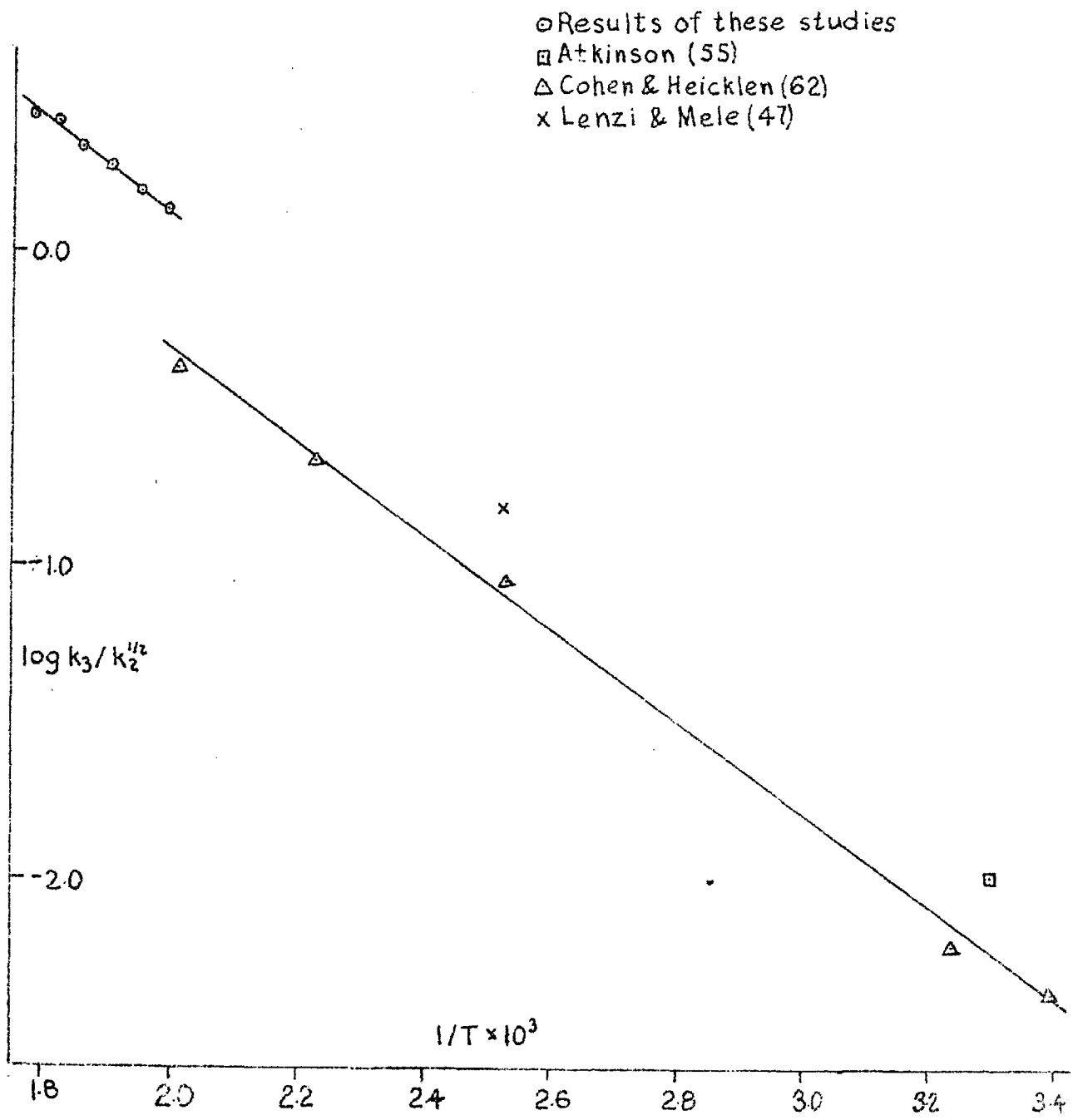

Figure 4.2

and have used pressures greater than 3cm. of Hg at only one temperature. At this temperature the results up to 30cm. are very scattered but do show a slight trend towards higher values of the rate constant ratio. Atkinson's result applies to a pressure of about 15cm. which would be near the high pressure region according to the results of the present study. Lenzi and Mele had too great a scatter in their determination to notice a variation th the rate constant ratio from 2 - 78cm. of Hg pressure. The agreement between the present results and the other work is good in view of the diversity in experimental methods.

The effect of pressure on the individual rate constants k_3 and k_2 may be considered in the following way. Suppose the active form of c - C_3F_6 is designated by c - $C_3F_6^*$; the processes in which it is involved may be described by :

$$c - C_3F_6 + M \xrightarrow{k_a} c - C_3F_6^* + M$$

$$c - C_3F_6^* + M \xrightarrow{k_b} c - C_3F_6 + M$$

$$c - C_3F_6^* \xrightarrow{k_c} CF_2 + C_2F_4$$

$$CF_2 + C_2F_4 \xrightarrow{k_d} c - C_3F_6^*$$

assuming a steady state concentration of $c\text{-}C_3F_6^*$:

$$k_a \left[c\text{-}C_3F_6\right] [M] = k_b \left[c\text{-}C_3F_6^*\right] [M] + k_c \left[c\text{-}C_3F_6^*\right] - k_d [CF_2][C_2F_4]$$

and $$\left[c\text{-}C_3F_6^*\right] = \frac{k_d \left[c\text{-}C_3F_6\right][M] + k_d \left[CF_2\right]\left[C_2F_4\right]}{k_b [M] + k_c}$$

at equilibrium :

$$k_c \left[c\text{-}C_3F_6^*\right] = k_d \left[CF_2\right]\left[C_2F_4\right]$$

$$k_a \left[c\text{-}C_3F_6\right][M] = k_b \left[c\text{-}C_3F_6^*\right][M]$$

Thus :

$$k_c k_a \left[c\text{-}C_3F_6\right] = k_d k_b \left[CF_2\right]\left[C_2F_4\right]$$

and $$K = \frac{\left[CF_2\right]\left[C_2F_4\right]}{\left[c\text{-}C_3F_6\right]} = \frac{k_c k_a}{k_d k_b}$$

The changes involving C_2F_4 may be expressed :

$$\frac{d\left[C_2F_4\right]}{dt} = k_c \left[c\text{-}C_3F_6^*\right] - k_d \left[CF_2\right]\left[C_2F_4\right] + k_2\left[CF_2\right]^2$$

where $$CF_2 + CF_2 \xrightarrow{k_2} C_2F_4$$

substituting in the value for $\left[c\text{-}C_3F_6^*\right]$:

$$\frac{d\left[C_2F_4\right]}{dt} = \frac{k_c}{k_b[M] + k_c}\left\{k_a \left[c\text{-}C_3F_6\right][M] + k_d \left[CF_2\right]\left[C_2F_4\right]\right\} - k_d[CF_2][CF_4]$$

$$+ k_2 \left[CF_2\right]^2$$

$$= \frac{k_c k_a \left[c\text{-}C_3F_6\right][M]}{k_b [M] + k_c} - \frac{k_d k_b [M]\left[CF_2\right]\left[C_2F_4\right]}{k_b [M] + k_c} + k_2 \left[CF_2\right]^2$$

The original form used without considering the detailed activation process for :

$$c\text{-}C_3F_6 \xrightarrow{k_1} CF_2 + C_2F_4$$

$$CF_2 + C_2F_4 \xrightarrow{k_3} c\text{-}C_3F_6,$$

was : $\frac{d[C_2F_4]}{dt} = k_1[c\text{-}C_3F_6] - k_3[CF_2][C_2F_4] + k_2[CF_2]^2$

Thus : $k_1 = \frac{k_c k_a [M]}{k_d[M] + k_c}$

$$k_3 = \frac{k_d k_b [M]}{k_b[M] + k_c} = \frac{k_c k_a [M]}{k_b[M] + k_c} \cdot \frac{1}{K}$$

$$= \frac{k_1}{K}$$

It is thus been shown that K is equal to the ratio of "quasi" constants k_1 & k_3 determined on the assumption of first and second order respectively, since they have the same dependence on pressure. The value of this equilibrium constant has been determined from $(k_3/k_2^{\frac{1}{2}})^{\infty}$ and k_2^{∞} (see section 4.1.5.). The latter is due to Dalby (48) who studied the flash photolysis of C_2F_4 in nearly one atmosphere of Argon and should be a high pressure value of k_2 unless it varies above this pressure. K does not vary with pressure and :

$$\left[\left(k_3/k_2^{\frac{1}{2}}\right)/k_1\right]_p = \frac{1}{K}\left(1/k_2^{\frac{1}{2}}\right)_p$$

Thus k_2 can be determined at various pressures by taking values of $k_3/k_2^{\frac{1}{2}}$ and k_1 at the same pressure.

This has been done for the experiments at 253° and the respective values of $(k_3/k_2^{\frac{1}{2}})_p$ and $(k_1)_p$ have been read from the lines through the points of figures 3.6 and 3.16. The calculated values of k_2 have been listed at the corresponding $1/p_o$ in the following table :

$1/p_o$ cm^{-1}	$k_2 \times 10^5$ l./mole sec.
0	1.392
0.2	1.372
0.4	1.365
0.6	1.369
0.8	1.376
1.0	1.386
1.2	1.394
1.4	1.406

k_2 varies by no more than 3% over the pressure range covered and no trend is observed; within experimental error k_2 is constant. This is suprising since for a

molecule of the complexity of C_2F_4 it is expected that the valve of k_2 would be pressure dependent at these pressures. It must be concluded that the C_2F_4 molecule formed by combination of difluoromethylene radicals need not have energy removed by collisions to remain stable.

4.1.5. The Equilibrium Constant and Heat of Reaction for the Dissociation of Perfluorocyclopropane. --

Equation (14) of section 3.2.2. may be written :

$$\left(\frac{k_3}{k_2^{\frac{1}{2}}}\right)^{\infty} = 1510 \exp.(-7030/RT) \ (\text{l/mole sec.})^{\frac{1}{2}}$$

These rate constants apply to the reactions :

$$2CF_2 \xrightarrow{k_2} C_2F_4; \quad \frac{d[C_2F_4]}{dt} = k_2[CF_2]^2$$

$$CF_2 + C_2F_4 \xrightarrow{k_3} c\text{-}C_3F_6$$

Dalby (48) (see section 1.4.4.) has measured the rate constant for the combination of CF_2 radicals to C_2F_4. He obtained for this bimolecular rate constant:

$$k = 1.3 \times 10^8 \left(\frac{T}{300^{\circ}K}\right)^{\frac{1}{2}} \exp.(-1200/RT) \ (\text{L/mole sec.})$$

$$(25\text{-}299^{\circ}C)$$

When his results were plotted in the ordinary Arrhenius form the following expression resulted :

$$k = 2{\cdot}82 \times 10^{8} \exp.(-1740/RT)(l/mole\ sec.)$$

Since Dalby defines his k by :

$$\frac{d[CF_2]}{dt} = -k[CF_2]^2,$$

the above expression must be divided by 2 to give the equivalent k_2 expression :

$$k_2^{\infty} = 1{\cdot}41 \times 10^{8} \exp.(-1740/RT)(l/mole.sec.).$$

When this expression is combined with the ratio of rate constants $(k_3/k_2^{\frac{1}{2}})^{\infty}$, the result is :

$$k_3^{\infty} = 1{\cdot}793 \times 10^{7} \exp.(-7900/RT)(l/mole.sec.).$$

The equilibrium constant for the reaction :

$$c\text{-}C_3F_6 \underset{k_3}{\overset{k_1}{\rightleftharpoons}} CF_2 + C_2F_4$$

may now be calculated using the expression (13) of section 3.2.1. for k_1^{∞} i.e.,

$$k_1^{\infty} = 8{\cdot}41 \times 10^{14} \exp.(-42{\cdot}55/RT)\ sec.^{-1}$$

where $$K = \frac{k_1}{k_3} = 4{\cdot}69 \times 10^{7} \exp.(-34{\cdot}65/RT)(mole/l.)$$

The heat of reaction at constant pressure may be calculated from the relation :

$$\Delta H = \Delta E + RT\Delta n$$

The heat of reaction at constant volume is 34·65 k.cal./mole and :

ΔH_{298} = 35.24 k.cal./mole

The heat of formation of c-C_3F_6 may now be determined. Assuming $\Delta H_F(CF_2)$ = -40k.cal./mole. (see section 1.4.2.) and $\Delta H_F(C_2F_4)$ = -152 k.cal./mole (160), then :

$\Delta H_F(c\text{-}C_3F_6)$ = -227 k.cal./mole.

4.1.6. Strain Energy in the Perfluorocyclopropane Ring.

Patrick (160) has tabulated the following bond energy terms for various substituted structures :

Structure	Bond	Energy (k.cal.)
Alkane	C - C	- 85·0
- CH_2 -	C - H	- 98·0
- CF_2-	C - F	- 110

These values may be used to estimate the energy associated with the bonds in perfluorocyclopropane. Thus for 3 C - C and 6 C - F bonds the total associated energy is - 915 k.cal. Thermochemical bond energy terms are derived from heats of atomization of molecules. Cottrell (161) has tabulated the following heats of atomization for various elements :

Reaction	ΔH (k.cal.)
$\frac{1}{2}$ H_2 ⟶ H	52·09
$\frac{1}{2}$ F_2 ⟶ F	18·5
C(graphite) ⟶ C	170·9

The heat of atomization of a molecule may be determined

if its heat of formation is known. Thus for :

$$c - C_3F_6 \longrightarrow 6F + 3C,$$

the heat of reaction or heat of atomization is : $3(170.9) + 6(18.5) + 227 = 851$ k.cal., where the heat of formation of $c - C_3F_6$ is - 227 k.cal. (see sect. 4.15). The difference between the heat of atomization and the sum of the energies associated with the bonds is a measure of the strain energy in the ring. For $c - C_3F_6$ this gives - 64 k.cal. This is somewhat greater than the upper limit of - 53 k.cal. estimated by Mitsch and Neuvar (45) on a somewhat more empirical basis for the perfluorocyclopropyl ring.

The heat of atomization of octafluorocyclobutane is estimated to be 1184 k.cal. using a heat of formation of - 352 k.cal.(160). The sum of the bond energy terms gives - 1220 k.cal. so that the strain energy is - 36 k.cal. For cyclopropane whose heat of formation has been reported by Frey (162) to be 12.7 k.cal. the heat of atomization is 812.5 k.cal. The sum of the bond energy terms gives - 843 k.cal. and thus a strain energy of -30.5 k.cal. The significantly greater reactivity of $c - C_3F_6$ can be attributed to increased strain energy. This is caused by the π character of the bonding in the fluorinated ring.

4.1.7. Chemical Equilibria and the Probable Course of Reaction.

The enthalpy change of a reaction may be used to estimate the equilibrium position. Generally speaking, the more negative the heat of reaction, the more negative is the free energy of reaction the larger is the equilibrium constant. In order to apply such considerations to compounds of interest in the present study, the following heats of formation have been used :

Material	Heat of Formation k.cal./mole.	Reference
CF_2	- 40	see sect. 1.4.2.
CH_2	86	Frey (162)
$CF_2= CF_2$	- 152	Patrick (160)
$CH_2= CH_2$	12·5	(150)
$c\text{-}C_3F_6$	- 227	this work
$c\text{-}C_3H_6$	12·7	Frey (162)
$CF_3\text{-} CF = CF_2$	- 259	Patrick (160)
$CH_3\text{-}CH = CH_2$	4·9	(150)

Perfluorocyclopropane was expected to decompose to give perfluoropropene. For this and the actually observed reaction :

$$c\text{-}C_3F_6 \rightarrow CF_3\text{-}CF = CF_2 \quad \Delta H = - 32 \text{ k.cal./mole.}$$

$$c\text{-}C_3F_6 \rightarrow CF_2 + CF_2= CF_2 \quad \Delta H = 35 \text{ k.cal./mole.}$$

The first process would seem preferred but undoubtedly has such a high activation energy due to the C - F bond strength that it is not important in the temperature range where decomposition has been studied. The activation energy for the latter process is low for two reasons. The resulting CF_2 is stabilized due to π bonding between the spare electrons on the carbon, and fluorine atoms, and the fluorinated C - 3 ring has a large amount of strain.

The analogous processes in the hydrocarbons yield the following information :

$$c - C_3H_6 \rightarrow CH_3 - CH = CH_2 \quad \Delta H = -7{\cdot}8 \text{ k.cal./mole.}$$

$$c - C_3H_6 \rightarrow CH_2 + CH_2 = CH_2 \quad \Delta H = 85{\cdot}8 \text{ k.cal./mole.}$$

The decomposition would be highly unlikely thermochemically. The isomerization has an activation energy of about 65 k.cal. and considering the more moderate strength of the C - H relative to the C - F bond an even greater value could be expected for $c - C_3F_6$ isomerization.

These considerations lead to speculation concerning the character of the intermediate in the reactions of cyclopropanes. The heats of formation

of the trimethylene and perfluorotrimethylene diradicals have been estimated from bond energy and heat of atomization data (see section 4.1.6). The Figures are :

$-CH_2-CH_2-CH_2-$ $\Delta H_F = 67$ k.cal./mole.

$-CF_2-CF_2-CF_2-$ $\Delta H_F \leqq -206$ k.cal./mol.

The upper limit in the second case allows for the stabilization energy due to the π bonding between the extra electrons on the carbons and the fluorine atoms.

If c - C_3F_6 proceeds directly to $CF_2 + C_2F_4$, the heat of reaction was found to be 35·3 k.cal/mole. However for :

$$c - C_3F_6 \rightarrow -CF_2-CF_2-CF_2- \quad \Delta H \leqq 21 \text{ k.cal/mole.}$$

Such a path would seem equally likely as an intermediate step. For the two possible subsequent steps :

$$-CF_2-CF_2-CF_2- \longrightarrow CF_2 + C_2F_4 \quad \Delta H \geqq 14 \text{ k.cal./mole.}$$

$$-CF_2-CF-CF_2- \longrightarrow CF_3-CF=CF_2 \quad \Delta H \geqq -57 \text{ k.cal./mole.}$$

The isomerization would seem preferred but a large activation energy could be expected because of a need to break a C - F bond. The absence of $CF_3 \cdot CF = CF_2$ in the products is some indication that the diradical is not the intermediate; in addition other reactions of this diradical which would be expected are not indicated by

the material balance results.

In the hydrocarbon case :

$$c - C_3H_6 \rightarrow -CH_2- CH_2- CH_2- \quad \Delta H = 54.5 \text{ k.cal./mole.}$$

which seems less likely than the direct isomerization where $\Delta H = -7.8$. Subsequent reactions of trimethylene could lead to :

$$-CH_2- CH_2- CH_2 \rightarrow CH_3- CH = CH_2 \quad \Delta H = -62.3$$

$$-CH_2- CH_2- CH_2 \rightarrow CH_2 + CH_2 = CH_2 \quad \Delta H = 31.3$$

Since the isomerization is preferred, the trimethylene may indeed be the intermediate in this case as has been suggested. Rabinovitch and co-workers (164) showed that during the isomerization of trans-1, 2-dideuterocyclopropane to propenes, the more rapid rearrangement to the cis compound did not result in carbon with D_2. This indicated a trimethylene intermediate which recyclized. More recently Cvetanovic and co-workers (163) have demonstrated that activated cyclopropane produced by photolysis of CD_2CO in the presence of C_2H_4 gave a D distribution in the products which clearly indicated the $\cdot CD_2 \cdot CH_2 \cdot CH_2$ trimethylene intermediate. It is thus fairly clear that the perfluorocyclopropane and cyclopropane thermal reactions are not anologous mechanistically.

4.2. The Unimolecular Rate Constant at Low Pressure and Consideration of Unimolecular Theory.

4.2.1. The Falloff in Rate Constant k_1.

As expected, the value of k_1 the unimolecular rate constant, falls off as pressure is reduced. The effect has been studied to the lowest practicable pressures, at 253 and 230°C and the results presented in figures 3.23 and 3.24. The falloff from the high pressure value of the rate constant is greater at higher temperature for the same pressure as shown in figure 4.3. where the curves of figures 3.23 and 3.24 have been superimposed.

Increase in reaction rate with temperature is due to the significantly greater number of activated molecules which are present at higher temperature. Thus if the populations of activated molecules are depleted by the effects causing falloff in overall rate constant, higher temperatures would be expected to exhibit a more noticable effect. Hence there is a sharper falloff at higher temperature.

As pressure is reduced the overall order of reaction should approach 2. For a molecule of the complexity of perfluorocyclopropane true second order kinetics of decomposition would not be expected at pressures which are experimentally convenient. In the review of Gill and

Pressure Dependence of k_1.

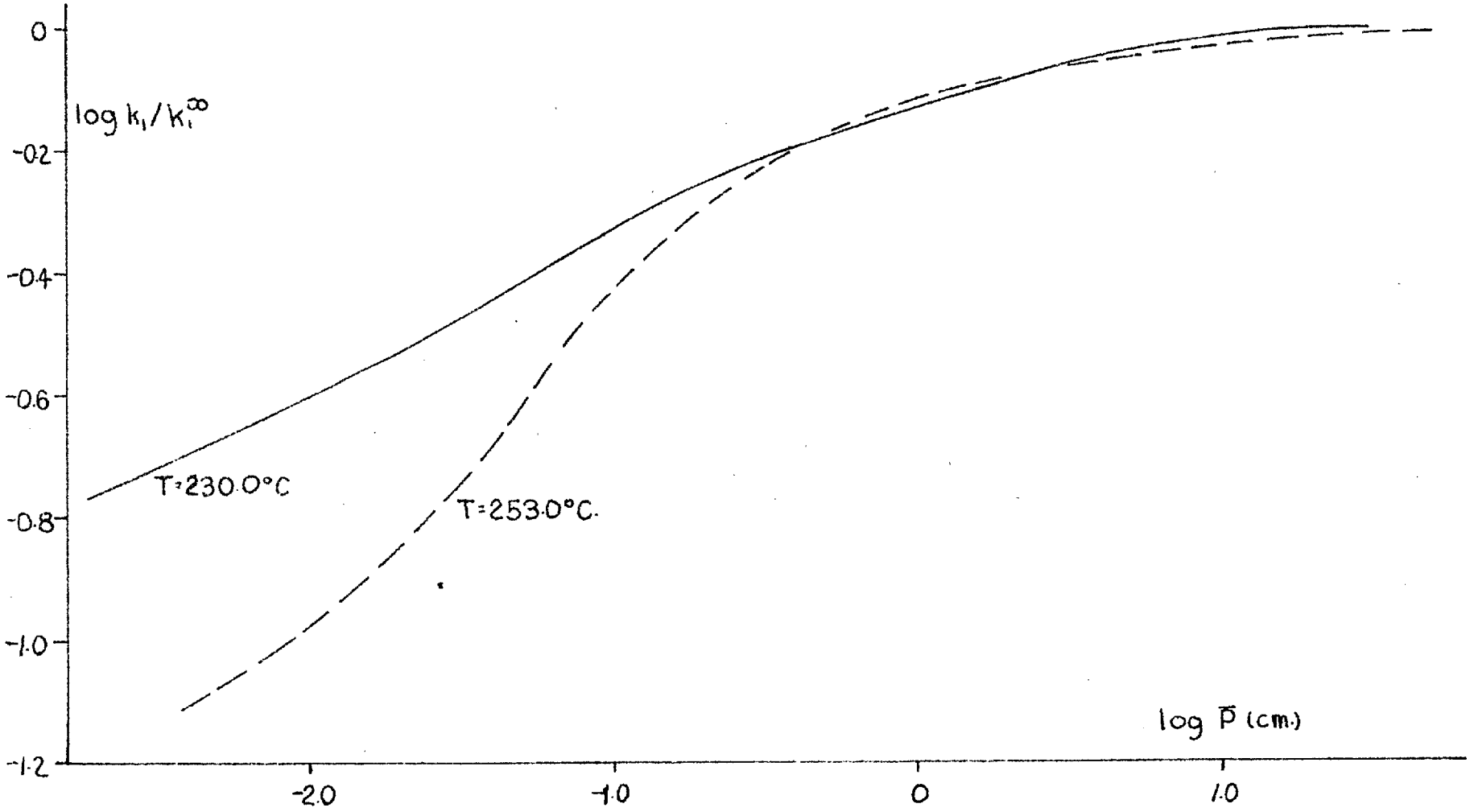

Figure 4.3

Laidler (12) only ozone, nitrous oxide and hydrogen peroxide had data suitable for comparison to predicted second order rates. At extremely low pressure the quasiunimolecular rate constant should depend on the first power of the total pressure and a log k - log p plot should be a straight line of slope one. In general the log k - log p curve should be approaching this condition asymptotically at low pressures.

This is indeed observed for molecules whose rates have been observed to a significant level of falloff such as cyclopropane (140) and nitryl chloride (4, P.179). In the case of perfluorocyclopropane such behaviour is apparant down to about 0.03 cm. in the falloff curve when an inflection point is observed and falloff with pressure is much less than expected. The homogeneity of the reaction has been confirmed in a number of experiments at high pressure. At low pressure where collisions with the walls are relatively more frequent an unimportant wall side reaction at high pressure could become significant. This might explain the higher rates than expected which have been observed in the present study at low pressure (see also sect 4.2.5).

4.2.2. Application of Transition-State Theory

The high pressure rate constant for $c\text{-}C_3F_6$ decomposition may be expressed from section 1.1.1.d as :

$$k_1^{\infty} = \frac{k\ T}{h} \quad \frac{\bar{Q}r^{\ddagger}}{\bar{Q}r} \quad \frac{\bar{Q}v^{\ddagger}}{\bar{Q}v} \quad \exp.(-Eo/RT).$$

where $\bar{Q}r$ and $\bar{Q}v$ are the rotation and vibration partition functions of the normal molecule, the double daggers apply to the transition state and Eo is the activation energy at absolute zero.

To calculate the moments of inertia of the normal molecule, the three carbons are assumed to be at the corners of an equilateral triangle with a 1.53 A^o c - c distance. The C - F distance is assumed 1.33 A^o. Both these values are normal fluorocarbon bond distances. The F-C-F angle is assumed to be 114^o since this was found to be about constant for the X-C-X angle in halogenated cyclopropanes (see Ito (82)). The moments of inertia about the principal axes in atomic weight and $\mathring{A}$ units are 303, 303, 323. The symmetry number of the normal $c\text{-}C_3F_6$ molecule is 6(symmetry D3h).

In the transition state one carbon moves away from the other two and the carbons are assumed to be at the points of an isosceles triangle. Two carbons are assumed to move together so that their distance

apart is reduced half way to the C=C distance in C_2F_4(1·313Å) i.e. 1·53 to 1·42Å . The distance of the third carbon from the C-C axis of the other two is increased by the amount the latter C-C distance has been reduced i.e. 1·325 + 0·11 = 1·435 Å . The two CF_2 groups on the approaching carbons are assumed to move half way through the 30° they origionally made with their own C-C axes, and the F-C-F angle is constant at 114° since this is the value in C_2F_4. The F-C-F angle on the third carbon is assumed to move half way from 114° to the value in CF_2(108°) i.e. 111° and the CF distance on the third carbon is reduced half way from 1.33 to the 1.32 in CF_2 i.e. 1.325. The moments of inertia calculated from these assumptions are : 289, 323 and 301. The symmetry number of the transition-state is 2 (symmetry C2v).

The ratio of rotational partition functions from these figures is :

$$\frac{\overline{Qr}^{\ddagger}}{\overline{Qr}} = 0{\cdot}925$$

The vibrational partition functions have been calculated from the normal mode frequencies of c-C_3F_6 discussed in appendix V; the changes in these frequencies in going to the transition state are also discussed in

this section. The normal molecule partition function is the product of 21 terms like :

$$\left(1 - \exp.\ (-h\nu / \underline{k}\,T)\right)^{-1} \quad \text{and}$$

for the transition state 20 such terms. The result is; for 526·15°K :

$$\frac{Q\nu^{\ddagger}}{Q\nu} = \frac{31490}{681}$$

The zero point energy may be estimated from the Arrhenius plot of k_1^{∞} (figure 3.15). This gives a value :

$$d(\ln k_1^{\infty}) / d\ (1/T) = - 0{\cdot}9298 \times 10^4$$

If the natural log of the transition-state expression for k_1^{∞} is taken and the result differentiated with respect to 1 / T, the result is :

$$d(\ln\ k_1^{\infty}) / d\ (1/T) =$$

$$- T - \frac{Eo}{R} + \sum_{\nu} \left(1 - \exp.(-h\nu/\underline{k}T)\right)^{-1} \times \frac{h\nu}{\underline{k}} \exp.(-h\nu/\underline{k}T).$$

The sum is taken over all vibration frequencies in the normal molecule and transition-state, the sign being changed for the transition-state values. The result using T = 526·15°K is :

$$Eo = 40{,}280 \text{ cal./mole.}$$

The value of k_1^{∞} can now be calculated in the original expression and at 526·15°K :

$$k_1^{\infty} = 8{\cdot}84 \times 10^{-3}$$

The actual value calculated from the experimental Arrhenius expression is :

$$k_1^{\infty} = 1.78 \times 10^{-3}$$

It is apparent from the calculations that slight adjustment upwards in the vibration frequencies assumed for the transition state would bring the values more into line so the agreement with experiment is quite good. It is none the less obvious that assumption of a fairly loose activated complex with reasonable assumptions about reduction of vibration frequencies over the normal molecule enables a fairly close value of the high pressure rate constant to be calculated by transition state theory.

4.2.3. Application of Kassel Theory

Classical Kassel theory is simple to apply to fall-off studies since the only experimental data required are the constants in the expression for the high pressure rate constant, although a collision diameter must also be assumed. The resulting expression for k/k^{∞} must be integrated numerically; however the tabulated integrations of Schlag and Rabinovitch (11) for typical parameters enable an estimate of the number of effective Kassel oscillators to be made by interpolation of their values. Their information has been applied to the data

for perfluorocyclopropane and the following quantities were used :

σ = 6·62 X 10^{-8} cm. (collision diameter - see appendix VI)

A = 8·41 x 10^{14}

E = 42·55 k.cal/mole.

The results for S = 11 and 15 have been plotted along with the experimental data at 253° and 230° in figures 4.4. and 4.5. (The solid lines have been traced from figures 3.23 and 3.24).

Kassel theory predicts the slope of the falloff curve to approach one asymptotically so that it cannot fit the perfluorocyclopropane data. In the region where normal falloff is observed the results are fitted by about S = 14. The falloff data for cyclopropane has been variously fitted to classical Kassel theory with S = 11 by Schlag (21) and S = 13 by Gill and Laidler (12). Thus the effective complexity of the two molecules is similar as would be expected from molecules of such similar structure. The quantum Kassel theory has been fitted by Schlag (21) to the falloff data for cyclopropane for S = 21, which is the number of vibrational degrees of freedom. This is a more satisfactory conclusion. The results of trajectory studies on model molecules as reviewed by Bunker (19) strongly support the idea that all vibrations are active. No attempt was made to

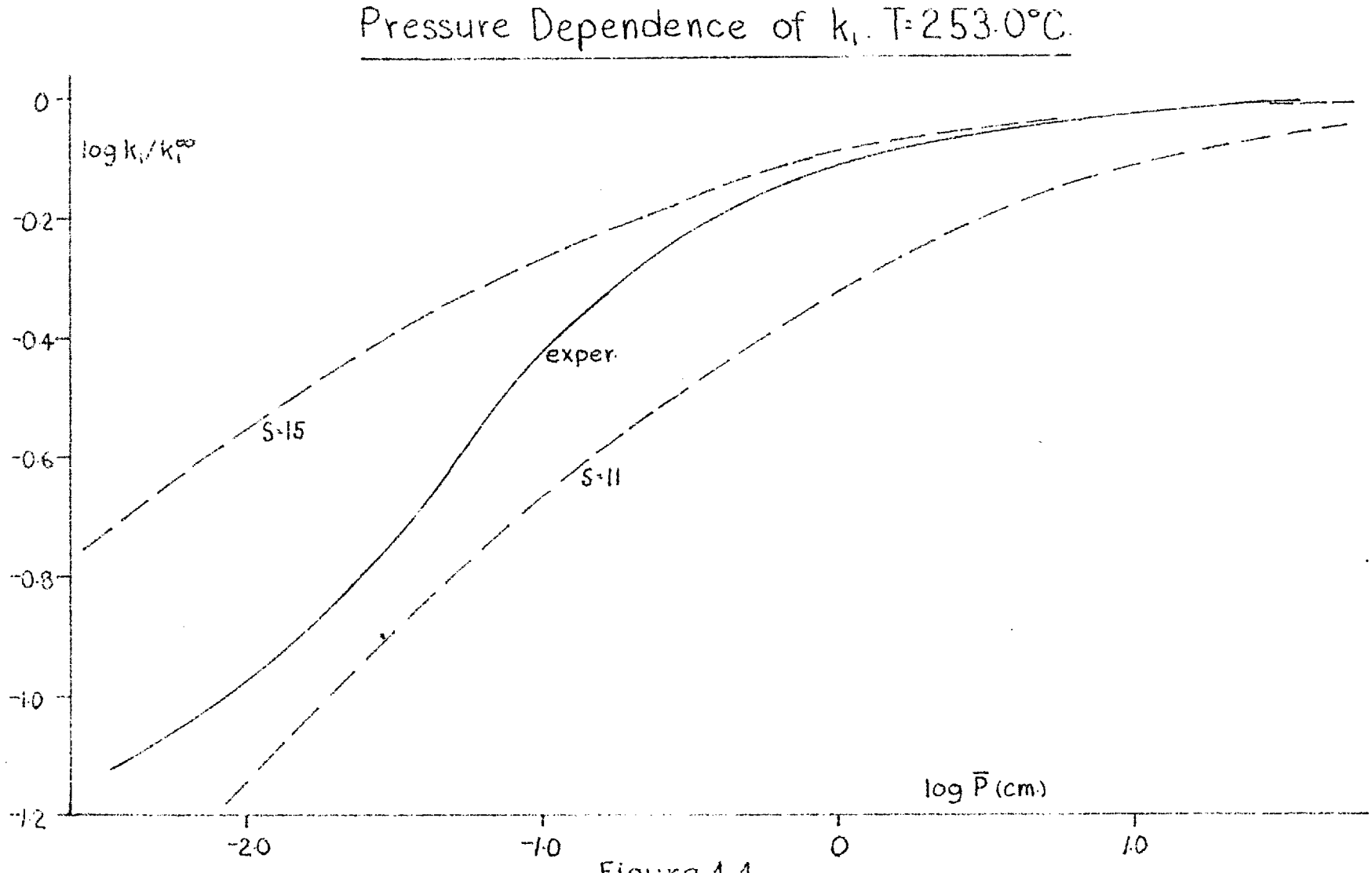
Pressure Dependence of k_1. T=253.0°C.
0
-0.2
-0.4
-0.6
-0.8
-1.0
-1.2
$\log k_1/k_1^{\infty}$
exper.
S=15
S=11
$\log \bar{P}$ (cm.)
-2.0
-1.0
0
1.0

Figure 4.4

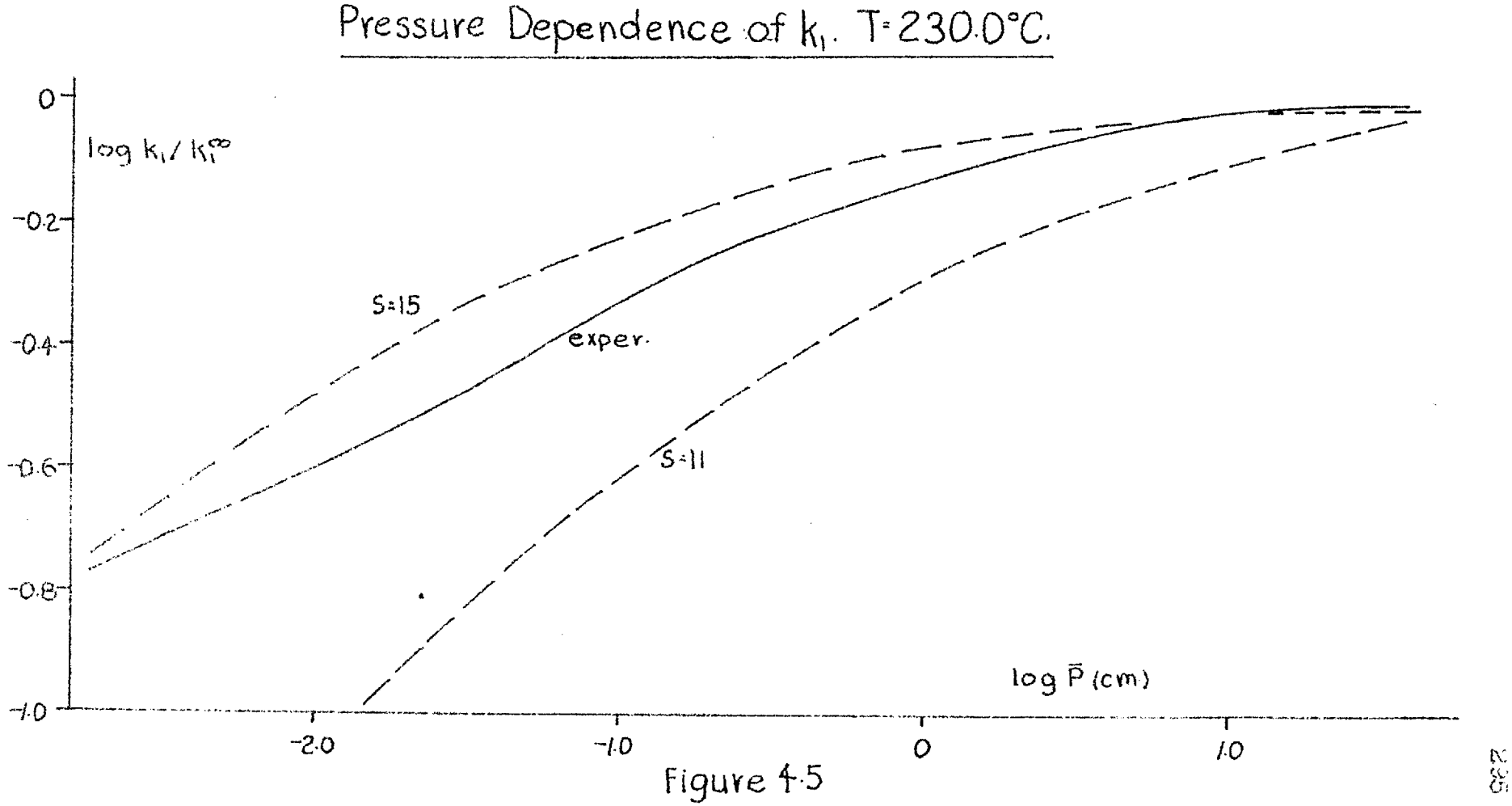
Pressure Dependence of k_1. T=230.0°C.
0
-0.2
-0.4
-0.6
-0.8
-1.0
log k_1 / k_1^{∞}
S=15
exper.
S=11
log $\bar{P}$ (cm)
-2.0
-1.0
0
1.0

Figure 4.5

apply the quantum theory to perfluorocyclopropane since this requires numerical integration of the fall-off equation.

The finding of a fit for 14 classical Kassel oscillations is suprising in comparison to the results of Trotman-Dickenson and co-workers (41, 42) for fluorinated cyclopropanes. They fitted falloff data for monofluorocyclopropane, 1,1-difluorocyclopropane, 1,1,2,2- trifluorocyclopropane, and 1, 1, 2, 2-tetrafluorocyclopropane with S = 13, 17, 18 and 21 respectively. They have attributed this increase in effective number of oscillators to the greater mechanical significance of the heavier fluorine atoms on internal vibrations. Perfluorocyclopropane does not fit into this pattern; however its high pressure activation energy fits into the decreasing trend with increasing fluorination of the other cyclopropanes and has a high prexponential factor in common with them (see table 12).

Benson (35) has shown that increasing the effective number of oscillators shifts the maximum in the energy distribution curve of reacting molecules to higher energies. Considered in terms of the Kassel prediction that falloff is sharper (i.e. greater at the same pressure) for a smaller number of oscillators, it is concluded

that the average energy of reacting molecules above the necessary minimum is greater with increased fluorination despite the trend of reduced activation energy. The sharp change in number of oscillators in the case of the fully fluorinated compound is consistent with a different reaction path, i.e. elimination of CF_2.

4.2.4. Application of Slater Theory

The vibrational analysis of the perfluorocyclopropane molecule (see appendix V) yields information about the force constants and kinetic energy coefficients (respectively the $\mathcal{K}_i$ and a_i in the Potential and Kinetic energy expressions of section 1.1.2b, page 48). These are related to the amplitude factors α_i which are required to apply Slater Theory.

The critical coordinate is assumed to be the distance from one carbon to the axis of the other two carbons. The favoured mechanism is one where CF_2 moves symmetrically away from a C_2F_4 part , simultaneously breaking two carbon-carbon bonds. It is the ring deformation frequencies which provide this motion; only A' and E' modes are considered since these vibrations effect the ring deformation motions.

The symbolism is that of section 1.1.2[b] for the parameters of interest. The amplitude factors α_i calculated for the effect of each frequency on the ring deformation frequency in each symmetry group are listed along with the appropriate frequency in the following table. In addition the amplitude factor ratios :

$$\mu_i = \frac{\alpha_i}{\alpha} = \alpha_i / (\Sigma \alpha_i^2)^{\frac{1}{2}}$$

have also been listed.

Vibrn. no.	1	2	3	8	9	10	11
freq. (cm^{-1})	1800	730	361	855	1385	524	216
$\alpha_i (x10^4)$	7·59	7·78	5·41	6·75	8·0	0·61	7·0
$\mu_i (x10)$	4·34	4·45	3·09	3·86	4·57	0·35	4·0

The approximations involved in the integration of Slater's general expression for the rate constant require that the μ_i are all nearly equal in magnitude. He suggests (4, P.181) that :

$$\mu_i < (4 \pi b)^{-\frac{1}{2}}$$

should be left out. The experimental high pressure activation energy is 42·55 k.cal./mole and at 526.15°K:

$$b = Eo/RT = 40·68$$

and $\mu_i < 0·140$

should be excluded. Thus mode 10 is omitted in the following analysis; the remaining amplitude factor

ratios are all of about the same magnitude.

For the remaining six frequencies a value $\alpha = 1{\cdot}75 \times 10^{-3}$ has been calculated; whence :

$$\nu = \frac{1}{\alpha} (\Sigma \alpha_i^2 \nu_i^2)^{\frac{1}{2}}$$

$$= 3{\cdot}254 \times 10^{13} \text{ sec.}^{-1}$$

The Arrhenius factor is three times this value since there are three identical ways in which the value of the critical coordinate may exceed that required for reaction. Thus $A = 9{\cdot}76 \times 10^{13}$ which differs by about an order of magnitude from the experimental value of $8{\cdot}41 \times 10^{14}$.

To consider the predicted effect of pressure on the rate constant, the following calculations have been performed at 253°C. For six vibrations :

$$m = \frac{1}{2} (n - 1) = 2{\cdot}5$$

For a collision diameter of $6{\cdot}62 \times 10^{-8}$cm. (see appendix VI) the collision frequency is:

$$\omega = 2{\cdot}333 \times 10^{8} \, P/T^{\frac{1}{2}},$$

where P, the pressure is in m.m. Further, referring to p.54 of this thesis:

$$b^m = 1{\cdot}055 \times 10^{4}$$

$$\Pi \mu_i = 4{\cdot}236 \times 10^{-3}$$

$$\gamma_n = 7{\cdot}869$$

$$\Theta = 0{\cdot}02485P \text{ (m.m.)}$$

Values of $k/k^{\infty} = Im(\Theta)$ can be determined from Slater's (4, p.169) Table 8·2(a). These indicate a falloff at m = 2·5 in a much higher pressure range than that observed experimentally. If the predicted and experimental relationship of log P and log k/k^{∞} are plotted together as in figure 4·6 with the predicted values displaced 2·5 log units in a negative direction, the experimental values are closely conformed to except at very low pressure.

Pritchard et.al. (166) found that they could predict the shape of the cyclopropane falloff curve by shifting the predicted curve by about 0·56 log units in a negative direction. The correction is greater in the present case but does confirm the ability of Slater Theory to predict the shape of falloff curves.

When the calculations are performed for 230°C the appropriate parameters are:

$$b^m = 1·18 \times 10^4$$

$$\Theta = 0·0284 \text{ P (m.m.)}$$

where Υn and $\overline{\Pi} \lambda i$ are as before. The Slater prediction displaced 2·5 log units in the negative direction does not conform to the experimental points to as low a pressure as in the higher temperature example. (See figure 4.7).

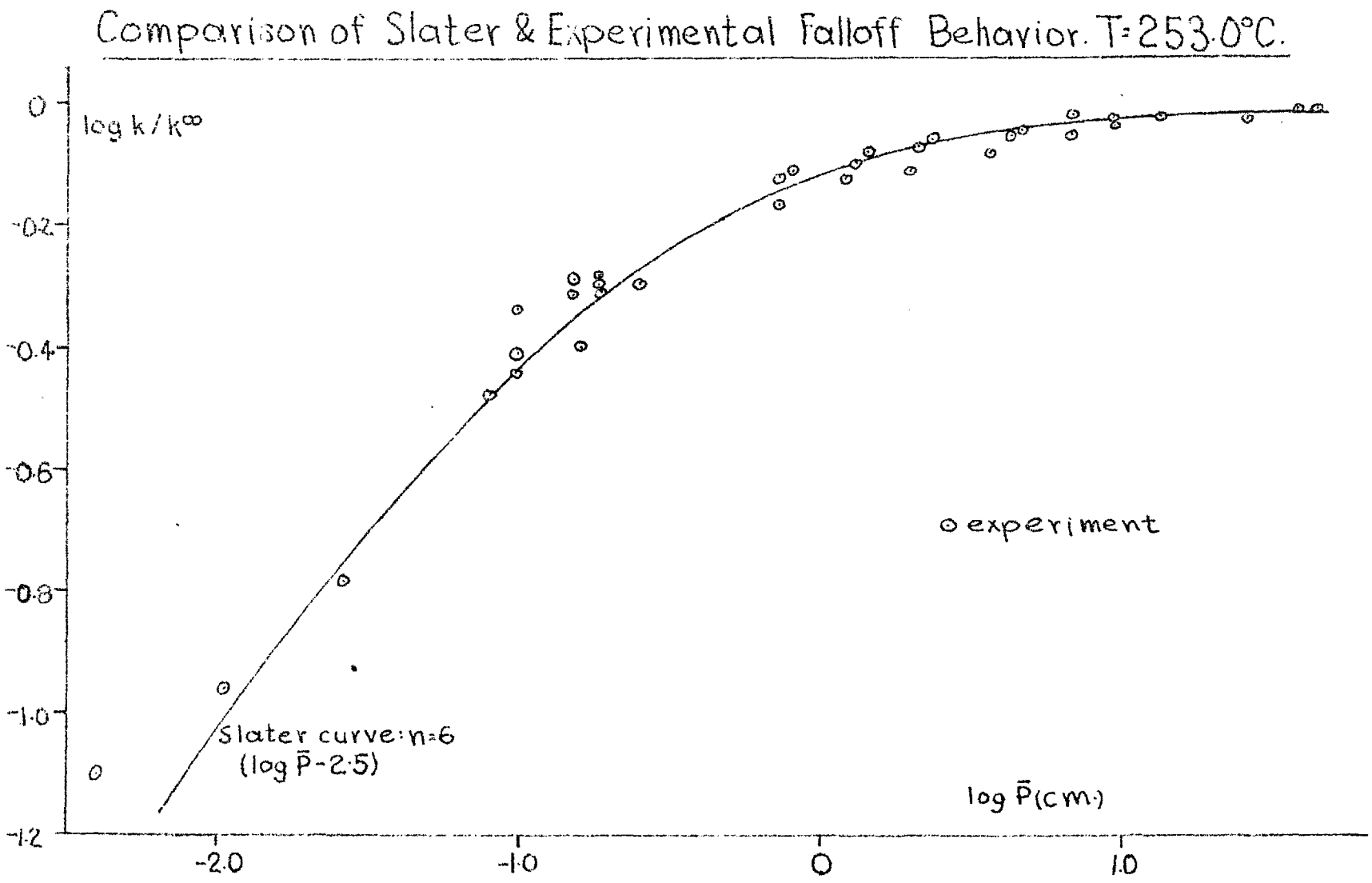
Comparison of Slater & Experimental Falloff Behavior. T=253.0°C.
log k/k∞
0
-0.2
-0.4
-0.6
-0.8
-1.0
-1.2
-2.0
-1.0
0
1.0
log P̄(cm.)
o experiment
Slater curve: n=6
(log F̄ - 2.5)

Figure 4.6

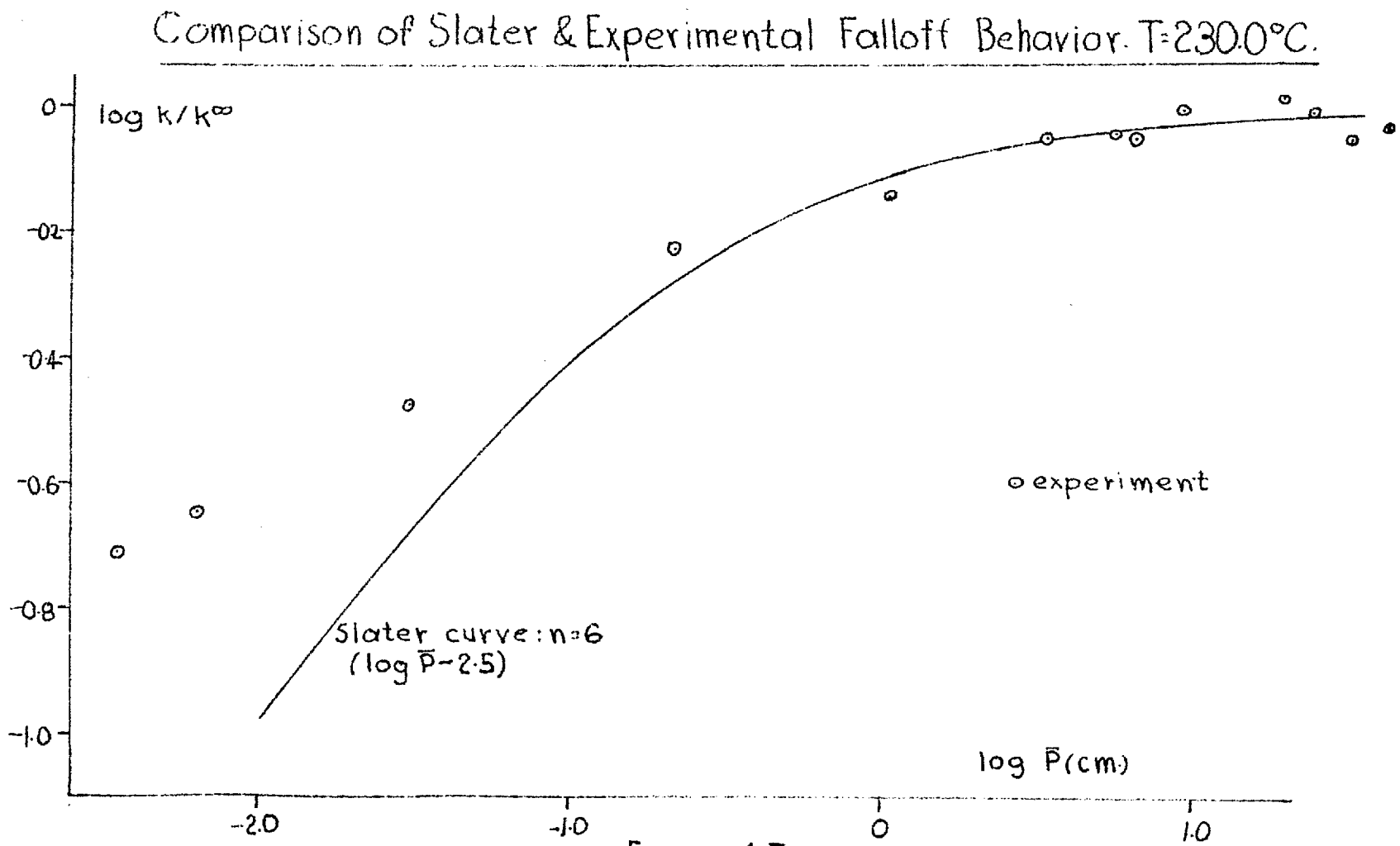
Comparison of Slater & Experimental Falloff Behavior. T=230.0°C.
log k/k∞
0
-0.2
-0.4
-0.6
-0.8
-1.0
-2.0
-1.0
0
1.0
log P̄(cm)
o experiment
Slater curve: n=6
(log P̄-2.5)

Figure 4.7

4.2.5. Third Body Effects in Unimolecular Reactions

The homogeneity of a unimolecular reaction is usually established by carrying it out in a reactor with a considerably increased surface area. If similar rates are found in both reactors homogeneity is assumed. The effect of surface is not usually studied in falloff experiments where at low pressure the collisions with the wall of the reactor are relatively more frequent.

Studies of unimolecular reactions in the presence of added gases indicate that a different distribution of energies of molecules is produced by the diluent. Thus for instance Chesick (141) found that nitrogen was only about 20% as effective as reactant in maintaining the high pressure distribution of active methylcyclopropane molecules. A similar significant effect might be found from the surface if the relative rates of collision with other gas molecules and the vessel walls were comparable.

The rates of collision with other molecules and walls may be estimated from the kinetic theory of gases. The rate of collision of like molecules is :

$$2\sigma^2 n^2 \left(\frac{\pi \underline{k}\ T}{m}\right)^{\frac{1}{2}}$$

where n is the molecule concentration/c.c. The rate

of collison with the walls per unit of area is:

$$\frac{n}{4}\left(\frac{8\ \underline{k}\ T}{\pi\ m}\right)^{\frac{1}{2}}$$

In the low pressure experiments of the present studies the reactor has a volume/surface ratio of 1·56 cm. and the per cent of total collisions with the walls have been estimated at various pressures using the above formulae; the figures are presented in the table.

Pressure cm.	% Collisions with wall.
0·001	7·9
0·005	1·7
0·01	0·9

Thus at low pressures in falloff studies there is some justification for comparing the behaviour in a packed reactor since wall effects which are insignificant at high pressure may be more noticeable at low pressure.

A similar shape of falloff curve to that of the present study has been observed by Kennedy and Pritchard (165) for cyclopropane at very low pressure. They studied the isomerization to propene in packed and unpacked reactors down to 6×10^{-4} m.m. At about 5×10^{-3} m.m. in the unpacked and 5×10^{-2} m.m. in the packed reactor the order of reaction again becomes first order. Both points are in the region where

molecule-wall collisions are about equal in number to molecule-molecule collisions. They suggest that this finding is consistent with the interpretation that collisions with the walls are 3 - 5 times as efficient as collisions with other cyclopropane molecules.

4.3. Suggestions for Further Work

4.3.1. Extension of the Present Works

The temperature range of the present study in the static reactor has been limited especially at lower temperature by side reactions e.g. the formation of octafluorocyclobutane and perfluoropropane. Perfluoropropene formation seems to be a surface reaction. Study of various seasoning procedures may reveal a technique which will effectively eliminate its formation. Alternatively a suitable coating may be found effective in preventing perfluoropropane formation. Halberstadt and Chesick (142) have found a metallic silicon coating produced by the thermal decomposition of an organic silane to reduce the effect of surface reactions.

Inclusion of the dimerization reaction of $CF_2=CF_2$ to octafluorocyclobutane considerably complicates the differential equation describing the kinetics in terms of one concentration variable. For the equations:

$$c\text{-}C_3F_6 \xrightarrow{k_1} CF_2 + C_2F_4$$

$$2\,CF_2 \xrightarrow{k_2} C_2F_4$$

$$C_2F_4 + CF_2 \xrightarrow{k_3} c\text{-}C_3F_6$$

$$2C_2F_4 \xrightarrow{k_4} c\text{-}C_4F_8$$

The system would probably best be treated as one of four first order differential equations describing the variation in concentration with time of the four species present. Since they are independent the system is soluble in principle. Standard computer programs have been written for the numerical integration of simultaneous differential equations, although the treatment may be complicated by the occurrence of square terms in the concentrations.

The effects of the dimerization reaction may be reduced by carrying out the c-C_3F_6 reaction in a relatively high pressure of inert diluent. If the studies are to be made with the pressure transducer, the backing-off circuit (see figure 2.9) would have to be redesigned. By reducing the resistance in series with the helipot a larger portion of the mallory cell voltage could be used to back off a large signal and still work with the highest transducer input (and hence sensitivity). Using an inert gas would also reduce the back reaction (CF_2 + C_2F_4) and first order kinetics could be assumed to a higher pressure of c-C_3F_6.

The procedure of studying the decomposition of c-C_3F_6 in the presence of a relatively high pressure of inert diluent would effectively eliminate falloff effects

if the total pressure was about 40 cm., as indicated by the falloff data of the present studies. The effect of other molecules in maintaining the high pressure distribution of active molecules would of course need consideration but for physically similar inert materials (e.g. perfluoropropane) the difference should be minimal. The rate of C_2F_4 dimerization would still depend only on the square of its concentration.

The use of high pressure brings up the problem of reactor cooling at the start of the reaction. This effect could be eliminated with a suitably "thick" metal reactor of large heat content and thermal conductivity.

Extending the $c\text{-}C_3F_6$ decomposition studies to higher temperatures undoubtedly involves the use of a flow reactor. The results would have to be followed by product analysis.

Improved low pressure results would be obtained with a larger reactor with a larger inlet line. The thermal transpiration corrections applied in the present studies are somewhat uncertain; these could be eliminated with a large bore inlet line (ref. Chesick (141)). A larger reactor would also give larger

samples and more accurate analyses as well as a minimisation of the increased dead space due to the larger bore inlet. A more suitable method of measuring the starting pressure would be to have some type of low pressure gauge in the line to measure the final pressure after expansion of starting material into the reactor.

If the equation which describes the kinetics of $c\text{-}C_3F_6$ decomposition, i.e.,

$$\frac{dPr}{dt} + k_1 Pr - a\,(Po - Pr)\left(-\frac{dPr}{dt}\right)^{\frac{1}{2}} = 0$$

were exactly integrable direct determination of k_1 and a would not necessarily result. Some fitting process would have to be found so that the values of k_1 and a which best fitted the experimental Pr-t data when put into the integrated expression would be determined. This could probably be brought about by a technique not unlike that used with the unintegrated form.

A computer program which could determine the best values of k_1 and a from experimental Pr-t data would be desirable. However with numerical integration being necessary for each k_1 - a pair as well as some judgement procedure for a number of experimental points being required, the computer time would be excessive. Hence the technique used is probably as good as can be expected. One unfortunate feature of the

system was however the variation of the factor α with the square root of pressure. Low pressure results invariably gave α values indistinguisable from zero so that the ratio of rate constants could not be determined below 1 cm. of Hg. pressure.

An extension of falloff results to lower pressures might be possible using direct machine integration of the kinetic equation.

4.3.2. Suggestions Concerning Other Systems.

In extending the work of the present kinetic studies it would be interesting to consider the effects of substituents on the cyclopropane ring. The decomposition of perfluoroallylcyclopropane (45) was found to have suprisingly similar rates of decomposition (about 2/3) compared to perfluorocyclopropane. Simpler molecules such as perfluoromethylperfluorocyclopropane would yield falloff data. This would be observed at a lower pressure than c-C_3F_6 due to the increased complexity but would make an interesting comparison to the relevant cyclopropane-methylcyclopropane results.

If saturated cyclopropane rings isomerize with the migration of an H atom, and perfluorinated rings decompose with the elimination of CF_2, then a different mode

of reaction would occur for a compound like tris-(trifluoromethyl)-perfluorocyclopropane :

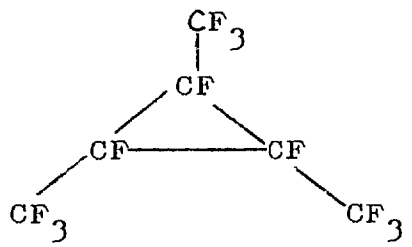

most probably CF_3 CF would be eliminated in the reaction step but the Arrhenius equation parameters for its decomposition would be interesting to compare to the other two types of cyclopropane ring reaction.

The field of unimolecular isomerization and decompositions of C_3 and C_4 hydrocarbon ring compounds has been extended to unsaturated systems. Carr and Walters (157) have studied the thermal isomerization of cyclobutene to 1,3-butadiene and Frey (158) the isomerization of methylcyclobutene to 1,3-pentadiene, for example. Schlag and Peatman (159) have studied the equilibrium between perfluorocyclobutene and perfluoro-1,3-butadiene. Cyclopropene is known to be quite unstable itself but to be stabilized by substitution. Mahler (124) has prepared the compound:

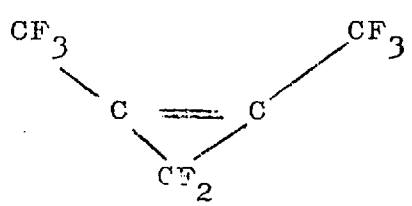

It would be interesting to compare the behaviour of the unsaturated perfluorinated cyclopropane to the saturated cyclopropane ring compounds.

However interesting a particular system might appear there are a number of problems which must be borne in mind. The availability of materials is always a consideration. However the literature of the past few years, partially reviewed in this thesis, has shown many ways in which interesting perfluorinated compounds can be prepared. The present work has demonstrated practically how this may be carried out in one particular case.

Application of the various theories to unimolecular reactions requires a complete vibrational analysis of the molecule in question. Parallel with any kinetic study in the future, of a unimolecular reaction, a detailed study of the molecule's vibrational spectrum should be made. Of particular interest in the application of these theories is the mechanism of decomposition. Every effort should be made by experimental methods to confirm the actual way in which a molecule reacts.

APPENDIX I

The following derivation due to Allen (46) describes the correction for dead space. Let N be the total number of moles in the hot part of the system, R' of these being moles of reactant. Let the ratio of the number of moles produced by the reaction to the number consumed be q. Now let dx moles react. The total increase in number of moles is (q-1) dx. This increase distributes itself between the hot and cold parts of the system at temperatures T_h and T_c respectively in accordance with the gas laws. It is assumed that no back diffusion occurs from the dead space; this must be true as long as the reaction is proceeding at any appreciable rate. If, of the increase in moles (q-1) dx, dN remain in the hot part, then the change in pressure in the hot part is:

$$dP_h = dN\ R\ \frac{T_h}{V_h}$$

where, R is the gas constant, V_h the volume at the reaction temperature. Thus to the cold section, (q-1) dx - dN must leak and the change in pressure in the cold section is:

$$dP_c = [(q-1)\ dx - dN]\ R\ \frac{T_c}{V_c}\ ,$$

where V_c is the dead space volume.

But $dP_h = dP_c$

Thus: $$dN \frac{T_h}{V_h} = [(q-1)dx - dN] \frac{T_c}{V_c},$$

and, $$dN = \frac{(T_c/V_c)(q-1)\ dx}{(T_h/V_h) + (T_c/V_c)}$$

$$= \frac{V_h(q-1)\ dx}{\frac{V_c T_h}{T_c} + V_h} = b(q-1)\ dx$$

where $1/b = (V_h + \frac{V_c T_h}{T_c})\ \frac{1}{V_h}$

Now the expansion of gas causes a loss of reactant from the hot part =

$$\frac{R'}{N}\ [(q-1)\ dx - dN].$$

Thus the total change in number of moles of reactant in the hot part is :

$$dR' = -dx - \frac{R'}{N}\ [(q-1)\ dx - dN]$$

and from above,

$$dR' = \frac{-dN}{b(q-1)} - \frac{R'}{N}\ [(q-1)\ dx - dN]$$

$$\frac{dR'}{dN} = \frac{-1}{b(q-1)} - \frac{R'}{N}\ (\frac{1}{b} - 1)$$

If it is assumed that: $N_o = R'_o$ at the start,

integration gives:

$$R' = \frac{q\, N_o^{1/b}}{(q-1)\, N^{(1/b)-1}} - \frac{N}{q-1}. \qquad (1)$$

This expression may be written in terms of pressure:

$$Pr = \frac{q\, P_o^{1/b}}{(q-1)P^{(1/b)-1}} - \frac{P}{q-1} = \frac{q\, P}{q-1}\left(\frac{P_o}{P}\right)^{1/b} - \frac{P}{q-1}. \qquad (2)$$

Since for the reaction under study, $q = 1.5$,

$$Pr = 3P(P_o/P)^{1/b} - 2P.$$

APPENDIX II

Using the terminology of Appendix I, the effect of dead space on an analysis when all of the material in the dead space and only part of that in the reactor is removed as a sample for analysis, will be considered. Suppose the reactor to consist of three zones:

(i) V_c (the dead space) at T_c

(ii) V_h' in the reaction section which is not removed on condensing out to get a sample for analysis

(iii) V_h'' in the reaction section at T_h which is removed along with the material in V_c for analysis.

Then the total volume V is:

$$V = V_c + V_h = V_c + V_h' + V_h''$$

In V_c let α be the moles of reactant and β the moles of product. Initially there is no product and:

$$P_o = \frac{\alpha_o RT_c}{V_c} = \frac{N_o RT_h}{V_h} \qquad (1)$$

At any time the pressures in each section are assumed equal so that

$$P_h = P_c, \text{ and}$$

$$\frac{N\ RT_h}{V_n} = (\alpha+\beta)\ \frac{RT_c}{V_c}\ . \qquad (2)$$

The material balance at any time can be expressed:

$$R' + \alpha + \frac{N-R'+\beta}{q} = R'_o+\alpha_o = N_o+\alpha_o \qquad (3)$$

From equation (2):

$$(\alpha+\beta) = \frac{N\ T_h\ V_c}{V_h\ T_c} \qquad (4)$$

From equations (3) and (4):

$$\beta = \frac{q}{q-1}\left[R\left(\frac{q-1}{q}\right) + N\left(\frac{T_h V_c}{V_n T_c} + \frac{1}{q}\right) - N_o\left(1 + \frac{V_c T_h}{T_c V_n}\right)\right]. \qquad (5)$$

At any time the value of R' may be expressed by equation (1) of Appendix I. Thus:

$$R' = \frac{N}{q-1}\left[q\left(\frac{N_o}{N}\right)^{1/b} - 1\right]. \qquad (6)$$

If at any time a sample is taken the concentration Z which is measured may be expressed:

$$Z = \frac{\text{moles reagent in } V_h'' + V_c}{\text{total moles in } V_h'' + V_c}$$

or

$$Z = \frac{(V_h''/V_h)\ R' + \alpha}{(NV_h''/V_h) + \alpha+\beta}. \qquad (7)$$

By substitution of equations (4),(5) and (6) into (7), the result is:

$$Z = \frac{\frac{V_h''}{V_h}\left[\frac{q(N_o/N)^{1/b}-1}{q-1}\right]\frac{T_hV_c}{V_hT_c} - \frac{q}{q-1}\left[\frac{q(N_o/N)^{1/b}-1}{q}\frac{T_hV_c}{V_hT_c} + \frac{1}{q}\frac{N_o}{N}\left(1+\frac{T_hV_c}{V_hT_c}\right)\right]}{\frac{V_h''}{V_h} + \frac{T_hV_c}{V_hT_c}} \quad (8)$$

In practice the ratio V_h''/V_h may be estimated from the pressure in the reactor before and after taking the sample for analysis. The ratio N_o/N may be replaced by P_o/P.

APPENDIX III

In the Fortran IV program reprinted on the following pages the symbol A replaces the α of eqn (12). The integration is performed for values of A from 0.05 to 12.05 in steps of 0.2. For each A the area under the curve is calculated for each Y from 1.0 to 0.6 in steps of 0.02. The print out is however only made for Y from 0.8 to 0.6 so that the top line would begin as shown in the "typical print out" of section 3.1.3.(page 196)

```
JOB  10C14010     D MCKEAGAN IBJOB    4.000 1000
          £EXECUTE       IBJOB
IBJOB VERSION 5 HAS CONTROL.
£IBJOB         FIOCS
£IBFTC DECK1
      DIMENSION Y(21),X(21),AR(20)
      DIMENSION W(51),U(51),H(51)
      DIMENSION YY(11),ARR(11)
      INTEGER P,Q,QQ,NN,PP
      INTEGER MM,S,T
      DO 50 MM=5,1205,20
      A=MM
      A=A/100.
      X(1)=1.
      DO 40 J=1,21,1
      I=80+20*J
      B=I
      Y(J)=1.-(B-100.)/1000.
      I=B
      IF(J.EQ.1) GO TO 40
      X(J)=AB(A,Y,J)
      D=1./X(J)-1./X(J-1)
      Q=500.*D
      Q=2*Q
      IF(Q.LT.50) GO TO 70
      Q=50
   70 E=Q
      R=.32/E
      Q=E
      Q=Q+1
C THE U ARE VALUES OF ORDINATE IN THE INTERVAL
      U(1)=Y(J)
      DO 27 QQ=2,Q,1
   27 U(QQ)=U(QQ-1)+R
C THE W ARE VALUES OF X IN THE INTERVAL
      DO 29 QQ=1,Q,1
   29 W(QQ)=AB1(A,U,QQ)
C THE H ARE VALUES OF 1/X IN THE INTERVAL
      DO 28 QQ=1,Q,1
   28 H(QQ)=1./W(QQ)
      NN=(Q-3)/2
      SUM=0
      DO 26 PP=1,NN,1
   26 SUM=SUM+4.*H(2*PP)+2.*H(2*PP+1)
      V=(R/3.)*(H(1)+H(QQ)+SUM+4.*H(QQ-1))
      IF(J.GT.2) GO TO 39
      AR(1)=V
      GO TO 40
   39 P=J-1
      AR(P)=AR(P-1)+V
      DO 91 S=1,51,1
      W(S)=0
      U(S)=0
```

```
   91 H(S)=0
      DO 43 T=1,11,1
      YY(T)=Y(T+ 9)
   43 ARR(T)=AR(T+ 9)
   40 CONTINUE
      IF(MM.GT.5) GO TO 49
      WRITE(6,41)(YY(T),T=1,11,1)
   41 FORMAT(1H,8X,11(F4.2,5X))
   49 CONTINUE
      WRITE(6,42)A,(ARR(T),T=1,11,1 )
   42 FORMAT(1H,F5.2,1X,11(F 9.5))
      DO 92 S=1,10,1
   92 AR(S)=0
   50 CONTINUE
      STOP
      END
£IBFTC CECK2
      REAL FUNCTION AB(A,Y,J)
      DIMENSION Y(11),X(11)
      AB=(((A*Y(J)-A)+((A-A*Y(J))**2.+4.*Y(J))**.5)/2.)**2.
      RETURN
      END
£IBFTC CECK3
      REAL FUNCTION AB1(A,U,QQ)
      DIMENSION U(51),W(51)
      INTEGER QQ
      AB1=(((A*U(QQ)-A)+((A-A*U(QQ))**2.+4.*U(QQ))**.5)/2.)**2.
      RETURN
      END
```

APPENDIX IV

Treatment of thermal transpiration effects in the region of transition between high pressure where no correction is needed and low pressure where conditions of true molecular flow exist, is theoretically difficult. The subject has been dealt with empirically by a number of workers but the relationships they obtain apply only to systems being measured which are below room temperature. The first attempt at a general treatment which could be applied to any system provided certain properties of the substance whose pressure was being measured, were known is due to Swift (151) and his treatment will be sketched here.

A familiar expression for the coefficient of viscosity η is:

$$\eta = \frac{1}{3} mn\bar{c}\lambda,$$

where m is the mass of a molecule, n the number of molecules per unit volume and $\bar{c}$ their average velocity. This expression is an approximation based on idealized resultant momentum interchanges between molecules. A more vigorous treatment due to Chapman (152) gives a form:

$$\eta = e\rho\bar{c}\lambda,$$

where e is a constant in the range 0.491 - 0.499 and ρ the density. $\bar{o}$, the average velocity of molecules

is obtained from Kinetic Theory assuming a Maxwell-Boltzmann distribution of velocities:

$$\bar{c} = 2\left(\frac{2RT}{\pi M}\right)^{\frac{1}{2}}$$

On a molar basis ρ can be written:

$$\rho = \frac{PM}{RT} ,$$

and if it is assumed that $e = 0.5$,

$$\eta = \left(\frac{2M}{RT\pi}\right)^{\frac{1}{2}} P\lambda . \qquad (1)$$

The mean free path of the molecules may also be calculated from the Kinetic Theory of Gases. Thus:

$$\lambda = \frac{1}{\sqrt{2}\ \pi n\sigma^2} = \frac{k\ T}{\sqrt{2}\ \pi\sigma^2 P} . \qquad (2)$$

Since λ varies with $1/P$, η is independent of pressure at the same temperature. This condition holds provided λ is small compared to the dimensions of the container. As the gas pressure is reduced the importance of impacts between molecules and the walls of the containing vessel increases relative to intermolecular impacts. A stage is eventually reached where collisions of the former type are predominant and each gas molecule moves independently of all the others in the vessel.

Under flow conditions at low pressure this effect is manifested as a changed velocity profile across an element in the flowing stream. Slip of the gas at the surface brings about this change. Where u is the slip velocity, the effect on the velocity profile, V, in the direction y perpendicular to the flow may be written:

$$u = \xi \frac{dV}{dy}$$

where ξ the coefficient of slip has the dimensions of length. Swift (151 p.249) has calculated ξ approximately from considerations of kinetic theory and stress analysis in the moving gas. He obtains:

$$\xi = 2e \left(\frac{2-f}{f}\right) \lambda,$$

where f is defined as the fraction of the gas molecules striking the surface which are diffusely reflected. Usually f is about 1 and for e = 0.5:

$$\xi = \lambda \qquad (3)$$

The condition of slip along the walls of a container such as a tube is also manifested where there is no flow if there is a temperature difference between the ends of the tube. The molecules from the hot end have larger momentum than those at the cold end due to higher velocity. The net result of collisions of all molecules with the walls of the fixed tube is a transfer of momentum to the

gas causing a drift of gas from the cold to the hot end. This effect is known as thermal transpiration. At low enough pressures that collisions between molecules can be neglected the resulting pressure differences may be expressed:

$$\frac{P_1}{P_2} = \sqrt{\frac{T_1}{T_2}} \tag{4}$$

At pressures intermediate between this region and high pressure where no pressure difference is observed, is a region where creep occurs at the walls and an opposing flow occurs at the centre of the tube set up by the pressure difference due to collisions between molecules. The resulting pressure difference is less than that expressed in equation (4). Swift (151) has approached the solution of this pressure difference and obtained an approximate relation. He derives an expression for the flow of gas under these conditions; an expression for the pressure difference at steady state results when the flow is equated to zero. Thus:

$$\frac{dP}{dx} = \frac{6\eta^2 R}{a^2 P(1+\frac{4\varepsilon}{a})M} \cdot \frac{dT}{dx}, \tag{5}$$

where x is the direction along the axis of the tube, and a the radius of the tube. The expression applies in the region where the Knudsen number K is less than 0.2, where $K = \frac{\lambda}{2a}$.

The expression (5) may be integrated for small temperature differences where it can be assumed that $\eta^2 = \bar{\eta}^2$ and $\xi = \bar{\xi}$, i.e. these quantities are constant. Thus:

$$\int P dP = \int \frac{6\bar{\eta}^2 \, R \, dT}{a^2(1+4\,\bar{\xi}/a)M} \text{ , and}$$

$$P_2 - P_1 = \frac{6\bar{\eta}_2 \, R(T_2 - T_1)}{\bar{P}(1+4\bar{\xi}/a)a^2 M} .$$

It equations (1) and (3) are substituted into this expression then:

$$P_2 - P_1 = \frac{12\,\bar{\lambda}^2\,\bar{P}\,(T_2 - T_1)}{\bar{T}\,\pi\,a^2\,(1+4\bar{\lambda}/a)} \qquad (6)$$

Swift (151) has shown that the expression (5) is similar to forms used by Knudsen (153) and Chu Liang (154) which predict the pressure effect but contain certain empirical constants. These relations are not applicable to the present work as they cover corrections to systems below room temperature.

At high pressures $(\lambda/a)^2$ becomes very small and $P_2 - P_1$ in equation (6) is zero as expected. At low pressures approaching the region where expression (4) is applicable, Knudsen has shown that a suitable expression for the pressure gradient is:

$$\frac{dP}{P} = \frac{3}{8}\,\Delta\,\frac{1}{1+\frac{2a}{\lambda}}\,\frac{dT}{T} , \qquad (8)$$

where Δ is an empirical constant. As $K = \lambda/2a$ becomes very large, Δ approaches 4/3. In the low pressure region Δ varies very little. Porter (155) has used such a form for K greater than 1. If Δ is assumed 4/3, then

$$\frac{P_2}{P_1} = \left(\frac{T_2}{T_1}\right)^{\frac{1}{2(1+2a/\lambda)}} \qquad (9)$$

At low pressure $2a/\lambda$ is negligible and (9) reduces to (4).

Application of equations (9) and (6) to the present work can only give approximate corrections for the transpiration effects. The true experimental temperatures for low pressure experiments, 230 and 253°C are far removed from room temperature at which the pressures have been measured. Averaged properties in equation (6) is a questionable assumption. It is also uncertain in what region of pressure equation (9) becomes applicable since this will differ between different molecules. Calculations have been performed for equations (6) and (9) using a tube diameter of 2 mm and a collision diameter of 6.62 Å for perfluorocyclopropane. These have been plotted for 230 and 253° in fig. IV.1 and IV.2. The correction was assumed to start deviating from equation (6), the high pressure curve at K = 0.2 and a curve was drawn arbitrarily so that it would fit the line of equation (9) by about 10^{-4}cm. The shape of the curve is not unlike that found by Porter (155) in about the same regions of pressure.

Thermal Transpiration Corrections. T=230.0°C.

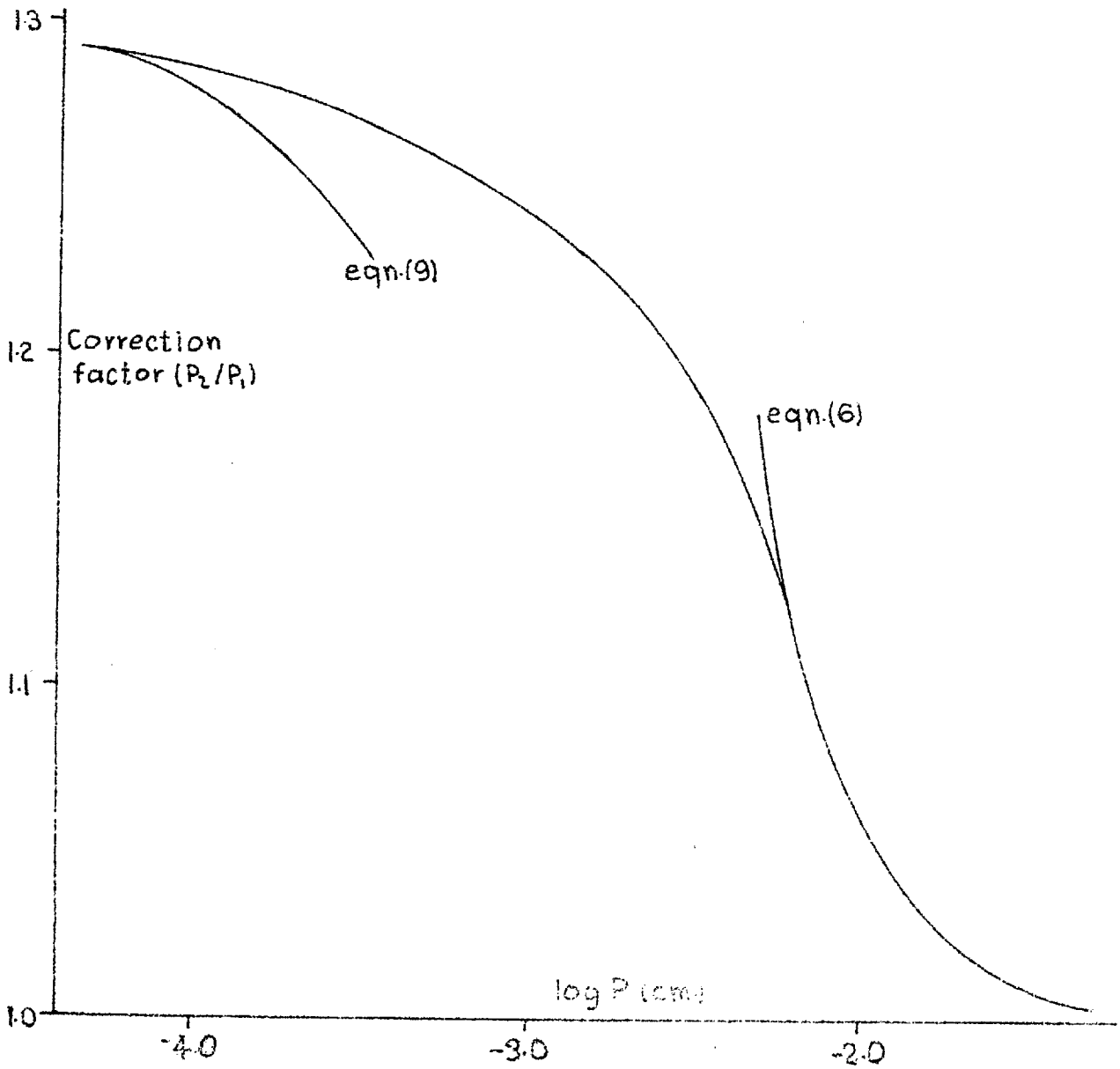

Figure IV.1

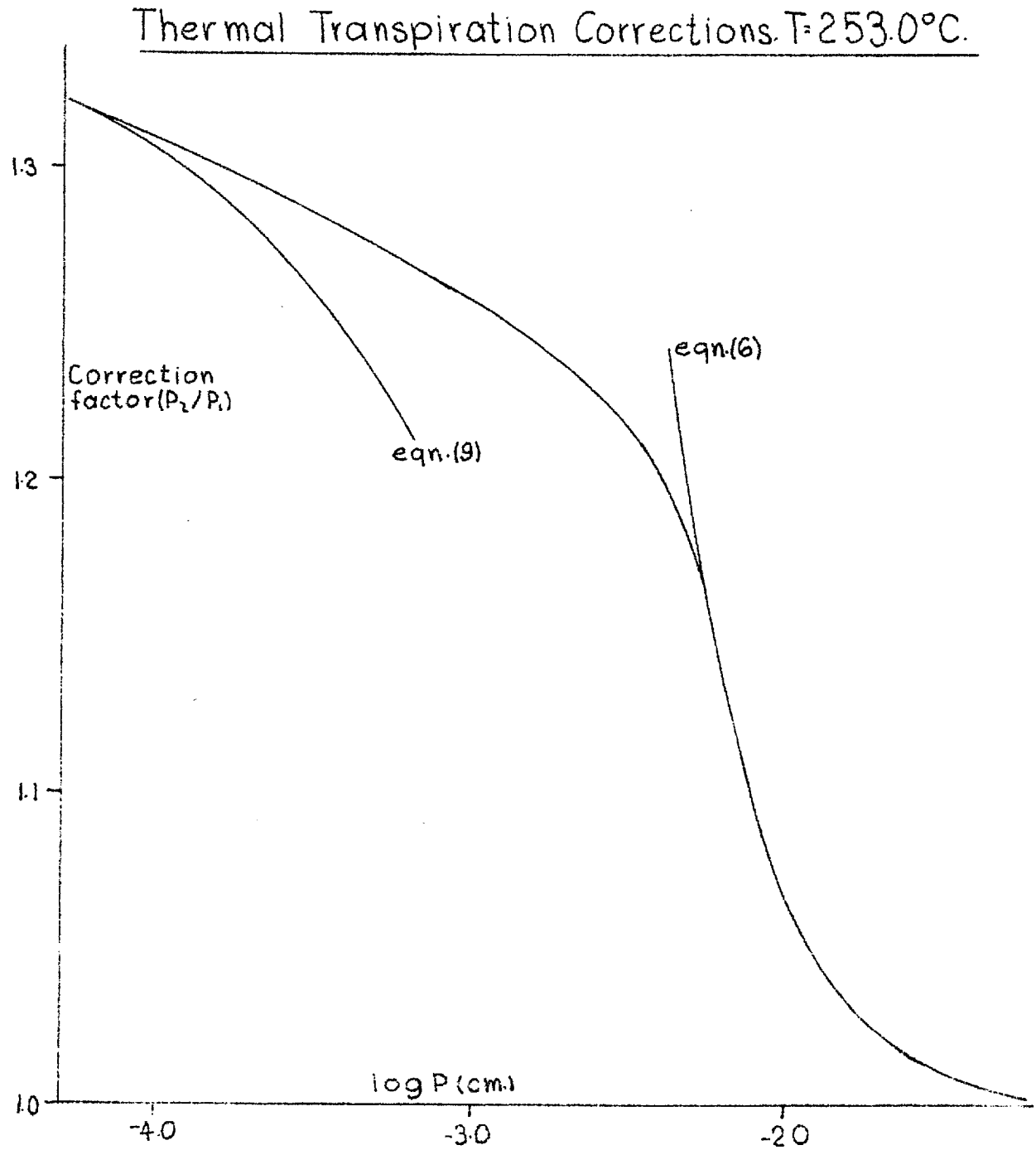
Thermal Transpiration Corrections. T=253.0°C.
1.3
1.2
1.1
1.0
Correction factor (P_2/P_1)
eqn.(6)
eqn.(9)
log P (cm.)
-4.0
-3.0
-2.0

Figure IV.2

APPENDIX V

The spectrum of perfluorocyclopropane has been studied in the far infra-red and a more complete assignment of the fundamental frequencies has resulted. A 10 cm. cell was used with polyethylene windows. A high pressure (60 cm.) of perfluorocyclopropane purified chromatographically but containing traces of C_2F_4 was put in the cell; a high pressure is required since resolution is generally reduced in this range of the infra-red. A Grubb-Parsons Spectromaster covered the range from 600 - 400 $cm.^{-1}$. In the range 500 - 200 $cm.^{-1}$ A Grubb-Parsons model DM4 double beam machine was used; compensating polythene strips were placed in the reference beam. A Grubb-Parsons model GM3 single beam spectrometer was employed over the range 200 - 50 $cm.^{-1}$.

New absorptions observed in the far infra-red where a medium strength absorption at 276 $cm.^{-1}$, a strong absorption at 245 $cm.^{-1}$ with pronounced shoulders at 255 and 237 $cm.^{-1}$ and a strong absorption at 200 $cm.^{-1}$. A large uncertainty (about 5 $cm.^{-1}$) in this latter peak could not be avoided and no resolution of shoulder peaks was possible since this figure is at the lower and upper limits of the DM4 and GM3 ranges. However a strong absorption was observed at about 200 $cm.^{-1}$ on both machines.

The weak 498 cm^{-1} absorption reported by Ito (82) has been definitely resolved and two illdefined shoulders noted using the Spectromaster. The lines at 443 and 552 cm^{-1} were definitely not observed and one probably due to impurities in Ito's sample. No absorptions are observed below 200 cm^{-1}.

On the basis of this new information Atkinson* has re-examined the fundamental vibrations of perfluorocyclopropane molecule and a complete analysis is shown in table V.1. For forbidden or unobserved transitions the values listed are combination frequencies or reasonable estimates from data of other molecules.

In order to calculate the vibrational partition functions of the transition state these frequencies have been modified as shown in table V.2.

Since the C=C stretching frequency is about 1700 cm^{-1} in C_2F_4 ν_1 has been left the same. One ring deformation frequency ν_8 has been removed for the vibration become translation in the transition state and the other ν_8 has been reduced to 200 since this motion would be more sluggish in the transition state.

---

* Atkinson, B., unpublished results.

Table V.1.

Fundamental Vibrations of Perfluorocyclopropane*

Species	Vibration No.	Approx. Mode of Vibration	Frequency cm^{-1}
A_1'	1	ring deformation	1800
	2	CF stretch	730
	3	CF_2 deformation	361
A_1''	4	CF_2 twist	200
A_2'	5	CF_2 wag	850
A_2''	6	CF stretch	1367
	7	CF_2 rock	200
E'	8	ring deformation	863
	9	CF stretch	1276
	10	CF_2 deformation	548
	11	CF_2 wag	252
E''	12	CF stretch	1552
	13	CF_2 rock	498
	14	CF_2 twist	276

* compare data of Ito (82) in table 1.3.

Table V.2.

Vibration Frequencies of Perfluorocyclopropane in the Transition State.

Vibration No.	Degeneracy	Frequency cm^{-1}
1	1	1800
2	1	730
3	1	361
4*	1	100
5	1	850
6	1	1367
7	1	200
8*	1	200
9	2	1276
10	2	548
11	1	252
11*	1	100
12	2	1552
13	1	498
13*	1	100
14*	1	300
14**	1	100

*,** These values have been changed from the vibrations of the normal molecule in table V.1.

The CF_2 angle assumed to be 114° in c-C_3F_6 (see appendix VI) is the same in C_2F_4 and changes only to 108° in CF_2 so that CF_2 deformations ν_3 and ν_{10} have not been changed.

The CF_2 twists in c-C_3F_6 are low frequency. Of the corresponding motions in C_2F_4, the in phase motions would be a rotation and the out of phase motions would be restricted due to the double bond. Hence one ν_{14} has been decreased to 100 and one increased to 300. The corresponding motion in CF_2 is also becoming a rotation and so ν_4 has been reduced to 100 cm^{-1}.

The wagging motion in the part of the molecule going to C_2F_4 would not change much in frequency; one ν_{11} and ν_5 have been kept the same. In the CF_2 part the motion becomes a rotation and so one ν_{11} has been reduced to 100. The same applies to the rocking frequencies. One ν_{13} has been reduced to 100; one ν_{13} and ν_7 have been left the same.

The CF stretching frequencies would increase slightly in C_2F_4 and CF_2 due to π bonding causing shorter bond lengths. Since they are already high in c-C_3F_6 ν_2, ν_6, ν_9 and ν_{12} have been left the same.

APPENDIX VI

The collision diameter of perfluorocyclopropane has been estimated in conjunction with the vibrational analysis reported in the previous appendix. From the assignments of Ito (82) for halogenated C_3 cyclopropanes, a constant CX_2 angle of 114° seems reasonable and this value has been assumed. Normal fluorocarbon bond distances have been assumed: 1.53 Å for the C-C and 1.33 Å for the C-F bond. A Van der Waals radius of 1.35 Å has been taken for fluorine. The collision diameter calculated as twice the distance from the centre of the C_3 triangle to the outer reach of a Van der Waals radius about any fluorine atom is 6.62 Å.

BIBLIOGRAPHY

1. Lindemann, F.A., Trans. Faraday Soc. 17, 598 (1922).
2. Howlett, K.E., Science Progress (Lon.) 50, 273 (1962).
3. Trotman-Dickenson, A.I., "Gas Kinetics", Academic Press, (1955).
4. Slater, N.B., "Theory of Unimolecular Reactions", Methuen, (1959).
5. Hinshelwood, C.N., "The Kinetics of Chemical Change" Oxford, (1940).
6. Rice, O.K., and Ramsperger, H.C., J.A.C.S. 49, 1617 (1927).
7. Kassel, L.S., J. Phys. Chem. 32, 225 (1928).
8. Kassel, L.S., "The Kinetics of Homogeneous Gas Reactions", Chapt.5, Chemical Catalog Co., (1932).
9. Kassel, L.S., J. Phys. Chem. 32, 1065 (1928).
10. Polanyi and Wigner, Z. physik. Chem., Haber-Band, 439 (1928).
11. Schlag, E.W., Rabinovitch, B.S., and Schneider, F.W., J. Chem. Phys. 32, 1599 (1960).
12. Gill, E.K. and Laidler, K.J., Proc. Roy. Soc. A250, 121 (1959).
13. Glasstone, S., Laidler, K.J. and Eyring, H. "The Theory of Rate Processes", McGraw-Hill Book Co., (1941).
14. Hinshelwood, C.N., Proc. Roy. Soc. A113, 230 (1926).

15. Herzberg, G., "Infrared and Raman Spectra of Polyatomic Molecules", D. Van Nostrand Co.Inc. (1945).

16. Marcus, R.A. and Rice, O.K., J. Phys. and Colloid Chemistry, 55, 894 (1951).

17. Wieder, G.M. and Marcus, R.A., J. Chem. Phys. 37, 1835 (1962).

18. Marcus, R.A., J. Chem. Phys. 20, 359 (1952).

19. Bunker, D.L., The International Encyclopaedia of Physical Chemistry: "Theory of Elementary Gas Reaction Rates", Chapt. 3, Pergamon Press, (1966).

20. Giddings, J.C. and Eyring, H., J. Chem. Phys. 22, 538 (1954).

21. Schlag, E.W., J. Chem. Phys. 35, 2117 (1961).

22. Slater, N.B., J. Chem. Phys. 24, 1256 (1956).

23. Thiele, E., J. Chem. Phys. 36, 1466 (1962).

24. Gowenlock, B.G., Quart. Rev. 14, 133 (1960).

25. Pritchard, H.O., J. Chem. Phys. 25, 267 (1956).

26. Atkinson, B. and Stedman, M., J. Chem. Soc. 512 (1962).

27. Steel, C., J. Chem. Phys. 31, 899 (1959).

28. Thiele, E. and Wilson, D.J., J. Phys. Chem. 64, 473 (1960).

29. Slater, N.B., J. Phys. Chem. 64, 476 (1960).

30. Wilson, D.J. and Thiele, E., J. Chem. Phys. 40, 3425 (1964).

31. Thiele, E., J. Chem. Phys. 45, 491 (1966).

32. Hoare, M., J. Chem. Phys. 38, 1630 (1963).

33. Wilson, D.J., J. Phys. Chem. 64, 323 (1960).

34. Mahan, B.H., J. Phys. Chem. 62, 100 (1958).

35. Benson, S.W., "Foundations of Chemical Kinetics", McGraw-Hill (1960).

36. Flowers, M. C. and Frey, H.M., J. Phys. Chem. 65, 373 (1961).

37. Brauner, J.W. and Wilson, D.J., J. Phys. Chem. 67, 1134 (1963).

38. Buff, F.P. and Wilson, D.J., J. Chem. Phys., 32, 677 (1960).

39. Buff, F.P. and Wilson, D.J., J. Chem, Phys., 45, 1444 (1966).

40. Elliott, C.S. and Frey, H.M., J. Chem. Soc. 4289 (1965).

41. Casas, F., Kerr, J.A. and Trotman-Dickenson, A.F., J. Chem. Soc. 3655 (1964).

42. Herbert, F.P., Kerr, J.A. and Trotman-Dickenson, A.F., J. Chem. Soc. 5710 (1965).

43. Placzek, D.W. and Rabinovitch, B.S., J. Phys. Chem. 69, 2141 (1965).

44. Atkinson, B. and McKeagan, D., Chem. Comm. 189 (1966).

45. Mitsch, R.A. and Neuvar, E.W., J. Phys. Chem. 70, 546 (1966).

46. Allen, A.D., J.A.C.S. 56, 2053 (1934).

47. Lenzi, M. and Mele, A., J. Chem. Phys. 43, 1974 (1965).

48. Dalby, F.W., J. Chem. Phys. 41, 2297 (1964).

49. Mitsch, R.A., J.A.C.S., 89, 758 (1965).

50. Benning et al. U.S. Pat.2,394,581 (Kinetic Chemicals Co.)

51. Young, E.G., Murray, W.S., J.A.C.S. 70, 2814 (1948).

52. Harmon, J., U.S. Pat. 2,404,374 (Dupont, 1946).

53. Br.Pat. 593,997 (Dupont, 1947).

54. Atkinson, B., Nature, 163, 291 (1949).

55. Atkinson, B., J. Chem. Soc. 2684 (1952).

56. Haszeldine, R.N., J. Chem. Soc. 3761 (1953).

57. Serpinet, J., Chim. anal. 41, 146 (1959).

58. "Chemistry of Carbon Compounds" Vol. II-A, p.31, Rodd, E.H. (Ed.) Elsevier Publishing Co.

59. Lovelace, A. et al. "Aliphatic Fluorine Compounds", Reinhold (1958) Chapt.2.

60. Heicklen, J. et al., J. Chem. Phys. 42, 221 (1965).

61. Heicklen, J. and Knight, V., J. Phys. Chem. 69, 2484, (1965).

62. Cohen, N. and Heicklen, J., J. Chem. Phys. 43, 871 (1965).

63. Heicklen, J. et al., U.S. Gov't. Res. Rept. 39, 23 (1964) No.19.

64. Heicklen, J. et al., U.S. Gov't. Res. Rept. 39, 18 (1964), No.18.

65. Miller, G.H. and Dacey, J.R., J. Phys. Chem. 69, 1434 (1965).

66. Andreades, S., Chem. Ind. (London) 782 (1962).

67. Kevan, L. and Hamlet, P., J. Chem. Phys. 42, 2255 (1965).

68. Cordischi, D. et al., Trans. Faraday Soc. 60, 2047, (1964).

69. Site, A.D. et al., J. Chem. Soc. 5430 (1964).

70. Cohen, N. and Heicklen, J., J. Phys. Chem. 70, 3082 (1966).

71. Heicklen, J. and Knight, V., J. Phys. Chem. 70, 3893 (1966).

72. Gozzo, F. and Carnaggi, G., Tetrahedron 22, 2181 (1966).

73. King, R.B. et al., J.A.C.S. 83, 3604 (1961).

74. Mahler, W., Inorg. Chem. 2, 230 (1963).

75. Clark, H.C. and Willis, C.J., J.A.C.S. 82, 1888 (1960).

76. Clark, H.C. and Willis, C.J., J.A.C.S. 84, 898 (1962).

77. Ayscough, P.B. and Emeleus, H.J., J. Chem. Soc. 3381, (1954).

78. Mitsch, R.A., J. Heterocyclic Chem. 1, 271 (1964).

79. Mitsch, R.A., J. Heterocyclic Chem. 3, 245 (1966).

80. Haszeldine, R.N., J. Chem. Soc. 3761 (1953).

81. Heicklen, J. et al., J. Phys. Chem. 69, 693 (1965).

82. Ito, M., Spectrochimica Acta 22, 1581 (1966).

83. Majer, J.R. and Patrick, C.R., Nature 192, 866 (1961).

84. Reed, R.I. and Snedden, W., Trans. Faraday Soc. 54, 301 (1958).

85. Majer, J.R. and Patrick, C.R., Nature 201, 1022 (1964).

86. Steele, W.C., J. Phys. Chem. 68, 2359 (1964).

87. Pottie, R.F., J. Chem. Phys. 42, 2607 (1965).

88. Farlow, M.W., U.S. Pat. 2,709,192 (May 24, 1955).

89. Stull, D.R., J.A.N. A.F. Thermochemical Tables (1961).

90. Wentink, T. and Isaacson, L., J. Chem. Phys. 46, 603, (1967).

91. Gozzo, F. and Patrick, C.R., Nature 202, 80 (1964).

92. Edwards, J.W. and Small, P.A., Nature 202, 1329 (1964).

93. Simons, J.P., Nature, 205, 1308 (1965).

94. Venkateswarlu, P., Phys. Revs. 77, 79 (1950).

95. Laird, R.K., Andrews, E.B. and Barrow, R.F., Trans. Faraday Soc. 46, 803 (1950).

96. Duchesne, J. and Burnelle, L., J. Chem. Phys. 21, 2005 (1953).

97. Mann, D.E. and Thrush, B.A., J. Chem. Phys. 33, 1732 (1960).

98. Simons, J.P. and Yarwood, A.J., Nature 187, 316 (1960).

99. Margrave, J.L. and Wieland, K., J. Chem. Phys. 21, 1552 (1953).

100. Simons, J.P. and Yarwood, A.J., Nature 192, 943 (1961).

101. Seyferth,D. et al., J.A.C.S. 87, 681 (1965).

102. Birchall, J.M. et al., Proc. Chem. Soc. 81 (1960).

103. Franzen, V., Abstracts of 141st meeting of The Amer. Chem. Soc. p.23; Franzen, V., Chem. Ber. 95, 1964 (1962).

104. Franzen, V., Angew. Chemie 72, 566 (1960).

105. Speziale, A.J. and Ratts, K.W., J.A.C.S. 84, 854-9 (1962).

106. Modica, A.P. and Le Graff, J.E., J. Chem. Phys. 43, 3383 (1965).

107. J.A.N.A.F. Tables, Advanced Research Projects Agency, Washington, D.C.

108. Mitsch, R.A., J. Heterocyclic Chem. 1, 233 (1964).

109. Hine, J. and Tanabe, K., J.A.C.S. 79, 2654 (1957).

110. Stockwell, P.B., Ph.D. Thesis, London University (1965).

111. Atkinson, B., Ph.D. Thesis, London University (1950)

112. Greene, S.A. and Wachi, F.M., Anal. Chem. 35, 928 (1963)

113. Heicklen, J. and Knight, V., J. Phys. Chem. 69, 3600 (1965).

114. Venkateswarlu, P., Phys. Revs. 77, 676 (1950).

115. Nelson, L.S. and Kuebler, N.A., J. Chem. Phys. 37, 47 (1962).

116. Heicklen, J., Cohen, N, and Saunders, D., J. Phys. Chem. 69, 1774 (1965).

117. U.S. Pat. 2,979,539 (1961).

118. U.S. Pat. 2,551,573.

119. McDonald, C.C., private communication to Dalby (48).

120. "Formation and Trapping of Free Radicals" 2, 53, Bass and Broida (Eds.) Acad. Press, New York (1960).

121. Porter, G. Disc. Faraday Soc. 14, 133 (1953).

122. Shen, T.Y., et al. Tetrahedron Letters 43 (1961).

123. Hine, J. and Tanabe, K., J.A.C.S. 81, 3002 (1958).

124. Mahler, J.A.C.S. 84, 4600 (1962).

125. Mastrangelo, S.V.R., J.A.C.S. 84, 1122 (1962).

126. Bass, A.M. and Mann, D.E., J. Chem. Phys. 36, 3501 (1962).

127. Simons, J.P., J. Chem. Soc. 5406 (1965).

128. Modica, A.P., J. Chem. Phys. 44, 1585 (1966).

129. Mathews, C.W., J. Chem. Phys. 45, 1068 (1966).

130. Modica, A.P. and La Graff, J.E., J. Chem. Phys. 45, 4729 (1966).

131. Fielding, W. and Pritchard, H.O., J. Phys. Chem. 64, 278 (1960).

132. Milligan, D.E., et al., J. Chem. Phys. 41, 1199 (1964).

133. Thrush, B.A. and Zwolenik, J.J., Trans. Faraday Soc. 59, 582 (1963).

134. Zeleznik, F.J. et al., NASA Tech. Note D-132 (1959).

135. Wiederkehr, R.R.V., J. Chem. Phys. 37, 1192 (1962).

136. Powell, F.X. and Lide, D.R., J. Chem. Phys. 45, 1067 (1966).

137. Genaux, C.T. et al., J.A.C.S. 75, 6196 (1953).

138. Atkinson, B. and Stockwell, P.B., J. Chem. Soc.(B), 984 (1966).

139. Kaesz, H.D., et al., J.A.C.S. 82, 6228 (1960).

140. Falconer, W.E., Hunter, T.F. and Trotman-Dickenson,A.F. J. Chem. Soc. 609 (1961).

141. Chesick, J.P., J.A.C.S. 82, 3277 (1960).

142. Halberstadt, M.L. and Chesick, J.P., J. Phys. Chem. 69, 429 (1965).

143. Atkinson, B. and Trenwith, A.B., J. Chem. Soc. 2082 (1953).

144. Lewis, E.E. and Naylor, M.A., J.A.C.S. 69, 1968 (1947).

145. Wellman, R.E. and Walters, W.D., J.A.C.S. 79, 1542 (1957).

146. Birchall, J.M., Haszeldine, R.N. and Roberts, D.W., Chem. Comm. 287 (1967).

147. Neuvar, E.W. and Mitsch, R.A., J. Phys. Chem. 71, 1229 (1967).

148. Haszeldine, R.N. and Young, J.C., Proc. Chem. Soc. 394 (1959).

149. Gale, D.M., Middleton, W.J. and Krespan, C.G., J.A.C.S. 87, 657 (1965).

150. "Handbook of Chemistry and Physics", 45th ed. Chemical Rubber Co. (Aug. '64).

151. Swift, J.D., in "Handbook of Vacuum Physics", Vol.1, Beck, A.H. (Ed.), Pergamon Press (1966).

152. Chapman, S., Phil. Trans. 217A, 115 (1918).

153. Knudsen, M., Ann. Physik. 83, 797 (1927).

154. Chu Liang, S., Can. J. Chem. 33, 279 (1955).

155. Porter, A.S., Disc. Faraday Soc. 8, 358 (1950).

156. Margenau, H. and Murphy, G.M. "The Mathematics of Physics and Chemistry", D. Van Nostrand Co.Ltd. (1943).

157. Carr, R.W. and Walters, W.D., J. Phys. Chem. 69, 1073 (1965).

158. Frey, H.M., Trans. Faraday Soc. 60, 83 (1964).

159. Schlag, E.W. and Peatman, W.B., J.A.C.S. 86, 1676 (1964).

160. "Advances in Fluorine Chemistry" Vol.2, Stacey, M. et al. (Eds.) Butterworths (1961).

161. Cottrell, T.L., "The Strength of Chemical Bonds", Butterworths (1958).

162. "Progress in Reaction Kinetics" Vol.2, Porter, G. (Ed.) Pergamon (1964).

163. Cvetanovic, R.J., et al., J. Chem. Phys. 46, 1993 (1967).

164. Rabinovitch, B.S., et al. J. Chem. Phys. 28, 504 (1958).

165. Kennedy, A.D. and Pritchard, H.O., J. Phys. Chem. 67, 161 (1963).

166. Pritchard, H.O., Sowden, R.G. and Trotman-Dickenson, A.F. Proc. Roy. Soc. A217, 563 (1953).